Host-directed therapy for intracellular bacterial Infections

Korbee, C.J.

Host-Directed Therapy for Intracellular Bacterial Infections

Proefschrift

ter verkrijging van

de graad van Doctor aan de Universiteit Leiden,

op gezag van Rector Magnificus Prof.mr. C.J.J.M. Stolker,

volgens besluit van het College voor Promoties

te verdedigen op woensdag 6 maart 2019

klokke 16:15 uur

door

Cornelis Jacob Korbee

geboren te Leiden

in 1982.

Promotor:
Prof. dr. T.H.M. Ottenhoff

Co-promotor:
Dr. M.C. Haks

Leden promotiecommissie:
Prof. dr. S.H. van den Burg
Prof. dr. J.J.C. Neefjes
Prof. dr. A.H. Meijer
Prof. dr. W. van Eden (*Universiteit Utrecht, Department of Infectious Diseases and Immunology*)
Prof. dr. J.T. van Dissel

Table of Contents

Scope and outline of this thesis

In this thesis we describe our work towards identifying novel targets and candidate drugs for host directed therapy (HDT) as a novel therapeutic approach for drug-resistant bacterial infections, focusing on the major human pathogens *Mycobacterium tuberculosis (Mtb*) and *Salmonella enterica* serovar Typhimurium (*Stm*).

Chapter 1 provides an introduction to the background of our studies, including the global health problems caused by *Mtb* and *Stm* and the rise in drug resistance in these pathogens. The concept of HDT is introduced and recent studies in this field are summarized. Finally, technical aspects and limitations of the identification of novel chemical compounds and host targets for HDT is discussed. The studies discussed in **Chapter 1** demonstrate the highly significant need for alternative and additional therapies to combat bacterial drug resistance, as well as the challenges that accompany identification of drugs, key host-targets and the subsequent development of therapies.

In **Chapter 2**, we describe novel techniques we developed, that allowed us to perform large-scale chemical compound and RNAi screens to identify human HDT targets and candidate drugs, using fluorescence-based human *Mtb* and *Stm* infection models. We describe a new flow cytometry-based screening assay that allows fast, medium-throughput screening and faithfully reproduces results from classical colony forming unit (CFU) assays, which can take weeks in case of *Mtb*, in contrast to the three days assay system we report here. Importantly, the assay also confirms published HDT compound data from literature. In addition, we propose and validate the MelJuSo cell line as a novel human phagocytic model for *Mtb* infection.

The novel screening assay and infection models are then applied for a large scale screening of a Library Of Pharmacologically Active Compounds (LOPAC) in **Chapter 3**. Here we report on the identification of a number of highly active HDT compounds for both *Stm* and *Mtb*. Furthermore, we also describe a newly developed *in silico* prediction model for analysis of large chemical screens. This model is then applied to identify novel compounds based on target profiles derived from compounds from the LOPAC library. Both the library screening as well as the *in silico* model identified inhibitors of receptor tyrosine kinases (RTKs) as novel drug candidates for TB HDT and proposed Dovitinib, AT9283 and ENMD-2076 as candidates for drug-repurposing.

The novel screening assay from **Chapter 2** is used for a chemical screen in **Chapter 4**. Based upon our previous identification of H-89 as a host-directed inhibitor of *Stm* and *Mtb*, we here report the screening of a novel library of H-89-analogue compounds, and identify lead compound 97i as a superior host-directed inhibitor of *Mtb* and *Stm*. Using kinase inhibition profiling and genetic silencing, we further identify PCTAIRE kinases as direct targets of 97i and regulators of intracellular survival of *Stm* and possibly *Mtb*.

An alternative approach to identification of HDT targets is reported in **Chapter 5.** Here, we employed a zebrafish TB model to uncover a role for DNA Damage-Regulated Autophagy Modulator (DRAM1) in regulating autophagy upon recognition of mycobacteria by TLRs. We demonstrate in zebrafish embryos that DRAM1 is up-regulated upon mycobacterial infection and, importantly, confirmed this mechanism in *Mtb*-infected primary human macrophages. We further show that signaling through the TLR-MYD88-NF-κB axis was responsible for the induction of DRAM1 and that autophagic encapsulation of mycobacteria was dependent on the cytosolic DNA sensor STING as well as the autophagy adaptor molecule p62. The TLR-MYD88-NF-κB-DRAM1 axis may therefore be exploited for HDT to induce autophagy-mediated control of intracellular (myco)bacteria.

In **Chapter 6**, the major findings of the above studies are summarized and discussed.

1 | General Introduction

Adapted from:
Barsacchi, R.*, Sundaramurthy, C.*, **Korbee, C.J.**, Neefjes, J.J., Ottenhoff, T.H.M., Scanu, T. and Zerial, M., 2012. **Systems Microbiology: Current Topics and Applications; Chapter 5 - Manipulating the Fight Between Human Host Cells and Intracellular Pathogens.** *Caister Academic Press.* ISBN: 978-1-908230-02-7.

* Contributed equally

Intracellular bacterial infections

Host-microbe interactions are complex phenomena spanning multiple levels of complexity, from environmental and ecological factors up to the cellular and genetic levels of host responses. At each of these levels a relationship is established between one or more microorganisms and the host, resulting in formation of various forms of associations ranging from symbiosis to parasitism. Pathogens have the potential to cause disease in their hosts through host-pathogen interactions in which host defenses are challenged by the invasive capacities of the pathogen. Below, we will discuss attempts made to unravel the components of host-pathogen interactions at the cellular and molecular levels and to discuss strategies to skew the balance in favor of the host, focusing on crucial intracellular pathogens causing globally relevant diseases such as *Mycobacterium tuberculosis* (*Mtb*) and *Salmonella enterica*.

Mycobacterium tuberculosis

Tuberculosis (TB) represents a critical health issue with one fourth of the human population carrying a latent *Mycobacterium tuberculosis* (*Mtb*) infection and around 1.3 million deaths in HIV negative cases and 0.4 million deaths in people infected with HIV in 2016 (World Health Organization figures February 2018; http://www.who.int/news-room/fact-sheets/detail/tuberculosis)[1-3]. *Mtb* is able to maintain infection throughout the entire life of the host in a dormant state, ready to be reactivated by as of yet largely unknown cues in normally immunocompetent individuals, or by immune suppression in immune-compromised patients (e.g. HIV patients or iatrogenically immunosuppressed patients, such as transplant recipients or patients on anti-inflammatory drugs). A large part of the "success" of *Mtb* in persisting in the host in a dormant state can be explained by its ability to exploit beneficial host cellular processes, blocking microbicidal ones and ultimately hijacking the host cell machinery to establish and maintain an intracellular survival niche.

Mtb infection is initiated upon aerosol-mediated entry into the bronchoalveolar space and the subsequent phagocytosis of *Mtb* by alveolar macrophages (Mϕs)[4]. The entry of *Mtb* into the Mϕ takes place through redundant receptor-mediated systems in which a large array of different molecules, such as complement receptors, mannose receptors, C-type 2 lectin receptors (DC-SIGN, Mincle, Dectin-1), Fc receptors and integrins have been implicated[5]. The peculiar and very diverse constituents of the *Mtb* cell wall might explain the redundant nature of host molecules in this process. Upon entry into the host cell *Mtb* employs several different strategies to escape the normal Mϕ innate immune functions. *Mtb* is able to interfere with the endocytic machinery by interfering with lipid signaling, by producing "host-like" factors (such as bacterial kinases that interact with host targets), it can interact with cell death-inducing pathways which are important for the establishment of immune reactions and bacterial clearance, it can inhibit normal calcium signaling functions, it can escape from the phagosome and it can inhibit Mϕ activation. These mechanisms are elaborated further below.

As a collective result of these events *Mtb* is able to establish a protected niche in which the bacterium can reside in a so-called dormant state for decades.

The interaction of *Mtb* with host lipid signaling occurs at the level of phosphatidylinositol 3-phosphate (PI(3)P). This signaling intermediate is a central relay in the process of docking of early endosomes on the phagosome, which in turn is critical for the progression of phagosome maturation. The bacterium is able to interfere with the activity of the phosophatidylinositol 3-kinase (PI(3)K) VPS34, preventing the generation of PI(3)P on the phagosome membrane. This is possibly achieved through the action of the bacterial cell wall lipid lipoarabinomannan (LAM)[6], as well as by secretion of the acidic host-like phosphatase SapM, which is thought to hydrolyze PI(3)P on the phagosomal membrane[7]. The combined effect of these events is an overall reduction of PI(3)P on the phagosome membrane, which as mentioned results in the inhibition of phagosome maturation. In addition, the *Mtb*-containing phagosome can retain its ability to interact with early and recycling endosomes through the action of RabGTPases 11 and 14[8]. This is thought to provide the bacterium with access to nutrients circulating through the recycling endosomes. Thus, *Mtb* blocks phagosome maturation progression both to avoid destructive late endosomal or lysosomal enzymes, and to gain access to nutrients that the host is internalizing. In addition to SapM, *Mtb* expresses Protein Kinase G (PknG), a soluble eukaryotic-like serine-threonine kinase whose function is proposed to be phosphorylation of an as yet unidentified host factor. The activity of this kinase is essential for inhibition of phagosome maturation by *Mtb* as intracellular trafficking of a PknG deletion mutant results in lysosomal delivery[9]. Another mechanism that *Mtb* employs to modulate host defenses is perturbation of calcium signaling. Recruitment of the host protein Coronin-1/TACO to the mycobacterial phagosome is critical for arresting phagosome maturation. Mycobacteria induce cytosolic calcium flux in a Coronin-1 dependent manner that results in activation of the calcium-dependent phosphatase Calcineurin. Thus, genetic ablation of Coronin-1 or chemical inhibition of Calcineurin results in release of mycobacterium-mediated phagosome maturation arrest *in vitro* and *in vivo* and subsequent killing of intracellular mycobacteria *in vitro*[10,11]. Other studies demonstrated that *Mtb* actively manipulates the host's innate immune response in order to promote its own survival and immune escape through several different mechanisms. First of all, *Mtb* induces decreased secretion of the pro-inflammatory cytokine IL-12. Nau *et al*. demonstrated this in 2002 by analysis of gene expression profiles of human Mϕs upon exposure to a panel of different bacterial strains and bacterial components. By analyzing *Mtb*-infection specific differentially regulated genes a marked decrease in expression of IL-12 was observed in response to infection with *Mtb* but not other bacteria. This was an indication that *Mtb* modulated other host signaling pathways in addition to those involved in Toll-like receptor (TLR) signaling[12]. Secondly, *Mtb* interferes with signaling pathways downstream of the IFNγ receptor (IFNγR), thus inhibiting a major protective cytokine pathway in human host defense to mycobacteria[13-17]. A third mechanism is down regulation of HLA class II antigen presentation molecules at the Mϕ cell surface to subvert $CD4^+$ T-cell responses[1,18-20]. Additionally, *Mtb* targets DC-SIGN (CD209), which has been shown to deactivate infected DCs and induce IL-10 production in specific settings[21], which further promotes immune deviation from

Th1 type immunity. *Mtb* also actively induces regulatory T cells, and the secretion of TGFβ and IL-10 from cells other than DCs such as M2 type macrophages, all of which are involved in dampening host immunity.

In recent years new severe health risks related to *Mtb* have emerged that have dramatically increased the urgency to find new drugs and targets against tuberculosis. Firstly, HIV co-infection enhances reactivation of latent *Mtb* and in turn *Mtb* could possibly augment the severity of disease in HIV-infected individuals[1]. HIV co-infects about one-fifth of those with *Mtb* infection in southern Africa, and TB is now the leading cause of mortality in HIV-infected individuals[22]. The severity of this co-infection is emphasized by the fact that a HIV infected person - compared to a HIV-negative *Mtb*-infected person - has a 20-fold greater chance to develop active TB[23]. Secondly, multi-, extensively and totally drug-resistant (MDR/XDR/TDR) *Mtb* strains have been emerging, underlining the necessity for new therapies, either through novel antibiotics or by host-directed approaches[23-25]. In 2016 490,000 people were estimated to be diagnosed with MDR-TB[3]. *Mtb* therefore is the leading anti-microbial resistant pathogen worldwide, urging for novel therapeutic drugs to treat MDR-TB as well as more effectively treat drug-susceptible TB such that regimens can be shortened, and thus help prevent newly emerging drug resistance. However, the scarcity of available novel bacterial targets for developing such compounds, and the lack of an integrative understanding of the exact host pathways manipulated by *Mtb* and the mechanisms involved impose a considerable bottleneck in research towards novel therapeutic approaches[26,27]. This is one reason why the field of TB research has witnessed increasingly large-scale screening and systems biological approaches to understand host-pathogen interactions, and to help identify new therapeutic targets in both the host and the pathogen, which will be discussed below.

Salmonella enterica

Salmonella enterica is another example of an intracellular bacterial pathogen that is successful in exploiting host functions to find an intracellular niche in which it is able to proliferate and perpetuate the infection. *Salmonella enterica* serovars Typhi (*S.* Typhi) and Paratyphi (*S.* Paratyphi) are facultative intracellular bacteria that cause gastroenteritis and typhoid fever, respectively, a chronic systemic illness with symptoms ranging from fever, abdominal pain and rash to possible transient diabetes. Typhoid fever has a mortality rate of 10-15% if left untreated and causes between 128,000 and 161,000 deaths annually (World Health Organization figures January 2018; http://www.who.int/news-room/fact-sheets/detail/typhoid). In contrast, *Salmonella enterica* serovar Typhimurium (*Stm*) is unable to cause typhoid fever in humans, but is a common causative agent of gastroenteritis. However, infection of a murine host with this pathogen can result in a systemic disease resembling human typhoid fever. Other *Salmonella* species, like *S. enteritidis*, are able to infect a wide range of other animals and cause transient enteritis in humans.

S*almonella* is generally contracted through the ingestion of contaminated food or water. The first line of contact with the host is the mucosa of the stomach, where the low gastric pH represents the initial defense against infection. After

entering the small bowel, *Salmonella* must traverse the intestinal mucosa, where it induces fluid and ion secretion into the lumen of the bowel as well as an acute inflammatory reaction[28]. The first level of cellular interaction with the host is represented by the contact with the intestinal epithelium. The overall strategy that the pathogen has evolved is to induce phagocytic-like behaviour in otherwise non-phagocytic competent cell types, like the intestinal epithelial M-cells. This process involves exploitation of host signalling pathways, trafficking systems and most importantly regulation of the actin cytoskeleton[29]. The ability to invade and populate the epithelial cell layer depends on a genetic locus termed the *Salmonella* Pathogenicity Island 1 (SPI1), which encodes a type III protein secretion system that is able to deliver a series of bacterial effector proteins to the cytoplasm of the host cell. Effectors coded by SPI1 known to be responsible for manipulation of the host cell machinery are SopB (an inositol 3-phosphatase), SopE and SopE2 (both guanine nucleotide exchange factors), which are activators of the RHO family GTPases CDC42 and RAC1[30]. This activation leads to the recruitment of WASP and Scar/WAVE family proteins, which together with Arp2/3 complexes initiate actin polymerization and permit the formation of the *Salmonella*-Containing Vesicle (SCV) in the non-phagocytic host cell population. Once formed, the SCV undergoes a maturation process, first by interacting transiently with early endosomes and subsequently with late endosomes[31]. During this maturation process, the fusion of the SCV with lysosomes is thought to be prevented, allowing *Salmonella* to survive. The SCV can, however, acquire and retain some lysosomal membrane markers like the glycoprotein LAMP-1[32]. *Salmonella* modulates the host's microtubular kinesin motors on phagosomes and manipulates dynein motor-driven transport of phagosomes to lysosomes to rescue *Salmonella* growth[33-35]. Moreover, *Salmonella* has been shown to activate host kinases, which might inhibit dynein motors to promote *Salmonella* replication[36]. This phase of intracellular invasion is then followed by passage into the sub-epithelial interstitium, where phagocytosis-competent neutrophils and Mϕs are able to ingest the pathogen. Here, the bacterium is able to survive in non-activated Mϕs, resulting in systemic spread and dissemination to various organs like regional lymph nodes, the liver and the spleen. *Salmonella's* intracellular Mϕ phase is characterized again by the processing of the SCV through a unique route of intracellular vesicular trafficking. In this case, the exploitation of host mechanisms is facilitated by the expression of a second genetic locus in the pathogen genome, called Salmonella Pathogenicity Island 2 (SPI2). SPI2 codes for another type III protein secretion system, which transports virulence factors from the pathogen to the host through the vacuolar membrane. The SPI2 locus codes for effectors that diffuse into the host cell cytoplasm, altering its physiology through formation of filamentous endosomes[37], decreased recruitment of NADPH oxidase[38] and changes in the SCV fusion pathways[36], as well as by controlling the actin cytoskeleton in close proximity to the SCV. One of the survival strategies of *Salmonella* is exerted through the action of the bacterial SpvB protein, which counteracts actin polymerization and is involved in triggering apoptosis. *In vitro*, Mϕs infected with *Salmonella* display a profound loss of actin filaments at 10 hours post infection. After 20-24 hours many of these cells have no more detectable polymerized actin and undergo DNA fragmentation in a process

resembling apoptosis. This is thought to permit the SCV to exit the cell with little exposure to the extracellular environment, allowing subsequent cycles of infections. Necrosis is probably not involved in dissemination of the bacteria as the vacuoles released by that process would lose their structural integrity and the bacterium would be exposed to the unfavourable extracellular milieu. Similar to TB, the problem of antibiotic resistance is increasing for treatment of typhoid fever[39]. Antibiotic resistance in *Salmonella* spp. started emerging in the 1970s with strains carrying plasmid-encoded chloramphenicol resistance genes. This led to increased application of second-line antimicrobials ampicillin and trimethoprim, leading to the emergence of MDR *Salmonella* strains in the late 1980s. Attempts to counter these MDR strains using fluoroquinolones were again met by antimicrobial resistance and the endemicity of MDR *Salmonella* strains has since vastly increased[40], urgently prompting for alternative approaches.

Bacterial drug resistance and the search for novel antibiotics

Following the emergence of antibiotic resistance in major human pathogens initial research focused almost exclusively on finding and developing novel antibiotics capable of treating otherwise resistant strains. However, in recent years it has become clear that possibilities for identification of novel antibiotics has diminished and the limited number of leads may prohibit effective development of novel therapeutics[41].

A major problem for development of novel antibiotics is the lack of targets that can be exploited in human pathogens. To illustrate this, a study reported by Becker *et al*. focusing on systematic analysis of 700 *Salmonella enterica* enzymes *in vivo* identified 64 enzymes that are both essential for *Salmonella* survival as well as conserved in other major human pathogens and thus potential drug targets. However, the metabolic pathways in which almost all of the 64 enzymes participate are already targeted by current antibiotics or have been identified in previous studies focusing on antibiotic development. Thus, the authors concluded that the pool of potential novel antibiotics targets is severely limited[42]. Despite this, several novel antibiotic candidates have recently been identified[43,44]. These included dinitrobenzamide derivatives and 1,3-benzothiazin-ones, which were identified as novel inhibitors of *Mtb* acting on cell wall synthesis by blocking formation of lipoarabinomannan, arabinogalactan and arabinose[45,46]. In an alternative approach, Willand *et al*. reported synthetic inhibitors of *Mtb* EthR that enhance the antibiotic activity of ethionamide. One of these inhibitors, BDM31343, enhanced the efficacy of low doses of ethionamide to reduce the *Mtb* bacterial load in a mouse model[47].

Even if promising drug candidates or targets are identified, other factors may contribute to the lack of development of novel clinically applicable antibiotics. Significant investments of time and money are required for drug development pipelines, consisting of drug and target identification, toxicity studies, efficacy testing in animal models and subsequent clinical trials. Especially the later phases

of drug development are usually carried out by pharmaceutical companies. However, development of novel antibiotics is not an attractive avenue for these companies for several reasons. Firstly, antibiotic treatment regimens are usually short, limiting the monetary return per treatment course. Secondly, the more successful and widely applied novel antibiotics are, the more rapidly drug resistance emerges, limiting their long term chances of generating revenue. Thirdly, the relevance of application of antibiotics for many indications (like bronchitis, otitis media and sinusitis) is currently being questioned, reducing the need for broad-spectrum antibiotics and further lowering revenue generated by antibiotic sales[41]. Finally, in poverty-related diseases financial return on investments may be particularly low as drugs have to be made available almost at cost prices[48].

Collectively, these developments illustrate the severity of the emergence of antibiotic resistance and call for new approaches to overcome this.

Host-Directed Therapy for intracellular bacterial infections

As described in the first part of this chapter, intracellular microbes interact extensively with their host environment and modulate it to suit their own survival, often resulting in a shifting of the equilibrium of several host functional modules. Hence, these interactions can be considered as perturbations favoured by host/pathogen co-evolution to primarily facilitate pathogen survival and transmission. Comprehensive understanding of the nature of these dynamic interactions might uncover entirely new targets to combat these pathogens and thus enable us to re-shift the equilibrium in favour of the host. In order to do so, novel tools to dissect the nature of these perturbations and approaches to integrate multi-platform and multi-omic data into functional networks will be essential. Several systematic approaches in the form of high throughput functional screens have been used in recent years to explore the interface between host and pathogen. A computational analysis of interaction nodes of known and experimentally validated pathogen proteins and their host interactors demonstrated that the host molecules that are most often targeted also tend to form crucial nodes in a number of key host pathways. Pathogens tend to target host molecules in a highly directed manner, specifically influencing components that are essential for the host cell and hence are not easily modifiable by the host in order to overcome the influence of the pathogen[49]. However, this could be turned to the advantage of the host in a therapeutic setting, since these nodes are usually well characterized. Hence, a wealth of information exists on the biology and pharmacology of these targets, which can potentially be exploited for rational drug design or drug repurposing in the fight against pathogens. Moreover, targeting the host to fight pathogens might have the additional advantage of reducing chances of drug resistance. The chances of a pathogen acquiring resistance to a host process are arguably lower than developing classical microbial drug resistance, since in the former case no direct selective pressure is exerted on the pathogen. Hence an emerging

approach in the field is to target host processes for development of host-directed therapies (HDT) to fight pathogens[50].

Identification of HDT drug candidates and targets

Although many interactions between viral and host proteins are documented and validated experimentally, this is not yet the case for bacteria and parasites. In fact, even for relatively well-studied bacteria like *Mtb* there are only few direct interactions mapped between bacterial proteins and their host interactors[51,52]. Previous studies from different labs have identified several host molecules involved in mycobacterial infection, which were verified by either RNA interference (RNAi)-mediated gene silencing and/or chemical compound treatment. Inhibition of the identified proteins restored intracellular balance in favour of the host.

Despite several successful examples, which will be discussed below, a system-wide understanding of interactions between mycobacteria and host cells is too incomplete to allow rational or systematic perturbation of host systems for therapeutic purposes. In an effort to fill this crucial gap, several laboratories are currently employing new technologies like arrayed RNAi or chemical compound libraries to probe host-pathogen systems and are using techniques such as automated microscopy, high content analysis, proteomics, microarrays and deep sequencing to visualize and analyze interactions between host and pathogen. Based on recent insights from this work, new HDT approaches are being developed now to improve bacterial inhibition, as shown in multiple recent studies (including our own), both *in vitro* in human and murine cells and *in vivo* in mouse, rabbit and zebrafish models[53-69]. The major targets and mechanisms identified in these studies are discussed below.

Kinases

Phosphorylation of proteins by kinases is an indispensable mechanism for relaying cellular signals in many signaling pathways. Due to their profound effects on signaling pathways and their downstream events, as well as the wealth of chemical inhibitors readily available, kinases are an evidently useful class of candidate targets for HDT. Several studies, including our own, have indeed identified a role for different kinases in regulating intracellular bacterial survival.

In one of the first studies in the area of chemical-genetic identification of drugable host regulators of intracellular *Stm* and *Mtb*, we focused on systematic perturbation of the human kinome[53]. In particular, the kinase PKB/AKT1 was identified as an important regulator of phagosome maturation. AKT1 is activated by *Salmonella* protein SopB, which is actively secreted into the host cytosol through the bacterial type III secretion system (TTSS). *Stm* likely benefits from activating AKT1 for several reasons: 1) AKT1 activation provides a survival signal for the cells, affording a continued niche for bacterial survival; 2) AKT1 ultimately activates the host kinase PAK4 which controls RAC1 activation and actin polymerization[53]. Actin plays an important role in the maintenance of

phagosomes; 3) AKT1 heavily phosphorylates the RAB14-GAP, AS160, which subsequently dissociates from the phagosomal membrane, thereby preventing AS160's ability to inactivate the GTPase RAB14. Active RAB14 prevents fusion of phagosomes with lysosomes and thereby promotes *Stm* survival. Of note, the same pathway appears to be activated by a series of unrelated intracellular bacteria such as *Mtb*, *Shigella* and *Chlamydia* strains[53].

In 2010, Kumar *et al.* reported genome wide siRNA screens to identify host factors involved in the regulation of the bacterial load of a virulent *Mtb* strain (H37Rv) in the THP-1 human monocytic leukaemia cell line[54]. In order to specifically study host factors involved in intracellular replication or degradation, but not uptake of *Mtb,* siRNA transfections were performed post infection, in contrast to the approach by Kuijl *et al.*, who used pre-infection siRNA. Using this post-infection siRNA approach the authors were unable to confirm a major role for AKT1 alone, but found that the combined knock-down of AKT1 and AKT2 significantly decreased *Mtb* proliferation. However, silencing of AKT1 *prior* to infection resulted in a ~50% decrease in *Mtb* bacterial load, in agreement with the findings of Kuijl *et al.*. Providing further validation, the genome-wide screen of Kumar *et al.* yielded an array of 275 host factors that influenced *Mtb* bacterial load in THP-1 cells, from which an '*Mtb* regulatory network' was constructed. This network of interactions was further subclustered based on gene ontology annotations[26]. Interestingly, several subnetworks in which the GO classes 'immunity/inflammation/stress', 'transcription regulation', 'signal transduction', 'metabolism' and 'cell cycle/growth' were enriched centered around AKT1, further emphasizing the importance of this kinase in the regulation of *Mtb* intracellular survival and replication. By silencing the 275 host factors identified in cells infected with several different *Mtb* field isolates (each with different virulence, antibiotic resistance and intracellular growth properties), 74 "common" host factors that were shared by all *Mtb* strains tested, including clinical isolates, could be identified[54].

Thus, activation of AKT1 was reported in multiple studies as a general mechanism exploited by intracellular pathogens to manipulate the host to facilitate pathogen survival. In agreement with this, a chemical inhibitor of AKT1 called H-89 was used in the study by Kuijl *et al*. as a lead compound for chemical genetics, and was shown to be effective in decreasing intracellular survival of both *Stm* and *Mtb* in human primary Mϕs. This indicated that similar signalling pathways might also play an important regulatory role in intracellular trafficking of *Mtb*. Inhibition of AKT1 was therefore proposed as a new strategy to eliminate intracellular bacteria*.* In addition, multi-drug resistant and extensively drug resistant strains of mycobacteria such as *Mtb* might still be susceptible to the effects of inhibition of AKT1.

Jayaswal *et al.* published another study in 2010 employing similar methods to those used by Kumar *et al.* The authors reported an RNAi screen focused on the kinome and phosphatome in the J774 murine Mϕ cell line, resulting in the identification of 41 host factors involved in the intracellular replication of *Mtb*, at least in a mouse cell line. Using a similar approach as Kumar *et al.*, a core set of 11 host factors was found to be effective in controlling intracellular *Mtb* independent of the origin of the strain. From these 11 genes the

TGFß type-1 receptor (TGFßRI) was studied in more detail, since the expression of both this receptor and another isoform (TGFß type-2 receptor, TGFßRII) and the ligands TGFßI and TGFßII were found to be up regulated in response to *Mtb* infection of mouse primary Mϕs by microarray analysis. In addition, casein kinase 1 (CSNK1) was studied, which is a kinase in the TGFßR1 axis and one of the 11 identified *Mtb* strain-independent host factors. A chemical inhibitor of both TGFßRI and CSNK1 was found to be effective in decreasing bacterial load after infection of mouse primary Mϕs with H37Rv or two different clinical field isolates. In addition, it was also effective in a murine *Mtb* infection model[55], as assessed by Colony Forming Unit (CFU) counts and histopathology of infected organs. This provides direct evidence of the feasibility of host-based therapeutic approaches to target mycobacteria.

The kinase ABL was identified as a host kinase essential for infection and survival of *Mtb* and *Mycobacterium marinum* (*Mm*) in a study by Napier *et al*.[58]. The ABL inhibitor imatinib (Gleevec) was subsequently shown to be efficacious in reducing bacterial loads in *Mtb*-infected mice. Importantly, administration of this drug was synergistic with first-line antibiotics in this murine model.

A direct interaction between an *Mtb* virulence factor and a host kinase is exemplified in a study focusing on kinase interactions of *Mtb* phosphatase PtpA[70]. Here, GSK3α was identified as a human host substrate of this phosphatase and dephosphorylation of GSK3α by PtpA resulted in diminished Mϕ apoptosis and thereby promoted *Mtb* survival.

Sogi *et al.* reported Gefitinib as a HDT candidate and used phosphoproteomic and transcriptional profiling to identify its mode of action[71]. The authors found that EGFR inhibitor Gefitinib in *Mtb* infected Mϕs inhibits STAT3, which is a transcription factor known to repress immune responses to *Mtb*. Furthermore Gefitinib upregulated genes involved in lysosomal biogenesis and increased both the number of lysosomes per cell and the trafficking of *Mtb* to the lysososmes, again underscoring the role of this pathway in controlling intracellular *Mtb* as well as highlighting its drugability by HDT.

Autophagy

In addition to studies focusing on phagosome maturation, also the modulation of autophagy-associated pathways has been an active topic in research on *Mtb* infection for several years. These studies have uncovered important new mechanisms, drug targets and drug candidates for HDT. Autophagy is a cellular degradative process that delivers intracellular structures like damaged organelles or cytoplasmic pathogens to the lysosomal pathway by enveloping them in double-membrane structures[72]. Several studies have shown that this process can be exploited to deliver intracellular pathogens, either in intact phagosomes or present in the cytosol, to the lysosomal pathway.

Based on the observation by Kumar *et al*. mentioned above that different field isolates of *Mtb* responded, in part, differently to specific RNAi-mediated host cell perturbations, targeted host-directed therapies must take into account heterogeneity in host mechanisms and signatures for different (myco)bacterial strains. As discussed in the previous section, however, there appeared to be a common core component of host pathways involved in host defense to all *Mtb*

isolates. When further studying this subset, the effect of silencing by 44 siRNAs could be reversed by inhibition of autophagy, indicating that the RNAi-targeted host factors might be involved in the negative regulation of autophagy. Although the anti-mycobacterial effects of autophagy have previously been shown[73], the extent of its interaction with mycobacterial infections was thus far not fully appreciated. This study suggested that inhibition of autophagy might be a central component of mycobacterial intracellular survival strategies[54]. Since mycobacteria actively inhibit autophagy, inducers of autophagy newly identified via independent chemical screens should therefore be tested for their potential use as anti-mycobacterial agents, thereby opening new avenues in treatment of tuberculosis. Identification of other critical host manipulated networks could therefore be important in expanding the arsenal of novel targeted host based therapies.

Another interesting observation was that IFN-γ stimulation appeared to enhance the bacterial load suppressive effect of silencing a number of host factors, in spite of the fact that the infected cells were relatively insensitive to IFN-γ as a single agent[54,74]. Two antipsychotics (Haloperidol and Prochlorperazine) and one antidepressant (Nortryptiline) were identified that inhibited mycobacterial infection by enhancing both phagocytic and autophagic Mϕ responses, as reported by Sundaramurthy *et al*.[56]. In screening a library of bioactive small molecules, Stanley *et al*. identified the EGFR inhibitor Gefitinib and the serotonin transport inhibitor fluoxetine as *Mtb*-inhibiting compounds, which upon further analysis appeared to enhance LC3-I to LC3-II conversion, suggesting that these compounds act through induction of autophagy[68]. Another study specifically focused on identifying FDA-approved drugs that inhibit mycobacteria through mTOR-independent induction of autophagy. The anticonvulsants carbamazepine and valproic acid were demonstrated to induce autophagy of intracellular *Mtb* through a pathway regulated by depletion of intracellular myo-inositol[66]. Both drugs were used in concentrations achievable in humans, and may therefore be good candidates for drug-repurposing.

Immunomodulation

Apart from studies focused on enhancing Mϕ microbicidal mechanisms, several recent studies have aimed to apply HDT in a broader immunomodulatory context, particularly targeting inflammation. Phosphodiesterase inhibitors were successfully applied in mouse and rabbit TB models, increasing bacterial susceptibility to antibiotics as a result of dampened innate immunity and inflammation[59-61]. Similarly, other anti-inflammatory agents such as Ibuprofen were shown to be beneficial by reducing bacterial loads and enhancing mouse survival in a murine TB model[62]. Another approach focused on restoring the Lipoxin A_4 and Leukotriene B_4 lipid mediator equilibrium in a zebrafish model, thereby balancing TNF production[75]. This was subsequently shown to be a feasible pathway that could be exploited for HDT in a mouse model using FDA-approved drugs like Zileuton, by augmenting prostaglandin E2 levels and IL-1β dependent protection[63]. Other studies also identified compounds and host targets involved in regulation of TNF-α. In the above mentioned study by Stanley *et al.* the small molecule fluoxetine was identified, which both induced autophagy and promoted TNF-α secretion[68]. The host molecule NAD(P)H:quinone oxidoreductase 1 (NQO1)

was identified in a study focusing on host genes enriched in Mϕs resistant to mycobacterial infection[69]. NQO1 was shown to enhance TNF-α and IL-1β secretion, as well as stimulate Mϕ differentiation and NF-κB activation. Dicoumarol, a selective inhibitor of NQO1, was shown to induce intracellular mycobacterial killing and was proposed as a HDT candidate.

Enhancing HDT drug granuloma delivery and antibiotic efficacy

Enhancing the efficacy of current and novel antibiotics and increasing their penetration into granulomas is another potential application for HDT strategies[64].

In a fashion similar to novel tumor immunotherapy regimens, approaches are being considered to enhance drug penetration and reduce induction of lesional hypoxia. This may be achieved by anti-angiogenic treatment. Two studies have now provided proof of principle for this in mycobacterial infection models. Firstly, Datta *et al*. demonstrated enhanced VEGF expression in human and rabbit TB granulomas. Treating *Mtb*-infected rabbits with an anti-VEGF antibody resulted in diminished hypoxic fractions in the granulomas and enhanced drug penetration as evidenced by increased small molecule tracer local delivery[64]. Secondly, the VEGF inhibitor Pazopanib was shown to reduce *Mm* bacterial loads in a zebrafish model as well as suppressed granuloma angiogenesis, identifying another HDT candidate pathway and corresponding candidate drug[65].

Alternatively, Skerry *et al*. identified Simvastatin as a novel HDT candidate for TB. In their study, Simvastatin treatment, both *in vitro* and *in vivo,* significantly increased the anti-tuberculous activity of isoniazid, and the authors proposed that Simvastatin may act by restricting access of *Mtb* to nutrient-rich lipid droplets present in the host cell.

Additional targets for HDT in infectious disease

Several additional studies have identified potential HDT drug candidates, and candidate mechanisms or targets for HDT next to the categories discussed above. Firstly, Machado *et al*. reported several compounds that inhibited *Mtb* via host mechanisms through enhancing phagosome acidification and lysosomal hydrolase activity, as well as by blocking efflux activity of the bacterium, thereby enhancing antibiotic efficacy[57]. This included the ion channel blockers Verapamil, Thioridazine, Chlorpromazine, Flupenthixol and Haloperidol. Interestingly, Haloperidol was also identified as a host-directed inhibitor of intracellular mycobacteria in the study by Sundaramurthy *et al*., where this compound was also linked to the autophagic response[56], indicating that this compound may have multiple modes of action (see also above). Secondly, an alternative approach for modulating phagosome maturation is the use of apoptotic body-like liposomes harboring bioactive lipids like phosphatidic acid and differentially phosphorylated phosphatidylinositol. This strategy was recently shown to inhibit intracellular mycobacteria, further meriting HDT approaches at the phagosome level[76]. Thirdly, by focusing on the metabolomics of virulent *Mtb* infection, Mehrotra *et al*. identified host metabolic pathways that were exploited by *Mtb,* which promoted necrotic cell death and pathogenesis, and thereby providing additional (metabolic) targets for HDT[77]. Further identifying metabolic targets involved in controlling intracellular bacterial infection, the anti-diabetic drug Metformin was identified as

a host-directed compound that inhibited *Mtb* by induction of autophagy and inducing generation of reactive oxygen species in an adenosine monophosphate-activated protein kinase (AMPK)-dependent manner[78].

Chemical genetics of host-pathogen interactions

Approaches focusing on various defined host and pathogen gene classes to unravel the intersection between host and pathogen using high-throughput or high-content technologies can pave the way towards a better understanding of dynamic host-pathogen interactions at a system biological level. Several of these have been discussed already above, and have provided a much-needed first step towards the systematic identification of genes involved in mycobacterium-host interactions. However, given the variability and differences in responses reported from different screens conducted in different experimental conditions using various methodologies, and the diverse criteria used to define 'hits', it will be important to better understand and correlate the data obtained by such broader screening studies. This will be an essential next step in developing an integrative understanding of the pathways regulating intracellular survival of mycobacteria and the interplay between host and pathogen that defines the generation, maintenance and eventual outcome of *Mtb* infection. Identifying host components involved in pathogenesis by RNAi-based screens as outlined above, is one way of finding host targets and processes involved in pathogenesis. This is an emerging area and several efforts are currently underway. A complementary approach is to identify chemical entities that perturb the host-pathogen system and from this knowledge identify possible target molecules involved in pathogenesis. Several different approaches have been employed towards target identification from cell based chemical screens. Literature in this field is evolving and several recent examples of different methodologies adopted to identify intracellular targets of hit compounds will be outlined further below. Although the methods described here have been used in the context of pathogen factors, many of them can be potentially adapted to identify host targets as well.

A different approach to better understand the intersection between *Mtb* and its host has been presented recently by Beaulieu *et al.*[74]. They have built a matrix of host effectors and bacterial mutants and screened this combinatorial space for phenotypes using an image based screening platform. Their system was geared to identify mycobacterial mutants that regulate host immunity and hence they engineered host cells to report on 12 different immune effectors of mycobacterial infections and scanned the whole mycobacterial genome for responses to these effectors. Despite the significant technical challenges in building this matrix and the undefined rates of false positives, they were able to identify several new *Mtb* genes that played a role in manipulating host immunity, with more than 200 *Mtb* genes as candidates for regulating these responses.

Approaches to identify HDT targets for the treatment of intracellular bacterial infections can also be informed by studies on other pathogens such as

viruses and parasites. Recently, two papers were published that vastly increased the publicly available repertoire of known anti-malarial compounds[79,80]. Interestingly, these papers described strategies to identify the mode of action of chemical compounds. Gamo *et al.*[79] screened approximately 2 million chemical compounds for their anti-malarial effect. The hit compounds were clustered based on their chemical structure. By following a similarity principle the authors reasoned that compounds within the same structural cluster might share a similar mode of action. In an effort to explore these compounds vis-à-vis the known target space, the authors classified compounds from different clusters based on their behaviour in diverse assays for different known human drug targets. Hypothesizing that similar targets may be found in the parasite, the authors then identified *P. falciparum* (*Pfal*) orthologs of these human targets and proposed a list of *Pfal* genes that might be considered as targets. Additionally, several compounds were identified that have no known orthologs in *Pfal*. Detailed studies on these might indeed help uncover previously underappreciated aspects of malarial physiology in general, and more specifically in the context of drug development. In an alternative approach, Guiguemde *et al.* screened approximately 400,000 compounds for anti-malarial activity in a whole cell based screen and identified and validated several of them as 'hits'[80]. To understand the mode of action of the hit compounds, the authors assessed the performance of 66 selected hits in assays for known anti-malarial mechanisms such as *Pfal* dihydro orotate dehydrogenase (PFDHOD), *Pfal* Falcipain-2 and hemazoin formation. Additionally, binding studies of these drugs were performed on a panel of 61 recombinant *Pfal* proteins. Using this approach, several combinations of possible mechanisms of action were identified for most of the drugs. Interestingly, five compounds were negative in all the assays tested despite having anti-malarial properties, thus showing novel mechanistic promise.

Volkman *et al.* proposed a different approach for identifying host cell targets for diverse perturbations such as toxins, drugs and viruses[52]. In this approach gene trap retroviruses were used to knock out genes, generating a library of nonessential null mutants in the human near-haploid cell line 7KBM7. This library of random knock-out clones was then screened for the effects of the different knock-outs by applying different agents that are normally toxic to the cell line. While most clones will die as a result of this perturbation, surviving clones are likely to be rendered resistant by disruption of the genes coding for the targets of the toxic agents by insertion of retroviral DNA. This approach was successfully validated by treating mutated cells with Gleevec, an anti-cancer drug - and a candidate HDT drug for *Mtb* infection[58], as discussed above - that specifically inhibits tyrosine kinase activity of ABL (and the fusion protein BCR-ABL that is constitutively active in certain tumour cells). Since 7KBM7 cells are sensitive to Gleevec, surviving clones are likely to harbour an insertion in their target genes. Indeed, five independent Gleevec-resistant clones contained insertions in genes closely functionally related to c-ABL. In this approach genes are functionally knocked out (due to insertional mutagenesis) as opposed to knocked down in RNAi screens. Therefore it could complement RNAi-based screens by overcoming the latter's significant drawbacks, such as incomplete and heterologous silencing between different oligos and off-target effects. However this tool is currently

restricted to the particular cell line 7KBM7, and therefore the biological processes supported by it, potentially limiting the exciting possibilities that it offers.

Functional and chemical genomics screens are powerful tools, but like every technology they are not free of caveats. Knockdown efficiency in a functional genomic screening setting is not homogeneous due to differences in efficacy between siRNA oligos, differences in mRNA and protein stability between targets, possible off-target effects, and possible redundancy of targets for which loss-of-function might be compensated by other factors in a single gene knockdown setting. On the other side chemical genomic screens are limited by other factors, such as bioavailability, the use of a narrow window of concentrations (at least in the primary campaigns), degradation of the compounds and unknown (often multiple) targets of the active compounds, complicating deconvolution steps. Moreover, the analysis of the results poses both traditional and new challenges, with lack of standards for statistical and bio-informatic analysis and varying quality of different databases for accurate gene annotations, chemical-protein or protein-protein interactions. The availability of new approaches such as multiparametric analysis[81] and population context analysis[82] to evaluate phenotypes with a finer granularity, as well as development of tools for correlation analysis across different screens, will help to extract more relevant information, refining our ability to filter false positives or negatives and, ultimately producing more defined new leads for prospective therapeutic interventions in human disease. Learning from similar and parallel efforts in developing HDT for cancer might accelerate, and be of great benefit to, the combat against major global killers such as TB.

References

1. Diedrich, C. R. & Flynn, J. L. HIV-1/mycobacterium tuberculosis coinfection immunology: how does HIV-1 exacerbate tuberculosis? *Infection and Immunity* **79,** 1407–1417 (2011).
2. Ottenhoff, T. H. M. The knowns and unknowns of the immunopathogenesis of tuberculosis. *Int. J. Tuberc. Lung Dis.* **16,** 1424–1432 (2012).
3. World Health Organization. *Global Tuberculosis Report 2017*. 1–249 (2017).
4. Kaufmann, S. H. How can immunology contribute to the control of tuberculosis? *Nat Rev Immunol* **1,** 20–30 (2001).
5. Brennan, P. J. & Nikaido, H. The envelope of mycobacteria. *Annu. Rev. Biochem.* **64,** 29–63 (1995).
6. Vergne, I., Chua, J. & Deretic, V. Mycobacterium tuberculosis phagosome maturation arrest: selective targeting of PI3P-dependent membrane trafficking. *Traffic* **4,** 600–606 (2003).
7. Saleh, M. T. & Belisle, J. T. Secretion of an acid phosphatase (SapM) by Mycobacterium tuberculosis that is similar to eukaryotic acid phosphatases. *Journal of Bacteriology* **182,** 6850–6853 (2000).

8. Kyei, G. B. *et al.* Rab14 is critical for maintenance of Mycobacterium tuberculosis phagosome maturation arrest. *The EMBO Journal* **25,** 5250–5259 (2006).
9. Walburger, A. *et al.* Protein kinase G from pathogenic mycobacteria promotes survival within macrophages. *Science* **304,** 1800–1804 (2004).
10. Jayachandran, R. *et al.* Survival of mycobacteria in macrophages is mediated by coronin 1-dependent activation of calcineurin. *Cell* **130,** 37–50 (2007).
11. Jayachandran, R. *et al.* RNA interference in J774 macrophages reveals a role for coronin 1 in mycobacterial trafficking but not in actin-dependent processes. *Mol. Biol. Cell* **19,** 1241–1251 (2008).
12. Nau, G. J. *et al.* Human macrophage activation programs induced by bacterial pathogens. *Proc. Natl. Acad. Sci. U.S.A.* **99,** 1503–1508 (2002).
13. Banaiee, N., Kincaid, E. Z., Buchwald, U., Jacobs, W. R. & Ernst, J. D. Potent inhibition of macrophage responses to IFN-gamma by live virulent Mycobacterium tuberculosis is independent of mature mycobacterial lipoproteins but dependent on TLR2. *J. Immunol.* **176,** 3019–3027 (2006).
14. Desvignes, L. & Ernst, J. D. Interferon-gamma-responsive nonhematopoietic cells regulate the immune response to Mycobacterium tuberculosis. *Immunity* **31,** 974–985 (2009).
15. Fortune, S. M. *et al.* Mycobacterium tuberculosis inhibits macrophage responses to IFN-gamma through myeloid differentiation factor 88-dependent and -independent mechanisms. *J. Immunol.* **172,** 6272–6280 (2004).
16. Benson, S. A. & Ernst, J. D. TLR2-dependent inhibition of macrophage responses to IFN-gamma is mediated by distinct, gene-specific mechanisms. *PLoS ONE* **4,** e6329 (2009).
17. Ottenhoff, T. H. M. *et al.* Genetics, cytokines and human infectious disease: lessons from weakly pathogenic mycobacteria and salmonellae. *Nat. Genet.* **32,** 97–105 (2002).
18. Kincaid, E. Z. & Ernst, J. D. Mycobacterium tuberculosis exerts gene-selective inhibition of transcriptional responses to IFN-gamma without inhibiting STAT1 function. *J. Immunol.* **171,** 2042–2049 (2003).
19. Noss, E. H. *et al.* Toll-like receptor 2-dependent inhibition of macrophage class II MHC expression and antigen processing by 19-kDa lipoprotein of Mycobacterium tuberculosis. *J. Immunol.* **167,** 910–918 (2001).
20. Ting, L. M., Kim, A. C., Cattamanchi, A. & Ernst, J. D. Mycobacterium tuberculosis inhibits IFN-gamma transcriptional responses without inhibiting activation of STAT1. *J. Immunol.* **163,** 3898–3906 (1999).
21. Appelmelk, B. J. *et al.* Cutting edge: carbohydrate profiling identifies new pathogens that interact with dendritic cell-specific ICAM-3-grabbing nonintegrin on dendritic cells. *J. Immunol.* **170,** 1635–1639 (2003).
22. Kaufmann, S. H. E. & Parida, S. K. Tuberculosis in Africa: learning from pathogenesis for biomarker identification. *Cell Host and Microbe* **4,** 219–228 (2008).

23. Jassal, M. S. & Bishai, W. R. Epidemiology and challenges to the elimination of global tuberculosis. *CLIN INFECT DIS* **50 Suppl 3,** S156–64 (2010).
24. Ottenhoff, T. H. M. Overcoming the global crisis: 'yes, we can', but also for TB ... ? *Eur. J. Immunol.* **39,** 2014–2020 (2009).
25. Ottenhoff, T. H. M. New pathways of protective and pathological host defense to mycobacteria. *Trends Microbiol.* **20,** 419–428 (2012).
26. Méresse, S. *et al.* Controlling the maturation of pathogen-containing vacuoles: a matter of life and death. *Nat Cell Biol* **1,** E183–8 (1999).
27. Vergne, I., Chua, J., Singh, S. B. & Deretic, V. Cell biology of mycobacterium tuberculosis phagosome. *Annu. Rev. Cell Dev. Biol.* **20,** 367–394 (2004).
28. Santos, R. L. *et al.* Animal models of Salmonella infections: enteritis versus typhoid fever. *Microbes Infect.* **3,** 1335–1344 (2001).
29. Guiney, D. G. & Lesnick, M. Targeting of the actin cytoskeleton during infection by Salmonella strains. *Clin. Immunol.* **114,** 248–255 (2005).
30. Hardt, W. D., Chen, L. M., Schuebel, K. E., Bustelo, X. R. & Galan, J. E. S. typhimurium encodes an activator of Rho GTPases that induces membrane ruffling and nuclear responses in host cells. *Cell* **93,** 815–826 (1998).
31. Brumell, J. H. & Grinstein, S. Salmonella redirects phagosomal maturation. *Current Opinion in Microbiology* **7,** 78–84 (2004).
32. Holden, D. W. Trafficking of the Salmonella vacuole in macrophages. *Traffic* **3,** 161–169 (2002).
33. Boucrot, E., Henry, T., Borg, J.-P., Gorvel, J.-P. & Méresse, S. The intracellular fate of Salmonella depends on the recruitment of kinesin. *Science* **308,** 1174–1178 (2005).
34. Harrison, R. E., Bucci, C., Vieira, O. V., Schroer, T. A. & Grinstein, S. Phagosomes fuse with late endosomes and/or lysosomes by extension of membrane protrusions along microtubules: role of Rab7 and RILP. *Molecular and Cellular Biology* **23,** 6494–6506 (2003).
35. Marsman, M., Jordens, I., Kuijl, C., Janssen, L. & Neefjes, J. Dynein-mediated vesicle transport controls intracellular Salmonella replication. *Mol. Biol. Cell* **15,** 2954–2964 (2004).
36. Uchiya, K. *et al.* A Salmonella virulence protein that inhibits cellular trafficking. *The EMBO Journal* **18,** 3924–3933 (1999).
37. Stein, M. A., Leung, K. Y., Zwick, M., García-del Portillo, F. & Finlay, B. B. Identification of a Salmonella virulence gene required for formation of filamentous structures containing lysosomal membrane glycoproteins within epithelial cells. *Molecular Microbiology* **20,** 151–164 (1996).
38. Vazquez-Torres, A. *et al.* Salmonella pathogenicity island 2-dependent evasion of the phagocyte NADPH oxidase. *Science* **287,** 1655–1658 (2000).
39. Smith, S. I., Seriki, A. & Ajayi, A. Typhoidal and non-typhoidal Salmonella infections in Africa. *Eur. J. Clin. Microbiol. Infect. Dis.* **35,** 1913–1922 (2016).
40. Crump, J. A., Sjölund-Karlsson, M., Gordon, M. A. & Parry, C. M. Epidemiology, Clinical Presentation, Laboratory Diagnosis, Antimicrobial

Resistance, and Antimicrobial Management of Invasive Salmonella Infections. *Clin. Microbiol. Rev.* **28,** 901–937 (2015).
41. Norrby, S. R., Nord, C. E., Finch, R.European Society of Clinical Microbiology and Infectious Diseases. Lack of development of new antimicrobial drugs: a potential serious threat to public health. *Lancet Infect Dis* **5,** 115–119 (2005).
42. Becker, D. *et al.* Robust Salmonella metabolism limits possibilities for new antimicrobials. **440,** 303–307 (2006).
43. Barry, C. E. & Blanchard, J. S. The chemical biology of new drugs in the development for tuberculosis. *Curr Opin Chem Biol* **14,** 456–466 (2010).
44. O'Neill, J. *Tackling drug-resistant infections globally: final report and recommendations*. (London: Wellcome Trust & HM Government, 2016).
45. Christophe, T. *et al.* High content screening identifies decaprenyl-phosphoribose 2' epimerase as a target for intracellular antimycobacterial inhibitors. *PLoS Pathog* **5,** e1000645 (2009).
46. Makarov, V. *et al.* Benzothiazinones kill Mycobacterium tuberculosis by blocking arabinan synthesis. *Science* **324,** 801–804 (2009).
47. Willand, N. *et al.* Synthetic EthR inhibitors boost antituberculous activity of ethionamide. *Nat. Med.* **15,** 537–544 (2009).
48. Tiberi, S. *et al.* Tuberculosis: progress and advances in development of new drugs, treatment regimens, and host-directed therapies. *Lancet Infect Dis* **18,** e183–e198 (2018).
49. Gabriel, G., Herwig, A. & Klenk, H.-D. Interaction of polymerase subunit PB2 and NP with importin alpha1 is a determinant of host range of influenza A virus. *PLoS Pathog* **4,** e11 (2008).
50. Walzl, G. *et al.* Tuberculosis: advances and challenges in development of new diagnostics and biomarkers. *Lancet Infect Dis* **18,** e199–e210 (2018).
51. Bach, H., Papavinasasundaram, K. G., Wong, D., Hmama, Z. & Av-Gay, Y. Mycobacterium tuberculosis virulence is mediated by PtpA dephosphorylation of human vacuolar protein sorting 33B. *Cell Host and Microbe* **3,** 316–322 (2008).
52. Volkman, H. E. *et al.* Tuberculous granuloma induction via interaction of a bacterial secreted protein with host epithelium. *Science* **327,** 466–469 (2010).
53. Kuijl, C. *et al.* Intracellular bacterial growth is controlled by a kinase network around PKB/AKT1. **450,** 725–730 (2007).
54. Kumar, D. *et al.* Genome-wide analysis of the host intracellular network that regulates survival of Mycobacterium tuberculosis. *Cell* **140,** 731–743 (2010).
55. Jayaswal, S. *et al.* Identification of host-dependent survival factors for intracellular Mycobacterium tuberculosis through an siRNA screen. *PLoS Pathog* **6,** e1000839 (2010).
56. Sundaramurthy, V. *et al.* Integration of chemical and RNAi multiparametric profiles identifies triggers of intracellular mycobacterial killing. *Cell Host and Microbe* **13,** 129–142 (2013).

57. Machado, D. *et al.* Ion Channel Blockers as Antimicrobial Agents, Efflux Inhibitors, and Enhancers of Macrophage Killing Activity against Drug Resistant Mycobacterium tuberculosis. *PLoS ONE* **11,** e0149326 (2016).
58. Napier, R. J. *et al.* Imatinib-sensitive tyrosine kinases regulate mycobacterial pathogenesis and represent therapeutic targets against tuberculosis. *Cell Host and Microbe* **10,** 475–485 (2011).
59. Subbian, S. *et al.* Phosphodiesterase-4 inhibition alters gene expression and improves isoniazid-mediated clearance of Mycobacterium tuberculosis in rabbit lungs. *PLoS Pathog* **7,** e1002262 (2011).
60. Subbian, S. *et al.* Phosphodiesterase-4 inhibition combined with isoniazid treatment of rabbits with pulmonary tuberculosis reduces macrophage activation and lung pathology. *Am. J. Pathol.* **179,** 289–301 (2011).
61. Koo, M.-S. *et al.* Phosphodiesterase 4 inhibition reduces innate immunity and improves isoniazid clearance of Mycobacterium tuberculosis in the lungs of infected mice. *PLoS ONE* **6,** e17091 (2011).
62. Vilaplana, C. *et al.* Ibuprofen therapy resulted in significantly decreased tissue bacillary loads and increased survival in a new murine experimental model of active tuberculosis. *Journal of Infectious Diseases* **208,** 199–202 (2013).
63. Mayer-Barber, K. D. *et al.* Host-directed therapy of tuberculosis based on interleukin-1 and type I interferon crosstalk. **511,** 99–103 (2014).
64. Datta, M. *et al.* Anti-vascular endothelial growth factor treatment normalizes tuberculosis granuloma vasculature and improves small molecule delivery. *Proc Natl Acad Sci USA* **112,** 1827–1832 (2015).
65. Oehlers, S. H. *et al.* Interception of host angiogenic signalling limits mycobacterial growth. **517,** 612–615 (2015).
66. Schiebler, M. *et al.* Functional drug screening reveals anticonvulsants as enhancers of mTOR-independent autophagic killing of Mycobacterium tuberculosis through inositol depletion. *EMBO Molecular Medicine* **7,** 127–139 (2015).
67. Skerry, C. *et al.* Simvastatin increases the in vivo activity of the first-line tuberculosis regimen. *J. Antimicrob. Chemother.* **69,** 2453–2457 (2014).
68. Stanley, S. A. *et al.* Identification of host-targeted small molecules that restrict intracellular Mycobacterium tuberculosis growth. *PLoS Pathog* **10,** e1003946 (2014).
69. Li, Q. *et al.* Novel high throughput pooled shRNA screening identifies NQO1 as a potential drug target for host directed therapy for tuberculosis. *Sci Rep* **6,** 27566 (2016).
70. Poirier, V., Bach, H. & Av-Gay, Y. Mycobacterium tuberculosis promotes anti-apoptotic activity of the macrophage by PtpA protein-dependent dephosphorylation of host GSK3α. *Journal of Biological Chemistry* **289,** 29376–29385 (2014).
71. Sogi, K. M., Lien, K. A., Johnson, J. R., Krogan, N. J. & Stanley, S. A. The Tyrosine Kinase Inhibitor Gefitinib Restricts Mycobacterium tuberculosis Growth through Increased Lysosomal Biogenesis and Modulation of Cytokine Signaling. *ACS Infect Dis* **3,** 564–574 (2017).

72. Deretic, V., Saitoh, T. & Akira, S. Autophagy in infection, inflammation and immunity. *Nat Rev Drug Discov* **13,** 722–737 (2013).
73. Gutierrez, M. G. *et al.* Autophagy is a defense mechanism inhibiting BCG and Mycobacterium tuberculosis survival in infected macrophages. *Cell* **119,** 753–766 (2004).
74. Beaulieu, A. M. *et al.* Genome-wide screen for Mycobacterium tuberculosis genes that regulate host immunity. *PLoS ONE* **5,** e15120 (2010).
75. Tobin, D. M. *et al.* Host genotype-specific therapies can optimize the inflammatory response to mycobacterial infections. *Cell* **148,** 434–446 (2012).
76. Poerio, N. *et al.* Liposomes loaded with bioactive lipids enhance antibacterial innate immunity irrespective of drug resistance. *Sci Rep* **7,** 45120 (2017).
77. Mehrotra, P. *et al.* Pathogenicity of Mycobacterium tuberculosis is expressed by regulating metabolic thresholds of the host macrophage. *PLoS Pathog* **10,** e1004265 (2014).
78. Singhal, A. *et al.* Metformin as adjunct antituberculosis therapy. *Science Translational Medicine* **6,** 263ra159–263ra159 (2014).
79. Gamo, F.-J. *et al.* Thousands of chemical starting points for antimalarial lead identification. **465,** 305–310 (2010).
80. Guiguemde, W. A. *et al.* Chemical genetics of Plasmodium falciparum. **465,** 311–315 (2010).
81. Collinet, C. *et al.* Systems survey of endocytosis by multiparametric image analysis. **464,** 243–249 (2010).
82. Snijder, B. *et al.* Population context determines cell-to-cell variability in endocytosis and virus infection. **461,** 520–523 (2009).

2 | A Novel Medium-Throughput siRNA and Chemical Compound Screening Assay for Host Regulation of Intracellular Bacterial Infections

Cornelis J. Korbee, Elisabeth van Strijen, Kees L. M. C. Franken, Louis Wilson, Nigel D. L. Savage, Mariëlle C. Haks**, Tom H. M. Ottenhoff**

Bacterial drug-resistance poses severe global health problems. Recent efforts to identify novel antibiotics yielded only a limited number of leads, prompting for novel approaches, including host-directed therapies. Intracellular pathogens like *Salmonellae* (*Stm*) and *Mycobacterium tuberculosis* (*Mtb*) manipulate host signaling networks to promote their survival but knowledge of the precise molecular interactions at the pathogen-host interface is limited. Chemical and genetic perturbation of host cell signaling and inflammation has been shown to inhibit growth of intracellular pathogens, but relatively few host targets or chemical compounds have been identified so far. To accelerate target identification, we have developed and validated a medium-throughput flow cytometry-based screening assay, employing highly manipulable, *Stm*- as well as *Mtb*-infectable human cell-lines, combined with (novel) (myco)bacterial fluorescent protein constructs. The assay is fast, highly reproducible, concurs with classical bacterial growth inhibition assays, provides an excellent screening window, is applicable to both siRNA and chemical compound screens and validates well in human primary macrophages.

Adapted from:
Korbee, C.J.*, Heemskerk, M.T.*, Kocev, D., van Strijen, E., Rabiee, O., Franken, K.L.M.C., Wilson, L., Savage, N.D.L., Džeroski, S., Haks, M.C.**, Ottenhoff, T.H.M.**, 2018. **Combined chemical genetics and data-driven bioinformatics approach identifies receptor tyrosine kinase inhibitors as host-directed antimicrobials.** *Nat Commun* **9**, 358. doi:10.1038/s41467-017-02777-6**.**

* Contributed equally
** Contributed equally

Introduction

Bacterial antibiotic resistance is a widespread and increasing problem in modern medicine. Although a number of novel candidate antibiotics have recently been identified[1], current antibiotics already cover the majority of druggable targets of pathogens, resulting in a continuous decline in the number of newly discovered and approved antibiotics[2-7]. Intracellular bacteria present additional challenges as they are often able to manipulate host cell signaling to induce a survival niche and thereby subvert both innate and adaptive immunity. Knowledge of the mechanisms involved, however, also creates new opportunities for treatment, for instance by pharmacological perturbation of host cell signaling or inflammation to induce killing of intracellular bacteria and to promote effective host defense[8]. Here, we focused on the major human pathogens *Salmonella enterica* and *Mycobacterium tuberculosis* (*Mtb*). *Salmonella enterica* serovar Typhimurium *(Stm*) is a common causative agent of gastroenteritis in humans and causes a systemic disease resembling human typhoid fever in a murine host[9]. Following ingestion by the host, the bacterium induces its uptake by otherwise non-phagocytic intestinal epithelial cells. This is mediated by Salmonella Pathogenicity Island 1 (SPI1) encoded effectors, which translocate to the host cytoplasm through a Type III Secretion System (T3SS). The effectors then induce actin cytoskeleton remodeling and the subsequent formation of the Salmonella-Containing Vesicle (SCV)[10]. The SCV interacts with both early and late endosomes, is relatively acidic and acquires lysosomal markers like LAMP-1[11,12]. *Mtb* is a facultative intracellular pathogen, which upon entry in the lung is phagocytosed by alveolar Mϕs[13]. By modulating the host cell microbicidal machinery *Mtb* establishes an intracellular niche in which it can survive and replicate[14]. The subsequent induction of granuloma formation enables *Mtb* to persist within the human host for decades[15]. With an estimated one fourth of the world population carrying a latent *Mtb* infection and a resulting 1.8 million annual deaths, TB remains a critical global health problem[16-20].

Several recent studies, including our own, have demonstrated the feasibility of host-directed approaches to combat bacterial drug-resistance both *in vitro*[21-25] and *in vivo*[26-36]. Using reciprocal chemical genetics focusing on systematic perturbation of the host cell kinome we identified AKT1 as a central regulator of *Stm* intracellular survival in human cells. Treatment of infected cells with H-89, a chemical inhibitor of AKT1, decreased the *Stm* bacterial load and this bacterial growth inhibition by H-89 was reproduced in *Mtb* infected human macrophages (Mϕs)[21]. However, HDT approaches have not yet led to clinically applicable drugs and additional chemical compounds for HDT and more detailed fundamental understanding of molecular host-pathogen interactions are needed for development of HDT strategies into feasible clinical applications.

There are several major challenges to be overcome to facilitate host-directed chemical-genetic studies targeting intracellular pathogens, particularly studies that aim at discovering key host pathways manipulated by *Mtb*. Firstly, it is extremely difficult to generate sufficient quantities of primary Macrophages (Mϕs), the natural target cells for *Mtb* infection, from human donors for medium-throughput screens, even by pheresis. Secondly, the often-used THP-1 monocytic

cell line requires PMA stimulation for differentiation, which massively affects cell signaling and vesicular trafficking[37,38], thus confounding cellular signaling studies. Thirdly, there is a lack of fast (compared to the classical 3-week *Mtb* Colony Forming Unit (CFU) assay), robust and widely applicable readouts for rapid screening. Finally, achieving stable genetic knockdown in human primary Mϕs is challenging, especially in large siRNA screens where knockdown efficiency of each individual gene cannot broadly be confirmed. To solve these problems, we have developed a rapid, medium-throughput, fluorescence-based screening assay to determine bacterial load by automated flow cytometry in the highly manipulable human HeLa and MelJuSo cell lines infected with (myco)bacteria expressing novel (myco)bacterial fluorescent protein constructs. Our identification of the MelJuSo cell line as a novel *Mtb* infection model has several important advantages: MelJuSo cells are suited to large scale screening assays as they are more homogenous than primary cells, do not require additional stimuli like PMA for maturation, can be efficiently manipulated using RNAi, and can be infected by mycobacteria[39]. We have shown in the past that human melanocytes can efficiently present mycobacterial antigens to HLA class II restricted CD4 T cells[40] and have successfully used MelJuSo to dissect molecular pathways of MHC class II presentation in human cells[41,42]. Our novel fluorescence-based bacterial growth assay is applicable for both siRNA and chemical compound screens, and is equally suitable for both *Stm* and *Mtb* despite the vast differences in their intracellular 'lifestyles' and replication rates (20 minutes and 18 hours, respectively)[8,9,13,14], demonstrating the versatility of this assay.

Results

A flow cytometry-based readout for intracellular bacterial load.

To uncover host pathways controlling intracellular bacterial survival, we developed a fast, robust and novel assay suitable for medium-throughput (96-well) compound and siRNA screening, employing flow cytometry as a readout for intracellular bacterial load using fluorescent strains of *Stm* and *Mtb.* We used the PKB/AKT1 kinase inhibitor H-89 as initial reference compound, since we had identified H89 as an effective HDT with antimicrobial activity against *Mtb* and *Stm* previously[21]. Optimization data for fluorescent reporters expressed in *Stm* and *Mtb* is described below. Importantly, our novel medium-throughput flow cytometry-based assay to screen compound and siRNA libraries allows accurate determination of *Mtb* bacterial load within 24h and 72h, respectively, which greatly shortens the time to readout compared to the classical 3-4 week CFU assay for *Mtb*. HeLa (cervical carcinoma) and MelJuSo (melanoma) human cell lines were selected as host models for *Stm* and *Mtb* infection, respectively. In contrast to non-phagocytic HeLa cells, melanocytes were previously reported to possess phagocytic capacity[39], a prerequisite for uptake of mycobacteria. Conversely, MelJuSo was not found to be a suitable target cell line for *Stm* infection as *Stm* did not propagate well in these cells, in line with the previously reported aberrant phenotype of *Stm* in MelJuSo[43]. As chemical compounds may exhibit auto-

fluorescence and therefore may cause false positive results when detecting increases in bacterial load, the assay for screening chemical compounds is ideally suited for detecting decreases in bacterial loads.

In HeLa cells infected with genetically-tagged DsRed-*Stm* both DsRed 'bright' and 'dim' infected cell populations were observed (**Figure 1A**). H-89 treatment markedly diminished the DsRed 'bright' population. Since H-89 treatment effectively reduced *Stm* bacterial numbers in HeLa cells as measured by CFU (**Figure 1E**) [21], this DsRed 'bright' population represents cells containing proliferating bacteria. The reduction in *Stm* bacterial load by H-89 treatment was corroborated by fluorescence microscopy (**Figure 1B**). Similarly, *Mtb* infection of MelJuSo cells could be visualized using flow cytometry (**Figure 1C**) and H-89 also decreased the bacterial load in this infection model (**Figure 1F**). Importantly, since alveolar Mϕs are the primary target cells for *Mtb in vivo*, we verified that infection of these cells can be similarly visualized using flow cytometry (**Figure 1D**) and that H-89 treatment decreased bacterial loads in primary human pro-inflammatory (Mϕ1) as well as anti-inflammatory (Mϕ2) cells similar to MelJuSo cells (**Figure 1G**). However, we observed considerable batch-to-batch variation in the proportion of infected Mϕs, further supporting the use of the homogenous MelJuSo cell line as an infection model for screening.

We next optimized both the reverse siRNA transfection strategy and bacterial infection conditions by varying cell density, multiplicity of infection (MOI), infection time point and the harvesting time point for analysis using the optimal fluorescent reporters in a medium-throughput setting (outlined below). Using the optimized conditions, knockdown of AKT1 resulted in a significant decrease of both *Stm* and *Mtb* survival in infected cells (**Figure 1H**), but again less so for *Mtb* than for *Stm*, mimicking the effect of treatment of infected cells with AKT1 inhibitor H-89 (**Figures 1E** and **F**).

In summary, we conclude that HeLa and MelJuSo cells represent new human model systems to study intracellular *Stm* and *Mtb* infection, respectively, providing novel models for medium-throughput screening of host-directed compounds and genetic manipulation to increase our understanding and treatment of intracellular bacterial infections. Importantly, our novel medium-throughput flow cytometry-based assay allows accurate determination of intracellular *Mtb* bacterial load in compound or siRNA treated cells within a significantly shorter time (2-3 days) window than classical CFU assays (3-4 weeks). The assay is suitable for *Stm, Mtb* and possibly other intracellular bacterial infection models, despite the vast differences in their intracellular 'lifestyles' and replication rates (20 minutes and 18 hours for *Stm* and *Mtb*, respectively)[8,9,13,14].

Optimization of fluorescent reporters for flow cytometry-based quantitation of bacterial infection.

To optimize our assay we explored different fluorescent reporters for expression in *Stm* or *Mtb*. Firstly, we monitored the long-term expression kinetics of GFP and DsRed transcribed from plasmids with an identical backbone in *Mtb* (**Table 1**). Despite hygromycin selection, the *Mtb* culture gradually lost GFP expression over

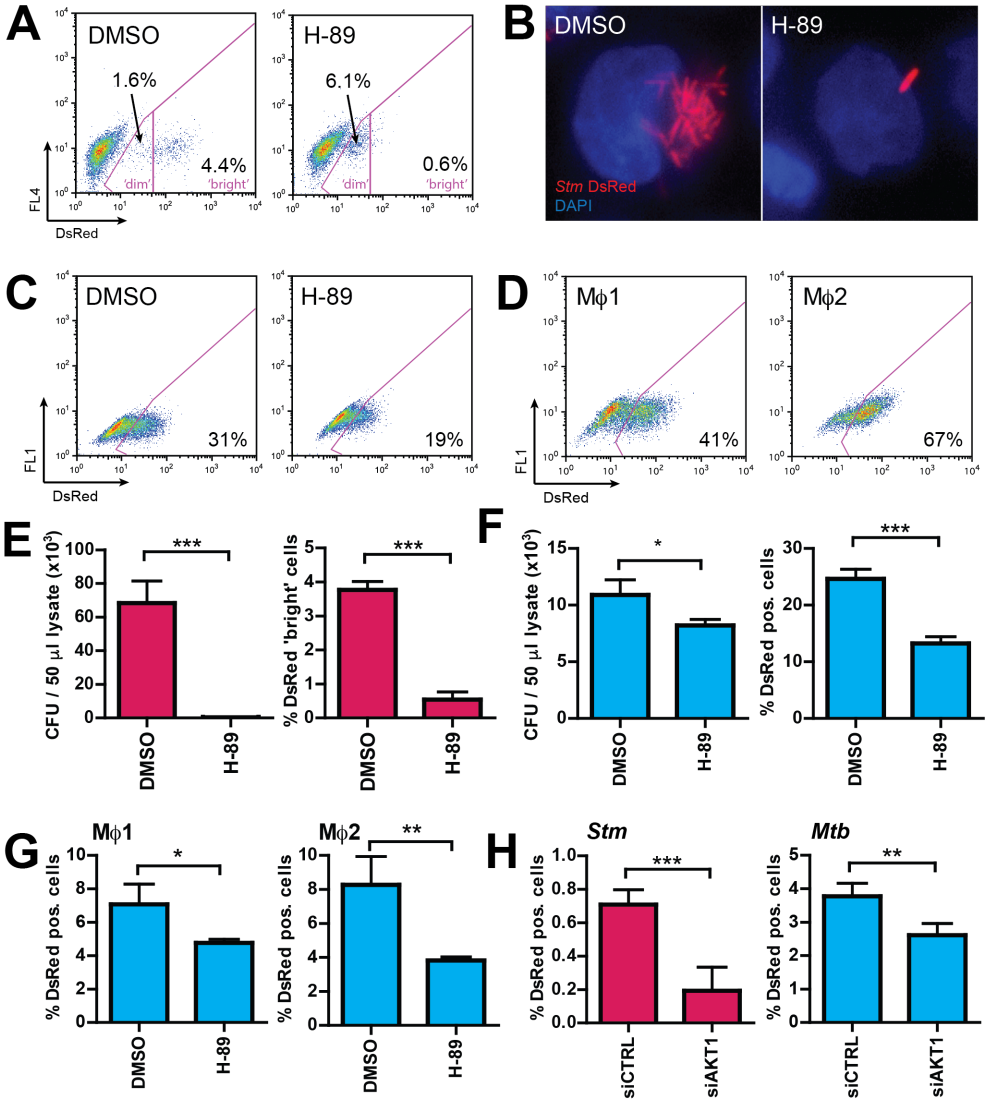

⬆ Figure 1. A flow cytometry-based readout for intracellular bacterial load.

A. Flow cytometry gating strategy. Shown are dot plots of HeLa cells infected with *Stm* constitutively expressing stable DsRed and treated with H-89 or DMSO at 10 µM as a negative control. Gates were drawn for separate analysis of total DsRed positive and DsRed 'bright' populations. Percentages of DsRed positive events in each gate are indicated. **B.** Fluorescence microscopy of HeLa cells infected and treated as in **A**. A representative infected cell is shown for both conditions. **C.** Flow cytometry gating strategy for MelJuSo cells infected with *Mtb* constitutively expressing stable DsRed and treated as in **A**. Percentages of DsRed positive events are indicated. **D.** Flow cytometry of human primary Mϕ1 (left panel) and Mϕ2 (right panel) macrophages infected with *Mtb* constitutively

expressing stable DsRed. Percentages of DsRed positive events are indicated. **E.** Comparison of CFU assay (left panel) to the flow cytometry-based screening assay (right panel) for HeLa cells infected and treated as in **A**. A representative result of 3 experiments is shown. Bars display mean ± standard deviation. Statistical significance was tested using a t-test. **F.** Comparison of CFU assays (left panel) to the flow cytometry-based screening assay (right panel) is shown for MelJuSo cells infected and treated as in **C**. A representative result of 3 experiments is shown. Bars display mean ± standard deviation. Statistical significance was tested using a t-test. **G.** Flow cytometry of Mϕ1 and Mϕ2 cells infected and treated as in **C**. Bars display mean ± standard deviation. Statistical significance was tested using a t-test. **H.** Infection of AKT1-silenced HeLa or MelJuSo cells with *Stm* expressing low pH-inducible, stable DsRed (left panel) and *Mtb* constitutively expressing destabilized DsRed (right panel), respectively, analyzed by flow cytometry. Bars display mean ± standard deviation. Statistical significance was tested using a t-test. Shown are results of 6 replicate samples from 1 representative screening plate out of more than 20 replicate plates.
(* = p-value <0.05, ** = p-value <0.01, *** = p-value <0.001).

time, whereas DsRed expression remained unaltered (**Figure 2A**). As loss of fluorescence would be detrimental to a flow-cytometry-based assay, GFP was excluded as a suitable fluorescent reporter in *Mtb*.

As demonstrated in **Figure 1**, constitutively expressed, stable DsRed constructs provided an excellent assay window to reliably evaluate the effect of chemical compound treatment on bacterial loads of both *Stm*- and *Mtb*-infected cells. Compared to compound treatment experiments, quantification of bacterial infection in siRNA transfected cells often resulted in more subtle phenotypes requiring further assay optimization: while the constitutive expression and high stability of fluorescent reporters can negatively impact the sensitivity of fluorescence-based bacterial growth inhibition assays, this can be overcome by employing conditionally expressed or destabilized fluorescent reporters (decreasing the half-life of DsRed from 4.6 days to several hours) [44,45]. To this end, different fluorescent reporter construct variants (**Table 1**) were expressed in *Stm* (constitutively-expressed stable DsRed, low pH-inducible expressed stable DsRed, or low pH-inducible expressed destabilized DsRed) or in *Mtb* (constitutively-expressed stable DsRed or constitutively-expressed destabilized DsRed) and these bacteria were subsequently used in our HeLa-*Stm* and MelJuSo-*Mtb* infection models following AKT1 silencing. As demonstrated in **Figure 2B**, a low pH-inducible expressed stable DsRed variant increased the assay window in *Stm*-infected HeLa cells following AKT1 silencing (Z' = 0.70) compared to constitutively-expressed stable DsRed (Z' = 0.58) and low pH-inducible expressed destabilized DsRed (Z' = 0.45). The effect of AKT1 silencing in *Mtb*-infected MelJuSo cells could only be visualized using an *Mtb* strain expressing a destabilized DsRed variant (**Figure 1H**), demonstrating that employing this novel fluorescent reporter overcomes a major limitation of fluorescent signal-based growth inhibition assays for slowly replicating bacteria.

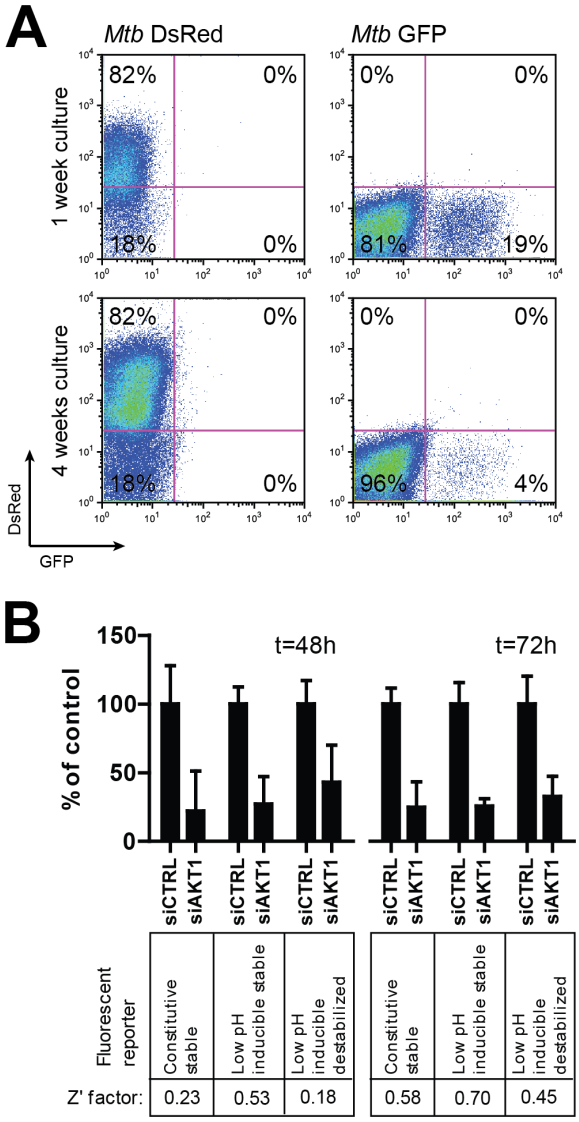

⬅ Figure 2. Optimization of the flow cytometry-based assay to monitor bacterial load using different fluorescent reporters.
A. Flow cytometric analysis of DsRed (left panel) and GFP (right panel) expression in *Mtb* cultured for either 1 week (top panel) or 4 weeks (bottom panel) after thawing of a frozen batch. **B.** Infection of HeLa cells using *Stm* strains expressing different fluorescent reporters (constitutive stable, low pH-inducible stable and low pH-inducible destabilized DsRed) at 48 hours (left panel) or 72 hours (right panel) post transfection with the indicated siRNA oligos. siCTRL: scrambled siRNA. The upper panel gives the level of inhibition of intracellular *Stm* in siAKT1 silenced cells expressed as a percentage of the control (siCTRL treated) condition ± standard deviation. The signal window resulting from infection with the indicated fluorescent *Stm* strains is expressed as a Z' factor.

HeLa-*Stm* and MelJuSo-*Mtb* infection models combined with a flow cytometry-based readout for intracellular bacterial load allow medium-throughput screening of siRNA libraries.

We next further optimized both the reverse siRNA transfection strategy and bacterial infection conditions by varying cell density, multiplicity of infection (MOI), infection time point and the harvesting time point for analysis using the optimal fluorescent reporters in a medium-throughput setting (96-well format). As shown in **Figure 3A**, knockdown of AKT1 was highly efficient in both HeLa and MelJuSo cells, routinely resulting in 87-97% knockdown at 72 hours post transfection. To determine an optimal infection window, knockdown kinetics were assessed until

96 hours post transfection. The largest decrease in AKT1 protein levels was observed between 48 and 72 hours post transfection, concurring with the reported 6 to 36 hour half-life of AKT1[46,47] (**Figure 3B**). AKT1 knockdown followed identical kinetics in both HeLa and MelJuSo cells. As cell over-confluence was observed at 96 hours post transfection the assay was not extended beyond this time point. By varying both the time point of infection (24-72 hours post transfection) and the time between infection and readout (24-72 hours) within a 96 hour timeframe, we determined that the optimal assay window for *Stm* infections

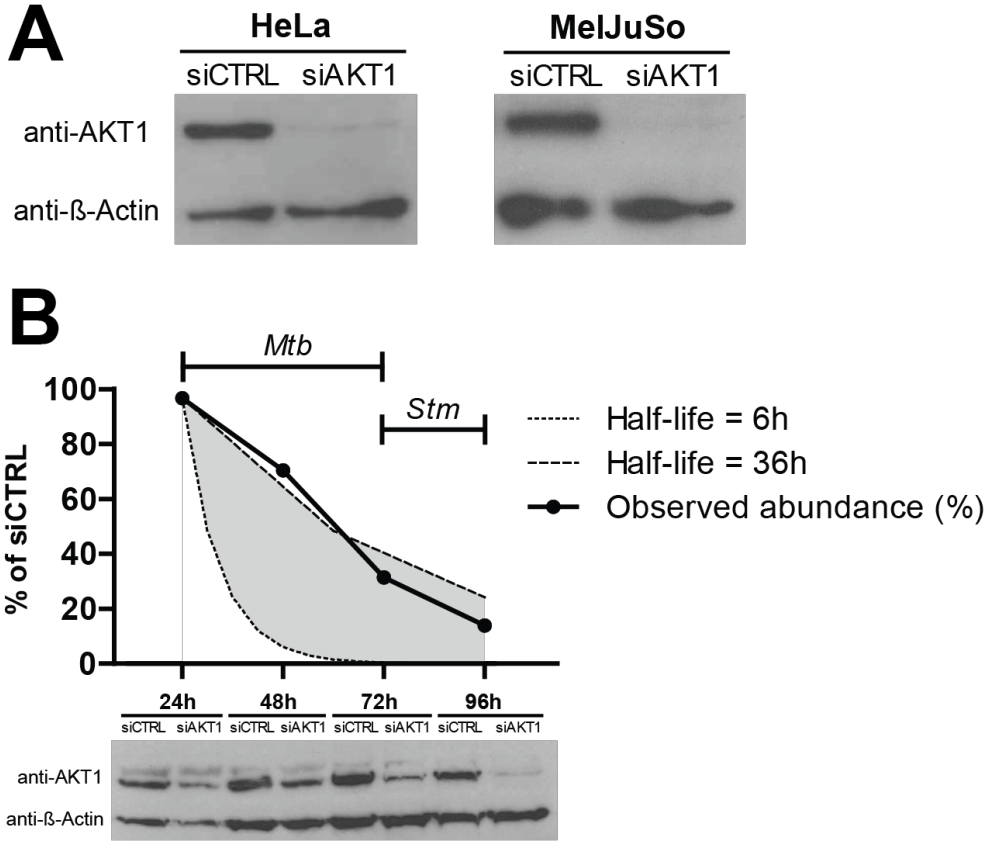

⬆ Figure 3. Knockdown of AKT1 in HeLa and MelJuSo cells.

A. Western blot showing AKT1 knockdown (siAKT1) compared to scrambled siRNA (siCTRL) in HeLa (left panel) and MelJuSo (right panel) whole cell lysates at 72 hours post transfection. β-Actin was included as loading control. **B.** Time course of AKT1 silencing by western blot analysis, normalized for β-Actin. AKT1 protein abundance is shown relative to cells transfected with scrambled siRNA between 24 to 96 hours post transfection (black line). The dotted and dashed lines represent theoretical 6 to 36-hour half-lives reported for AKT1, respectively. The horizontal bars depict the infection time windows for both *Stm* and *Mtb* used in the final screening assay.

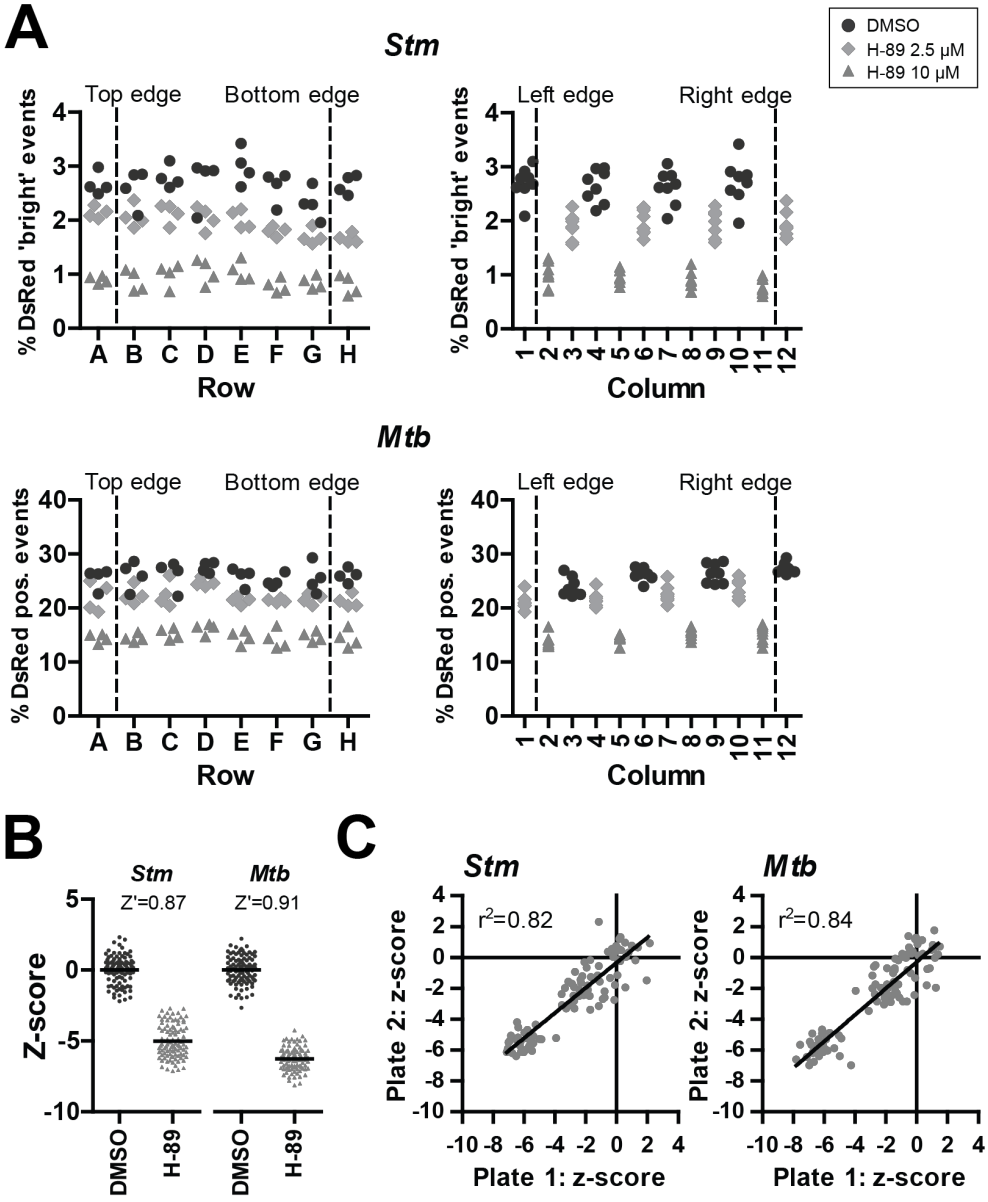

← Figure 4. Screening assay window, reproducibility, uniformity and validation.

A. Plate uniformity test using HeLa cells infected with *Stm* constitutively expressing stable DsRed (top panel) or MelJuSo cells infected with *Mtb* constitutively expressing stable DsRed (bottom panel) and treated with 2.5 µM H-89, 10 µM H-89 or DMSO at equal v/v. The percentage of gated 'bright' (top panel) or total (bottom panel) DsRed positive events from individual wells were grouped either by row (left panel) or by column (right panel). The dashed lines

indicate the wells on the edges of the plates to identify edge effects. **B.** Assay windows for both the HeLa-*Stm* and the MelJuSo-*Mtb* infection models (as in **A**) following assay optimization. Z' factors are displayed for each infection model. Shown are 96 individual replicates of infected cells treated with 10 μM H-89 or DMSO. Percentages of DsRed 'bright' cells (HeLa-*Stm*) and DsRed positive cells (MelJuSo-*Mtb*) are expressed as a z-score. **C.** Comparison of individual plates from plate uniformity tests for HeLa-*Stm* (left panel) and MelJuSo-*Mtb* (right panel) infection models (as in **A**). Z-scores were plotted for individual wells and a correlation coefficient was calculated by linear regression.

was obtained when HeLa cells were infected 72 hours post transfection followed by a 24 hour incubation until readout by flow cytometry, while *Mtb* infections resulted in the largest possible assay window when MelJuSo cells were infected 24 hours post transfection followed by a 48 hour incubation until readout by flow cytometry (**Figure 3B**).

Screening assay window, reproducibility, uniformity and validation.

To further confirm assay uniformity and reproducibility, plate uniformity assays were performed and the assay conditions were optimized according to any drift or edge effects that were observed. Results from representative 96-well plates using the optimized screening conditions for *Stm* and *Mtb* are displayed in **Figure 4A**, indicating that the assay generates highly uniform results within the assay plates. The assay yielded an assay window (expressed as a Z' factor) of 0.87 for infections with *Stm* and 0.91 for *Mtb*, greatly exceeding the minimal acceptable Z' factor of 0.4 (**Figure 4B**). In addition, inter-plate reproducibility was high for both infection models (r^2 = 0.82 for *Stm* infections and r^2 = 0.84 for *Mtb* infections) (**Figure 4C**).

Validation of the MelJuSo-*Mtb* model and the novel screening assay

To validate the MelJuSo model system, we tested already published host-directed compounds with known activity against *Mtb* here in this model; indeed, as expected these known compounds also reduced *Mtb* loads in MelJuSo cells and in human Mϕs upon short (overnight) treatment (at standard 10 μM concentrations). As shown in **Figure 5**, Imatinib, D4476, and LY-364947 all decreased the *Mtb* bacterial load in our model, well in agreement with previous studies[23,26]. In addition, we also confirmed that a dual inhibitor of TGFbetaR1 and Casein Kinase 1 (D4476) inhibited *Mtb* more potently than the individual inhibitors of TGFbetaR1 (LY-364947) and Casein Kinase 1 (IC261) alone, confirming data from Jayaswal *et al*.[23] (**Figure 5**). Finally, during the work described in this thesis also Haloperidol[24] was confirmed to inhibit both *Stm* and *Mtb* in our model and these results will be discussed in more detail in **Chapter 3**. Thus, the results obtained in our novel MelJuSo-*Mtb* infection model and flow cytometry-based readout of intracellular infection faithfully reproduce the reported inhibitory effects of previously published compounds, providing important biological plausibility for

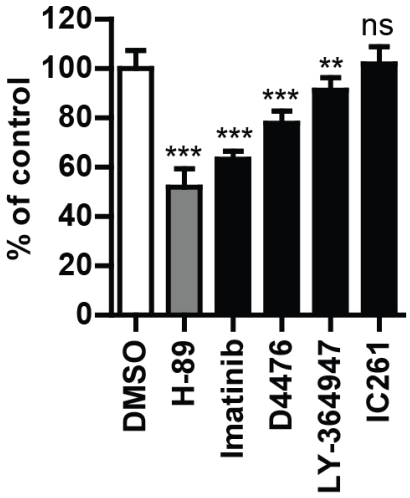

← Figure 5. Verification of host-directed *Mtb* inhibitors from literature in the novel screening assay.
Overnight treatment of MelJuSo cells infected with *Mtb* constitutively expressing stable DsRed with compounds that were previously reported to be active against *Mtb* at 10 μM or with DMSO at equal v/v. H-89 is used as a positive control at 10 μM[21]. The *Mtb* bacterial load is displayed as a percentage of the DMSO control +/- standard deviation to indicate the extent of bacterial inhibition. Statistically significant difference compared to DMSO was tested using a one-way ANOVA. (ns = not significant, ** = p-value < 0.01, *** = p-value < 0.001).

the system. Of note, none of the published compounds evaluated above was more potent in inhibiting intracellular *Mtb* than our reference compound H-89. We therefore used our assay to screen chemical libraries to identify host-directed inhibitors with more potent activity than H-89 in **Chapters 3** and **4**.

Discussion

Here, we report the development and validation of a novel fluorescence-based screening assay that is able to rapidly quantify intracellular bacterial infection in human cells, as described here we think is important since it helps shortening the readout from a classical 3-week CFU assay for *Mtb* to 24-72h using flow cytometry. The assay is highly reproducible, medium-throughput, provides an excellent assay window, and is suitable for screening both chemical compound and siRNA libraries. Taking advantage of the previously reported phagocytic capability of melanocytes[39], we also report the human melanoma cell line MelJuSo as a novel model for *Mtb* infection studies, particularly for studies encompassing chemical and RNAi screens. This model has considerable potential to facilitate advanced research into host-directed therapies in TB for several reasons. Firstly, due to their clonal origin cell lines are substantially more homogeneous than primary cells from different donors. This greatly enhances reproducibility and enables substantial upscaling of the assay. Secondly, MelJuSo cells do not require any additional stimulation in contrast to the often-used THP-1 infection model, avoiding skewing of cell signaling prior to experimental stimuli. Thirdly, MelJuSo cells are highly manipulable by siRNA and their transfectability enables studying intracellular *Mtb* in cell lines overexpressing a gene of interest or expressing fluorescently tagged proteins. Each of these properties render MelJuSo cells ideally suitable for the high-content screening stages of host-directed chemical

genetics research, which can then be followed by validation of a limited selection of hits in human primary Mϕs. Importantly, our assay faithfully reproduces the inhibitory effect of several previously published host-directed compounds (that were identified using different strategies, approaches and models) on *Mtb* intracellular survival as well as HDT results obtained in human primary Mϕs, further validating our novel infection model.

High stability of reporter proteins can pose major problems in fluorescent assays for bacteria viability, especially in case of slowly proliferating bacteria like *Mtb*. In our experiments chemical compound treatment induced a robust phenotype resulting in strong changes in the fluorescent signal when using stable fluorescent proteins such as DsRed. In contrast, siRNA induced more subtle phenotypes, likely due to relatively specific gene targeting, protein stability and potential target redundancy. In this case decreased bacterial viability resulting from host gene knockdown may be masked by residual stable fluorescence. Importantly, we here showed that conditional or destabilized DsRed constructs for (myco)bacterial expression can aid in overcoming this problem, by sufficiently increasing the assay sensitivity for host-directed siRNA screens. In our experiments, both the reference compound H-89 and AKT1 silencing were unable to induce complete host-mediated *Mtb* inhibition. Considering that none of the compounds displayed in **Figure 5** surpassed the *Mtb* inhibitory potency of H-89, more and substantially better chemical compounds and drugable targets must be identified to firmly establish host-directed therapy as a feasible option for complementary treatment of TB. To this end, we employed the screening assay reported here for chemical compound screens of up to 1,200 compounds and siRNA screens of up to 1,000 siRNA pools (results in **Chapters 3** and **4**), yielding highly reproducible results with a good signal window and identifying chemical compounds and siRNA pools that perform considerably better than H-89 and AKT1 silencing, respectively. Importantly, top hit compounds from these screens were subsequently successfully validated in human primary Mϕs.

The advent of high-throughput screens for host-directed intervention in intracellular bacterial infections gave rise to several different screening efforts employing methods ranging from traditional CFU assays[22,23] to bioluminescent assays[48,49] and automated microscopy[24,50] all with their individual merits and pitfalls. Despite being the golden standard in TB research, CFU assays are not ideally suitable for high-throughput screens due to their laborious nature and the slow proliferation of *Mtb*. Additionally, individual *Mtb* colonies are often hard to distinguish due to their irregular morphology and variable size, adding to the inaccuracy of the assay. As an alternative to CFU assays, efforts have been made to optimize bioluminescent constructs for expression in mycobacteria[48] and to develop bioluminescent screening assays[49]. Though reliable and rapid, bioluminescent assays are severely limited when compared to flow cytometry or microscopy based readouts, due to their single-parameter measurement at the well level rather than at the (sub)cellular or population levels. In contrast, phenotypic screens using automated microscopy can be tremendously informative but automated microscopy platforms require a major investment and analysis is often dependent on proprietary image analysis software. The computational infrastructure for the complex analyses and storage of the

excessive quantities of data generated using this method in a high-content setting are not currently in place in many laboratories. Our novel flow cytometry-based screening assay bridges the gap between the methods outlined above, combining the simplicity, ease of use and straightforward analysis of bioluminescent assays with the multiparametric readout, versatility and high quantifiability of fluorescence microscopy.

Experimental procedures

Reagents

H-89 dihydrochloride, D4476, IC261, LY-364947, Rifampicin and Kanamycin were purchased from Sigma-Aldrich, Zwijndrecht, The Netherlands. Hygromycin B was acquired from Life Technologies-Invitrogen, Bleiswijk, The Netherlands. Imatinib mesylate was from Enzo Life Sciences, Raamsdonksveer, The Netherlands. Ampicillin was purchased from Calbiochem Merck-Millipore, Darmstadt, Germany.

Cell culture

HeLa cells and the MelJuSo human melanoma cell line were maintained at 37°C and 5% CO_2 in Gibco Iscove's Modified Dulbecco's Medium (IMDM; Life Technologies-Invitrogen) with 10% fetal bovine serum (FBS, Greiner Bio-One, Alphen a/d Rijn, The Netherlands), 100 units/ml Penicillin and 100 µg/ml Streptomycin (Life Technologies-Invitrogen). Pro-inflammatory Mϕ1s and anti-inflammatory Mϕ2s were generated from monocytes isolated from whole blood of healthy donors by FICOLL separation and CD14 MACS sorting (Miltenyi Biotec, Teterow, Germany) followed by 6 days differentiation with 5 ng/ml granulocyte macrophage-colony stimulating factor (GM-CSF; BioSource Life Technologies-Invitrogen) or 50 ng/ml macrophage-colony stimulating factor (M-CSF; R&D Systems, Abingdon, United Kingdom) respectively, as previously reported[51]. Mϕs were cultured in Gibco Roswell Park Memorial Institute (RPMI) 1640 medium (Life Technologies-Invitrogen) with 10% FBS and 2 mM L-Alanyl-L-Glutamine (PAA, Linz, Austria).

Bacterial culture

Bacterial strains used are displayed in **Table 1**. Mycobacteria were cultured in Difco Middlebrook 7H9 broth (Becton Dickinson, Breda, The Netherlands) supplemented with 10% ADC (Becton Dickinson), 0.5% Tween-80 (Sigma-Aldrich) and appropriate antibiotics. *Stm* was cultured on Difco Luria-Bertani (LB) agar (Becton Dickinson) or in Difco LB broth (Becton Dickinson) supplemented with appropriate antibiotics.

Stm and *Mtb* infections

One day before infection, mycobacterial cultures were diluted to a density corresponding with early log phase growth (optical density at 600 nm (OD_{600}) of 0.4). *Stm* was grown either in LB broth or on LB agar with appropriate antibiotics. After overnight incubation *Stm* liquid cultures were diluted 1:33 and cultured for an

Table 1. Bacterial strains, plasmids used for fluorescent protein expression and their respective antibiotic selection markers.

Base strain	Plasmid	Antibiotic resistance (source, concentration)
Stm SL1344.	pMW211[C.10E/DsRed] (Constitutive promoter).	Ampicillin (plasmid, 100 µg/ml).
Stm SL1344.	pMW215[PpagC/DsRed] (Low-pH inducible promoter).	Ampicillin (plasmid, 100 µg/ml).
Stm SL1344.	pMW266[PpagC/destabilized DsRed] (Low-pH inducible promoter).	Ampicillin (plasmid, 100 µg/ml).
Mtb H37Rv.	pSMT3[Phsp60/DsRed].	Hygromycin (plasmid, 50 µg/ml).
Mtb H37Rv.	pSMT3[Phsp60/GFP].	Hygromycin (plasmid, 50 µg/ml).
Mtb H37Rv.	pSMT3[Phsp60/destabilized DsRed].	Hygromycin (plasmid, 50 µg/ml).

additional 3-4 hours while plate grown *Stm* was suspended in PBS by rinsing the agar plates. Bacterial density was determined by measuring the OD_{600} and the bacterial suspension was diluted in cell culture medium without antibiotics to reach a multiplicity of infection (MOI) of 10 (unless indicated otherwise). Accuracy of bacterial density measurements was verified by a standard colony forming unit (CFU) assay. Cell cultures (HeLa for *Stm* infections and MelJuSo for *Mtb* infections), seeded in 96-well flat-bottom plates as described below, were inoculated with 100 µl of the bacterial suspension, centrifuged for 3 minutes at 800 rpm and incubated at 37°C/5% CO_2 for 20 minutes if infected with *Stm* or 60 minutes if infected with *Mtb*. Plates were then washed with culture medium containing 30 µg/ml gentamicin sulfate (Lonza BioWhittaker, Basel, Switzerland) and incubated at 37°C and 5% CO_2 in medium containing 5 µg/ml gentamicin and indicated chemical compounds until readout by flow cytometry or CFU, as indicated.

Chemical compound treatment

10,000 HeLa or MelJuSo cells were seeded per well in 96-well flat-bottom plates or 300,000 primary Mϕs were seeded per well in 24-well plates in appropriate culture medium without antibiotics one day prior to infection with *Mtb* or broth-grown *Stm*. Infected cells were treated overnight with chemical compounds at 10 µM (unless indicated otherwise) or DMSO at equal v/v in medium containing 5 µg/ml gentamicin.

siRNA transfections

3,000 HeLa or MelJuSo cells were reverse-transfected with ON-TARGETplus siRNA pools (Thermo Fisher Dharmacon, Waltham Massachusetts, USA) at a 50 nM concentration using 0.2 µl Dharmafect1 (Thermo Fisher Dharmacon) per well in

a flat-bottom 96-well plate in appropriate culture medium without antibiotics. Knockdown efficiency was verified by immunoblotting at indicated time points. Cells transfected with siRNA were infected with *Mtb* at MOI 1000 24 hours post transfection and incubated for an additional 48 hours and infections with agar-grown *Stm* were carried out at MOI 500 72 hours post transfection and incubated overnight, unless indicated otherwise.

Colony forming unit assay

CFU assays were performed using the track dilution method described previously[52]. In short, bacterial suspensions were serially diluted and 10 µl drops were plated on square agar plates, which were subsequently placed at an angle to allow the drops to spread over a larger surface area.

Generation of a mycobacterial destabilized DsRed construct and expression in *Mtb* H37Rv

The destabilized DsRed gene (DsRed C-terminally fused to amino acids 422-461 of the mouse ornithine decarboxylase (MODC) to induce ubiquitin-independent proteasomal degradation[30]) was amplified from the pMW266[PpagC/destabilized DsRed] plasmid by PCR and cloned into the Gateway (Invitrogen) adapted mycobacterial expression plasmid pSMT3[31]. In this vector, expression of destabilized DsRed is constitutive and controlled by the hsp60 promoter. Electrocompetent *Mtb* H37Rv were freshly prepared from a 100 ml log-phase culture by incubation at 4°C for 90 minutes followed by suspension of the bacteria in 1 ml ice cold PBS containing 10% glycerol. 100 µl Bacterial suspension was then transformed with 1 µg plasmid DNA by electroporation. Transformed bacteria were suspended in 10 ml 7H9 broth, incubated overnight at 37°C and subsequently plated on Difco Middlebrook 7H10 agar (Becton Dickinson, Breda, The Netherlands) under Hygromycin (50 µg/ml) selection (Life Technologies-Invitrogen, Bleiswijk, The Netherlands). DsRed expression of individual clones was verified by flow cytometry.

Fluorescence microscopy

100,000 HeLa or MelJuSo cells were grown on glass coverslips (Menzel-Gläser, Braunschweig, Germany) in 24-well plates and infected as described above. Samples were fixed for 30 minutes at RT with 4% paraformaldehyde, embedded in VectaShield with DAPI (Brunschwig Chemie, Amsterdam, The Netherlands) and examined on an Axioskop 2 fluorescence microscope (Carl Zeiss, Sliedrecht, The Netherlands).

Screening assay validation and screening statistics

The flow cytometry-based screening assay for *Stm* and *Mtb* infection of human cell lines was developed adhering to guidelines published by the NIH Chemical Genomics Center[53]. Cells were transfected and infected with *Stm* or *Mtb* in flat-bottom 96-wells plates as described above. Cells were harvested by trypsinization and fixed with 1% paraformaldehyde prior to readout using a FACSCalibur (Becton Dickinson) with high-throughput sampler (HTS) extension (Becton

Dickinson). Data was analyzed using FlowJo for Mac OS X version 8.8.7 (TreeStar, Ashland, OR, USA) and both the total and bright DsRed positive populations expressed as a frequency of the parent forward/side-scatter gate and the total event counts were extracted for further analysis. Z' factors (to determine the assay window) were calculated using the formula $Z' = \frac{\left(AVG_{DMSO} - \frac{3SD_{DMSO}}{\sqrt{n}}\right) - \left(AVG_{H\text{-}89} + \frac{3SD_{H\text{-}89}}{\sqrt{n}}\right)}{AVG_{DMSO} - AVG_{H\text{-}89}}$, where AVG is the average percentage of DsRed positive events measured after DMSO or H-89 treatment, SD is the standard deviation of these measurements and n is the number of replicates. Z-scores were calculated using the formula $z = \frac{x - AVG_{DMSO}}{STDEV_{DMSO}}$ where the difference between the percentage of DsRed positive events (bacterial load) or the total event count (cell viability) of a single replicate of an experimental condition (x) and the average percentage of DsRed positive events or the total event count of the DMSO control (AVG_{DMSO}) is divided by the standard deviation of the DMSO control ($STDEV_{DMSO}$). An average z-score ≤ -2 or ≥ 2 was used as a hit cut-off, unless otherwise indicated.

Immunoblotting

Cells were lysed by heating in loading buffer (250 mM Tris, 8% w/v SDS, 20% glycerol, 20% β-mercaptoethanol and 0.002% w/v bromophenolblue) for 5 minutes at 99°C. Proteins from lysates of 50,000 cells were mass-separated by SDS-PAGE gel electrophoresis and subsequently blotted on a PVDF membrane. Following fixation in pure methanol for 15 seconds at RT, membranes were blocked for 1 hour at RT with 5% w/v milk. Blots were then incubated overnight at 4°C with mouse anti-human AKT1 IgG1 (1:5,000; Cell Signaling Technology, Leiden, The Netherlands) diluted in 5% w/v milk. After incubation, membranes were washed for 1 hour at RT with PBS containing 0.1% Tween-20, refreshing the wash buffer every 10 minutes. Blots were incubated with HRP-labelled goat anti-mouse IgG (1:12,500; Thermo Scientific, Bleiswijk, The Netherlands) and HRP-labelled goat anti-human actin (1:80,000; Santa Cruz, Heidelberg, Germany) diluted in 5% w/v milk for 1 hour at RT and washed as above. Protein bands were visualized on a photosensitive film by Enhanced ChemiLuminescence (ECL Plus, Amersham-GE Healthcare, Freiburg, Germany). Relative protein abundance was quantified by calculating the area under the curve (AUC) for each band using ImageJ (version 1.43n) and each lane was normalized against the AUC of the actin band.

Statistics

Student's T-test, one-way ANOVA and linear regression were performed using GraphPad Prism version 6.0 for Mac OS X (GraphPad Software, San Diego California, USA; www.graphpad.com).

References

1. Barry, C. E. & Blanchard, J. S. The chemical biology of new drugs in the development for tuberculosis. *Curr Opin Chem Biol* **14,** 456–466 (2010).

2. Norrby, S. R., Nord, C. E., Finch, R.European Society of Clinical Microbiology and Infectious Diseases. Lack of development of new antimicrobial drugs: a potential serious threat to public health. *Lancet Infect Dis* **5,** 115–119 (2005).
3. Becker, D. *et al.* Robust Salmonella metabolism limits possibilities for new antimicrobials. **440,** 303–307 (2006).
4. Makarov, V. *et al.* Benzothiazinones kill Mycobacterium tuberculosis by blocking arabinan synthesis. *Science* **324,** 801–804 (2009).
5. Christophe, T. *et al.* High content screening identifies decaprenyl-phosphoribose 2' epimerase as a target for intracellular antimycobacterial inhibitors. *PLoS Pathog* **5,** e1000645 (2009).
6. Willand, N. *et al.* Synthetic EthR inhibitors boost antituberculous activity of ethionamide. *Nat. Med.* **15,** 537–544 (2009).
7. Lawn, S. D. & Zumla, A. I. Tuberculosis. *Lancet* **378,** 57–72 (2011).
8. Ottenhoff, T. H. M. New pathways of protective and pathological host defense to mycobacteria. *Trends Microbiol.* **20,** 419–428 (2012).
9. Santos, R. L. *et al.* Animal models of Salmonella infections: enteritis versus typhoid fever. *Microbes Infect.* **3,** 1335–1344 (2001).
10. Guiney, D. G. & Lesnick, M. Targeting of the actin cytoskeleton during infection by Salmonella strains. *Clin. Immunol.* **114,** 248–255 (2005).
11. Holden, D. W. Trafficking of the Salmonella vacuole in macrophages. *Traffic* **3,** 161–169 (2002).
12. Brumell, J. H. & Grinstein, S. Salmonella redirects phagosomal maturation. *Current Opinion in Microbiology* **7,** 78–84 (2004).
13. Kaufmann, S. H. How can immunology contribute to the control of tuberculosis? *Nat Rev Immunol* **1,** 20–30 (2001).
14. Vergne, I., Chua, J., Singh, S. B. & Deretic, V. Cell biology of mycobacterium tuberculosis phagosome. *Annu. Rev. Cell Dev. Biol.* **20,** 367–394 (2004).
15. Cooper, A. M. Cell-mediated immune responses in tuberculosis. *Annu. Rev. Immunol.* **27,** 393–422 (2009).
16. Diedrich, C. R. & Flynn, J. L. HIV-1/mycobacterium tuberculosis coinfection immunology: how does HIV-1 exacerbate tuberculosis? *Infection and Immunity* **79,** 1407–1417 (2011).
17. Ottenhoff, T. H. M. The knowns and unknowns of the immunopathogenesis of tuberculosis. *Int. J. Tuberc. Lung Dis.* **16,** 1424–1432 (2012).
18. World Health Organization. *Global tuberculosis report 2015*. (2015).
19. Ottenhoff, T. H. M. Overcoming the global crisis: 'yes, we can', but also for TB ... ? *Eur. J. Immunol.* **39,** 2014–2020 (2009).
20. Jassal, M. S. & Bishai, W. R. Epidemiology and challenges to the elimination of global tuberculosis. *CLIN INFECT DIS* **50 Suppl 3,** S156–64 (2010).
21. Kuijl, C. *et al.* Intracellular bacterial growth is controlled by a kinase network around PKB/AKT1. **450,** 725–730 (2007).
22. Kumar, D. *et al.* Genome-wide analysis of the host intracellular network that regulates survival of Mycobacterium tuberculosis. *Cell* **140,** 731–743 (2010).

23. Jayaswal, S. *et al.* Identification of host-dependent survival factors for intracellular Mycobacterium tuberculosis through an siRNA screen. *PLoS Pathog* **6,** e1000839 (2010).
24. Sundaramurthy, V. *et al.* Integration of chemical and RNAi multiparametric profiles identifies triggers of intracellular mycobacterial killing. *Cell Host and Microbe* **13,** 129–142 (2013).
25. Machado, D. *et al.* Ion Channel Blockers as Antimicrobial Agents, Efflux Inhibitors, and Enhancers of Macrophage Killing Activity against Drug Resistant Mycobacterium tuberculosis. *PLoS ONE* **11,** e0149326 (2016).
26. Napier, R. J. *et al.* Imatinib-sensitive tyrosine kinases regulate mycobacterial pathogenesis and represent therapeutic targets against tuberculosis. *Cell Host and Microbe* **10,** 475–485 (2011).
27. Subbian, S. *et al.* Phosphodiesterase-4 inhibition alters gene expression and improves isoniazid-mediated clearance of Mycobacterium tuberculosis in rabbit lungs. *PLoS Pathog* **7,** e1002262 (2011).
28. Subbian, S. *et al.* Phosphodiesterase-4 inhibition combined with isoniazid treatment of rabbits with pulmonary tuberculosis reduces macrophage activation and lung pathology. *Am. J. Pathol.* **179,** 289–301 (2011).
29. Koo, M.-S. *et al.* Phosphodiesterase 4 inhibition reduces innate immunity and improves isoniazid clearance of Mycobacterium tuberculosis in the lungs of infected mice. *PLoS ONE* **6,** e17091 (2011).
30. Vilaplana, C. *et al.* Ibuprofen therapy resulted in significantly decreased tissue bacillary loads and increased survival in a new murine experimental model of active tuberculosis. *Journal of Infectious Diseases* **208,** 199–202 (2013).
31. Mayer-Barber, K. D. *et al.* Host-directed therapy of tuberculosis based on interleukin-1 and type I interferon crosstalk. **511,** 99–103 (2014).
32. Datta, M. *et al.* Anti-vascular endothelial growth factor treatment normalizes tuberculosis granuloma vasculature and improves small molecule delivery. *Proc Natl Acad Sci USA* **112,** 1827–1832 (2015).
33. Oehlers, S. H. *et al.* Interception of host angiogenic signalling limits mycobacterial growth. **517,** 612–615 (2015).
34. Schiebler, M. *et al.* Functional drug screening reveals anticonvulsants as enhancers of mTOR-independent autophagic killing of Mycobacterium tuberculosis through inositol depletion. *EMBO Molecular Medicine* **7,** 127–139 (2015).
35. Skerry, C. *et al.* Simvastatin increases the in vivo activity of the first-line tuberculosis regimen. *J. Antimicrob. Chemother.* **69,** 2453–2457 (2014).
36. Stanley, S. A. *et al.* Identification of host-targeted small molecules that restrict intracellular Mycobacterium tuberculosis growth. *PLoS Pathog* **10,** e1003946 (2014).
37. Liu, W. S. & Heckman, C. A. The sevenfold way of PKC regulation. *Cell. Signal.* **10,** 529–542 (1998).
38. Wu-zhang, A. X. & Newton, A. C. Protein kinase C pharmacology: refining the toolbox. *Biochem. J.* **452,** 195–209 (2013).
39. Le Poole, I. C. *et al.* Phagocytosis by normal human melanocytes in vitro. *Exp. Cell Res.* **205,** 388–395 (1993).

40. Le Poole, I. C. *et al.* A novel, antigen-presenting function of melanocytes and its possible relationship to hypopigmentary disorders. *J. Immunol.* **151,** 7284–7292 (1993).
41. van Ham, S. M. *et al.* HLA-DO is a negative modulator of HLA-DM-mediated MHC class II peptide loading. *Curr. Biol.* **7,** 950–957 (1997).
42. van Ham, M. *et al.* Modulation of the major histocompatibility complex class II-associated peptide repertoire by human histocompatibility leukocyte antigen (HLA)-DO. *J. Exp. Med.* **191,** 1127–1136 (2000).
43. Martínez-Lorenzo, M. J., Méresse, S., de Chastellier, C. & Gorvel, J. P. Unusual intracellular trafficking of Salmonella typhimurium in human melanoma cells. *Cellular Microbiology* **3,** 407–416 (2001).
44. Verkhusha, V. V. *et al.* High stability of Discosoma DsRed as compared to Aequorea EGFP. *Biochemistry* **42,** 7879–7884 (2003).
45. Li, X. *et al.* Generation of destabilized green fluorescent protein as a transcription reporter. *J. Biol. Chem.* **273,** 34970–34975 (1998).
46. Basso, A. D. *et al.* Akt forms an intracellular complex with heat shock protein 90 (Hsp90) and Cdc37 and is destabilized by inhibitors of Hsp90 function. *J. Biol. Chem.* **277,** 39858–39866 (2002).
47. Liao, Y. *et al.* Peptidyl-prolyl cis/trans isomerase Pin1 is critical for the regulation of PKB/Akt stability and activation phosphorylation. *Oncogene* **28,** 2436–2445 (2009).
48. Andreu, N. *et al.* Optimisation of bioluminescent reporters for use with mycobacteria. *PLoS ONE* **5,** e10777 (2010).
49. Eklund, D. *et al.* Validation of a medium-throughput method for evaluation of intracellular growth of Mycobacterium tuberculosis. *Clin. Vaccine Immunol.* **17,** 513–517 (2010).
50. Brodin, P. *et al.* High content phenotypic cell-based visual screen identifies Mycobacterium tuberculosis acyltrehalose-containing glycolipids involved in phagosome remodeling. *PLoS Pathog* **6,** e1001100 (2010).
51. Verreck, F. A. W., de Boer, T., Langenberg, D. M. L., van der Zanden, L. & Ottenhoff, T. H. M. Phenotypic and functional profiling of human proinflammatory type-1 and anti-inflammatory type-2 macrophages in response to microbial antigens and IFN-gamma- and CD40L-mediated costimulation. *Journal of Leukocyte Biology* **79,** 285–293 (2006).
52. Jett, B. D., Hatter, K. L., Huycke, M. M. & Gilmore, M. S. Simplified agar plate method for quantifying viable bacteria. *BioTechniques* **23,** 648–650 (1997).
53. Singhal, A. *et al.* Metformin as adjunct antituberculosis therapy. *Science Translational Medicine* **6,** 263ra159–263ra159 (2014).

3 | Combined Chemical Genetics and Data-driven Bioinformatics Approach Identifies Receptor Tyrosine Kinase Inhibitors as Host-directed Antimicrobials

Cornelis J. Korbee*, Matthias T. Heemskerk*, Dragi Kocev, Elisabeth van Strijen, Omid Rabiee, Kees L. M. C. Franken, Louis Wilson, Nigel D. L. Savage, Sašo Džeroski, Mariëlle C. Haks**, Tom H. M. Ottenhoff**

Antibiotic-resistance poses rapidly increasing global problems in combating multidrug-resistant (MDR) infectious diseases like MDR tuberculosis, prompting for novel approaches including host-directed therapies (HDT). Intracellular pathogens like *Salmonellae* and *Mycobacterium tuberculosis* (*Mtb*) exploit host pathways to survive. Only very few HDT compounds targeting host pathways are currently known. In a Library Of Pharmacologically Active Compounds (LOPAC) based drug-repurposing screen, we identify multiple compounds, which target Receptor Tyrosine Kinases (RTKs) and inhibit intracellular *Mtb* and *Salmonellae* more potently than currently known HDT-compounds. By developing a data-driven *in silico* model based on confirmed targets from public databases, we successfully predict additional efficacious HDT compounds. These compounds target host RTK signaling and inhibit intracellular (MDR-)*Mtb*. A complementary human kinome siRNA screen independently confirms the role of RTK signaling and kinases (BLK, ABL1 and NTRK1) in host control of *Mtb*. These approaches validate RTK signaling as a drugable host pathway for HDT against intracellular bacteria.

Adapted from:
Korbee, C.J.*, Heemskerk, M.T.*, Kocev, D., van Strijen, E., Rabiee, O., Franken, K.L.M.C., Wilson, L., Savage, N.D.L., Džeroski, S., Haks, M.C.**, Ottenhoff, T.H.M.**, 2018. **Combined chemical genetics and data-driven bioinformatics approach identifies receptor tyrosine kinase inhibitors as host-directed antimicrobials.** *Nat Commun* **9**, 358. doi:10.1038/s41467-017-02777-6**.**

* Contributed equally
** Contributed equally

Introduction

With an estimated 1/4 of the world population carrying a latent *Mycobacterium tuberculosis* (*Mtb*) infection, 10.5 million new cases and 1.8 million deaths annually, tuberculosis (TB) is an increasing global health issue[1-3]. This is further aggravated by the emergence of multi-, extensively- and totally drug-resistant (MDR/XDR/TDR) *Mtb* strains, threatening to render TB untreatable using current antibiotics[4-6]. In 2015 480,000 patients suffered from MDR-TB.

Although novel candidate antibiotics have recently been identified[7], current antibiotics already cover the majority of druggable targets of pathogens, resulting in a continuous decline in the number of new and approved antibiotics[8-13]. Intracellular bacteria such as *Salmonellae* and *Mtb* pose additional challenges by manipulating host signaling pathways to subvert innate and adaptive immunity. This, however, also creates potential for novel treatment strategies like host-directed therapy (HDT), to reprogram the host immune system by pharmacological and chemical-genetic manipulation. Importantly, HDT-driven manipulation of host signaling pathways may be effective also against drug-resistant bacteria, and help to restore host control of infection in metabolically perturbed cells[14,15]. Several recent studies, including our own, have demonstrated the feasibility of HDT approaches to inhibit bacteria both *in vitro* in human and murine cells[16-20] and *in vivo* in mice, rabbits and zebrafish[21-31]. Using reciprocal chemical-genetics targeting the human kinome, we previously identified AKT1 as a central regulator of *Salmonella enterica* serovar Typhimurium (*Stm*), *Mtb*, and MDR-*Mtb* survival. Treatment of infected cells with the kinase inhibitor H-89 significantly decreased intracellular bacterial loads. Despite H-89 being known as a PKA inhibitor, we demonstrated that this compound inhibited intracellular bacteria by targeting AKT1[16]. However, H-89 had a substantially lower impact on intracellular growth of *Mtb* compared to *Stm*, suggesting that *Mtb* modulates additional host signaling pathways to survive. This is in agreement with reports that *Mtb* arrests vesicle maturation at an earlier stage than *Stm*[16,32,33]. Other studies identified additional drugable human kinases that regulate *Mtb* survival, including TGFβRI and CSNK1[18] and imatinib-sensitive kinases ABL1 and ABL2[21]. In addition to kinases and kinase inhibitors, other potential targets and compounds for TB HDT were identified, including two antipsychotics (Haloperidol and Prochlorperazine) and an antidepressant (Nortryptiline)[19], phosphodiesterase inhibitors[22,23], anti-inflammatory agents like Ibuprofen[25], the FDA-approved drug Zileuton[26], the anti-diabetic drug Metformin[34], phenylbutyrate[35,36] and human metabolic targets[37,38]. Nevertheless, the field of TB HDT has not fully progressed towards clinical application and many interactions between host and bacterium remain to be deciphered. Therefore, better compounds are urgently needed as drug candidates for TB HDT as well as for the identification of cellular events occurring at the host-pathogen interface, which may enable rational drug design for HDT.

We used the screening assay described in **Chapter 2** in drug-repurposing screens, and identified compounds with host-directed anti-(myco)bacterial activity

against *Mtb* and *Stm*, outperforming published HDT compounds' activities. Based on these data, together with confirmed target profiles of the screened compounds we next developed a predictive *in silico* model in order to be able to identify additional HDT compounds. This model was applied to predict host-directed compounds amongst all compounds present in the PubChem repository and to identify their key targets with predicted activity against intracellular *Stm* or *Mtb*. Interestingly, both our experimental wet lab screens as well as the novel *in silico* predictive model identified inhibitors of (growth factor) receptor tyrosine kinases (RTKs) and downstream intermediates of RTK signaling as candidate host-directed drugs to control intracellular infection. Moreover, an siRNA screen of the human kinome in *Mtb*-infected human cells independently validated a key role for RTK signaling in host control of *Mtb*. Thus, using two independent chemical genetic experimental approaches as well as a computational method, we find and validate RTK signaling as a novel important host pathway that controls intracellular *Mtb* (including MDR-*Mtb*) survival. This pathway is druggable by compounds and drugs including clinical drugs Dovitinib, AT9283 and ENMD-2076. These findings offer new approaches to combat intracellular infectious diseases in the face of rapidly rising multi drug resistance.

Results

Identification of host-directed antimicrobial compounds

We applied the novel screening assay described in **Chapter 2** for a TB drug-repurposing screen of a library of 1260 pharmacologically active compounds (LOPAC) in order to identify host-directed compounds with stronger activity against intracellular *Mtb* than H-89. The primary screen in the MelJuSo-*Mtb* intracellular infection model identified 110 compounds that significantly reduced and 16 compounds that increased intracellular bacterial loads. Ninety of these did not affect host cell viability (**Figure 1A** and **Table 1**) and were therefore pursued further. Seven compounds decreased *Mtb* bacterial load more potently than H-89 (**Table 2**). A rescreen of these 7 compounds confirmed their activity and 5 of these compounds again surpassed H-89 (SU 6656, Quinacrine, SB 216763, GW 5074 and Tyrphostin AG 494; **Figure 1B** and **Table 2**). **Figure 1B** shows z-score values in the left panel, with the actual percentage inhibition of *Mtb* growth shown in the middle panel, expressed as the % of control value. These latter data confirmed the strong inhibitory effect of these HDT compounds on intracellular *Mtb*. We next confirmed that these compounds exerted their antimicrobial effects via the host by excluding any direct microbicidal activity against extracellular *Mtb* (**Figure 1C**). As a control, the classical *Mtb* antibiotic rifampicin significantly inhibited *Mtb*.

To investigate whether also compounds existed with host-directed activity against *Stm*, and whether their activity was selective for *Mtb*, *Stm* or both, we also screened the same LOPAC library using the very similar HeLa-*Stm* infection model (**Figure 2A**). Twelve compounds were identified that significantly reduced the *Stm* bacterial load and 10 of these did not affect host cell viability (**Table 3**). 173

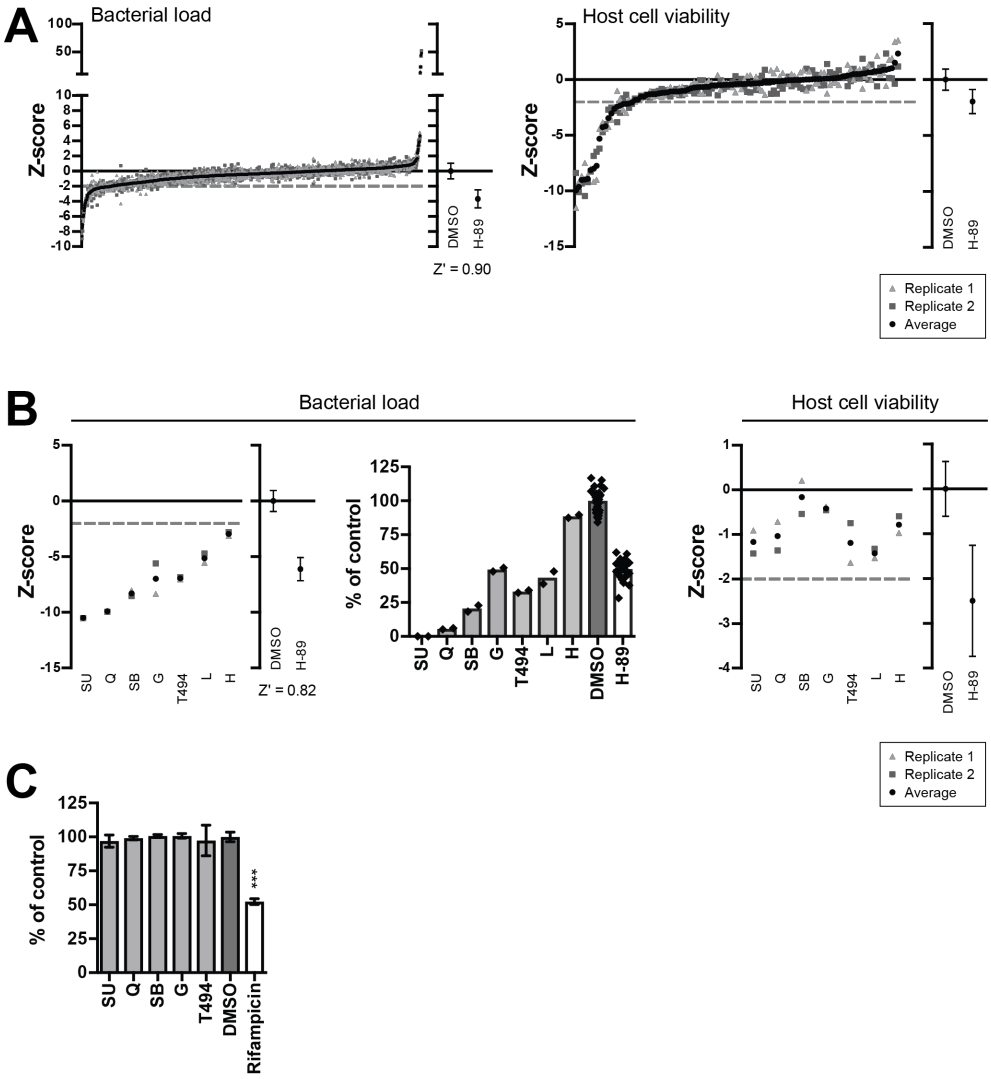

⬆ Figure 1. Identification of host-directed compounds inhibiting *Mtb*.

A. Results of a screen of 1260 compounds of the LOPAC library at 10 μM in the MelJuSo-*Mtb* infection model using *Mtb* constitutively expressing stable DsRed, expressed as z-scores (left panel). Individual replicates of the screened compounds are shown as grey points and the average z-score for each compound is displayed in black. The average z-score and standard deviation of the controls (DMSO and H-89) are displayed separately and the assay window expressed as a Z'-factor is shown below. Cell viability z-scores of the 110 hit compounds are shown in the right panel. The dashed line depicts a cut-off at a z-score of -2. **B.** A rescreen of the hit compounds that were superior to H-89 without affecting cell viability at 10 μM is shown as in **A**. The bacterial load is expressed as z-score in the utmost left panel and as a percentage of control

value in the middle panel to indicate the extent of bacterial inhibition. Individual screening datapoints are overlayed on the bar graph. Compound abbreviations: SU = SU 6656, Q = Quinacrine, SB = SB 216763, G = GW5074, T494 = Tyrphostin AG 494, L = L-594,881, H = Haloperidol. **C.** 6-Day treatment of an *Mtb* broth culture with the 5 hit compounds of the *Mtb* screen at 10 μM. Rifampicin (20 μg/ml) was used as a positive control. The average bacterial density +/- standard deviation of 4 replicates from a representative experiment (out of 3 experiments) is shown, expressed as a percentage of the DMSO control. Statistically significant difference compared to DMSO was tested using a one-way ANOVA ($F_{(6,25)} = 81.66$; *** = p-value < 0.001).

Table 1. LOPAC MelJuSo-*Mtb* primary screen hits using a bacterial load cut-off at z<-2 and a host cell viability cut-off at z>-2.

Bacterial load z-score	Cell viability z-score	Compound name
-6.02	**-1.36**	**SB 216763**
-5.79	**-0.33**	**SU 6656**
-5.25	**-1.14**	**Quinacrine dihydrochloride**
-4.86	**0.38**	**GW5074**
-3.87	-0.14	3',4'-Dichlorobenzamil hydrochloride
-3.83	**-1.01**	**Tyrphostin AG 494**
-3.77	-1.20	Haloperidol
-3.43	-1.55	Metaproterenol hemisulfate
-3.16	2.35	Serotonin hydrochloride
-3.14	0.96	Hydrocortisone 21-hemisuccinate sodium salt
-2.98	-1.07	Nortriptyline hydrochloride
-2.95	-0.88	LY-294,002 hydrochloride
-2.94	-0.14	Emodin
-2.93	-0.77	NNC 55-0396
-2.92	-0.64	Metrifudil
-2.91	0.76	LY-367,265

Bacterial load z-score	Cell viability z-score	Compound name
-2.78	-1.31	Fluspirilene
-2.75	0.06	nor-Binaltorphimine dihydrochloride
-2.66	-0.38	R-(-)-Fluoxetine hydrochloride
-2.65	-1.30	Loperamide hydrochloride
-2.63	0.08	BU224 hydrochloride
-2.62	-1.23	Nylidrin hydrochloride
-2.57	1.52	Farnesylthiosalicylic acid
-2.50	-0.46	PD 168,077 maleate
-2.48	-1.80	GR 127935 hydrochloride hydrate
-2.48	-0.49	5-Hydroxyindolacetic acid
-2.47	-0.46	Fenoldopam monohydrobromide
-2.47	0.01	S-Nitrosoglutathione
-2.44	-0.04	L-Histidine hydrochloride
-2.43	0.65	L-165,041
-2.41	0.04	4-Hydroxybenzhydrazide
-2.41	-1.83	Forskolin
-2.40	-0.38	AMN082
-2.36	-0.45	NAN-190 hydrobromide
-2.36	-0.68	Labetalol hydrochloride
-2.35	-0.41	Hexahydro-sila-difenidol hydrochloride, p-fluoro analog
-2.35	-0.01	L-Canavanine
-2.33	0.05	BRL 50481
-2.31	-0.11	N-Methyl-beta-carboline-3-carboxamide
-2.31	0.23	B-HT 933 dihydrochloride
-2.30	-1.05	Tyrphostin AG 527
-2.30	-0.52	1,3-Dimethyl-8-phenylxanthine

Bacterial load z-score	Cell viability z-score	Compound name
-2.30	0.10	Dopamine hydrochloride
-2.29	-1.17	A-77636 hydrochloride
-2.28	-1.53	Formoterol fumarate dihydrate
-2.25	-0.22	cis-(Z)-Flupenthixol dihydrochloride
-2.25	0.18	5-hydroxydecanoic acid sodium salt
-2.24	0.64	Isoguvacine hydrochloride
-2.23	-0.38	Nimesulide
-2.23	-0.66	alpha-Lobeline hydrochloride
-2.20	-0.67	Hydroxyurea
-2.19	-1.31	Fenoterol hydrobromide
-2.17	-0.34	L-733,060 hydrochloride
-2.17	-0.05	Minocycline hydrochloride
-2.17	-0.71	3-Nitropropionic acid
-2.17	0.41	LFM-A13
-2.16	-1.01	Nalidixic acid sodium salt
-2.16	-1.07	1,3,5-tris(4-hydroxyphenyl)-4-propyl-1H-pyrazole
-2.16	0.57	CR 2249
-2.15	1.02	p-MPPF dihydrochloride
-2.15	-0.04	Naltrexone hydrochloride
-2.15	0.87	Fluphenazine dihydrochloride
-2.14	-1.08	(-)-Tetramisole hydrochloride
-2.14	-0.31	Hydralazine hydrochloride
-2.14	0.09	(+)-Hydrastine
-2.12	0.54	MHPG sulfate potassium
-2.12	-0.67	6-Hydroxy-DL-DOPA
-2.12	-0.52	Ro 90-7501

Bacterial load z-score	Cell viability z-score	Compound name
-2.12	0.75	Neostigmine bromide
-2.11	-0.20	4-Amino-1,8-naphthalimide
-2.10	0.26	Flunarizine dihydrochloride
-2.09	-0.39	2-Methyl-5-hydroxytryptamine maleate
-2.09	0.01	L-368,899 hydrochloride
-2.09	-0.48	Tyrphostin AG 528
-2.09	-0.50	Lamotrigine
-2.09	-0.38	VER-3323 hemifumarate salt
-2.09	0.51	BU99006
-2.09	0.11	GYKI 52466 hydrochloride
-2.09	0.51	Hexamethonium bromide
-2.09	0.49	Flutamide
-2.07	0.05	Hypotaurine
-2.06	-0.06	NCS-356 sodium salt hydrate
-2.06	-0.07	(±)-7-Hydroxy-DPAT hydrobromide
-2.06	0.88	Hydroxylamine hydrochloride
-2.05	0.14	MDL 26,630 trihydrochloride
-2.04	-0.23	4-Hydroxy-3-methoxyphenylacetic acid
-2.03	-0.35	Fenofibrate
-2.03	-0.02	(±)-8-Hydroxy-DPAT hydrobromide
-2.02	-0.25	5-Hydroxy-L-tryptophan
-2.01	0.78	Methiothepin mesylate

Hit compounds that performed better than H-89 in both the primary screen and the rescreen are displayed in bold.

Compounds increased the *Stm* bacterial load without affecting host cell viability. Four of the hit compounds that decreased the bacterial load (Trimethoprim, Haloperidol, Mibefradil and Ofloxacin) were superior to H-89 in inhibiting

Table 2. Details of validated hit compounds from the *Mtb* and *Stm* LOPAC screens.

Abbr.	Compound name	Alternative name(s)	Primary screen z-score	Rescreen z-score	Activity
Mycobacterium tuberculosis					
SU	SU 6656	2,3-Dihydro-N,N-dimethyl-2-oxo-3-[(4,5,6,7-tetrahydro-1H-indol-2-yl)methylene]-1H-indole-5-sulfonamide	**-5.79**	**-10.51**	Src family kinase inhibitor
Q	Quinacrine dihydrochloride		**-5.25**	**-9.90**	MAO inhibitor
SB	SB 216763	3-(2,4-Dichlorophenyl)-4-(1-methyl-1H-indol-3-yl)-1H-pyrrole-2,5-dione	**-6.02**	**-8.29**	GSK-3 kinase inhibitor
G	GW5074	3-(3, 5-Dibromo-4-hydroxybenzylidine-5-iodo-1,3-dihydro-indol-2-one)	**-4.86**	**-6.98**	Raf1 kinase inhibitor
T494	Tyrphostin AG 494	N-Phenyl-3,4-dihydroxybenzylidenecyanoacetamide	**-3.83**	**-6.93**	EGFR kinase inhibitor
L	3',4'-Dichlorobenzamil hydrochloride	L-594,881	**-3.87**	-5.13	$Na^+/Ca2^+$ exchanger inhibitor
H	Haloperidol		**-3.77**	-2.96	D2/D1 dopamine receptor antagonist
Salmonella Typhimurium					
T	Trimethoprim		**-4.06**	-12.18	Antibiotic; dihydrofolate reductase inhibitor
H	Haloperidol		**-3.90**	-12.09	D2/D1 dopamine receptor antagonist
M	Mibefradil dihydrochloride	Ro 40-5967; (1S,2S)-2-[2[[3-(2-benzimidazolylpropyl]methylamino]ethyl]-6-fluoro-1,2,3,4-tetrahydro-1-isopropyl-2-naphthyl methoxyacetate dihydrochloride	**-3.64**	**-12.76**	$Ca2^+$ channel blocker
O	Ofloxacin	Ofloxacine; DL-8280; HOE-280	**-3.45**	-11.60	Antibiotic; DNA synthesis inhibitor

Z-scores lower than the z-score of H-89 are displayed in bold.

intracellular *Stm* (**Table 2**). Mibefradil again exceeded the inhibitory effect of H-89 in a rescreen (**Figure 2B**), while all four compounds consistently and strongly decreased the *Stm* bacterial load. While **Figure 2A** and the left panel of **Figure 2B** show z score values, the percentage inhibition of intracellular *Stm* growth is shown in the middle panel of **Figure 2B**, expressed as the % of control value, demonstrating the strong inhibitory effect of these HDT compounds on intracellular *Stm*. We next excluded any direct microbicidal activity of these HDT-compounds against extracellular *Stm* (**Figure 2C**). By contrast, Trimethoprim and Ofloxacin (both known antibiotics), which were part of the LOPAC library and therefore tested here as well, directly inhibited extracellular *Stm* as expected. The

fact that these known antibiotics for *Stm* were hits in our screen further confirms the strength and validity of our approach, showing that we can clearly distinguish antibiotics from host-directed compounds. Taken together, Haloperidol (a known HDT inhibitor[19]) and Mibefradil (newly discovered here) were confirmed and identified, respectively, as host-directed inhibitors of *Stm*.

Interestingly, a comparison of the *Mtb* and *Stm* HDT compound screening results revealed a highly limited overlap between hits in the two infection models (**Figure 2D**). This observation agrees well with reports that *Mtb* and *Stm* arrest

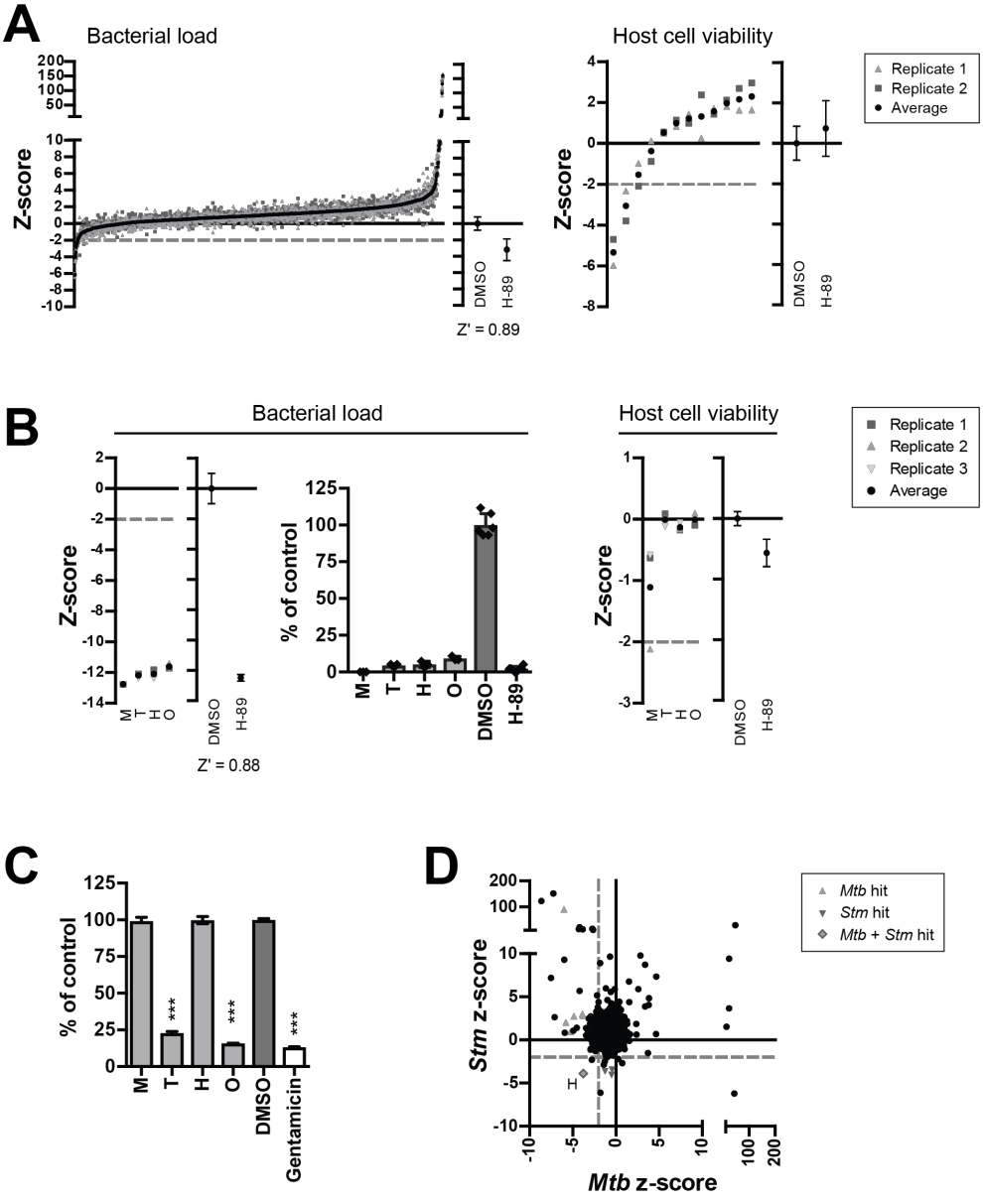

Table 3. LOPAC HeLa-*Stm* primary screen hits using a bacterial load cut-off at z<-2 and a host cell viability cut-off at z>-2.

Bacterial load z-score	Cell viability z-score	Compound name
-4.06	-1.54	Trimethoprim
-3.90	0.98	Haloperidol
-3.64	**1.57**	**Mibefradil dihydrochloride**
-3.45	1.21	Ofloxacin
-2.86	1.96	Demeclocycline hydrochloride
-2.70	-0.38	Doxazosin mesylate
-2.47	2.29	Metergoline
-2.30	1.31	Fluspirilene
-2.20	0.52	8-(3-Chlorostyryl)caffeine
-2.00	2.15	GW2974

Hit compounds that performed better than H-89 in both the primary screen and the rescreen are displayed in bold.

⬅ Figure 2. Identification of host-directed compounds inhibiting *Stm*.

A. Screen of the LOPAC library in the HeLa-*Stm* infection model using *Stm* constitutively expressing stable DsRed, as in **Figure 2A**. **B.** Rescreen of the hit compounds from the HeLa-*Stm* screen that were superior to H-89 without affecting cell viability, displayed as in **Figure 2B**. The bacterial load is expressed as z-score in the utmost left panel and as a percentage of control value +/- standard deviation in the middle panel to indicate the extent of bacterial inhibition. Compound abbreviations: T = Trimethoprim, H = Haloperidol, M = Mibefradil, O = Ofloxacin. **C.** Overnight treatment of a *Stm* broth culture with the hit compounds at 10 µM. Gentamicin (50 µg/ml) was used as a positive control. The average bacterial density +/- standard deviation of 6 replicates from a representative experiment out of 3 experiments is shown. The bacterial load is expressed percentage of the DMSO control value to indicate the extent of bacterial inhibition. Statistically significant difference compared to DMSO was tested using a one-way ANOVA ($F_{(5,30)}$ = 4871; *** = p-value < 0.001). **D.** Comparison of the *Stm* and *Mtb* primary screening data. Compounds that were superior to H-89 and subsequently confirmed in a rescreen are indicated in grey triangles. H = haloperidol.

vesicle maturation at different stages[16,32,33]. Haloperidol was the only compound that inhibited both *Mtb* and *Stm*.

Identification of HDT compounds using an *in silico* model

We next decided to use the above experimental data obtained in our LOPAC screens, and combine these with bioactivity assay based data available for all

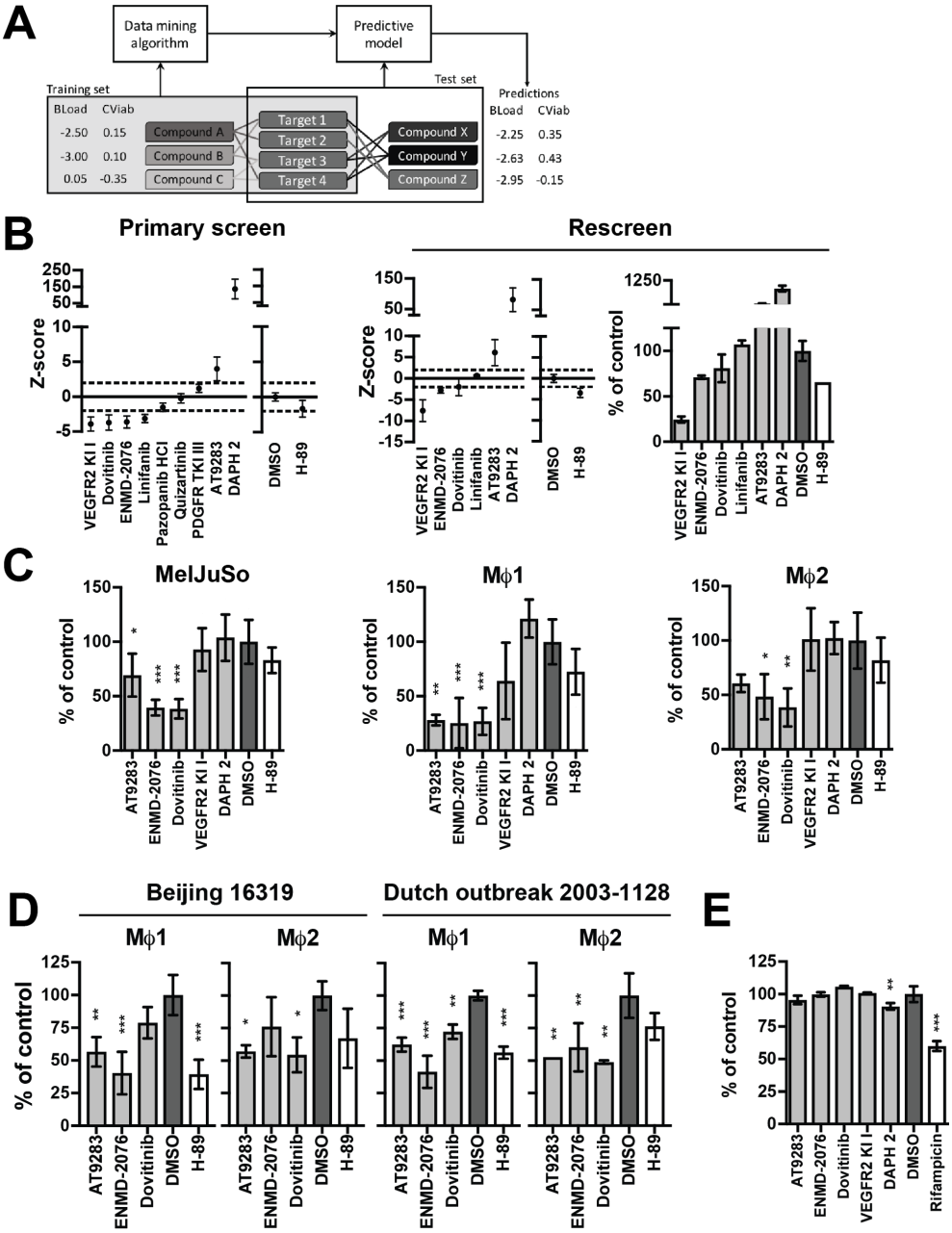

1260 LOPAC compounds in PubChem, to develop a novel bioinformatics predictive model using machine learning. The model was constructed to predict new chemical compounds with host-directed activity against intracellular *Stm* or *Mtb*, based on target protein profiles identified by machine learning from our own LOPAC screening data (**Figure 3A**). An extended description of the machine learning methods describing the predictive model is provided as **Supplementary Information** at the end of this chapter. In brief, we first linked all LOPAC

⬅ Figure 3. Screen of *in silico* predicted compounds active against intracellular *Mtb*.

A. Schematic of the predictive model. Abbreviations: BLoad = bacterial load z-score; CViab = cell viability z-score. **B.** Compound primary screen (left panel) and rescreen (middle panel) at 10 µM in the MelJuSo-*Mtb* model using *Mtb* constitutively expressing stable DsRed, expressed as mean z-scores +/- standard deviation. Dashed lines indicate a hit cut-off at a z-score of 2 or -2. Average z-score and standard deviations of controls (DMSO and H-89) are displayed separately. To indicate the extent of bacterial inhibition, rescreen results are expressed both as z-score and as percentage of control value +/- standard deviation in the right panel. **C.** CFU assay of MelJuSo (left panel) and human primary Mϕ1 (middle panel) and Mϕ2 (right panel) *Mtb* infection models treated with the hit compounds from **B** at 10 µM. Mϕ1 and Mϕ2 models have been described by Verreck *et al.*[39]. Shown are representative data out of 3 experiments (MelJuSo) and data from a representative donor (Mϕs) out of 2 (Mϕ1) or 5 (Mϕ2) blood bank donors. To indicate the extent of bacterial inhibition, results are expressed as percentage of control +/- standard deviation. Replicates in the MelJuSo model: AT9283 and ENMD-2076: n=6; Dovitinib, VEGFR KI I and DAPH2: n=5; DMSO and H-89: n=9. Replicates in the Mϕ models: AT9283, ENMD-2076, Dovitinib, VEGFR KI I and DAPH 2: n=3; DMSO and H-89: n=5. Statistically significant difference compared to DMSO was tested by one-way ANOVA (MelJuSo: $F_{(6,39)} = 16.35$; Mϕ1: $F_{(6,18)} = 10.88$; Mϕ2: $F_{(6,18)} = 5.23$; * = p-value < 0.05, ** = p-value <0.01, *** = p-value < 0.001). **D.** CFU assay of the Mϕ1 and Mϕ2 models infected with MDR-*Mtb* (Beijing family China 16319 and Dutch outbreak 2003-1128) and treated with the validated hit compounds from **C** at 10 µM. Shown are data (n=3 technical replicates) from a representative donor out of 4 different blood bank donors, displayed as percentage of the DMSO control +/- standard deviation. Statistically significant differences compared to DMSO were tested by one-way ANOVA (Mϕ1 Beijing: $F_{(4,10)} = 11.43$; Mϕ2 Beijing: $F_{(4,10)} = 3.72$; Mϕ1 Dutch outbreak: $F_{(4,10)} = 29.09$; Mϕ2 Dutch outbreak: $F_{(4,10)} = 8.81$; * = p-value < 0.05, ** = p-value <0.01, *** = p-value < 0.001). **E.** Six-day treatment of *Mtb* cultures with hit compounds at 10 µM. Rifampicin (20 µg/ml) was used as a positive control. Average bacterial density +/- standard deviation of 3 replicates is shown, expressed as a percentage of the DMSO control. Displayed are representative results out of 3 individual experiments. Statistically significant difference compared to DMSO was tested by one-way ANOVA ($F_{(6,25)} = 101.4$; ** = p-value <0.01, *** = p-value < 0.001).

compounds to PubChem, and retrieved bioassay data by using a pre-processing pipeline (**Supplementary Figure 1A**), which identified 1058 confirmed human protein targets for these 1260 compounds. This resulted in a data table comprising all LOPAC compounds annotated with their corresponding impact on intracellular bacterial survival and host cell viability from our screens, expressed as z-scores, combined with their PubChem bioassay activity for each confirmed human target. An example of the table structure is shown in **Supplementary Table 1**. This was then used as a training set to learn ensembles of predictive clustering trees (PCTs; **Supplementary Figure 2**) to predict impact on intracellular bacterial survival and host cell viability. We next employed this *in silico* tool (the learned model) to identify and select candidate compounds from PubChem with predicted host-directed antimicrobial activity. Querying PubChem for compounds that are known to target one or more of the above 1058 confirmed human protein targets yielded 460,580 compounds, which were then annotated with their bioassay data and fed into the predictive model as a testing set. Using the ensembles of PCTs learned from the training data to predict the intracellular bacterial survival and host cell viability z-scores of these 460,580 compounds, we identified 47 candidate compounds predicted to affect intracellular *Mtb* load (**Table 4**) and 30 compounds predicted to affect intracellular *Stm* load (**Table 5**). From these two lists of compounds, commercially available compounds (**Table 6**) were ordered and screened in the MelJuSo-*Mtb* and HeLa-*Stm* infection models. As the PubChem BioAssay data contains compound-target relations based only on IC50 and EC50 values as well as binding constants, the predictive model was able to identify only compound-target interactions rather than the direction of the target effects. Thus, as we were therefore unable to predict whether compounds would actually inhibit or activate their associated targets, predicted negative z-scores might result in experimentally positive z-scores in *in vitro* intracellular bacterial inhibition tests and vice versa. In the *Mtb* screen 6 out of 9 compounds predicted to affect the bacterial load indeed decreased or increased the bacterial load (**Figure 3B, left panel**). A rescreen of the hit compounds confirmed 5 out of 6 hits (VEGFR KI I, ENMD-2076, Dovitinib, AT9283 and DAPH 2; **Figure 3B, middle and right panels**). Results are shown as z-scores as well as the percentage inhibition of *Mtb* growth expressed as the % of control value, to confirm the strong inhibitory effect of these HDT compounds on intracellular *Mtb* (**Figure 3B, utter right panel**).

As compound autofluorescence might result in false positive z-scores in our assay, we further validated all the confirmed hit compounds independently in classical CFU assays, both in cell lines and in primary human Mϕs. The compounds AT9283, ENMD-2076 and Dovitinib significantly decreased *Mtb* CFUs in both MelJuSo cells and human primary Mϕs (**Figure 3C**; results are shown as percentage inhibition of *Mtb* growth expressed as % of control value). Importantly, AT9283, ENMD-2076 and Dovitinib also reduced CFUs in human primary Mϕs infected with two different MDR-*Mtb* strains (Beijing family China 16319 and Dutch outbreak 2003-1128; **Figure 3D**). These data independently confirm and validate the results obtained in our novel screening and prediction pipeline, and -importantly- extend the newly identified HDT-compounds' effects to intracellular multidrug resistant bacteria. Finally, none of the compounds directly affected

Table 4. Complete list of compounds identified as potential hits from the *Mtb* predictive model output.

PubChem ID	Predicted bacterial load z-score	Predicted cell viability z-score	Reliability
6604502	-2.59	-0.59	0.61
46233889	-2.38	-0.84	0.54
46235770	-2.38	-0.84	0.54
56945171	-2.38	-0.84	0.54
56945172	-2.38	-0.84	0.54
56945173	-2.38	-0.84	0.54
56945174	-2.38	-0.84	0.54
56945175	-2.38	-0.84	0.54
56945277	-2.38	-0.84	0.54
24995659	-2.35	-0.96	0.61
10113978	-2.29	-0.91	0.53
11496629	-2.27	-0.95	0.54
10907042	-2.24	-0.87	0.54
59627005	-2.21	-0.93	0.54
16041424	-2.15	-0.89	0.54
9977819	-2.14	-0.93	0.53
6419834	-2.14	-0.93	0.53
67161540	-2.13	-0.94	0.52
11485656	-2.10	-0.87	0.54
16757867	-2.09	-0.73	0.68
6711154	-2.08	-0.93	0.68
10142586	-2.07	-0.99	0.52
657806	-2.07	-0.48	0.66
9532258	-2.05	-0.86	0.71
10209082	-2.01	-0.93	0.66
24889392	-2.00	-0.87	0.65
5782470	-1.99	-0.64	0.75
660914	-1.95	-0.22	0.67
1552034	-1.91	-0.50	0.79
3246585	-1.89	-0.55	0.66
5284352	-1.86	-0.48	0.62
16235522	-1.84	-0.42	0.71
5284416	-1.84	-0.72	0.65
661761	-1.83	-0.23	0.66
6097179	-1.82	-0.43	0.65
1745927	-1.82	-0.34	0.75
3246543	-1.82	-0.63	0.63
6918515	-1.81	0.31	0.75
5765289	-1.80	-0.47	0.78
664864	-1.78	-0.25	0.66
1363897	-1.78	-0.19	0.71
3246495	-1.78	-0.50	0.65
6604530	-1.78	-0.50	0.65
663169	-1.78	-0.50	0.65
456214	-1.78	-0.45	0.63
660368	-1.77	-0.40	0.65
660838	-1.77	-0.52	0.65

Commercially available compounds selected for the study are indicated in bold.

Table 5. Complete list of compounds identified as potential hits from the *Stm* predictive model output.

PubChem ID	Predicted bacterial load z-score	Predicted cell viability z-score	Reliability
5035	-1.88	0.60	0.65
50994498	-1.68	0.52	0.72
202478	-1.58	0.47	0.71
7333	-1.56	0.04	0.66
44474938	-1.55	0.54	0.73
57402462	-1.55	0.54	0.73
11743300	-1.52	0.44	0.73
13998486	-1.52	0.44	0.73
15163141	-1.52	0.44	0.73
185834	-1.52	0.44	0.73
4416	-1.52	0.44	0.73
44303090	-1.52	0.44	0.73
44398003	-1.52	0.44	0.73
44398036	-1.52	0.44	0.73
44398114	-1.52	0.44	0.73
47641	-1.52	0.44	0.73
50266	-1.52	0.44	0.73
5474589	-1.52	0.44	0.73
6437849	-1.52	0.44	0.73
6439331	-1.52	0.44	0.73
65638	-1.52	0.44	0.73
6713949	-1.52	0.44	0.73
72027	-1.52	0.44	0.73
73345319	-1.52	0.44	0.73
93365	-1.52	0.44	0.73
9799239	-1.52	0.44	0.73
9841596	-1.52	0.44	0.73
9951886	-1.52	0.44	0.73
9954083	-1.52	0.44	0.73
9417	-1.51	0.15	0.68

Commercially available compounds selected for the study are indicated in bold.

Table 6. Compounds selected from the predictive model output.

PubChem ID	Compound name	Predicted bacterial load z-score	Predicted cell viability z-score	Reliability score	Primary screen z-score	Rescreen z-score	Activity
Mycobacterium tuberculosis							
10113978	Pazopanib·HCl	-2.30	-0.91	0.53	-1.50	N.D.	Receptor Tyrosine Kinase (RTK) inhibitor
11496629	AT9283	-2.27	-0.95	0.54	**4.01**	**6.09**	JAK/Aurora kinase inhibitor
16041424	ENMD-2076	-2.15	-0.89	0.54	**-3.62**	**-2.83**	RTK/Aurora A inhibitor
11485656	Linifanib (ABT-869)	-2.11	-0.87	0.54	**-3.13**	0.66	VEGFR/PDGFR inhibitor
10907042	PDGFR Tyrosine Kinase Inhibitor III	-2.24	-0.88	0.53	1.19	N.D.	PDGFR inhibitor
9977819	Dovitinib (TKI-258, CHIR-258)	-2.14	-0.93	0.53	**-3.70**	**-2.02**	RTK inhibitor
6419834	VEGFR2 Kinase Inhibitor I	-2.14	-0.93	0.53	**-3.91**	**-7.63**	VEGFR2 inhibitor
6711154	DAPH 2	-2.08	-0.93	0.68	**136.21**	**80.77**	PKC inhibitor
24889392	Quizartinib	-2.00	-0.87	0.65	-0.24	N.D.	FLT3 inhibitor
Salmonella Typhimurium							
4416	Nafoxidine hydrochloride	-1.52	0.44	0.73	**-3.06**	**-2.33**	Estrogen receptor modulator
7333	1,3-Di-o-tolylguanidine	-1.56	0.04	0.66	-0.42	N.D.	Sigma 1 receptor agonist
47641	Naftifine hydrochloride	-1.52	0.44	0.73	-0.61	N.D.	Fungal squalene epoxidase inhibitor
9417	Opipramol	-1.51	0.15	0.69	**-4.01**	**-4.21**	Sigma receptor agonist

Z-scores exceeding the cut-off (2 < z-score <-2) are displayed in bold, N.D. = not determined.

extracellular bacterial growth in liquid cultures, while classical antibiotics (rifampicin) did, confirming that the mode of action of the new HDT-compounds is via modulation of host and not direct bacterial mechanisms (**Figure 3E**).

Using this same screening and validation approach for *Stm* in the HeLa-*Stm* infection model, we confirmed that 2 out of 4 compounds predicted to affect *Stm* survival indeed decreased the bacterial load of *Stm*-infected cells in a primary screen (**Figure 4A, left panel**). Both of these hits (Opipramol and Nafoxidine) were subsequently confirmed in a rescreen (**Figure 4A, middle and right panels**; results shown as z-scores and as % inhibition of *Stm* growth expressed as the % of control value). Both hit compounds also reduced the *Stm* bacterial load independently in classical CFU assays (**Figure 4B**), again without directly affecting bacterial growth in a liquid overnight *Stm* culture (**Figure 4C**), confirming their HDT

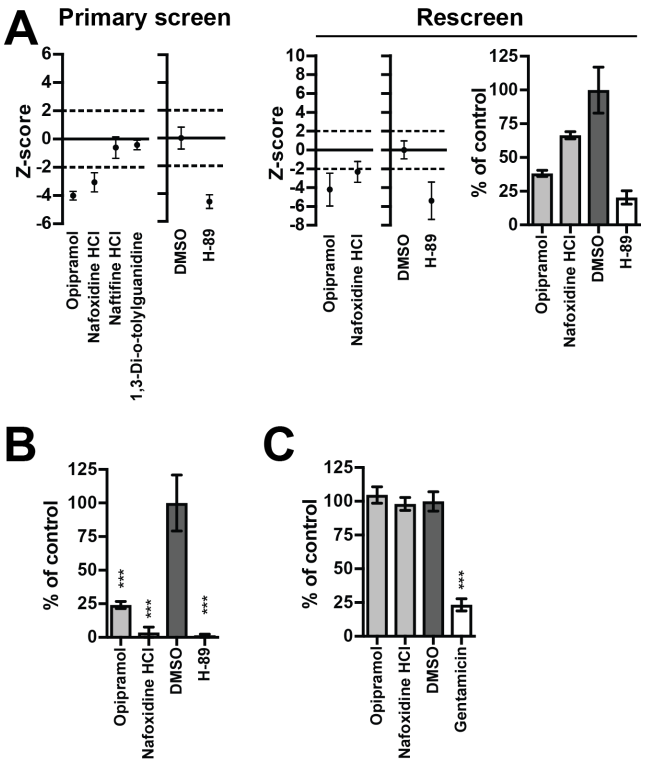

⬆ Figure 4. Screen of *in silico* predicted compounds active against intracellular *Stm*.

A. Chemical compound primary screen (left panel) and rescreen (middle panel) at 10 µM in the HeLa-*Stm* infection model using *Stm* constitutively expressing stable DsRed, expressed as mean z-scores +/- standard deviation. Horizontal dashed lines indicate a hit cut-off at a z-score of 2 or -2. The average z-scores and standard deviations of the controls (DMSO and H-89) are displayed separately. To indicate the extent of bacterial inhibition, rescreen results are expressed as percentage of control value +/- standard deviation in the right panel. **B.** CFU assay of the HeLa-*Stm* infection model treated with the validated hit compounds from **A** at 10 µM. Shown are representative data out of 3 independent experiments, displayed as a percentage of the DMSO control. The average +/- standard deviation of 3 replicates is shown. Statistically significant differences compared to DMSO were tested using a one-way ANOVA ($F_{(3,8)}$ = 56.31; *** = p-value < 0.001). **C.** Overnight treatment of *Stm* broth cultures with the hit compounds at 10 µM. The *Stm* antibiotic Gentamicin (50 µg/ml) was used as a positive control. The average bacterial density +/- standard deviation of 3 replicates is shown, expressed as a percentage of the DMSO control. Displayed are representative results out of 3 individual experiments. Statistically significant differences compared to DMSO were tested using a one-way ANOVA ($F_{(3,38)}$ = 579.5; *** = p-value < 0.001).

mode of action. These data therefore confirm and validate our novel screening and prediction pipeline not only for *Mtb* but also *Stm*.

Thus, we have successfully developed and used a data-driven novel *in silico* predictive model to identify host-directed compounds with antimicrobial activity against intracellular bacteria. The model significantly enhanced the identification of *de novo* hit compounds (5 out of 9 (55.6%) and 2 out of 4 (50%) for *Mtb* and *Stm*, respectively) compared to random LOPAC library primary screening (126 out of 1260 (10%) for *Mtb* and 185 out of 1260 (14.6%) for *Stm*). In addition, the results were replicated and validated in primary human Mϕs infected with *Mtb*, strongly agreeing with and further validating the MelJuSo-*Mtb* model used in our novel flow cytometry-based screening assay.

RTK signaling is a novel host pathway controlling *Mtb*

As AT9283, ENMD-2076 and Dovitinib are RTK inhibitors[40-42] we used a chemical genetics approach to confirm a role for RTK signaling in host-mediated *Mtb* control. We first retrieved human protein targets of AT9283, ENMD-2076 and Dovitinib from the Compound Bioactivity section in ChEMBL (http://www.www.ebi.ac.uk/chembl/) and further downselected targets for which the compounds were annotated as 'Active'. Because no targets annotated as 'Active' could be retrieved for AT9283 and ENMD-2076, we first constructed a STRING protein network and performed gene ontology (GO) analysis using the targets of Dovitinib (n=86 proteins; **Figure 5A**). Due to the hierarchical organization of GO-terms, general cellular and molecular functions tend to be highly enriched in GO term enrichment analyses. Therefore, we focused on identifying the highest ranked GO terms that described distinct pathways rather than the overall highest ranked GO terms. As expected from the reported target specificities of Dovitinib[42], 'transmembrane receptor protein tyrosine kinase signaling pathway' (GO:0007169, false discovery rate (FDR) 3.82E-33) was the highest ranking enriched pathway and 40 protein targets participated in this pathway (**Figure 5A** and **Figure 6A**). We next verified that both AT9283 and ENMD-2076 target RTKs by retrieving human protein targets from the Target Summary section in ChEMBL and performed an identical STRING analysis (**Figures 6B** and **6C**). Even though this analysis resulted in small networks due to the limited number of studied targets and the lists of targets from the Target Summary section also include non-confirmed targets, the GO-term 'transmembrane receptor protein tyrosine kinase signaling pathway' (GO:0007169) was again highly enriched in the target networks of AT9283 (FDR 1.11E-12) and ENMD-2076 (FDR 6.47E-5).

To independently confirm RTK signaling as a functional pathway that controls intracellular survival of *Mtb*, we next performed an unbiased siRNA screen of the human kinome in the MelJuSo-*Mtb* infection model (**Figure 5B**), agnostic to the above data. The siRNA screen identified 20 targets that decreased and 21 that increased the *Mtb* bacterial load whilst not affecting host cell viability (**Table 7**). These 41 hit kinases were then used in a STRING protein network and GO analysis. Independently confirming the STRING analysis of the targets of Dovitinib, AT9283 and ENMD-2076, also in this analysis 'transmembrane receptor protein tyrosine kinase signaling pathway' (GO:0007169, FDR 1.32E-13) was the highest-ranking enriched pathway, and 18 hit kinases from the siRNA screen

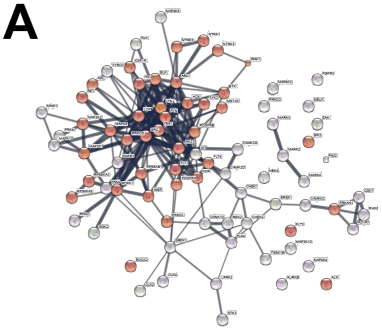

#pathway ID	pathway description	gene count	FDR
GO.0006468	protein phosphorylation	78	1.82E-104
GO.0006796	phosphate-containing compound metabolic process	77	5.02E-75
GO.0046777	protein autophosphorylation	48	5.02E-75
GO.0006464	cellular protein modification process	77	2.12E-62
GO.0018108	peptidyl-tyrosine phosphorylation	37	3.82E-55
GO.0018193	peptidyl-amino acid modification	51	3.73E-48
GO.0035556	intracellular signal transduction	57	3.48E-40
GO.0007169	**transmembrane receptor protein tyrosine kinase signaling pathway**	40	3.82E-35
GO.0001934	positive regulation of protein phosphorylation	40	7.72E-33
GO.0007167	enzyme linked receptor protein signaling pathway	41	7.77E-32

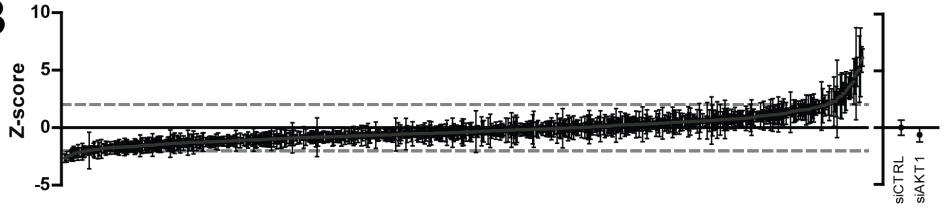

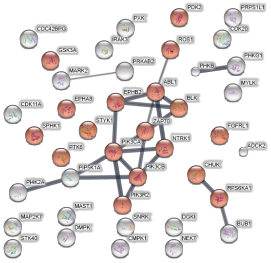

#pathway ID	pathway description	gene count	FDR
GO.0016310	phosphorylation	36	2.07E-38
GO.0006468	protein phosphorylation	29	1.86E-29
GO.0044267	cellular protein metabolic process	30	1.32E-13
GO.0007169	**transmembrane receptor protein tyrosine kinase signaling pathway**	18	1.32E-13
GO.0018108	peptidyl-tyrosine phosphorylation	10	3.76E-10
GO.0035556	intracellular signal transduction	21	6.49E-10
GO.0046777	protein autophosphorylation	10	2.44E-09
GO.0007166	cell surface receptor signaling pathway	20	5.30E-08
GO.0044237	cellular metabolic process	35	7.52E-08
GO.0046834	lipid phosphorylation	6	7.52E-08

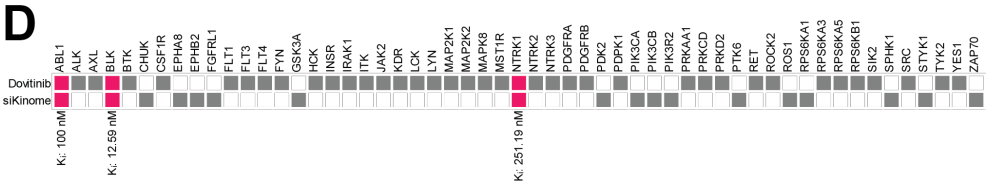

participated in this pathway (**Figure 5C** and **Figure 6D**). Three of the kinases (ABL1, BLK and NTRK1) were both hits in the siRNA screen and confirmed targets of Dovitinib (**Figure 5D**). Of these 3 kinases, only ABL1 was present in the potential target networks of AT9283 and ENMD-2076 (**Figures 6B** and **6C**). However, a lower dissociation constant (K_i) is reported in ChEMBL for the interaction between Dovitinib and BLK (K_i: 12.59 nM) than between Dovitinib and ABL1 (K_i: 100 nM), suggesting that BLK is targeted more strongly by Dovitinib. To identify the top enriched RTK signaling pathway targeted by Dovitinib and siRNA, we used the kinases shown in **Figure 5D** in a STRING analysis. This identified the neurotrophin signaling pathway as the top enriched KEGG pathway (**Figure 7**)[43]. Silencing of Neurotrophic Receptor Tyrosine Kinase 1 (NTRK1) resulted in an increased *Mtb* bacterial load (**Table 7**), establishing a functional link between

⬅ Figure 5. Identification of host kinases controlling intracellular *Mtb* survival.
A. STRING network of confirmed targets of Dovitinib retrieved from the ChEMBL repository Compound Bioactivity section (left panel). Individual proteins are displayed as nodes. Lines represent protein-protein interactions and the thickness of the lines indicates confidence. Proteins participating in the 'transmembrane receptor tyrosine kinase signaling pathway' are displayed in red. The top 10 enriched GO terms in the 'Biological Function' category are displayed along with the number of genes/proteins annotated with the indicated GO terms and the false discovery rate (FDR) of the enrichment (right panel). **B.** Results of a siRNA screen of the human kinome in the MelJuSo-*Mtb* infection model using *Mtb* constitutively expressing destabilized DsRed, expressed as z-scores. The average z-score +/- standard deviation for each siRNA pool is displayed. A hit cut off at z=2 or z=-2 is displayed as a dashed line. The average z-score and standard deviation of the controls (siCTRL and siAKT) are displayed separately. SiCTRL: non-targeting siRNA pool. **C.** STRING network of the siRNA screen hits (left panel) is displayed along the top 10 enriched GO terms in the 'Biological Function' category (right panel), as in **A**. **D.** Participation of individual targets of Dovitinib (top row) or hits from the siRNA screen (bottom row) in the 'transmembrane receptor tyrosine kinase signaling pathway' is indicated by filled squares. Proteins that are both targeted by Dovitinib and were a hit in the siRNA screen are shown in magenta. Dissociation constants (K_i) retrieved from ChEMBL are shown below for the interaction between Dovitinib and ABL1, BLK and NTRK1.

➡ Figure 6 (next page). STRING analysis of targets of Dovitinib, AT9283, ENMD-2076 and siRNA screening hits.
A. Association of individual targets of Dovitinib with the top 10 enriched GO terms is indicated by filled squares. **B.** STRING network of potential targets of AT9283 retrieved from the ChEMBL repository Target Summary section (top panel). Individual proteins are displayed as nodes. Lines represent protein-protein interactions and the thickness of the lines indicates confidence. Proteins participating in the 'transmembrane receptor tyrosine kinase signaling pathway' are displayed in red. The top 10 enriched GO terms in the 'Biological Function' category are displayed along with the number of genes/proteins annotated with the indicated GO terms and the false discovery rate (FDR) of the enrichment (bottom panel). **C.** STRING network of potential targets of ENMD-2076 retrieved from the ChEMBL repository Target Summary section (top panel) and the top 18 enriched GO terms in the 'Biological Function' category (bottom panel) are displayed as in **B**. **D.** Association of individual siRNA hit kinases with the top 10 enriched GO terms is indicated by filled squares.

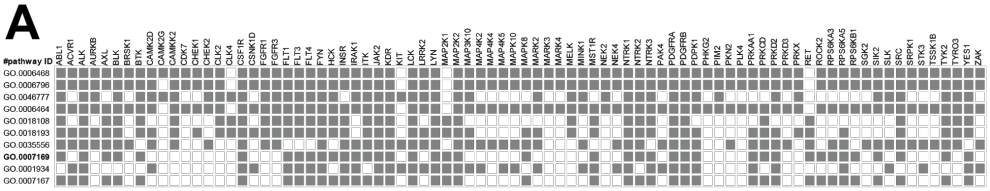

neurotrophin signaling and *Mtb* survival.

Thus, using independent chemical genetic, functional and computational approaches, we find and validate that (1) RTK signaling is a novel host pathway that controls intracellular (MDR)-*Mtb* survival and that (2) repurposable drugs such as Dovitinib, AT9283 and ENMD-2076 that target RTK signaling are new candidates for HDT in treating TB, including MDR-*Mtb*.

Table 7. siKinome screen hits in the MelJuSo-*Mtb* infection model.

GenBank Accession	Gene Symbol	Z-score
NM_006213	PHKG1	-2,65
NM_133494	NEK7	-2,65
NM_018425	PI4KII	-2,50
NM_032017	MGC4796	-2,47
NM_019884	GSK3A	-2,44
NM_014975	SAST	-2,42
NM_006219	PIK3CB	-2,34
NM_001079	ZAP70	-2,25
NM_005157	ABL1	-2,19
NM_012119	CCRK	-2,18
NM_017525	HSMDPKIN	-2,17
NM_007199	IRAK3	-2,16
NM_001715	BLK	-2,15
NM_001278	CHUK	-2,14
NM_000293	PHKB	-2,11
NM_002611	PDK2	-2,09
NM_017771	PXK	-2,08
NM_005399	PRKAB2	-2,02
NM_021923	FGFRL1	-2,01
NM_004717	DGKI	-2,00
NM_005027	PIK3R2	2,02
NM_021972	SPHK1	2,12
NM_001100594	SNRK	2,20
NM_006218	PIK3CA	2,26
NM_175886	PRPS1L1	2,26

GenBank Accession	Gene Symbol	Z-score
NM_005975	PTK6	2,27
NM_033487	CDC2L1	2,51
NM_001007792	NTRK1	2,62
NM_001081562	DMPK	2,69
NM_001006665	RPS6KA1	2,72
NM_016308	UMP-CMPK	2,77
NM_002944	ROS1	3,31
NM_004336	BUB1	3,50
NM_182493	MLCK	3,58
NM_001006943	EPHA8	3,70
NM_052853	ADCK2	3,80
NM_018423	STYK1	4,02
NM_001039468	MARK2	4,46
NM_145185	MAP2K7	4,85
NM_003557	PIP5K1A	6,10
NM_017449	EPHB2	7,68

➡ **Figure 7. STRING analysis of the siKinome screening data.**
STRING analysis to identify enriched KEGG pathways using the kinases from **Figure 5D**. Displayed are the top 10 enriched KEGG pathways along with the number of genes/proteins annotated with the indicated GO terms and the false discovery rate (FDR) of the enrichment (left panel). Involvement of individual proteins is overlaid on the 'neurotrophin signaling pathway' KEGG pathway retrieved from the Kyoto Encyclopedia of Genes and Genomes (http://www.genome.jp/kegg/). Proteins in grey are targeted by Dovitinib only, blue proteins were siRNA screening hits and proteins in red are both targeted by Dovitinib and silencing of these genes affected the *Mtb* bacterial load.

#pathway ID	pathway description	gene count	FDR
4722	Neurotrophin signaling pathway	15	1.95e-19
4014	Ras signaling pathway	15	2.01e-15
4151	PI3K-Akt signaling pathway	16	3.13e-14
4664	Fc epsilon RI signaling pathway	10	1.12e-13
4015	Rap1 signaling pathway	13	3.15e-13
4510	Focal adhesion	13	3.15e-13
4660	T cell receptor signaling pathway	10	3.99e-12
4380	Osteoclast differentiation	10	3.56e-11
4062	Chemokine signaling pathway	11	4.34e-11
5200	Pathways in cancer	13	6.08e-11

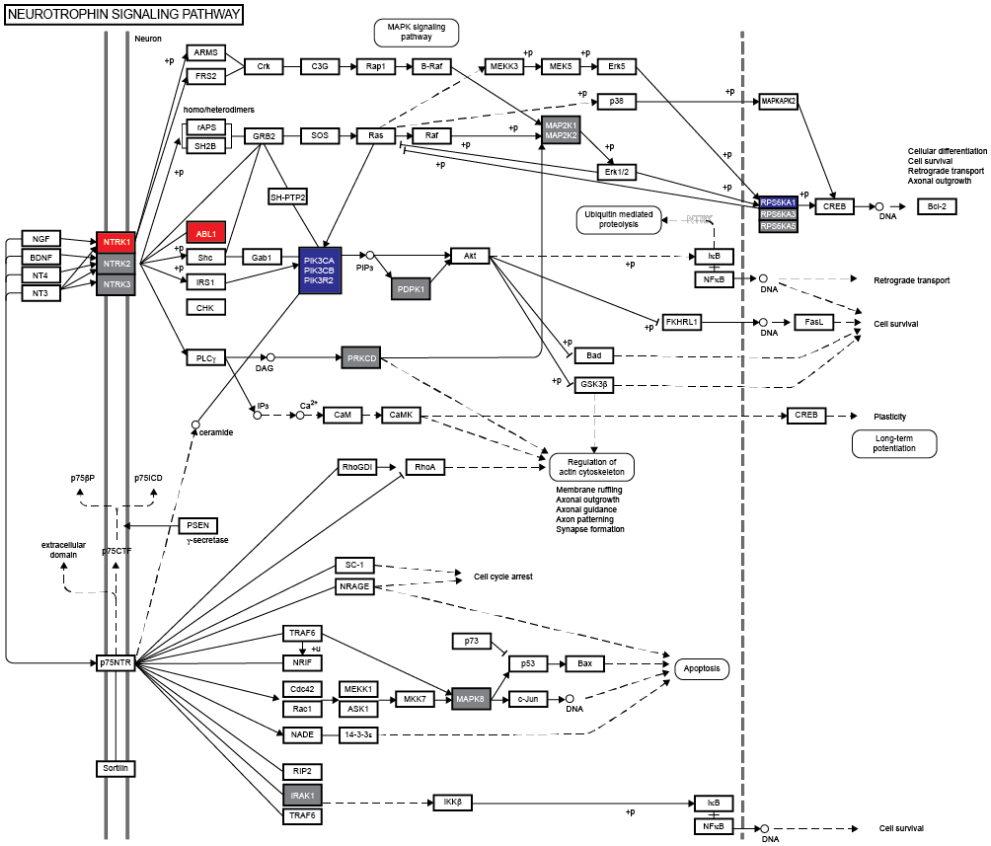

Discussion

Employing chemical genetic screens complemented with newly developed computational approaches, we have identified host-directed therapy (HDT) compounds and drugs (Dovitinib, AT9283 and ENMD-2076) that target human RTK signaling to control intracellular *Mtb* survival, including MDR-*Mtb*. Perhaps more importantly, our findings pave the way towards identifying additional compounds targeting human RTK signaling to improve control of intracellular *Mtb* infection since all compounds were confirmed to be effective in primary human Mϕ infection models.

Current efforts to develop HDT are a topic of interest for infectious diseases and cancer (reviewed recently[38]). In order to be able to screen larger HDT-compound libraries for novel leads with activity against intracellular *Mtb* and *Stm*, we have developed a new robust and rapid fluorescence-based intracellular screening assay (**Chapter 2**). This assay allowed us to identify host-directed *Mtb*-inhibiting compounds (SU 6656, Quinacrine, SB 216763, GW5074 and Tyrphostin AG 494) and host-directed *Stm*-inhibiting compounds (Mibefradil), which performed significantly better than our best reference compound H-89, in a LOPAC library drug-repurposing screening effort. We were also able to confirm the activity of previously published HDT compounds in our screening approach (Imatinib, D4476, LY-364947, Haloperidol), lending strong plausibility and validity to our strategy.

We next developed a novel *in silico* model which was data-driven and based on known and confirmed targets from public databases, by which we could successfully predict and verify additional compounds with host-directed activity against *Mtb* (Dovitinib, AT9283 and ENMD-2076) and *Stm* (Nafoxidine and Opipramol). Using STRING network analysis we uncovered RTK signaling as a novel host pathway controlling *Mtb* intracellular survival, which is targeted by compounds identified in this study. Finally we performed an independent unbiased siRNA screen of the human kinome, which confirmed a role for RTK signaling in control of intracellular *Mtb* survival. Collectively, our results uncover new host signaling pathways as well as corresponding active chemical compounds targeting these to control intracellular bacterial infections, including MDR-TB and *Stm*.

Our LOPAC screen provides important and general proof-of-principle for drug repurposing, since we successfully identified several candidate compounds that displayed host-directed antimicrobial activity while their known targets have not previously been associated with infectious diseases. Strikingly, 4 of the 5 hit compounds that consistently outperformed H-89 in controlling *Mtb* infection are known to affect (growth factor) RTK signaling. Tyrphostin AG 494, SU 6656, SB 216763 and GW5074 are inhibitors of EGFR, SRC Family Kinases (SFKs), GSK-3 and RAF1, respectively, which are all kinases participating in RTK pathways[44-48]. In addition to compounds affecting RTK signaling we identified 3 other host-directed *Mtb*-inhibiting compounds with vastly different target specificities. Firstly, Quinacrine was originally developed as an antimalarial drug but has displayed

activity in a myriad of diseases via a wide range of targets[49]. Interestingly, reported targets of Quinacrine include AKT1 and NF-κB as well as phospholipase A2[50]. The latter is a central enzyme in the eicosanoid pathway, which was recently shown to be involved in *Mtb* control by balancing the type I interferon response[26]. Secondly, Haloperidol is an antipsychotic drug targeting dopamine receptors[51]. Importantly, Haloperidol was recently shown to affect survival of intracellular mycobacteria in a host-directed fashion[19], providing important additional and independent validation of our screening strategy and models. Finally, 3',4'-Dichlorobenzamil is an amiloride-analogue Na+/Ca2+ exchanger inhibitor[52]. This compound may act by inhibiting Ca2+ transport in the cell, as activation of calcineurin by increased Ca2+ levels has previously been proposed as a mechanism for inhibition of phagosome maturation in *Mtb*-infected cells[53].

A similar LOPAC library screen in the HeLa-*Stm* infection model resulted in 4 compounds that more strongly reduced the bacterial load than our reference compound H-89, and Mibefradil was further confirmed to surpass H-89's activity in a rescreen. However, H-89 is already a highly potent host-directed inhibitor of *Stm* and all 4 compounds consistently and significantly reduced the *Stm* bacterial load. Two of the 4 hit compounds from the primary screen were known antibiotics (Trimethoprim and Ofloxacin) but these were tested nevertheless in our screen because they were part of the LOPAC. Of the remaining 2 HDT compounds, Haloperidol, which was already found in a previous HDT screen study in TB, was confirmed as a HDT compound with activity against *Mtb*, but we extend these results here to *Stm* as well. These data again show the validity of our screening and prediction approach since we are able to consistently and faithfully confirm already available knowledge. The data on Haloperidol also suggest that this compound may be applicable for HDT in a broader spectrum of intracellular bacterial infections. The second hit compound, Mibefradil, is a Ca2+ channel blocker[54]. The majority of screening hits in the HeLa-*Stm* infection model exacerbated bacterial loads and even though these compounds can therefore not be used for drug repurposing, all of the identified compounds may be important starting points for gaining deeper mechanistic insight into *Stm*-host interactions. The limited overlap between the hit compounds from *Mtb* and *Stm* screens likely reflects the vastly different intracellular 'lifestyles' of these pathogens. Notwithstanding this, several compounds display consistent intracellular antimicrobial activity in both *Mtb* and *Stm* infection models, such as Haloperidol. These compounds are therefore promising candidate drugs with wider application against (antibiotic resistant) intracellular bacterial infections.

Selecting hits for follow-up analysis in large (chemical) screens poses substantial challenges. Here, we employed two complementary strategies for screening follow-up. Firstly, as we aimed to identify compounds with superior host-directed antimicrobial activity, we focused on compounds performing better than the reference compound H-89, resulting in a strictly data-driven hit cut-off. Using this strategy we identified SU 6656, Quinacrine, SB 216763, GW5074 and Tyrphostin AG 494 as the most promising candidate compounds for TB and Mibefradil for salmonellosis, as well as confirmed Haloperidol as an attractive drug for HDT against both *Mtb* and *Stm*. Secondly, as screening outcome may be strongly influenced by compound properties such as solubility, hydrophobicity,

concentration, IC50 and target selectivity, using a strict cut-off may mask valuable data hidden in the large dataset and will be lost to follow-up. We therefore used a complementary follow-up approach by developing an innovative *in silico* compound predictive model to uncover relevant chemical compound classes and target profiles in screening data. Focusing on confirmed target profiles by automated extraction of bioassay data from PubChem we were able to both discern compound targets and predict novel active compounds. As the target profiles were ranked without using a hit cut-off, this approach enabled unbiased validation and follow-up of the primary chemical compound screen. The use of simple numerical values as predictive parameters renders this prediction model highly adaptable and easily applicable to other chemical screens. The model significantly enhanced the identification of de novo hit compounds (55.6% and 50% for *Mtb* and *Stm*, respectively) compared to random LOPAC library primary screening (10% for *Mtb* and 14.6% for *Stm*). Remarkably, the predicted *Mtb* hit compounds AT9283, ENMD-2076 and Dovitinib were all (growth factor) RTK inhibitors[40-42].

As inhibitors of RTK signaling molecules were already observed to be over-represented in the hits from our drug-repurposing screen, our predictive model successfully provided an unbiased validation of this observation and prompted us to further focus our screening endeavor on RTK inhibitors. RTK inhibitors are widely studied in cancer research for their anti-neoplastic properties[55]. Phase II clinical trials have been performed with both AT9283 and ENMD-2076 and Dovitinib has already passed phase III clinical trials[56-61] (http://www.clinicaltrials.gov), enabling swift future drug repurposing as host-directed antimicrobials. Our unbiased siRNA screen of the human kinome independently identified and validated RTK signaling as a host pathway regulating *Mtb* survival, identifying BLK, ABL1 and NTRK1 as host kinases controlling intracellular *Mtb* and possible drugable targets. BLK is an SFK involved in B-cell receptor signaling and the insulin response to glucose uptake in pancreatic islet cells[62,63]. The non-receptor tyrosine kinase ABL1 was previously linked to mycobacterial infection and its commonly used inhibitor Imatinib was shown to exert host-directed *Mtb* inhibiting activity *in vivo*[15,21], providing independent validation of our siRNA screening. Finally, NTRK1 is an RTK involved in peripheral nervous system development and synaptic function and plasticity[64]. Various cells of the hematopoietic lineage have been shown to produce the NTRK ligand nerve growth factor during inflammation and autoimmunity[65] and expression of NTRKs in monocytes has been previously reported[66]. Next to the confirmation of these compound targets by genetic silencing as described here, there were other siRNA hits involved in RTK signaling which might represent as yet unknown molecular targets for these or other hit compounds. Conversely, confirmed compound targets that were not identified in our siRNA screen may still contribute to *Mtb* control due to redundancy and possible incomplete genetic knockdown inherent to siRNA screens.

A role for growth factors in mycobacterial infection has been previously reported. The growth factor VEGF was linked to mycobacterial infection in a zebrafish Mycobacterium marinum (*Mm*) infection study[28] as well as in a rabbit *Mtb* infection model[27]. However, in both studies the reported effect of VEGF was

primarily systemic rather than (sub)cellular, inducing enhanced angiogenesis in granulomas. Our data strongly suggest that an intracellular response to growth factor receptor signaling via RTKs may be another important determinant for mycobacterial infection outcome. Interestingly, Oehlers *et al*. used Pazopanib, one of the compounds identified by our predictive model to show an inhibitory effect of VEGF receptor (VEGFR) inhibition on vascularization around nascent granulomas in their model. Though not meeting our strict hit selection criteria, Pazopanib statistically significantly (z-score -1.50) decreased *Mtb* loads in our screen (and thus in the absence of a vascular system), suggesting that cellular *Mtb* inhibition by Pazopanib might precede or complement the vascularization effects observed *in vivo* by Oehlers *et al*. Additionally, epidermal growth factor receptor (EGFR) signaling has previously been linked to mycobacterial infection through a chemical screen identifying EGFR inhibitor Gefitinib as a compound that restricts *Mtb* growth[31]. Our study significantly expands this knowledge by introducing additional RTK-targeting compounds that can be used for drug repurposing, including compounds targeting VEGFR (Dovitinib) and EGFR (Tyrphostin AG 494) signaling.

Our *in silico* predictive model successfully identified two compounds (Nafoxidine, an estrogen receptor modulator and Opipramol, a Sigma receptor agonist) with host-directed *Stm*-inhibiting activity. Interestingly, Haloperidol (a hit in both the *Mtb* and *Stm* LOPAC screens) was previously reported to interact with Sigma receptors with high affinity[67], suggesting mechanistic involvement of Sigma receptors in host control of intracellular bacteria.

In conclusion, the results from our chemical genetic and novel bioinformatics approach provide an important proof-of-concept of HDT for intracellular infections, such as (MDR) TB and salmonellosis. Moreover, our results identify human RTK signaling as a signaling pathway targetable by novel repurposable drugs, providing a new and promising therapeutic starting point for drug development against *Mtb*, including MDR-*Mtb*.

Experimental procedures

Reagents

H-89 dihydrochloride, DAPH 2, Nafoxidine hydrochloride, 1,3-Di-o-tolylguanidine, Naftifine hydrochloride, Opipramol, Rifampicin, Kanamycin and the Library of Pharmacologically Active Compounds (LOPAC) were purchased from Sigma-Aldrich, Zwijndrecht, The Netherlands. Hygromycin B was acquired from Life Technologies-Invitrogen, Bleiswijk, The Netherlands. VEGFR2 Kinase Inhibitor I and Ampicillin were purchased from Calbiochem Merck-Millipore, Darmstadt, Germany. Pazopanib HCl, AT9283 and Linifanib (ABT-869) were acquired from Selleck Chemicals, Munich, Germany. Quizartinib was purchased from MedChemExpress, Stockholm, Sweden. Santa Cruz BioTechnology, Heidelberg, Germany was the supplier of PDGFR Tyrosine Kinase Inhibitor III. Dovitinib

(TKI-258, CHIR-258) was from APExBIO, Houston, TX, USA. The siKinome library was acquired from Thermo Fisher Dharmacon, Waltham Massachusetts, USA.

Cell culture

HeLa cells and the MelJuSo human melanoma cell line were maintained at 37°C and 5% CO_2 in Gibco Iscove's Modified Dulbecco's Medium (IMDM; Life Technologies-Invitrogen) with 10% fetal bovine serum (FBS, Greiner Bio-One, Alphen a/d Rijn, The Netherlands), 100 units/ml Penicillin and 100 µg/ml Streptomycin (Life Technologies-Invitrogen). Pro-inflammatory Mϕ1s and anti-inflammatory Mϕ2s were generated from monocytes isolated from whole blood of healthy donors by FICOLL separation and CD14 MACS sorting (Miltenyi Biotec, Teterow, Germany) followed by 6 days differentiation with 5 ng/ml granulocyte macrophage-colony stimulating factor (GM-CSF; BioSource Life Technologies-Invitrogen) or 50 ng/ml macrophage-colony stimulating factor (M-CSF; R&D Systems, Abingdon, United Kingdom) respectively, as previously reported[68]. Mϕs were cultured in Gibco Roswell Park Memorial Institute (RPMI) 1640 medium (Life Technologies-Invitrogen) with 10% FBS and 2 mM L-Alanyl-L-Glutamine (PAA, Linz, Austria).

Bacterial culture

Bacterial strains used are displayed in **Table 8**. Mycobacteria were cultured in Difco Middlebrook 7H9 broth (Becton Dickinson, Breda, The Netherlands) supplemented with 10% ADC (Becton Dickinson), 0.5% Tween-80 (Sigma-Aldrich) and appropriate antibiotics. *Stm* was cultured on Difco Luria-Bertani (LB) agar (Becton Dickinson) or in Difco LB broth (Becton Dickinson) supplemented with appropriate antibiotics.

Table 8. Bacterial strains, plasmids used for fluorescent protein expression and their respective antibiotic selection markers.

Base strain	Plasmid	Antibiotic resistance (source, concentration)
Stm SL1344.	pMW211[C.10E/DsRed] (Constitutive promoter).	Ampicillin (plasmid, 100 µg/ml).
Mtb H37Rv.	pSMT3[Phsp60/DsRed].	Hygromycin (plasmid, 50 µg/ml).
Mtb H37Rv.	pSMT3[Phsp60/ destabilized DsRed].	Hygromycin (plasmid, 50 µg/ml).
MDR *Mtb* Beijing family China (Kremer 43) 16319	None.	Rifampicin, Isoniazid, Ethambutol, Pyrazinamide (intrinsic, n/a).
MDR *Mtb* Dutch outbreak 2003-1128.	None.	Rifampicin, Isoniazid, Streptomycin, Claritromycin (intrinsic, n/a).

Stm and *Mtb* infections

One day before infection, mycobacterial cultures were diluted to a density corresponding with early log phase growth (optical density at 600 nm (OD_{600}) of 0.4). *Stm* was grown either in LB broth or on LB agar with appropriate antibiotics. After overnight incubation *Stm* liquid cultures were diluted 1:33 and cultured for an additional 3-4 hours while plate grown *Stm* was suspended in PBS by rinsing the agar plates. Bacterial density was determined by measuring the OD_{600} and the bacterial suspension was diluted in cell culture medium without antibiotics to reach a multiplicity of infection (MOI) of 10 (unless indicated otherwise). Accuracy of bacterial density measurements was verified by a standard colony forming unit (CFU) assay. Cell cultures (HeLa for *Stm* infections and MelJuSo for *Mtb* infections), seeded in 96-well flat-bottom plates as described below, were inoculated with 100 µl of the bacterial suspension, centrifuged for 3 minutes at 800 rpm and incubated at 37°C/5% CO_2 for 20 minutes if infected with *Stm* or 60 minutes if infected with *Mtb*. Plates were then washed with culture medium containing 30 µg/ml gentamicin sulfate (Lonza BioWhittaker, Basel, Switzerland) and incubated at 37°C and 5% CO_2 in medium containing 5 µg/ml gentamicin and indicated chemical compounds until readout by flow cytometry or CFU, as indicated.

Chemical compound treatment

10,000 HeLa or MelJuSo cells were seeded per well in 96-well flat-bottom plates or 300,000 primary Mϕs were seeded per well in 24-well plates in appropriate culture medium without antibiotics one day prior to infection with *Mtb* or broth-grown *Stm*. Infected cells were treated overnight with chemical compounds at 10 µM (unless indicated otherwise) or DMSO at equal v/v in medium containing 5 µg/ml gentamicin.

siRNA transfections

3,000 HeLa or MelJuSo cells were reverse-transfected with ON-TARGETplus siRNA pools (Thermo Fisher Dharmacon, Waltham Massachusetts, USA) at a 50 nM concentration using 0.2 µl Dharmafect1 (Thermo Fisher Dharmacon) per well in a flat-bottom 96-well plate in appropriate culture medium without antibiotics. Cells transfected with siRNA were infected with *Mtb* at MOI 1000 24 hours post transfection and incubated for an additional 48 hours and infections with agar-grown *Stm* were carried out at MOI 500 72 hours post transfection and incubated overnight, unless indicated otherwise.

Colony forming unit assay

CFU assays were performed using the track dilution method described previously[69]. In short, bacterial suspensions were serially diluted and 10 µl drops were plated on square agar plates, which were subsequently placed at an angle to allow the drops to spread over a larger surface area.

Bacterial growth assay

100 µl *Stm* or *Mtb* culture (OD_{600} of 0.1) was plated in a flat-bottom 96-well plate containing 100 µl of indicated chemical compounds at 20 µM in LB (*Stm*) or 7H9 (*Mtb*) broth. The plate was incubated at 37°C overnight for *Stm* or during a period of 15 days for *Mtb* and absorbance was measured at a 550 nm wavelength on a Mithras LB 940 plate reader (Berthold Technologies, Bad Wildbad, Germany).

Compound identification within the PubChem repository and retrieval of BioAssay data

Structure-data format (SDF) data supplied with the LOPAC library was converted to InChIKey using the OpenBabel toolbox (http://www.openbabel.org). InChIKeys were subsequently mapped to PubChem IDs and correct identification was checked manually. Compounds were manually linked to PubChem IDs if InChIKey information was insufficient for automated identification. For each of the identified compounds, BioAssay data was retrieved from the PubChem repository (as of July 25th, 2014). Human protein targets for which compounds were confirmed to be active were then extracted from the BioAssay data. Compounds were subsequently described with their confirmed protein targets, as well as z-scores for bacterial load and cell viability from the primary screening data. All remaining compounds in the PubChem repository that were not included in the LOPAC library were described with their confirmed protein targets as above. Compounds that were not confirmed to target any of the protein targets identified for the LOPAC compounds were excluded from analysis and the remaining compounds were used as a testing set for the predictive model.

Predictive model

Using LOPAC compounds as a training set, BioAssay data obtained from PubChem (descriptive variables) were related to the z-scores for bacterial load and cell viability from the primary screening data (target variables) using the predictive modelling approach of multi-target regression to simultaneously predict both target variables. Predictive models were constructed within the predictive clustering framework[35,36], using predictive clustering trees (PCTs) as predictive models for multi-target regression. Ensembles of predictive clustering trees were generated[37,38] using the Bagging ensemble learning method[70,71] as implemented in the data mining tool CLUS (http://clus.sourceforge.net). Multiple predictive models were constructed using different bootstrap samples of the training dataset and their predictions were averaged to obtain an overall prediction. The variance of the predictions for the two target variables across the models in the ensemble was calculated for each target variable separately, averaged between the two targets and then used as a reliability estimation score[72].

STRING analysis

Protein interaction networks were generated using STRING version 10 (http://string-db.org/)[73] using experiments and databases as data sources and a minimal confidence score of 0.4.

Statistics

Student's T-test, one-way ANOVA and linear regression were performed using GraphPad Prism version 6.0 for Mac OS X (GraphPad Software, San Diego California, USA; www.graphpad.com). Z' factors were calculated using the formula $Z' = \frac{\left(AVG_{DMSO} - \frac{3SD_{DMSO}}{\sqrt{n}}\right) - \left(AVG_{H\text{-}89} + \frac{3SD_{H\text{-}89}}{\sqrt{n}}\right)}{AVG_{DMSO} - AVG_{H\text{-}89}}$, where AVG is the average percentage of DsRed positive events measured after DMSO or H-89 treatment, SD is the standard deviation of these measurements and n is the number of replicates (as in **Chapter 2**). Z-scores were calculated using the formula $z = \frac{x - AVG_{DMSO}}{STDEV_{DMSO}}$, where the difference between the percentage of DsRed positive events (bacterial load) or the total event count (cell viability) of a single replicate of an experimental condition (x) and the average percentage of DsRed positive events or the total event count of the DMSO control (AVG_{DMSO}) is divided by the standard deviation of the DMSO control ($STDEV_{DMSO}$). Z-scores for the primary screens were calculated using a similar formula, where the average percentage of fluorescent events and the standard deviation of all samples on each plate (instead of the DMSO control) were used (to provide plate normalization). The average DMSO z-score was then subtracted from each sample. An average z-score ≤ -2 or ≥ 2 was used as a hit cut-off, unless otherwise indicated.

Data availability

The data that support the findings of this study are available from the corresponding authors upon request.

Code availability

The code of the machine learning software CLUS that was used to build the in-silico models for predicting compound activity is available for download from the SourceForge repository (at https://sourceforge.net/projects/clus/).

Supplementary Information: Development and use of an *in silico* model for predicting compound activity.

Machine learning in a nutshell.

Machine learning studies computer programs/algorithms that have the ability to learn (improve with experience) where the experience is given in the form of data examples (instances). The input to a typical machine learning algorithm is a single flat table comprising a number of records (rows) and attributes (columns). In general, each row represents an object and columns represent properties of objects{Dzeroski:2001di}. An excerpt of the data table that we used to learn a predictive model is given in **Supplementary Table 1**. Here, rows correspond to individual compounds and columns contain different properties of these compounds, including bioactivity profiles retrieved from PubChem, intracellular

Supplementary Table 1. Excerpt from the data table for the *Mtb* screen used to learn the predictive models.

	Descriptive/Input space (PubChem BioAssay accession)					Target/Output space	
PubChem ID	gi: 10864009	gi: 10880131	gi: 10937869	gi: 112938	...	Bacterial load z-score	Cell viability z-score
ID1	1[a]	0	0	1	...	-2.61	0.29
ID2	0	0	0	1	...	-1.57	-0.43
ID3	0	0	0	0	...	0.47	0.22
ID4	0	0	1	0	...	-0.83	-0.13
ID5	1	1	0	0	...	-2.58	-0.53
ID6	0	1	0	0	...	1.78	0.97
...	...	...	...	...	...	...	...

[a] **'1' indicates that the compound has the corresponding protein as a confirmed target in a PubChem BioAssay.**

bacterial survival z-scores and host cell viability z-scores. The task formulated here is to predict the intracellular bacterial survival and the host cell viability z-scores for a novel compound using the information from its PubChem bioactivity profile. In machine learning terminology, this translates into a predictive modelling task (or supervised learning) where the two z-scores are called target (or output or dependent) variables/attributes and the variables describing the bioactivity profile are called descriptive (or input or independent) variables/attributes. Furthermore, considering that there are two numeric target variables, the task at hand is called multi-target regression[74]. This is illustrated in the data excerpt in **Supplementary Table 1**. The output of a data mining algorithm is typically a predictive model (or a set of predictive models) valid for the given data. The dataset used to learn the models is usually called training dataset. The model can then be applied to a different set of data, usually called testing dataset.

Data pre-processing

In this study, the training set of compounds consisted of our reference compound H-89 and the LOPAC library compounds that were screened in our HeLa-*Stm* and MelJuSo-*Mtb* infection models, while the testing set consisted of all other compounds available in the PubChem public repository. We performed separate analyses on the *Mtb* and *Stm* datasets, but the pre-processing of the data and the data analysis were performed following identical procedures. A schematic overview of the complete pre-processing pipeline is displayed in **Supplementary Figure 1A**.

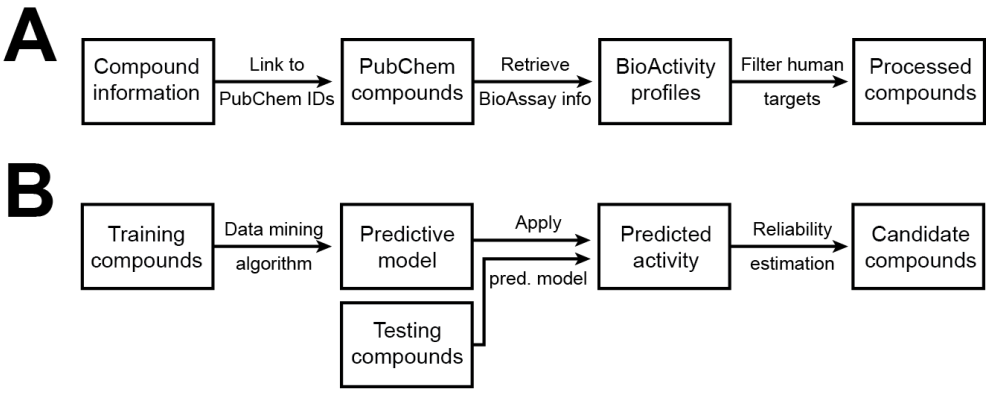

⬆ Supplementary Figure 1. Data pre-processing pipeline.

A. Pre-processing pipeline used to link compounds described by structured-data files to compounds in the PubChem database of compounds. **B.** Data analysis pipeline from the pre-processed compounds to the new candidate compounds for wet-lab experiments.

The first step of the data pre-processing was to uniquely identify the LOPAC compounds by linking them to their corresponding PubChem IDs. Based on the structure-data format (SDF) information provided by the compound supplier, we linked the LOPAC compounds to compounds from PubChem. To this end, SDF information of the compounds was first converted into InChIKey using the OpenBabel toolbox (http://www.openbabel.org) and then mapped to PubChem IDs. Next, we manually checked whether the mapping was correct and provided manual mapping where the InChIKey information was not sufficient, obtaining a list of PubChem compounds that were used in our study. Next, biological activity information was retrieved for the LOPAC compounds from each compounds' 'bioassays' section in PubChem. From the bioassays, only human protein targets for which compounds were confirmed to be active were extracted, yielding a total of 1058 protein targets. This resulted in the columns on the left-hand side of **Supplementary Table 1** (the descriptive variables). At the end of the pre-processing pipeline, each compound is described with both its protein targets (as descriptive attributes for machine learning) and experimental measurements of activity and viability (as target attributes for the machine learning). These compound descriptions comprise our training set. Finally, we considered all of the remaining compounds from PubChem as potential candidates for drug repurposing (**Supplementary Figure 1A**). We applied the pre-processing pipeline on each of these compounds as described above. Only compounds confirmed to target at least one of the 1058 human target proteins were included, thus obtaining a testing set of 460,580 compounds. Note that the compounds from the testing set have information only for the bioactivity profiles (the descriptive attributes), while the intracellular bacterial survival and host cell viability z-scores are not known but the goal is to predict these. We obtained these predictions by applying the predictive model (predictive clustering tree) learned from the training

data to each of the compounds from the testing set, as described in more detail below.

Predictive clustering trees

To analyze the data and learn a predictive model, we used the machine learning tool CLUS (available at http://clus.sourceforge.net). Specifically, we used predictive clustering trees (PCTs) for multi-target regression as models[74,75]. PCTs are a generalization of regression trees, a machine learning approach commonly used for regression. An example PCT is shown in **Supplementary Figure 2**. Similar to regression trees, PCTs are tree-like structures that have internal nodes and leaves. The internal nodes contain tests on the descriptive variables (i.e. asking whether a given protein is targeted or not), while leaves give predictions for the target variables (the predicted z-scores for intracellular bacterial survival and host cell viability). We opted to use PCTs because they are able to implicitly exploit

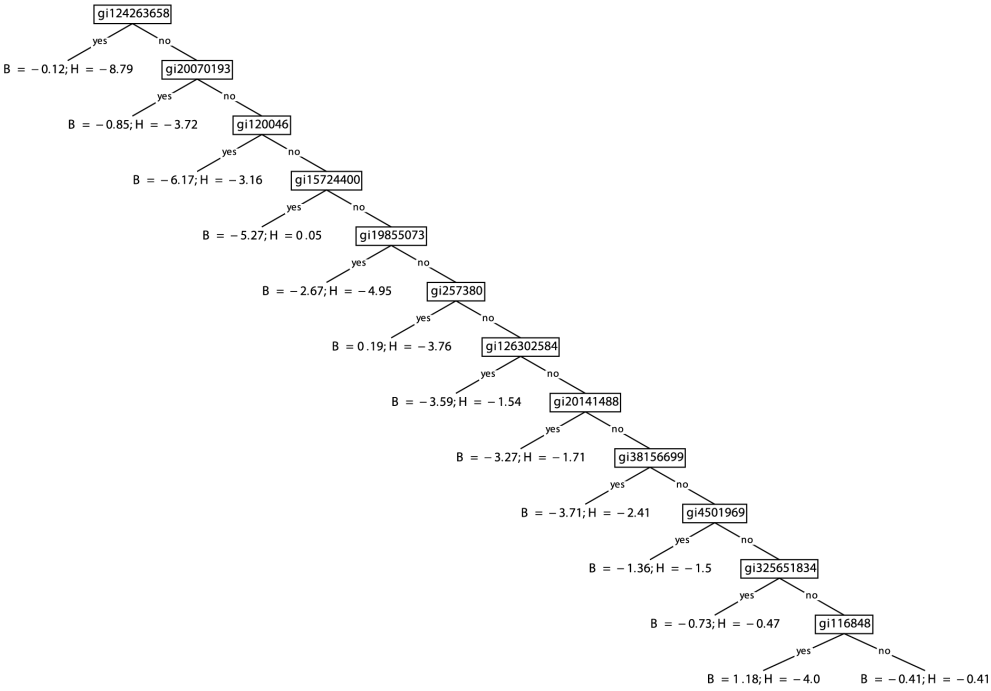

⬆ Supplementary Figure 2. Example predictive clustering tree.

Example predictive clustering tree (PCT) obtained from the screening data for *Mtb*. The internal nodes of the tree refer to the descriptive variables and check whether or not a compound targets a given protein. The leaves then give the predictions for the intracellular bacterial survival and the host cell viability z-scores. For example, compounds that target *gi15724400*, but not *gi14263638*, *gi20070193* or *gi120046*, are predicted to drastically reduce bacterial load (z-score of -5.27) and not affect cell viability (z-score of 0.05).

the relation between the target variables during model construction. Furthermore, PCTs are easily interpretable. A PCT can be viewed as a hierarchy of clusters with each node corresponding to a cluster. The top-node of a PCT corresponds to one cluster (group) containing all data points. This cluster is recursively partitioned into smaller clusters while moving down the tree. The leaves represent the clusters at the lowest level of the hierarchy and each leaf is labeled with its cluster's centroid/ prototype (the averages of the target variables are the prediction made by the leaf).

PCTs are built with a greedy recursive top-down induction algorithm. This learning algorithm starts by selecting a test for the root node by using a heuristic function computed on the training examples. The goal of the heuristic is to guide the algorithm towards small trees with good predictive performance. Based on the selected test, the training set is partitioned into subsets according to the test outcome. This is recursively repeated to construct the subtrees. The partitioning process stops when a stopping criterion is satisfied (i.e. the minimal number of examples per leaf is reached or the heuristic score no longer changes). In that case, the prototype (the prediction) is calculated as the averages of the target variables and stored in a leaf.

Ensembles of PCTs

An ensemble is a set of predictive models (called base models). The prediction of an ensemble for a new example is obtained by combining the predictions of all base models from the ensemble. These predictions can be combined by averaging them. The ensemble learning procedure is illustrated in **Supplementary Figure 3**. Here, we consider ensembles of PCTs for multi-target regression[74]. For constructing the base models, we used the Bagging method[76]. Bagging is an ensemble method that constructs the base models in the ensemble by making bootstrap samples (E_i) of the training set (also called bootstrap replicates) and using each of these replicates to construct a predictive model. Each bootstrap sample is obtained by randomly sampling training instances, with replacement, from the original training set, until an equal number of instances as in the training set is obtained.

Reliability scores

A very important aspect of using a predictive model is the ability to estimate the reliability of the predictions it makes. This reliability indicates how confident the model is about its prediction. Ensembles offer a natural way of estimating the reliability of their predictions by exploiting their voting mechanism[77]. When a prediction is made for an unlabeled example (these are examples that do not have z-score values for intracellular bacterial survival and host cell viability) by an ensemble, we consider it reliable if the predictions of the individual models in the ensemble are coherent, i.e., if the variance of the predictions is low. Here, we get the reliability score for a prediction of two targets by averaging the variances of the predictions for each of the two targets (the variances of the predicted z-scores for intracellular bacterial survival and host cell viability).

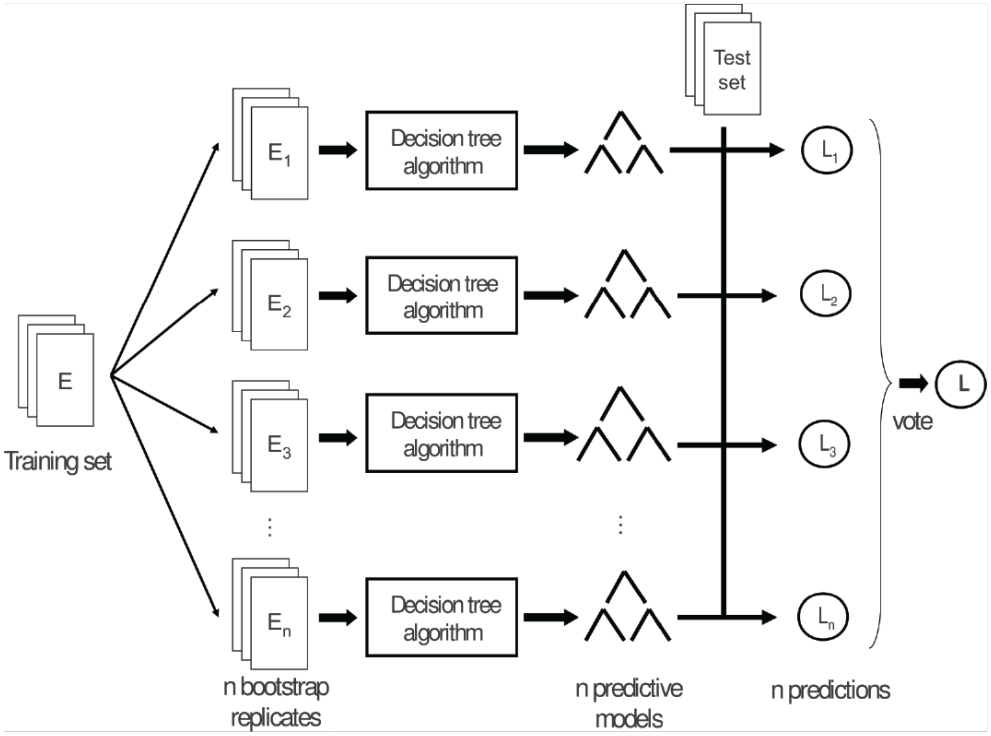

⬆ Supplementary Figure 3. Illustration of the ensemble learning method of bagging.
From the training set of examples E, n bootstrap samples are created (E_1, E_2, ..., E_n). Predictive models are then constructed (using a tree construction algorithm) on each of the n replicates. The predictions of the base predictive models (L_1, L_2... L_n) are combined by a voting (averaging) scheme into the final prediction (L) of the ensemble.

Data analysis workflow

To identify candidate compounds in the set of testing compounds to screen in our MelJuSo-*Mtb* or HeLa-*Stm* infection models, we followed the data analysis workflow outlined in **Supplementary Figure 1B**. First, we used the training dataset to construct a predictive model (a PCT) using a data-mining algorithm (the PCT algorithm). Next, the predictive model was applied to the testing set to obtain the predictions for the activity of the compounds, expressed as z-scores. Finally, we calculated a reliability score for each prediction for a test compound.

This data analysis workflow resulted in a small set of selected candidate compounds from all of the 460,580 compounds in the testing set. Predicted *Mtb* hits were defined as compounds with a predicted intracellular bacterial survival z-score below -2 and a host cell viability z-score between -1 and 1 with a prediction reliability greater than 0.5, or an intracellular bacterial survival z-score below -1.75,

a host cell viability z-score between -0.75 and 0.75 and a prediction reliability higher than 0.75. This yielded a total of 47 candidate compounds (**Table 4**). Predicted *Stm* hits were defined as compounds with a predicted intracellular bacterial survival z-score below -2, a host cell viability z-score between -1 and 1 and a prediction reliability greater than 0.5 or an intracellular bacterial survival z-score below -1.5, a host cell viability z-score between -0.75 and 0.75 and a prediction reliability higher than 0.5. This yielded a total of 30 candidate compounds (**Table 5**). From the resulting lists of predicted hits, compounds were then selected for further experiments based on their commercial availability.

References

1. Diedrich, C. R. & Flynn, J. L. HIV-1/mycobacterium tuberculosis coinfection immunology: how does HIV-1 exacerbate tuberculosis? *Infection and Immunity* **79,** 1407–1417 (2011).
2. Ottenhoff, T. H. M. The knowns and unknowns of the immunopathogenesis of tuberculosis. *Int. J. Tuberc. Lung Dis.* **16,** 1424–1432 (2012).
3. World Health Organization. *Global tuberculosis report 2015*. (2015).
4. Ottenhoff, T. H. M. Overcoming the global crisis: 'yes, we can', but also for TB ... ? *Eur. J. Immunol.* **39,** 2014–2020 (2009).
5. Jassal, M. S. & Bishai, W. R. Epidemiology and challenges to the elimination of global tuberculosis. *CLIN INFECT DIS* **50 Suppl 3,** S156–64 (2010).
6. Ottenhoff, T. H. M. New pathways of protective and pathological host defense to mycobacteria. *Trends Microbiol.* **20,** 419–428 (2012).
7. Barry, C. E. & Blanchard, J. S. The chemical biology of new drugs in the development for tuberculosis. *Curr Opin Chem Biol* **14,** 456–466 (2010).
8. Norrby, S. R., Nord, C. E., Finch, R.European Society of Clinical Microbiology and Infectious Diseases. Lack of development of new antimicrobial drugs: a potential serious threat to public health. *Lancet Infect Dis* **5,** 115–119 (2005).
9. Becker, D. *et al.* Robust Salmonella metabolism limits possibilities for new antimicrobials. **440,** 303–307 (2006).
10. Makarov, V. *et al.* Benzothiazinones kill Mycobacterium tuberculosis by blocking arabinan synthesis. *Science* **324,** 801–804 (2009).
11. Christophe, T. *et al.* High content screening identifies decaprenyl-phosphoribose 2' epimerase as a target for intracellular antimycobacterial inhibitors. *PLoS Pathog* **5,** e1000645 (2009).
12. Willand, N. *et al.* Synthetic EthR inhibitors boost antituberculous activity of ethionamide. *Nat. Med.* **15,** 537–544 (2009).
13. Lawn, S. D. & Zumla, A. I. Tuberculosis. *Lancet* **378,** 57–72 (2011).
14. Guler, R. & Brombacher, F. Host-directed drug therapy for tuberculosis. *Nature Chemical Biology* **11,** 748–751 (2015).

15. Hawn, T. R., Shah, J. A. & Kalman, D. New tricks for old dogs: countering antibiotic resistance in tuberculosis with host-directed therapeutics. *Immunol. Rev.* **264,** 344–362 (2015).
16. Kuijl, C. *et al.* Intracellular bacterial growth is controlled by a kinase network around PKB/AKT1. **450,** 725–730 (2007).
17. Kumar, D. *et al.* Genome-wide analysis of the host intracellular network that regulates survival of Mycobacterium tuberculosis. *Cell* **140,** 731–743 (2010).
18. Jayaswal, S. *et al.* Identification of host-dependent survival factors for intracellular Mycobacterium tuberculosis through an siRNA screen. *PLoS Pathog* **6,** e1000839 (2010).
19. Sundaramurthy, V. *et al.* Integration of chemical and RNAi multiparametric profiles identifies triggers of intracellular mycobacterial killing. *Cell Host and Microbe* **13,** 129–142 (2013).
20. Machado, D. *et al.* Ion Channel Blockers as Antimicrobial Agents, Efflux Inhibitors, and Enhancers of Macrophage Killing Activity against Drug Resistant Mycobacterium tuberculosis. *PLoS ONE* **11,** e0149326 (2016).
21. Napier, R. J. *et al.* Imatinib-sensitive tyrosine kinases regulate mycobacterial pathogenesis and represent therapeutic targets against tuberculosis. *Cell Host and Microbe* **10,** 475–485 (2011).
22. Subbian, S. *et al.* Phosphodiesterase-4 inhibition alters gene expression and improves isoniazid-mediated clearance of Mycobacterium tuberculosis in rabbit lungs. *PLoS Pathog* **7,** e1002262 (2011).
23. Subbian, S. *et al.* Phosphodiesterase-4 inhibition combined with isoniazid treatment of rabbits with pulmonary tuberculosis reduces macrophage activation and lung pathology. *Am. J. Pathol.* **179,** 289–301 (2011).
24. Koo, M.-S. *et al.* Phosphodiesterase 4 inhibition reduces innate immunity and improves isoniazid clearance of Mycobacterium tuberculosis in the lungs of infected mice. *PLoS ONE* **6,** e17091 (2011).
25. Vilaplana, C. *et al.* Ibuprofen therapy resulted in significantly decreased tissue bacillary loads and increased survival in a new murine experimental model of active tuberculosis. *Journal of Infectious Diseases* **208,** 199–202 (2013).
26. Mayer-Barber, K. D. *et al.* Host-directed therapy of tuberculosis based on interleukin-1 and type I interferon crosstalk. **511,** 99–103 (2014).
27. Datta, M. *et al.* Anti-vascular endothelial growth factor treatment normalizes tuberculosis granuloma vasculature and improves small molecule delivery. *Proc Natl Acad Sci USA* **112,** 1827–1832 (2015).
28. Oehlers, S. H. *et al.* Interception of host angiogenic signalling limits mycobacterial growth. **517,** 612–615 (2015).
29. Schiebler, M. *et al.* Functional drug screening reveals anticonvulsants as enhancers of mTOR-independent autophagic killing of Mycobacterium tuberculosis through inositol depletion. *EMBO Molecular Medicine* **7,** 127–139 (2015).
30. Skerry, C. *et al.* Simvastatin increases the in vivo activity of the first-line tuberculosis regimen. *J. Antimicrob. Chemother.* **69,** 2453–2457 (2014).

31. Stanley, S. A. *et al.* Identification of host-targeted small molecules that restrict intracellular Mycobacterium tuberculosis growth. *PLoS Pathog* **10,** e1003946 (2014).
32. Vergne, I., Chua, J., Singh, S. B. & Deretic, V. Cell biology of mycobacterium tuberculosis phagosome. *Annu. Rev. Cell Dev. Biol.* **20,** 367–394 (2004).
33. Brumell, J. H. & Grinstein, S. Salmonella redirects phagosomal maturation. *Current Opinion in Microbiology* **7,** 78–84 (2004).
34. Singhal, A. *et al.* Metformin as adjunct antituberculosis therapy. *Science Translational Medicine* **6,** 263ra159–263ra159 (2014).
35. Coussens, A. K., Wilkinson, R. J. & Martineau, A. R. Phenylbutyrate Is Bacteriostatic against Mycobacterium tuberculosis and Regulates the Macrophage Response to Infection, Synergistically with 25-Hydroxy-Vitamin D3. *PLoS Pathog* **11,** e1005007 (2015).
36. Mily, A. *et al.* Significant Effects of Oral Phenylbutyrate and Vitamin D3 Adjunctive Therapy in Pulmonary Tuberculosis: A Randomized Controlled Trial. *PLoS ONE* **10,** e0138340 (2015).
37. Mehrotra, P. *et al.* Pathogenicity of Mycobacterium tuberculosis is expressed by regulating metabolic thresholds of the host macrophage. *PLoS Pathog* **10,** e1004265 (2014).
38. Kaufmann, S. H. E., Dorhoi, A., Hotchkiss, R. S. & Bartenschlager, R. Host-directed therapies for bacterial and viral infections. *Nat Rev Drug Discov* (2017). doi:10.1038/nrd.2017.162
39. Verreck, F. A. W. *et al.* Human IL-23-producing type 1 macrophages promote but IL-10-producing type 2 macrophages subvert immunity to (myco)bacteria. *Proc. Natl. Acad. Sci. U.S.A.* **101,** 4560–4565 (2004).
40. Howard, S. *et al.* Fragment-based discovery of the pyrazol-4-yl urea (AT9283), a multitargeted kinase inhibitor with potent aurora kinase activity. *J. Med. Chem.* **52,** 379–388 (2009).
41. Tentler, J. J. *et al.* Assessment of the in vivo antitumor effects of ENMD-2076, a novel multitargeted kinase inhibitor, against primary and cell line-derived human colorectal cancer xenograft models. *Clinical Cancer Research* **16,** 2989–2998 (2010).
42. Trudel, S. *et al.* CHIR-258, a novel, multitargeted tyrosine kinase inhibitor for the potential treatment of t(4;14) multiple myeloma. *Blood* **105,** 2941–2948 (2005).
43. Kanehisa, M., Furumichi, M., Tanabe, M., Sato, Y. & Morishima, K. KEGG: new perspectives on genomes, pathways, diseases and drugs. *Nucleic Acids Res.* **45,** D353–D361 (2017).
44. Lemmon, M. A. & Schlessinger, J. Cell signaling by receptor tyrosine kinases. *Cell* **141,** 1117–1134 (2010).
45. Levitzki, A. & Gazit, A. Tyrosine kinase inhibition: an approach to drug development. *Science* **267,** 1782–1788 (1995).
46. Varga, E. V. *et al.* Involvement of Raf-1 in chronic delta-opioid receptor agonist-mediated adenylyl cyclase superactivation. *Eur. J. Pharmacol.* **451,** 101–102 (2002).

47. Cicha, I., Zitzmann, R. & Goppelt-Struebe, M. Dual inhibition of Src family kinases and Aurora kinases by SU6656 modulates CTGF (connective tissue growth factor) expression in an ERK-dependent manner. *Int. J. Biochem. Cell Biol.* **46,** 39–48 (2014).
48. Coghlan, M. P. *et al.* Selective small molecule inhibitors of glycogen synthase kinase-3 modulate glycogen metabolism and gene transcription. *Chem. Biol.* **7,** 793–803 (2000).
49. Al-Bari, M. A. A. Chloroquine analogues in drug discovery: new directions of uses, mechanisms of actions and toxic manifestations from malaria to multifarious diseases. *J. Antimicrob. Chemother.* **70,** 1608–1621 (2015).
50. Ehsanian, R., Van Waes, C. & Feller, S. M. Beyond DNA binding - a review of the potential mechanisms mediating quinacrine's therapeutic activities in parasitic infections, inflammation, and cancers. *Cell Commun. Signal* **9,** 13 (2011).
51. Lako, I. M., van den Heuvel, E. R., Knegtering, H., Bruggeman, R. & Taxis, K. Estimating dopamine D_2 receptor occupancy for doses of 8 antipsychotics: a meta-analysis. *J Clin Psychopharmacol* **33,** 675–681 (2013).
52. Blaustein, M. P. & Lederer, W. J. Sodium/calcium exchange: its physiological implications. *Physiol. Rev.* **79,** 763–854 (1999).
53. Jayachandran, R. *et al.* Survival of mycobacteria in macrophages is mediated by coronin 1-dependent activation of calcineurin. *Cell* **130,** 37–50 (2007).
54. Osterrieder, W. & Holck, M. In vitro pharmacologic profile of Ro 40-5967, a novel Ca2+ channel blocker with potent vasodilator but weak inotropic action. *J. Cardiovasc. Pharmacol.* **13,** 754–759 (1989).
55. Gaumann, A. K. A. *et al.* Receptor tyrosine kinase inhibitors: Are they real tumor killers? *Int. J. Cancer* **138,** 540–554 (2016).
56. Hay, A. E. *et al.* A phase II study of AT9283, an aurora kinase inhibitor, in patients with relapsed or refractory multiple myeloma: NCIC clinical trials group IND.191. *Leuk. Lymphoma* **57,** 1463–1466 (2016).
57. Moreno, L. *et al.* A phase I trial of AT9283 (a selective inhibitor of aurora kinases) in children and adolescents with solid tumors: a Cancer Research UK study. *Clinical Cancer Research* **21,** 267–273 (2015).
58. Schäfer, N. *et al.* Phase I trial of dovitinib (TKI258) in recurrent glioblastoma. *J. Cancer Res. Clin. Oncol.* **142,** 1581–1589 (2016).
59. Cheng, A.-L. *et al.* Randomized, Open-Label Phase 2 Study Comparing Frontline Dovitinib vs Sorafenib in Patients With Advanced Hepatocellular Carcinoma. *Hepatology* (2016). doi:10.1002/hep.28600
60. Lim, S. H. *et al.* Efficacy and safety of dovitinib in pretreated patients with advanced squamous non-small cell lung cancer with FGFR1 amplification: A single-arm, phase 2 study. *Cancer* (2016). doi:10.1002/cncr.30135
61. Yee, K. W. L. *et al.* A phase I trial of the aurora kinase inhibitor, ENMD-2076, in patients with relapsed or refractory acute myeloid leukemia or chronic myelomonocytic leukemia. *Invest New Drugs* (2016). doi: 10.1007/s10637-016-0375-2

62. Gauld, S. B. & Cambier, J. C. Src-family kinases in B-cell development and signaling. *Oncogene* **23,** 8001–8006 (2004).
63. Borowiec, M. *et al.* Mutations at the BLK locus linked to maturity onset diabetes of the young and beta-cell dysfunction. *Proc Natl Acad Sci USA* **106,** 14460–14465 (2009).
64. Skaper, S. D. The biology of neurotrophins, signalling pathways, and functional peptide mimetics of neurotrophins and their receptors. *CNS Neurol Disord Drug Targets* **7,** 46–62 (2008).
65. Aloe, L., Rocco, M. L., Bianchi, P. & Manni, L. Nerve growth factor: from the early discoveries to the potential clinical use. *J Transl Med* **10,** 239 (2012).
66. Ehrhard, P. B., Ganter, U., Stalder, A., Bauer, J. & Otten, U. Expression of functional trk protooncogene in human monocytes. *Proc. Natl. Acad. Sci. U.S.A.* **90,** 5423–5427 (1993).
67. Maurice, T. & Su, T.-P. The pharmacology of sigma-1 receptors. *Pharmacol. Ther.* **124,** 195–206 (2009).
68. Verreck, F. A. W., de Boer, T., Langenberg, D. M. L., van der Zanden, L. & Ottenhoff, T. H. M. Phenotypic and functional profiling of human proinflammatory type-1 and anti-inflammatory type-2 macrophages in response to microbial antigens and IFN-gamma- and CD40L-mediated costimulation. *Journal of Leukocyte Biology* **79,** 285–293 (2006).
69. Jett, B. D., Hatter, K. L., Huycke, M. M. & Gilmore, M. S. Simplified agar plate method for quantifying viable bacteria. *BioTechniques* **23,** 648–650 (1997).
70. Liu, W. S. & Heckman, C. A. The sevenfold way of PKC regulation. *Cell. Signal.* **10,** 529–542 (1998).
71. Wu-zhang, A. X. & Newton, A. C. Protein kinase C pharmacology: refining the toolbox. *Biochem. J.* **452,** 195–209 (2013).
72. Le Poole, I. C. *et al.* Phagocytosis by normal human melanocytes in vitro. *Exp. Cell Res.* **205,** 388–395 (1993).
73. Szklarczyk, D. *et al.* STRING v10: protein-protein interaction networks, integrated over the tree of life. *Nucleic Acids Res.* **43,** D447–52 (2015).
74. Kocev, D., Vens, C., Struyf, J. & Džeroski, S. Tree ensembles for predicting structured outputs. *Pattern Recognition* (2013).
75. Blockeel, H., De Raedt, L. & Ramon, J. Top-down induction of clustering trees. *ICML Proceedings of the Fifteenth International Conference on Machine Learning* 55–63 (1998).
76. Breiman, L. Bagging predictors. *Machine learning* (1996).
77. Levatić, J., Ceci, M., Kocev, D. & Džeroski, S. Self-training for multi-target regression with tree ensembles. *Knowledge-Based Systems* (2017). doi: 10.1016/j.knosys.2017.02.014

4 | Novel Host-Directed Chemical Compounds Inhibit Intracellular Bacteria by Targeting PCTAIRE Kinases

Cornelis J. Korbee*, Matthias T. Heemskerk*, Kimberley V. Walburg, Rian van den Nieuwendijk, Elisabeth van Strijen, Coenraad Kuijl, Conrad Schreuders, Janneke Eken, Nigel D.L Savage, Jacques J. Neefjes, Hermen S. Overkleeft, Tom H. M. Ottenhoff**, Mariëlle C. Haks**

Rapidly increasing drug-resistance poses severe problems in combatting many bacterial infectious diseases, including tuberculosis (TB) and *Salmonella* infections. Recent attempts to identify novel antibiotics have yielded only limited numbers of leads, prompting for novel approaches, including host-directed therapies. Intracellular pathogens like *Mycobacterium tuberculosis* (*Mtb*) and *Salmonellae* manipulate host signaling networks to promote their survival, but very few host targets and chemical compounds have been identified for host-directed therapies. Using a chemical genetic approach focused on a novel, proprietary library of chemical compounds derived from the host-directed inhibitor of intracellular bacteria H-89, we here identify novel kinase inhibitor 97i as a host-directed inhibitor of intracellular *Mtb* and *Salmonella* typhimurium (*Stm*). 97i Strongly inhibited both (MDR-)*Mtb* and *Stm* infection in human (phagocytic) cell lines and in primary Mϕ1 and Mϕ2 macrophages. Importantly, we identify the PCTAIRE-family kinase CDK18 as a novel host factor controlling intracellular *Stm*, and as a direct target of 97i. Together, these results identify PCTAIRE kinases as novel putative target molecules for host-directed therapies (HDT) and 97i as a strong basis for HDT drug development for intracellular bacterial infections.

Manuscript in preparation

* Contributed equally
** Contributed equally

Introduction

Tuberculosis (TB) remains a critical global health problem with an estimated one fourth of the world population carrying a latent *Mycobacterium tuberculosis* (*Mtb*) infection and 10.4 million new cases and 1.8 million deaths annually[1,2]. The emergence of multi-, extensively- and totally drug-resistant (MDR/XDR/TDR) strains of *Mtb* further aggravates this situation, threatening to render current antibiotics inadequate for future TB treatment[3-5]. An estimated 490,000 people were diagnosed with MDR-TB in 2016[2].

Salmonella enterica infections are major causes of morbidity and mortality worldwide as well, particularly *S. enterica* serovar Typhi (the causative agent of typhoid fever), which causes between 128,000 and 161,000 deaths annually (World Health Organization figures January 2018; http://www.who.int/news-room/fact-sheets/detail/typhoid). As with TB, antibiotic resistance is becoming an increasing problem for treatment of typhoid fever, prompting for novel approaches[6].

Several novel candidate antibiotics have recently been identified[7], but because current antibiotics already cover the majority of drugable targets of pathogens, it is increasingly difficult to discover new classes of antibiotics[8-14]. However, new drugs are urgently needed to combat the rapidly increasing global drug resistance for many human pathogens. Intracellular bacteria such as *Salmonellae* and *Mtb* present additional challenges to treatment and eradication by host defense mechanisms, as they are able to manipulate host-signaling networks to inhibit phagosome maturation, apoptosis, autophagy and MHC restricted antigen presentation to T cells, thereby subverting both innate and adaptive immunity. Better knowledge of the mechanisms that these and other intracellular pathogens deploy to escape host defense is critical to discover opportunities for novel therapies, including treatment strategies that target host rather than pathogen molecules (host-directed therapy; HDT). Importantly, chemical-genetic and pharmacological reprogramming of host immune functions may not only be effective against drug-resistant bacteria, but also help to restore host control of infected cells that are metabolically perturbed[15,16]. The feasibility of such HDT approaches to improve bacterial inhibition both *in vitro* in human cells and *in vivo* in mouse, rabbit and zebrafish models has recently been shown in several studies, including our own[17-34].

In one of the first studies in this area, we used reciprocal chemical-genetics focusing on systematic perturbation of the human kinome and identified AKT1 as a central molecule regulating intracellular survival of *Salmonella enterica* serovar Typhimurium *(Stm)* and *Mtb*, including MDR-*Mtb*[17]. We demonstrated that by targeting AKT1 the kinase inhibitor H-89 significantly decreased intracellular bacterial loads in human cell lines and in primary macrophages. However, compared to treatment of *Stm*-infected cells, inhibition of intracellular *Mtb* by H-89 was less efficient, suggesting that *Mtb* also modulates other host signaling pathways to subvert its intracellular killing that are not affected by H-89. Indeed, *Mtb* has been reported to arrest vesicle maturation at an earlier stage than *Stm*[17,35,36], such that other regulators of phagosome maturation, including kinases, may need to be targeted. In agreement with this notion, Kumar *et al*.

demonstrated that silencing of AKT1 alone was not sufficient to induce efficient killing of *Mtb*, and found that the combined knock-down of AKT1 and AKT2 resulted in a significant decrease in bacterial outgrowth[18]. Collectively, these studies suggest that in addition to AKT1, the perturbation of other host targets or combinations of host targets will be essential to efficiently inhibit intracellular *Mtb* by HDT, but the precise molecular host targets remain largely unknown.

Other kinases that may be involved in host-mediated inhibition of *Mtb* include Imatinib-sensitive kinases like ABL1 and ABL2, and enhanced control of *Mtb* could be achieved in Imatinib-treated mice[22]. Our most recent work used chemical genetic experimental and computational approaches, and uncovered receptor and non-receptor tyrosine kinase (RTK) signaling as a novel important host pathway controlling intracellular *Mtb* survival. This pathway was drugable by compounds and drugs currently in clinical trials for other diseases including Dovitinib, AT9283 and ENMD-2076, thus offering new approaches to combat TB in the face of rapidly rising multi-drug resistance[34]. In particular, inhibitors of growth factor receptor tyrosine kinases were identified in this study, corroborating other studies linking growth factor receptors like epidermal growth factor receptor (EGFR) and vascular endothelial growth factor receptor (VEGFR) and corresponding inhibitors like gefitinib and pazopanib to *Mtb* infection outcome[29,32,37].

In addition to kinases and kinase inhibitors, several other potential targets and compounds for HDT for TB were recently identified, ranging from immunomodulatory drugs to metabolic targets. Sundaramurthy *et al*. identified two antipsychotics (Haloperidol and Prochlorperazine) and an antidepressant (Nortryptiline) that displayed host-directed mycobacterial inhibition by enhancing phagocytic and autophagic macrophage responses[20]. Machado *et al*. identified the ion channel blockers Verapamil, Thioridazine, Chlorpromazine, Flupenthixol and Haloperidol as *Mtb*-inhibiting compounds that enhance efficacy of antibiotics by inhibiting efflux activity in the bacterium. Interestingly, these compounds also displayed host-mediated bacterial inhibition by enhancing phagosome acidification and upregulating lysosomal hydrolase activity[21]. Singhal *et al.* reported the anti-diabetic drug Metformin as a host-directed compound that inhibited *Mtb* by increasing production of mitochondrial reactive oxygen species and promoting phagosome-lysosome fusion[38].

Another challenge in TB therapy that may be overcome by HDT strategies is the limited antibiotics efficacy and their limited penetration in granulomas[28]. Similar to tumor treatment strategies, antiangiogenic treatment may decrease hypoxic fractions of granulomas and enhance drug penetration. Using anti-VEGF antibodies or inhibitors of the VEGF pathway were demonstrated to be a promising strategy to achieve this *in vitro* and in rabbit and zebrafish models[28,29,34]. In another report, Simvastatin was identified as a drug repurposing candidate for TB[31]. The authors reported that Simvastatin treatment both *in vitro* and *in vivo* greatly enhanced isoniazid efficacy, possibly by limiting access of *Mtb* to intracellular nutrient-rich lipid droplets.

Despite all these recent advances, HDT drug development for intracellular bacterial infections has not yet led to clinically applicable and efficacious drug regimens. A better understanding of the host-pathogen interactions and in

particular the molecular host targets which are critical to controlling intracellular infection is needed to rationally design or repurpose drugs that can be applied clinically.

In the current study we have explored the kinase inhibitor chemical space, using different chemical and functional infection biology approaches, and identified novel chemical compounds that are active in controlling intracellular bacterial infection. Structure-activity analysis of the compound library revealed a correlation between compounds' structural features and their ability to inhibit AKT1, which directly corresponded to their ability to inhibit intracellular *Stm*. However, no such correlation was observed when assessing the compounds' ability to inhibit intracellular *Mtb*, suggesting involvement of kinases other than AKT1 in host regulation of intracellular *Mtb*. Perhaps most importantly, the host-mediated antimicrobial activity induced by kinase inhibitor 97i greatly exceeded that of currently known HDT drug candidates. Finally, we demonstrate that the PCTAIRE kinase CDK18 is a target of 97i that is central to host control of intracellular *Stm* and possibly (MDR-)*Mtb.*

Results

H-89 treatment and AKT1 silencing efficiently decrease intracellular *Stm* bacterial loads but are less efficient against intracellular *Mtb*.

We previously identified AKT1 as a central regulator of *Stm* intracellular survival in primary human macrophages and the AKT1 inhibitor H-89 as a novel host-directed inhibitor of *Stm* and *Mtb*[17]. More recently we reported the development of a fast and versatile flow cytometry-based assay to allow for medium-throughput screening of chemical and genetic libraries in cell lines infected with *Stm* or *Mtb*[34]. As important validation data we first verified the bacterial inhibition resulting from AKT1 silencing and H-89 treatment in this new model, using *Stm* and *Mtb* human (phagocytic) cell line based infection models. Indeed, both H-89 treatment and AKT1 silencing significantly reduced the bacterial load in HeLa cells infected with *Stm* and in MelJuSo cells infected with *Mtb* H37Rv, lending important validation of our previous findings in macrophages as well as providing key validation of the model for further application in chemical genetic screens (**Figure 1**).

As previously also reported, the extent of the effect of H-89 treatment and AKT1 silencing was much less pronounced for *Mtb* than for *Stm* (**Figure 1**), indicating that host kinases other than those targeted by H-89 may be important in regulating *Mtb* intracellular survival. To identify these, we explored the kinase inhibitor chemical space by following a chemical genetic screening approach using a newly synthesized chemical compound library based on the H-89 backbone.

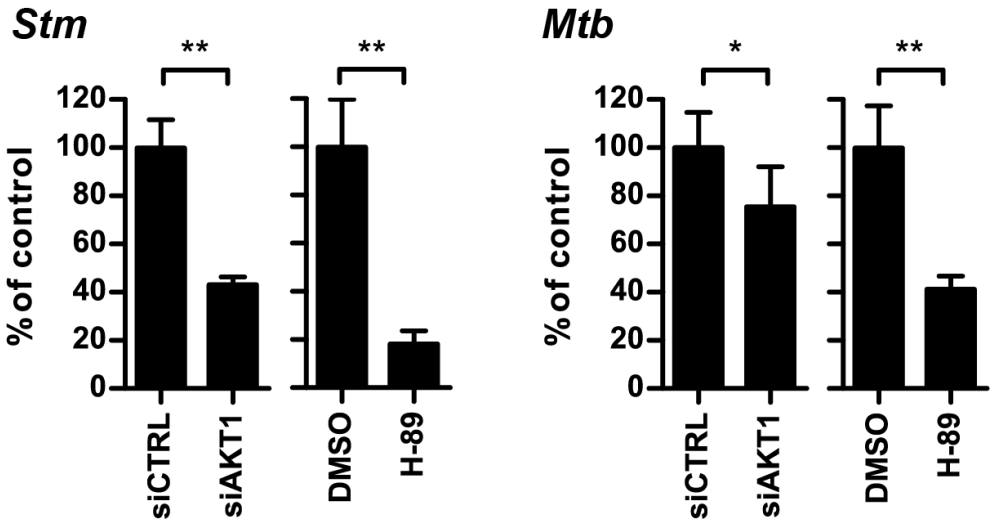

⬆ Figure 1. Inhibition or silencing of AKT1 decreases *Stm* and *Mtb* bacterial load.
AKT1 silencing by siRNA or treatment with 10 μM H-89 or DMSO at equal v/v in HeLa cells infected with *Stm* (left panel) or MelJuSo cells infected with *Mtb* (right panel). Bacterial load was determined by flow cytometry and is displayed as percentage of the appropriate negative control (DMSO for compounds and siCTRL for siRNA, respectively). Bars display mean ± standard deviation of 6 technical replicates. A representative result out of at least 10 experiments is shown. Statistical significance was tested using a t-test.
(* = p-value <0.05, ** = p-value <0.01).

Identification of novel kinase inhibitors with enhanced activity against *Mtb* and *Stm*.

We synthesized a novel library of 76 H-89-analogue compounds by systematically altering residues on 3 key positions at the styrene moiety of the chemical backbone of H-89 (**Figure 2**; synthesis described in "Synthetic studies on kinase inhibitors and cyclic peptides: strategies towards new antibiotics", Adriaan W. Tuin, 2008) and screened this library using our novel flow cytometry-based assay[34]. Using this assay, a population of *Stm*-infected cells with high fluorescence intensity (*Stm* 'bright') can be discerned, which is indicative of cells harboring proliferating bacteria. This population was found to be sensitive to H-89 treatment. In contrast, H-89 treatment did not affect the total fraction of *Stm*-infected cells (*Stm* total). Screening of the compound library yielded 5 compounds that reduced the *Stm* bacterial load (z-score ≤ -2) and no compounds that enhanced bacterial survival when analyzing the *Stm* 'bright' population (**Figure 3A, top panel**; z-score ≥ 2). In contrast, the total *Stm* infected population was decreased by 2 compounds (97a and 97i), while 8 compounds increased *Stm* total (**Figure 3A, middle panel**). In the MelJuSo-*Mtb* model, 36 compounds

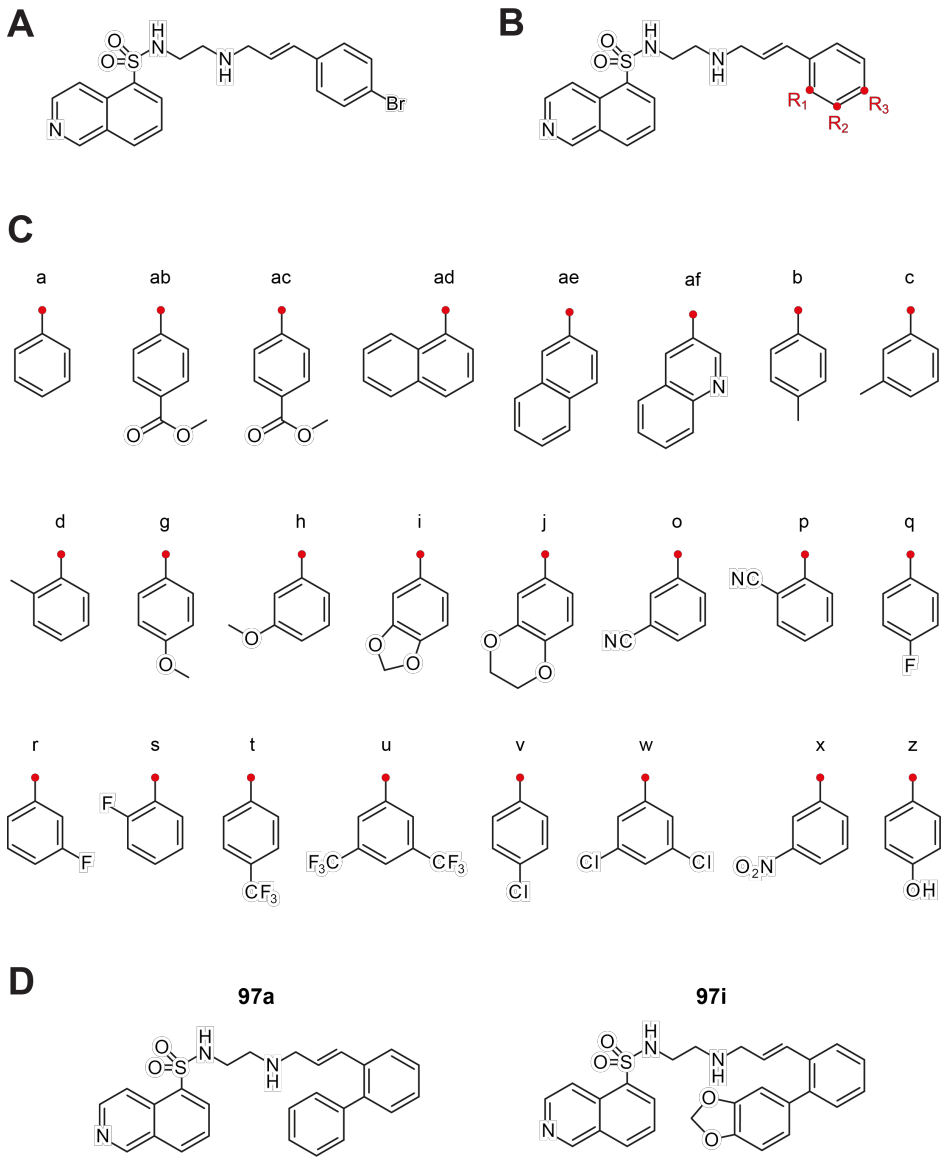

⬆ Figure 2. Construction of the H-89-based chemical library and structure of lead compounds.

A. Chemical structure of H-89. **B.** H-89-derived chemical backbone of the inhibitor library. Red nodes indicate the positions (R_1, R_2 and R_3) where chemical residues were attached to construct the library. **C.** Names and chemical structures of the residues attached to the chemical backbone on either the R_1, R_2 or R_3 positions. The red nodes correspond to the R_1, R_2 or R_3 positions on the chemical backbone depicted in **A**. **D.** Chemical structures of compounds 97a (left panel) and 97i (right panel).

significantly inhibited *Mtb* and none of the compounds increased the bacterial load (**Figure 3A, bottom panel**). The two compounds that reduced the *Stm* total population (97a and 97i) also displayed remarkably strong inhibition of intracellular *Mtb.* As a strong inhibitory effect was observed in *Stm*- as well as in *Mtb*-infected cells, 97a and 97i might induce an inhibitory mechanism that is common for both *Stm* and *Mtb* infection. Inhibition of intracellular *Stm* and *Mtb* by 97a and 97i was subsequently confirmed in a rescreen and the effect of both compounds on host cell viability was assessed by analyzing total cell counts (**Figure 3B**). As 97a strongly affected host cell viability (especially in the MelJuSo-*Mtb* model), 97i was selected as our top candidate compound. To exclude that 97i exerted bacterial inhibition by a direct bactericidal or bacteriostatic mechanism instead of acting on host targets, we treated bacteria with 97i in bulk bacterial culture in the absence of human cells. No effect of H-89, 97a and 97i was seen on *Mtb* or *Stm* growth at a 10 μM concentration, either at neutral pH or for *Stm* grown in acidic broth (**Figure 3C**). As expected, *Mtb* did not proliferate in acidic broth regardless of compound treatment (data not shown).

The applicability of 97i as a novel TB HDT-drug was further explored in cell-based assays. As host-directed compounds do not directly affect bacteria, targeting the host should be equally effective in both WT and drug-resistant bacterial strains. Therefore, we treated primary human pro-inflammatory Mϕ1s and anti-inflammatory Mϕ2s infected with drug sensitive *Mtb* H37Rv (used in the experiments above) or MDR *Mtb* (Dutch outbreak 2003-1128 and Beijing strain 16319, specified in **Table 1**) with 97i. This resulted in a similar decrease in the bacterial loads of both MDR and non-MDR *Mtb* strains (**Figure 4A**). Thus, 97i-mediated *Mtb* inhibition by human macrophages is independent of bacterial drug resistance, further emphasizing the potential of host-directed therapeutic approaches for TB treatment. As host-directed treatment and antibiotics by

➡ Figure 3. Chemical compound screen of H-89 analogues.
A. HeLa-*Stm* (top and middle panels) and MelJuSo-*Mtb* (bottom panel) model-based chemical compound primary screening results at 10 μM concentration sorted by z-score. The top panel shows z-scores based on the percentage of brightly fluorescent cells (*Stm* 'bright'), while z-scores based on the total *Stm*-infected population (*Stm* total) are shown in the middle panel. Data points display the mean z-score ± standard deviation of 3 replicates. A z-score of 2 or -2 was used as a cut-off value for hit selection (indicated by dashed lines). **B.** Rescreen of compounds 97a and 97i in the MelJuSo-*Mtb* and HeLa-*Stm* infection models performed as in **A**, expressed as a percentage of the DMSO control. 97a, 97i and H-89 were used at 10 μM and DMSO at equal v/v was included as a negative control. Data are the mean percentage of the DMSO control ± standard deviation of 3 replicates. Statistical significance was tested using a one-way ANOVA. **C.** *Stm* and *Mtb* growth in liquid culture during treatment with 10 μM 97i or DMSO at equal v/v at pH 7.0 and pH 4.5. Fifty μg/ml gentamicin and 20 μg/ml rifampicin are displayed as positive controls for *Stm* and *Mtb* growth inhibition, respectively.
(** = p-value <0.01, *** = p-value <0.001).

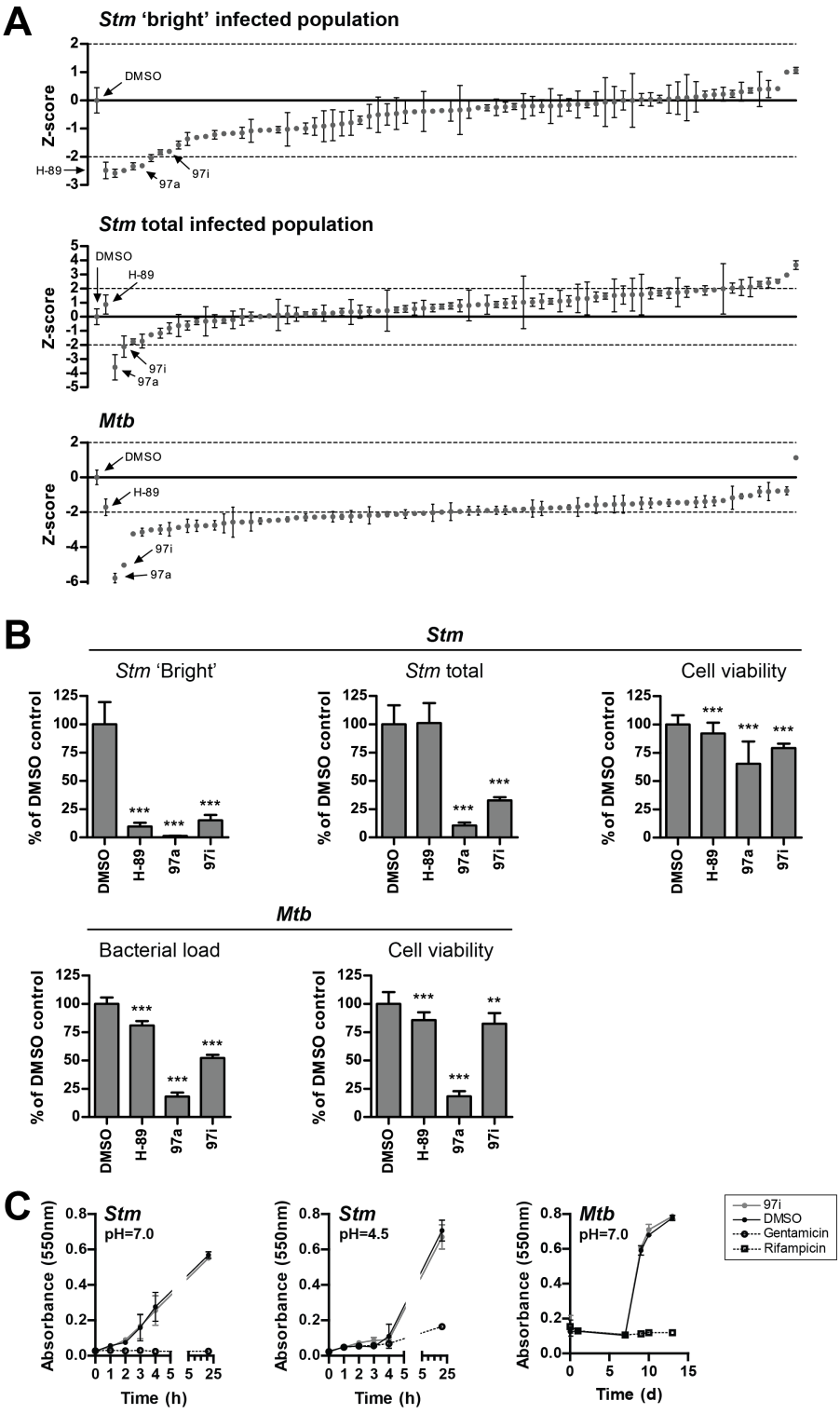
A
Stm 'bright' infected population
Z-score
DMSO
H-89
97a
97i
Stm total infected population
Mtb
B
Stm
Stm 'Bright'
Stm total
Cell viability
% of DMSO control
DMSO
H-89
97a
97i
Mtb
Bacterial load
Cell viability
C
Stm
pH=7.0
pH=4.5
Mtb
pH=7.0
Absorbance (550nm)
Time (h)
Time (d)
97i
DMSO
Gentamicin
Rifampicin

definition act on different pathways, we expected that treatment with host-targeting compounds might augment the effect of classical antibiotics. Indeed, treatment of MelJuSo cells infected with *Mtb* with a combination of rifampicin and 97i resulted in an additional decrease in bacterial survival as compared to rifampicin alone, both at optimal and suboptimal antibiotic concentrations (**Figure 4B**).

Thus, 97i is a novel H-89-analogue kinase inhibitor that strongly inhibits intracellular *Stm* and *Mtb* in a host-directed fashion. 97i Had no effect on extracellular bacteria, did not affect cell viability and offered added value in combination with antibiotic treatment.

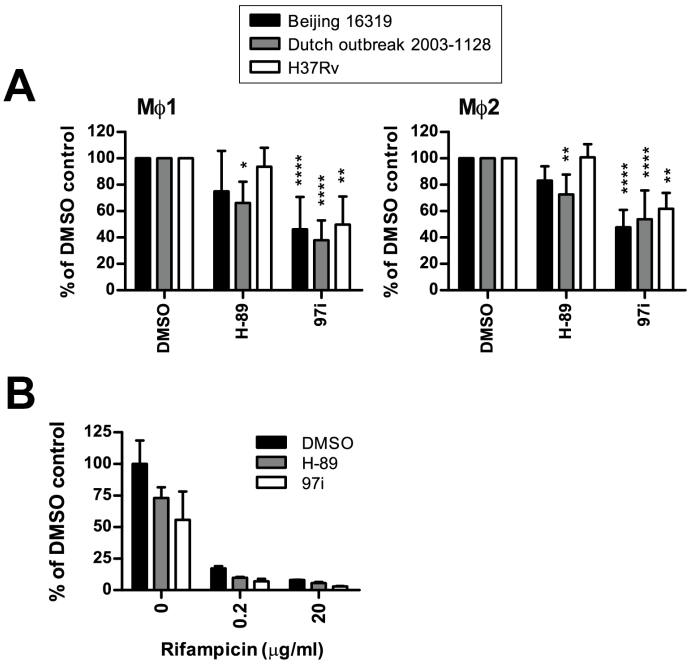

⬆ Figure 4. 97i efficacy testing in MDR-*Mtb* infections and in combination with antibiotics.

A. CFU assay of human type 1 and type 2 Mϕs infected with *Mtb* Beijing strain 16319, Dutch outbreak *Mtb* strain 2003-1128 or H37Rv, and treated with 10 μM H-89 or 97i or DMSO at equal v/v. Bars depict pooled results from macrophages from at least 3 individual donors, expressed as a percentage of the DMSO control. Statistical significance was tested using a two-way ANOVA with Dunnett multiple test correction. **B.** CFU assay of MelJuSo cells infected with *Mtb* and treated with a combination of rifampicin and 10 μM of either H-89 or 97i. Rifampicin was used at a concentration within the range of patient serum concentrations (20 μg/ml)[39], or at a suboptimal concentration (0.2 μg/ml). Data are expressed as a percentage of the DMSO control not treated with rifampicin.
(* = p-value <0.05, ** = p-value <0.01, *** = p-value <0.001, **** = p-value <0.0001).

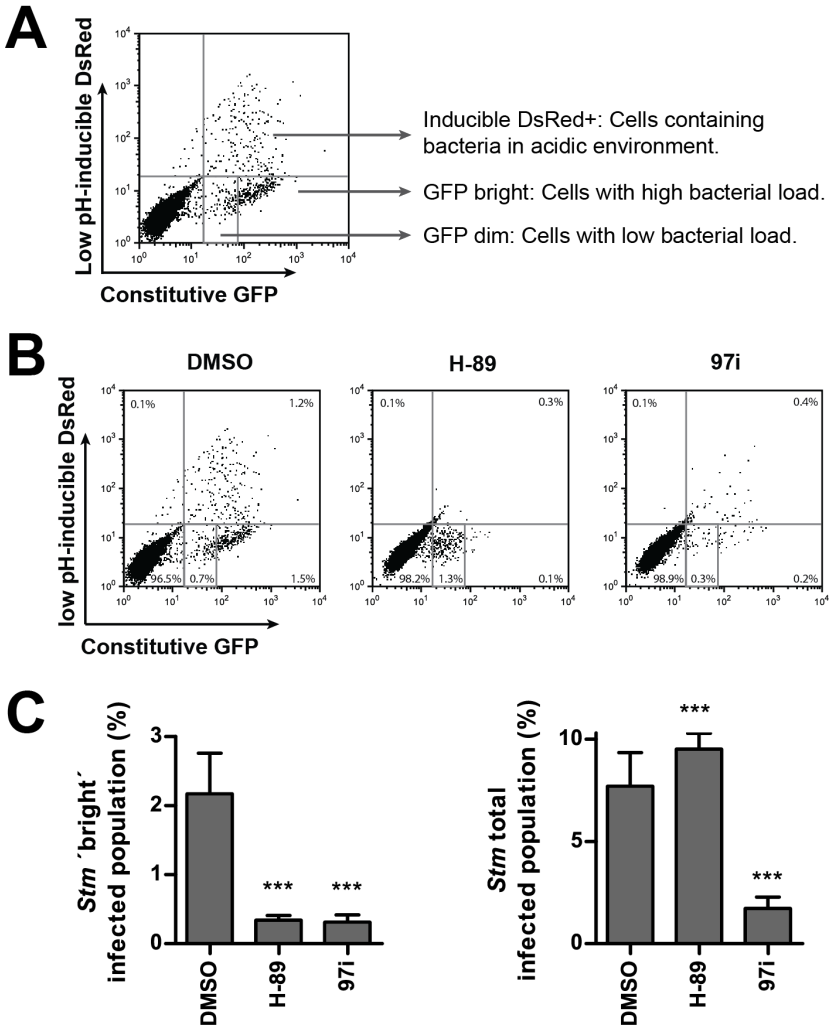

⬆ Figure 5. Analysis of *Stm* intracellular trafficking upon 97i treatment.

A. Example dot-plot from flow cytometric analysis of HeLa cells infected with dual-reporter (constitutive GFP and low pH-inducible DsRed) *Stm*. Interpretation of the different fluorescent cell populations is indicated. **B.** Flow cytometry dot-plots of HeLa cells infected with dual-reporter *Stm* treated with 10 μM H-89 or 97i or DMSO at equal v/v are displayed as in **A**. **C.** Quantification of different fluorescent populations in HeLa cells infected with dual-reporter *Stm* treated with 10 μM H-89 or 97i or DMSO at equal v/v. The percentage of GFP 'bright' cells is displayed in the left panel, while the right panel shows the total percentage of GFP positive cells. Data are the mean ± standard deviation of 20 replicates. A representative experiment out of at least 3 experiments is shown. Statistical significance was tested using one-way ANOVA.
(*** = p-value <0.001).

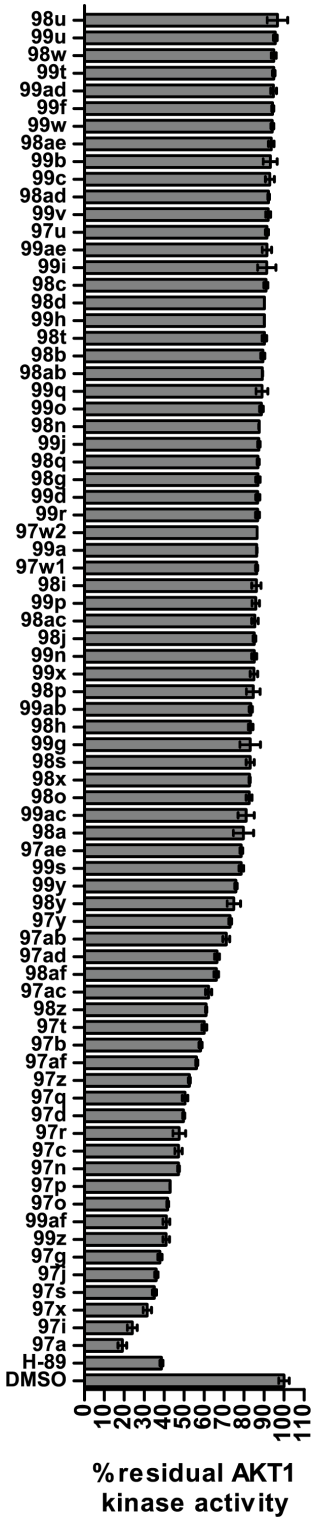

⬅ Figure 6. Analysis of *in vitro* AKT1 inhibition by the H-89 analogue compound library.
In vitro AKT1 inhibition assay using the compound library of H-89 analogues. Graph shows the percentage of residual AKT1 activity in the presence of chemical compounds at a 1.7 μM concentration (previously determined as an optimal concentration for AKT1 inhibition by H-89 *in vitro*[17]) compared to DMSO at equal v/v. Data are expressed as a percentage of the DMSO control value ± standard deviation.

Analysis of intracellular trafficking of *Stm* upon 97i treatment.

To gain insight into the possible mechanism of action of 97i, particularly its impact upon bacterial trafficking to different intracellular compartments, we employed a HeLa infection model using a dual-reporter *Stm.* This *Stm* strain constitutively expresses GFP and is capable of low pH-inducible expression of destabilized DsRed to visualize *Stm* trafficking to non-acidic (GFP+/DsRed-) as well as acidic (GFP+/DsRed+) compartments. Using this model, cells containing high or low bacterial loads can also be clearly distinguished based on fluorescence intensity (**Figure 5A**), as previously reported[34]. H-89 treatment resulted in clearance of all *Stm* from acidic compartments, while a dim GFP signal still remained present (**Figure 5B**). Quantification of these data demonstrated that despite equal inhibition of *Stm* proliferation by both H-89 and 97i (**Figure 5C, left panel**), the total GFP positive cell population did not decrease upon H-89 treatment (**Figure 5C, right panel**). This indicated that either non-proliferating bacteria, dead (but intact) bacteria or free GFP remained intracellularly after H-89 treatment. In contrast, 97i almost completely abrogated fluorescent signals from the cells (**Figure 5B** and **Figure 5C, right panel**), indicating induction of a mechanism resulting in degradation of all *Stm*-associated proteins.

In summary, 97i reduced a population of *Stm*-infected cells that is not sensitive to H-89, indicating that 97i induces a different inhibitory mechanism than H-89.

Structure-activity relationship analysis confirms molecularly that *Mtb* survival is regulated by host kinases other than AKT1.

To study the role of AKT1 inhibition in the intracellular bacterial inhibition exerted by our novel compounds, an *in vitro* AKT1 kinase inhibition screen was performed for all synthesized compounds (**Figure 6**) and cross-referenced with the *Stm* and *Mtb* inhibition screening data from **Figure 3A** (**Figure 7A**). In the AKT1 inhibition screen, 97i was identified as a strong AKT1 inhibitor. However, a group of compounds that strongly inhibited intracellular *Mtb* without affecting AKT1 activity was also identified (**Figure 7A, right panel**), suggesting that inhibition of other kinases might contribute to *Mtb* inhibition. Stratification of the *Stm* 'bright' screening data by AKT1 inhibitory activity (using the median AKT1 inhibition of the whole dataset as a cut-off) revealed that compounds exerting strong AKT1 inhibition were significantly stronger inhibitors of *Stm* (**Figure 7B, left panel**), confirming our previous findings[17]. An identical analysis of the *Mtb* screening data revealed no difference in *Mtb* inhibition by either weak or strong AKT1 inhibitors. Despite this lack of correlation between AKT1 inhibition and the *Mtb* bacterial

➡ Figure 7 (next page). Comparison of *in vitro* AKT1 inhibition and intracellular bacterial inhibition by the H-89 analogue compound library.
A. AKT1 inhibition *in vitro* was compared to the *Stm* 'bright' (left panel), *Stm* total (middle panel) and *Mtb* (right panel) compound screening data (**Figure 3A**). The percentage of residual kinase activity is plotted on the y-axis against the effect of compound treatment on the bacterial load (expressed as a z-score) on the x-axis for each compound. Each data point represents an individual compound. H-89 is indicated in black and 97i is shown as an open circle. A group of weak AKT1 inhibitors that decreased *Mtb* intracellular survival is indicated by a dashed box (short dashes). Dashed line (long dashes): hit cut-off from *Stm* and *Mtb* compound screens (see legend **Figure 3A**). **B.** *Stm* 'bright' (left panel), *Stm* total (middle panel) and *Mtb* (right panel) compound screening data (from **Figure 3A**) expressed as a z-score and stratified using a cut-off at the median AKT1 inhibition of the whole dataset. Data points represent individual compounds. H-89 is indicated in black and 97i is shown as an open circle. Statistical significance was tested using a Mann-Whitney test. **C.** Relationship between chemical structure and AKT1 inhibitory activity for compounds carrying a residue at the R_1, R_2 or R_3 positions. Residual AKT1 activity *in vitro* is plotted for individual compounds. An open circle indicates 97i. Dashed line: level of AKT1 inhibition by H-89. Statistical significance was tested using a one-way ANOVA with Bonferroni multiple comparison test. **D.** Structure-activity relationship for compounds carrying a residue at the R_1, R_2 or R_3 positions against bacterial infection loads, comparing the *Stm* 'bright' (left panel), *Stm* total (middle panel) and *Mtb* (right panel) compound screening data (from **Figure 3A**). An open circle indicates 97i. Dashed line: bacterial load upon H-89 treatment. Statistical significance was tested using a one-way ANOVA with Bonferroni multiple comparison test.
(* = p-value <0.05, ** = p-value <0.01, *** = p-value <0.001).

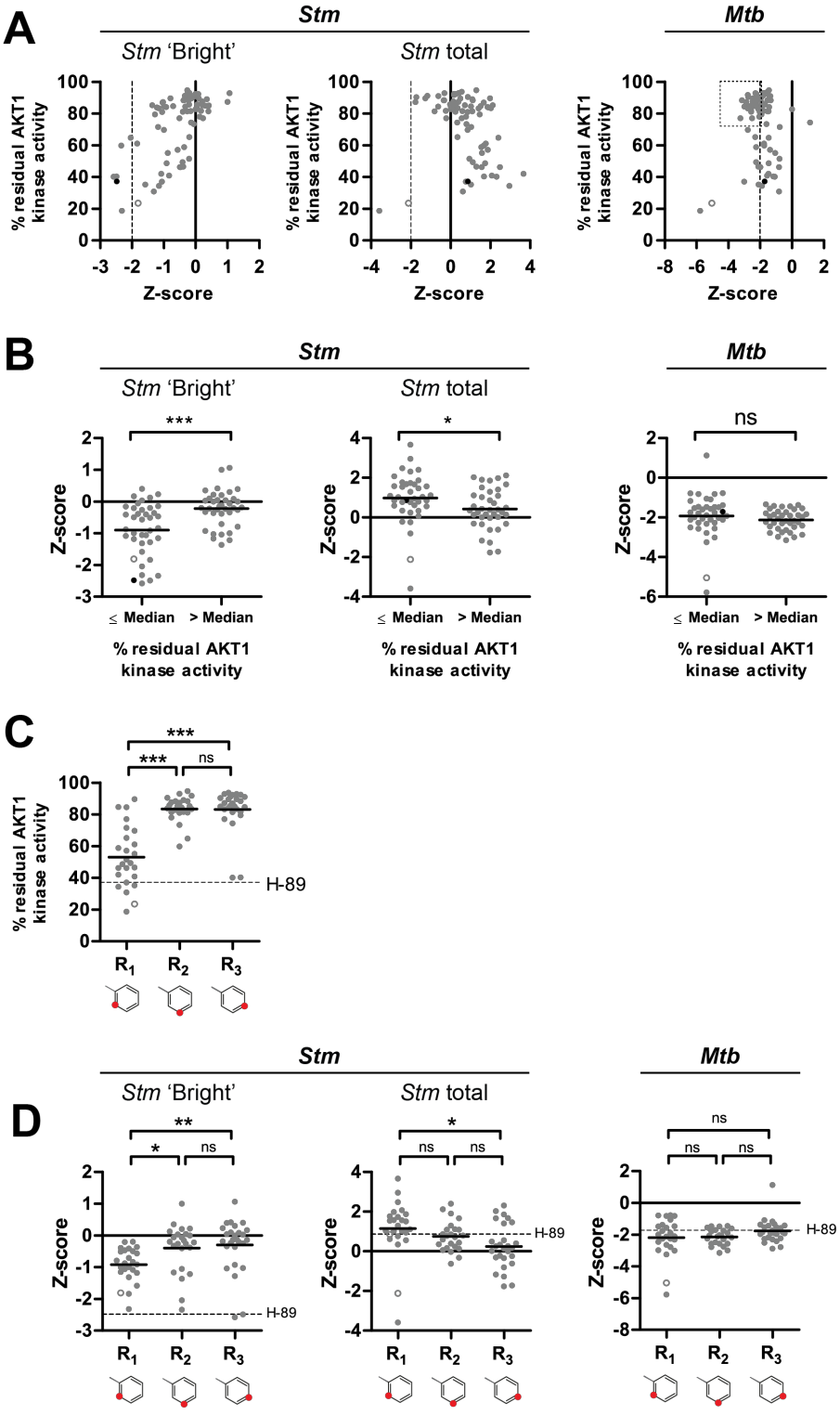
A
Stm
Mtb
Stm 'Bright'
Stm total
% residual AKT1 kinase activity
Z-score
B
***
*
ns
≤ Median
> Median
% residual AKT1 kinase activity
C
***
***
ns
H-89
R1
R2
R3
D
**
*
ns
*
ns
ns
ns
ns
ns
H-89
R1
R2
R3

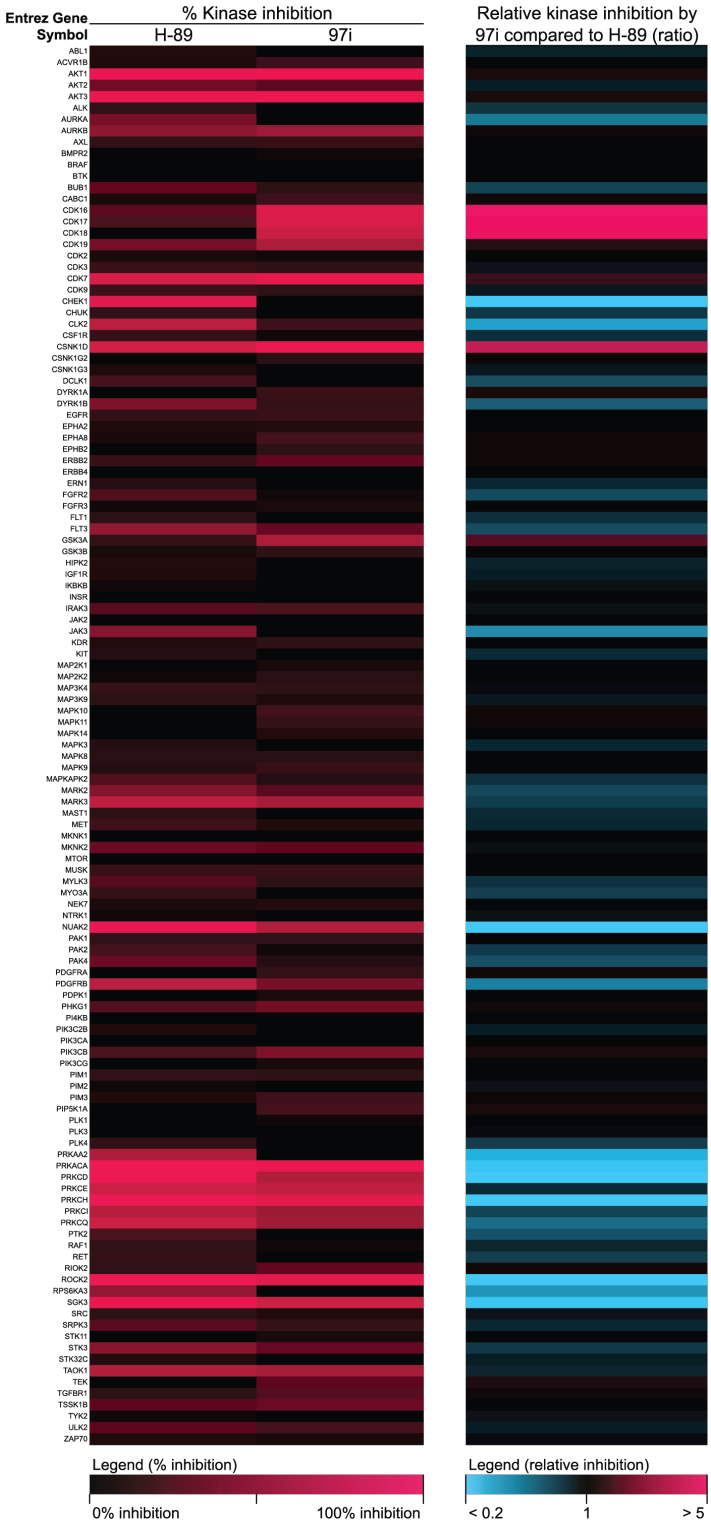

← Figure 8. Kinase inhibition profiles of compounds H-89 and 97i. Heat maps displaying *in vitro* kinase inhibition by compounds H-89 and 97i. The left panel shows the actual percentage of kinase inhibition by the compounds for the indicated kinases. The right panel shows the relative kinase inhibition of 97i compared to H-89 expressed as a ratio.

load, 97i strongly decreased both the total *Stm* infected and *Mtb* infected populations, indicating that kinases other than AKT1 may be involved in inhibiting intracellular *Mtb* (**Figure 7B, right panel**) and decreasing the total *Stm*-infected population (**Figure 7B, middle panel**).

Next, we studied whether the chemical conformation of the inhibitors (**Figure 2**) was associated with their AKT1 inhibitory activity. Compounds carrying any residue at the R_1 position were significantly better AKT1 inhibitors than compounds carrying residues at R_2 or R_3 positions (**Figure 7C**). This structure-activity relationship resulted in functional consequences as compounds carrying a residue at R_1 inhibited *Stm* intracellular survival significantly better than the R_2 or R_3 variants when analyzing the *Stm* 'bright' population (**Figure 7D, left panel**). Again, no difference was observed between compound groups for *Mtb* intracellular survival (**Figure 7D, right panel**). In contrast, 97i (a compound from the R_1 group) strongly decreased the *Stm* total and *Mtb* infected populations, further indicating that bacterial inhibition exerted by 97i is dependent on AKT1 and one or more additional kinase(s).

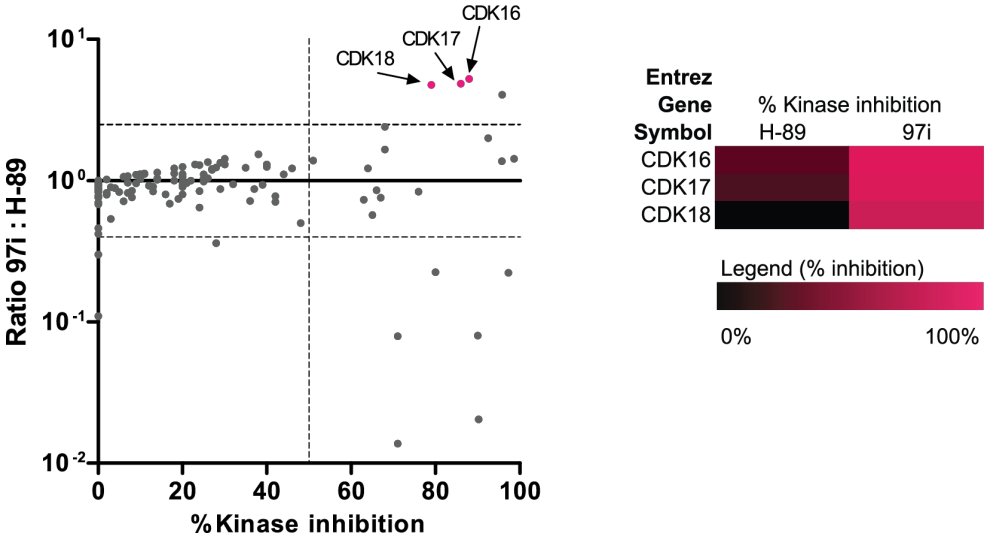

⬆ Figure 9. Identification of candidate target kinases of 97i.

A scatterplot displaying relative kinase inhibition by 97i compared to H-89 as a function of the percentage of kinase inhibition by 97i is displayed in the left panel. Each data point represents an individual kinase. Horizontal dashed lines indicate a 2.5-fold (higher or lower) difference in kinase inhibition compared to H-89. The vertical dashed line is a cut-off at 50% kinase inhibition. Data points in magenta represent the three kinases (CDK16, CDK17 and CDK18) that were not strongly inhibited by H-89 (< 50% inhibition), were inhibited by at least 50% by 97i and displayed at least a 2.5-fold enhanced inhibition by 97i compared to H-89. The right panel shows the percentage of kinase inhibition of CDK16, CDK17 and CDK18 by 97i and H-89 as a heat map as in **Figure 8**.

Taken together, these data strongly suggest a role for kinases other than AKT1 in regulation of *Mtb* intracellular survival, whereas in contrast AKT1 alone plays a dominant role in regulating *Stm* intracellular survival.

Identification of CDK18 as a target of 97i and as a putative host regulator of intracellular bacterial survival.

As 97i likely induced a different inhibitory mechanism than H-89, and both H-89 and 97i inhibit AKT1, we next set out to identify other kinases that are targeted by 97i but not by H-89. To this end we compared the *in vitro* kinome inhibitory capacity of H-89 and 97i by screening them against a panel of 123 kinases representing all major branches of the human protein kinase phylogeny (**Figure 8**). The results of this kinome scan revealed a high (but not complete) degree of similarity between the target profiles of 97i and H-89 and confirmed that both compounds similarly inhibited AKT1. To identify the kinases responsible for the enhanced bacterial inhibition by 97i compared to H-89, we focused on kinases that 1) were not strongly inhibited (< 50%) by H-89; 2) were inhibited significantly (≥ 50%) by 97i and 3) displayed at least a 2.5-fold increased inhibition by 97i compared to H-89. Kinases CDK16, CDK17 and CDK18 fulfilled these criteria and were therefore selected as targets of 97i (**Figure 9**). We next explored whether inhibition of CDK16, 17 or 18 by 97i is responsible for the enhanced reduction of bacterial load compared to H-89. Therefore, we employed siRNA to silence CDK16, 17 or 18 in the presence or absence of H-89 treatment (**Figure 10**). Indeed, a combination of H-89 treatment and CDK18 silencing mimicked the strong inhibitory effect of 97i in our HeLa-*Stm* infection model (**Figure 10**). No such effect was observed when silencing CDK16 or CDK17 either alone or in combination with H-89 treatment (data not shown).

In conclusion, we have identified CDK16, CDK17 and CDK18 as novel target kinases of 97i and demonstrated that targeting CDK18 in addition to kinases inhibited by H-89 exerts superior host-mediated *Stm* inhibition.

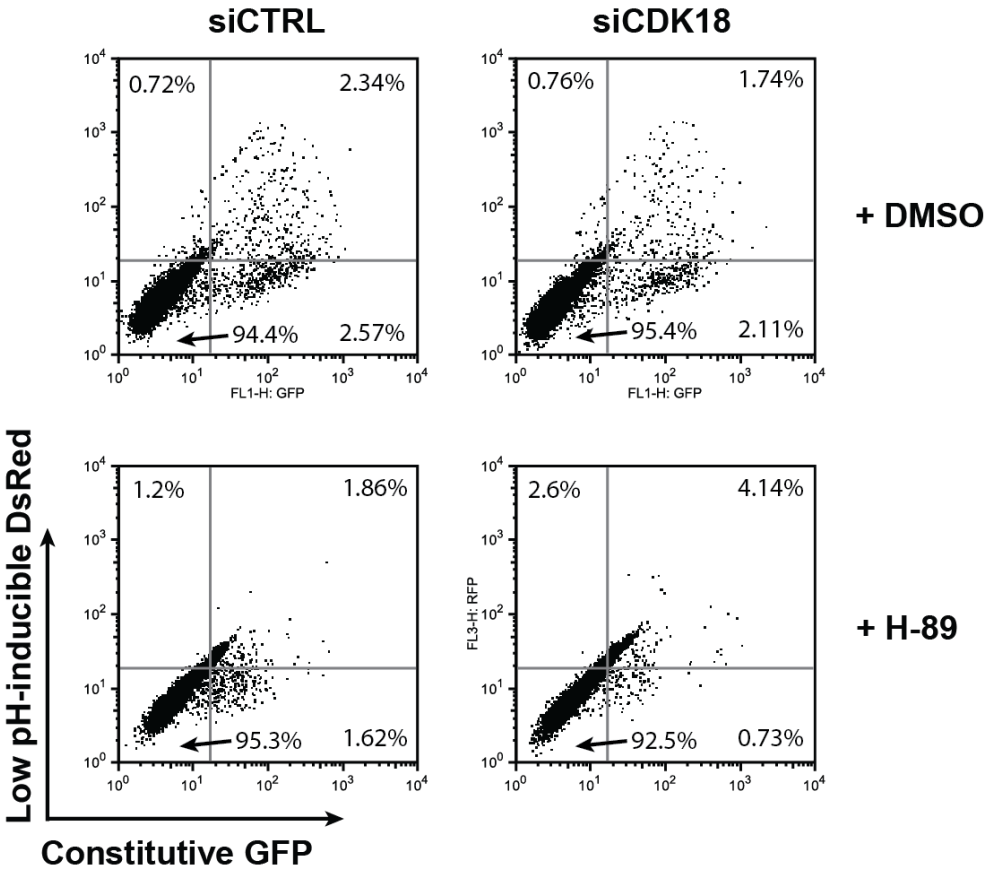

⬆ Figure 10. Confirmation of CDK18 as a regulator of intracellular bacterial survival.
Flow cytometry dot-plots of siRNA-silenced HeLa cells infected with dual-reporter *Stm* either treated with 10 μM H-89 or DMSO at equal v/v are displayed as in **Figure 5A**. CDK18 was silenced (siCDK18), while a scrambled siRNA pool (siCTRL) was used as a negative control.

Discussion

Here we report the chemical genetic identification of a novel host-directed kinase inhibitor, 97i, which targets the PCTAIRE-family kinase member CDK18 to enhance host control of *Stm* and possibly other major intracellular human pathogens, including *Mtb*, MDR-*Mtb* and other *Salmonella* species, in human cells. Greatly increased host-mediated *Mtb* inhibition was achieved by enhancing the chemical structure of H-89, modifying its target specificity to include CDK18, alongside kinases readily targeted by H-89. We previously demonstrated that H-89 is able to partially inhibit intracellular *Mtb,* indicating that pathways targeted by H-89,

including AKT1, are involved in *Mtb* control. Here we demonstrate that supplementation of H-89 treatment with genetic silencing of CDK18 mimicked the effect of 97i treatment in our HeLa-*Stm* infection model. These data suggest that the inability of H-89 to inhibit CDK18 might also be responsible for its inability to achieve significant *Mtb* inhibition.

The PCTAIRE kinases are a distinct family of cyclin-dependent kinases (CDKs) consisting of CDK16, CDK17 and CDK18 (PCTAIRE-1, PCTAIRE-2 and PCTAIRE-3, respectively) [40]. Despite being part of the CDK family, the role of PCTAIRE kinases in cell cycle regulation is still under debate and their cellular-molecular functions are poorly understood. However, several recent publications have begun to shed light on their cellular and molecular functions. In contrast to other CDKs, the PCTAIRE family of kinases can display a cytosolic localization. The PCTAIRE kinases CDK16 and CDK18 were previously shown to interact with COPII to modulate secretory cargo transport from the ER, indicating a role in vesicle transport. Interestingly, this process could be partly inhibited by H-89[41]. Here, we demonstrate that H-89 partly inhibits CDK16 and CDK17, but not CDK18. In contrast, 97i inhibits all three PCTAIRE family members. In our study we confirmed CDK18 as an important PCTAIRE kinase for control of intracellular bacterial infection. Further studies on HDT drugs will need to focus on identifying the contribution of individual PCTAIRE kinases in controlling of bacterial infection, and subsequently to improve inhibitor selectivity for the relevant kinases involved. In several recent studies in cancer, selective inhibitors of CDK16 were employed, providing a possible starting point for further chemical modifications and rational drug design[42,43]. In further support of a role for CDK18 in vesicle transport as well as a possible link between CDK18 and phagocytosis, Matsuda *et al*. recently reported that CDK18 is a negative regulator of the kinase FAK, which in turn regulates the RhoGTPases Rac1 and RhoA[44]. Rac1 and RhoA are central regulators of actin cytoskeleton reorganization[45], which is not only linked to cell motility and adhesion, but is also an essential mechanism driving phagocytosis and phagosome maturation[46]. Therefore, CDK18 might be directly involved in regulation of phagosome maturation, e.g. via FAK. Our own (unpublished) data agree with a role for FAK in the regulation of intracellular bacterial survival, as silencing of FAK increased the bacterial load of both *Stm* and *Mtb*.

Other potential functions of PCTAIRE kinases in intracellular bacterial infection might be related to immune modulation. Recently, CDK16 knockdown was shown to sensitize tumor cells to TNF-family cytokines[43]. Even though this may have not been a contributing factor in our infection models, 97i might exert an additional immunomodulatory effect *in vivo* by sensitizing infected macrophages to TNF-family cytokines through its inhibition of multiple PCTAIRE kinases. Further studies in more complex (*in vitro* and *in vivo*) model systems should be performed to confirm this potentially beneficial immunomodulatory effect of 97i. In another study focusing on inhibition of the IL-1β-induced inflammatory response by *Klebsiella pneumoniae* (*K. pneumoniae*), CDK18 was identified as one of the proteins required for this inhibition and this process was dependent on the epidermal growth factor receptor (EGFR) [47]. This suggests another potential immunomodulatory role for CDK18 in *Mtb* infection, as IL-1β was previously demonstrated to balance type I interferon production towards a

protective phenotype during *Mtb* infection[27]. As we previously also identified growth factor receptor tyrosine kinase signaling (including via EGFR) as a central host regulatory pathway controlling *Mtb* infection[34], similar inhibitory mechanisms might be employed by both *K. pneumoniae* and *Mtb*.

Though not extensively studied, CDK18 was previously linked to *Stm* infection and may be one of the host targets actively manipulated by the bacterium. Bioinformatics analysis of phosphoproteomics data of *Stm*-infected cells identified CDK18 as a possible upstream regulator involved in phosphorylation events in infected cells induced by *Stm* infection[48]. Even though CDK18 was not selected as a top candidate in the study by Rogers *et al.*, our own data show that CDK18 may indeed be mechanistically involved in *Stm* infection outcome.

Our chemical genetic approach emphasizes the complexity of interactions between *Mtb* and the host. The demonstration that inhibition of multiple kinases is essential for *Mtb* control points to a potential limitation of single gene based RNAi approaches since identification of kinase interactions and interaction networks is not feasible in a single-knockdown setting. Therefore, the chemical lead optimization approach and subsequent target identification as we have followed here might be a powerful alternative for identifying novel drug targets for TB, by virtue of the fact that chemical compounds rarely have a single target.

Regardless of their mode of action, the novel inhibitors identified in our screens display promising effects in our infection models. First of all, the ability of these compounds to further reduce the *Mtb* bacterial load following *in vitro* rifampicin treatment provides proof-of-principle that host-directed compounds can be used to either induce further inhibition of bacteria that are less susceptible to antibiotics or to render them more susceptible to the microbicidal effects of antibiotics. If further developed, similar compounds might offer ways to shorten the unusually long (minimum 6 months) antibiotic course of TB treatment as well as decrease the probability of *de novo* antibiotic resistance by targeting the host rather than the bacterium[15,16]. Importantly, our novel kinase inhibitors are equally active against both a laboratory strain (H37Rv) as well as clinical (MDR) isolates. This provides an important proof-of-concept that host-directed compounds such as 97i can be applied to complement classical antibiotics for treatment of MDR bacterial infections.

In conclusion, we identified 97i as a novel host-directed kinase inhibitor, which controls major intracellular human pathogens, including *Mtb*, MDR-*Mtb* and *Salmonella* species in human cells. We further demonstrated that 97i inhibited intracellular *Stm* by not only targeting AKT1 but also the PCTAIRE-family kinase member CDK18. Further work is required to confirm whether these kinases are also involved in controlling intracellular *Mtb*. The potent new chemical inhibitor 97i may be used as a basis for next-generation host-directed therapeutics against intracellular bacterial infections.

Materials & Methods

Synthesis of the kinase inhibitor library

Synthesis of the compound library is described in "Synthetic studies on kinase inhibitors and cyclic peptides: strategies towards new antibiotics", Adriaan W. Tuin, 2008 (https://openaccess.leidenuniv.nl/bitstream/handle/1887/13365/Proefschrift+AW_Tuin+alles.pdf?sequence=7).

Reagents

H-89 dihydrochloride, Rifampicin and Kanamycin were purchased from Sigma-Aldrich, Zwijndrecht, The Netherlands. Ampicillin was acquired from Calbiochem Merck-Millipore, Darmstadt, Germany. Hygromycin B was supplied by Life Technologies-Invitrogen, Bleiswijk, The Netherlands.

Cell culture

Cell culture was performed as previously described[34]. In short, HeLa and MelJuSo cell lines were maintained at 37°C and 5% CO_2 in Gibco Iscove's Modified Dulbecco's Medium (IMDM, Life Technologies-Invitrogen) supplemented with 10% fetal bovine serum (FBS, Greiner Bio-One, Alphen a/d Rijn, The Netherlands), 100 units/ml Penicillin and 100 µg/ml Streptomycin (Life Technologies). Type 1 and type 2 Mϕs were generated by differentiating monocytes of healthy donors for 6 days with 5 ng/ml recombinant granulocyte macrophage-colony stimulating factor (GM-CSF, BioSource Life Technologies-Invitrogen) or 50 ng/ml recombinant macrophage-colony stimulating factor (M-CSF, R&D Systems, Abingdon, United Kingdom) respectively, as previously reported[49]. Mϕs were maintained in Gibco Roswell Park Memorial Institute (RPMI) 1640 medium (Life Technologies-Invitrogen) supplemented with 10% FBS and 2 mM L-Alanyl-L-Glutamine (PAA, Linz, Austria).

Bacterial culture

Bacterial strains used are displayed in **Table 1**. Mycobacteria were cultured in Difco Middlebrook 7H9 broth (Becton Dickinson, Breda, The Netherlands) supplemented with 10% ADC (Becton Dickinson), 0.5% Tween-80 (Sigma-Aldrich) and appropriate antibiotics. *Stm* was cultured on Difco Luria-Bertani (LB) agar (Becton Dickinson) or in Difco LB broth (Becton Dickinson) supplemented with appropriate antibiotics.

Stm and *Mtb* infections

Stm and *Mtb* infections were performed as previously described[34]. In short, 10,000 HeLa or MelJuSo cells seeded in 96-well flat-bottom plates were inoculated with 100 µl of the bacterial suspension at MOI 10 (unless otherwise indicated), centrifuged for 3 minutes at 800 rpm and incubated at 37°C/5% CO_2 for 20 minutes if infected with *Stm* or 60 minutes if infected with *Mtb*. Plates were then washed with culture medium containing 30 µg/ml gentamicin sulfate (Lonza BioWhittaker, Basel, Switzerland) and incubated at 37°C and 5% CO_2 in medium containing 5 µg/ml gentamicin and indicated chemical compoundsat 10 µM

Table 1. Bacterial strains, plasmids used for fluorescent protein expression and their respective antibiotic selection markers.

Base strain	Plasmid	Antibiotic resistance *(source, concentration)*
Mtb H37Rv.	pSMT3[Phsp60/DsRed].	Hygromycin *(plasmid, 50 µg/ml).*
Mtb H37Rv.	pSMT3[Phsp60/destabilized DsRed].	Hygromycin *(plasmid, 50 µg/ml).*
Mtb Beijing family China (Kremer 43) 16319.	None.	Rifampicin, Isoniazid, Ethambutol, Pyrazinamide *(intrinsic, n/a).*
Mtb Dutch outbreak 2003-1128.	None.	Rifampicin, Isoniazid, Streptomycin, Claritromycin *(intrinsic, n/a).*
Stm SL1344.	pMW211[C.10E/DsRed] (Constitutive promotor).	Ampicillin *(plasmid, 100 µg/ml).*
Stm SL1344.	pMW215[PpagC/DsRed] (Low-pH inducible promotor).	Ampicillin *(plasmid, 100 µg/ml).*
Stm SL1344.	pMW215[PpagC/DsRed] (Low pH-inducible promotor). pMW211[C.10E/GFP] (Constitutive promotor).	Ampicillin *(plasmid, 100 µg/ml).* Kanamycin *(plasmid, 100 µg/ml).*

concentration (unless indicated otherwise) until readout by flow cytometry or CFU, as indicated.

Chemical compound treatment

10,000 HeLa or MelJuSo cells or were seeded per well in 96-well flat-bottom plates or 300,000 primary Mϕs were plated in 24-well flat-bottom plates in appropriate culture medium without antibiotics one day prior to infection with *Mtb* or broth-grown *Stm.* Infected cells were treated overnight with chemical compounds at a 10 µM concentration (unless otherwise indicated) in medium containing 5 µg/ml gentamicin.

siRNA transfections

3,000 HeLa or MelJuSo cells were reverse-transfected with ON-TARGETplus siRNA pools (Thermo Fisher Dharmacon, Waltham Massachusetts, USA) at a 50 nM concentration using 0.2 µl Dharmafect1 (Thermo Fisher Dharmacon) per well in a flat-bottom 96-well plate in appropriate culture medium without antibiotics. Cells transfected with siRNA were infected with *Mtb* at MOI 1000 24 hours post transfection and incubated for an additional 48 hours and infections with agar-grown *Stm* were carried out at MOI 500 72 hours post transfection and incubated overnight, unless otherwise indicated.

Colony forming unit assay

CFU assays were performed using the track dilution method described previously[50]. In short, serial dilutions of bacterial suspensions and 10 µl drops were spotted on square agar plates (Becton Dickinson). The plates were then placed at an angle to allow the drops to spread out on the plates.

Bacterial growth assay

100 µl *Mtb* or *Stm* culture (OD_{600} of 0.1) was plated in a flat-bottom 96-well plate containing 100 µl of indicated chemical compounds at 20 µM in 7H9 broth for *Mtb* or LB broth for *Stm*. The plate was incubated at 37°C and absorbance was measured at a 550 nm wavelength at indicated time points on a Mithras LB 940 plate reader (Berthold Technologies, Bad Wildbad, Germany).

AKT1 kinase inhibition assay

AKT1 kinase inhibition assays were performed as previously reported[17]. Compounds were tested at 1,7 µM concentration in the presence of 100 µM ATP.

Kinase inhibitor profiling

Kinase inhibitor target profiling was performed commercially at 10 µM using the ScanEDGE panel for the KINOMEscan platform (DiscoveRx, Fremont California, USA).

Statistics

Student's T-test (two groups, normally distributed), Mann-Whitney test (two groups, non-parametric), one-way ANOVA with Dunnett's multiple comparison test (multiple groups) and two-way ANOVA with Bonferroni post test (multiple comparisons, grouped data) were performed using GraphPad Prism version 7.0 for Mac OS X (GraphPad Software, San Diego California USA, www.graphpad.com). Screening statistics were performed as previously reported[34], according to guidelines from the NIH Chemical Genomics Center[38]. Z-scores were calculated by dividing the difference between the percentage of gated fluorescent events (bacterial load) of each screening replicate and the average percentage of fluorescent events of the DMSO control by the DMSO control's standard deviation. For the primary compound screen data, z-scores were calculated using the same formula, but the average percentage of fluorescent events and the standard deviation of all samples on each plate (instead of the DMSO control) was used to provide plate normalization. Subsequently, the average DMSO z-score was subtracted from each sample.

Acknowledgements

This project was funded by the European Union's Seventh Programme for research, technological development and demonstration under grant agreement N° PhagoSys HEALTH-F4-2008-223451; NEWTBVAC HEALTH.F3.2009 241745, TANDEM project Grant Agreement N° 305279. We also gratefully acknowledge the support of the Netherlands Organization for Health Research and Development

(ZonMw-TOP grant 91214038) and Technology Foundation STW (grant 13259). The funders had no role in study design, data collection and analysis, decision to publish, or preparation of the manuscript.

We thank Dick van Soolingen and Kirsten Kremer (RIVM, Bilthoven, the Netherlands) for providing the MDR-*Mtb* strains.

References

1. Ottenhoff, T. H. M. The knowns and unknowns of the immunopathogenesis of tuberculosis. *Int. J. Tuberc. Lung Dis.* **16,** 1424–1432 (2012).
2. World Health Organization. *Global Tuberculosis Report 2017*. 1–249 (2017).
3. Ottenhoff, T. H. M. Overcoming the global crisis: 'yes, we can', but also for TB ... ? *Eur. J. Immunol.* **39,** 2014–2020 (2009).
4. Jassal, M. S. & Bishai, W. R. Epidemiology and challenges to the elimination of global tuberculosis. *CLIN INFECT DIS* **50 Suppl 3,** S156–64 (2010).
5. Ottenhoff, T. H. M. New pathways of protective and pathological host defense to mycobacteria. *Trends Microbiol.* **20,** 419–428 (2012).
6. Smith, S. I., Seriki, A. & Ajayi, A. Typhoidal and non-typhoidal Salmonella infections in Africa. *Eur. J. Clin. Microbiol. Infect. Dis.* **35,** 1913–1922 (2016).
7. Barry, C. E. & Blanchard, J. S. The chemical biology of new drugs in the development for tuberculosis. *Curr Opin Chem Biol* **14,** 456–466 (2010).
8. Norrby, S. R., Nord, C. E., Finch, R.European Society of Clinical Microbiology and Infectious Diseases. Lack of development of new antimicrobial drugs: a potential serious threat to public health. *Lancet Infect Dis* **5,** 115–119 (2005).
9. Becker, D. *et al.* Robust Salmonella metabolism limits possibilities for new antimicrobials. **440,** 303–307 (2006).
10. Makarov, V. *et al.* Benzothiazinones kill Mycobacterium tuberculosis by blocking arabinan synthesis. *Science* **324,** 801–804 (2009).
11. Christophe, T. *et al.* High content screening identifies decaprenyl-phosphoribose 2' epimerase as a target for intracellular antimycobacterial inhibitors. *PLoS Pathog* **5,** e1000645 (2009).
12. Willand, N. *et al.* Synthetic EthR inhibitors boost antituberculous activity of ethionamide. *Nat. Med.* **15,** 537–544 (2009).
13. Lawn, S. D. & Zumla, A. I. Tuberculosis. *Lancet* **378,** 57–72 (2011).
14. O'Neill, J. *Tackling drug-resistant infections globally: final report and recommendations*. (London: Wellcome Trust & HM Government, 2016).
15. Guler, R. & Brombacher, F. Host-directed drug therapy for tuberculosis. *Nature Chemical Biology* **11,** 748–751 (2015).
16. Hawn, T. R., Shah, J. A. & Kalman, D. New tricks for old dogs: countering antibiotic resistance in tuberculosis with host-directed therapeutics. *Immunol. Rev.* **264,** 344–362 (2015).
17. Kuijl, C. *et al.* Intracellular bacterial growth is controlled by a kinase network around PKB/AKT1. **450,** 725–730 (2007).
18. Kumar, D. *et al.* Genome-wide analysis of the host intracellular network that regulates survival of Mycobacterium tuberculosis. *Cell* **140,** 731–743 (2010).
19. Jayaswal, S. *et al.* Identification of host-dependent survival factors for intracellular Mycobacterium tuberculosis through an siRNA screen. *PLoS Pathog* **6,** e1000839 (2010).

20. Sundaramurthy, V. *et al.* Integration of chemical and RNAi multiparametric profiles identifies triggers of intracellular mycobacterial killing. *Cell Host and Microbe* **13,** 129–142 (2013).
21. Machado, D. *et al.* Ion Channel Blockers as Antimicrobial Agents, Efflux Inhibitors, and Enhancers of Macrophage Killing Activity against Drug Resistant Mycobacterium tuberculosis. *PLoS ONE* **11,** e0149326 (2016).
22. Napier, R. J. *et al.* Imatinib-sensitive tyrosine kinases regulate mycobacterial pathogenesis and represent therapeutic targets against tuberculosis. *Cell Host and Microbe* **10,** 475–485 (2011).
23. Subbian, S. *et al.* Phosphodiesterase-4 inhibition alters gene expression and improves isoniazid-mediated clearance of Mycobacterium tuberculosis in rabbit lungs. *PLoS Pathog* **7,** e1002262 (2011).
24. Subbian, S. *et al.* Phosphodiesterase-4 inhibition combined with isoniazid treatment of rabbits with pulmonary tuberculosis reduces macrophage activation and lung pathology. *Am. J. Pathol.* **179,** 289–301 (2011).
25. Koo, M.-S. *et al.* Phosphodiesterase 4 inhibition reduces innate immunity and improves isoniazid clearance of Mycobacterium tuberculosis in the lungs of infected mice. *PLoS ONE* **6,** e17091 (2011).
26. Vilaplana, C. *et al.* Ibuprofen therapy resulted in significantly decreased tissue bacillary loads and increased survival in a new murine experimental model of active tuberculosis. *Journal of Infectious Diseases* **208,** 199–202 (2013).
27. Mayer-Barber, K. D. *et al.* Host-directed therapy of tuberculosis based on interleukin-1 and type I interferon crosstalk. **511,** 99–103 (2014).
28. Datta, M. *et al.* Anti-vascular endothelial growth factor treatment normalizes tuberculosis granuloma vasculature and improves small molecule delivery. *Proc Natl Acad Sci USA* **112,** 1827–1832 (2015).
29. Oehlers, S. H. *et al.* Interception of host angiogenic signalling limits mycobacterial growth. **517,** 612–615 (2015).
30. Schiebler, M. *et al.* Functional drug screening reveals anticonvulsants as enhancers of mTOR-independent autophagic killing of Mycobacterium tuberculosis through inositol depletion. *EMBO Molecular Medicine* **7,** 127–139 (2015).
31. Skerry, C. *et al.* Simvastatin increases the in vivo activity of the first-line tuberculosis regimen. *J. Antimicrob. Chemother.* **69,** 2453–2457 (2014).
32. Stanley, S. A. *et al.* Identification of host-targeted small molecules that restrict intracellular Mycobacterium tuberculosis growth. *PLoS Pathog* **10,** e1003946 (2014).
33. Li, Q. *et al.* Novel high throughput pooled shRNA screening identifies NQO1 as a potential drug target for host directed therapy for tuberculosis. *Sci Rep* **6,** 27566 (2016).
34. Korbee, K. J. *et al.* Combined chemical genetics and data-driven bioinformatics approach identifies receptor tyrosine kinase inhibitors as host-directed antimicrobials. *Nat Commun* **9,** 358 (2018).
35. Vergne, I., Chua, J., Singh, S. B. & Deretic, V. Cell biology of mycobacterium tuberculosis phagosome. *Annu. Rev. Cell Dev. Biol.* **20,** 367–394 (2004).

36. Brumell, J. H. & Grinstein, S. Salmonella redirects phagosomal maturation. *Current Opinion in Microbiology* **7,** 78–84 (2004).
37. Sogi, K. M., Lien, K. A., Johnson, J. R., Krogan, N. J. & Stanley, S. A. The Tyrosine Kinase Inhibitor Gefitinib Restricts Mycobacterium tuberculosis Growth through Increased Lysosomal Biogenesis and Modulation of Cytokine Signaling. *ACS Infect Dis* **3,** 564–574 (2017).
38. Singhal, A. *et al.* Metformin as adjunct antituberculosis therapy. *Science Translational Medicine* **6,** 263ra159–263ra159 (2014).
39. Peloquin, C. A. Using therapeutic drug monitoring to dose the antimycobacterial drugs. *Clin. Chest Med.* **18,** 79–87 (1997).
40. Mikolcevic, P., Rainer, J. & Geley, S. Orphan kinases turn eccentric: a new class of cyclin Y-activated, membrane-targeted CDKs. *Cell Cycle* **11,** 3758–3768 (2012).
41. Palmer, K. J., Konkel, J. E. & Stephens, D. J. PCTAIRE protein kinases interact directly with the COPII complex and modulate secretory cargo transport. *Journal of Cell Science* **118,** 3839–3847 (2005).
42. Dixon-Clarke, S. E. *et al.* Structure and inhibitor specificity of the PCTAIRE-family kinase CDK16. *Biochem. J.* **474,** 699–713 (2017).
43. Yanagi, T., Shi, R., Aza-Blanc, P., Reed, J. C. & Matsuzawa, S.-I. PCTAIRE1-knockdown sensitizes cancer cells to TNF family cytokines. *PLoS ONE* **10,** e0119404 (2015).
44. Matsuda, S., Kawamoto, K., Miyamoto, K., Tsuji, A. & Yuasa, K. PCTK3/CDK18 regulates cell migration and adhesion by negatively modulating FAK activity. *Sci Rep* **7,** 45545 (2017).
45. Groves, E., Dart, A. E., Covarelli, V. & Caron, E. Molecular mechanisms of phagocytic uptake in mammalian cells. *Cell. Mol. Life Sci.* **65,** 1957–1976 (2008).
46. Kinchen, J. M. & Ravichandran, K. S. Phagosome maturation: going through the acid test. *Nat Rev Mol Cell Biol* **9,** 781–795 (2008).
47. Frank, C. G. *et al.* Klebsiella pneumoniae targets an EGF receptor-dependent pathway to subvert inflammation. *Cellular Microbiology* **15,** 1212–1233 (2013).
48. Rogers, L. D., Brown, N. F., Fang, Y., Pelech, S. & Foster, L. J. Phosphoproteomic analysis of Salmonella-infected cells identifies key kinase regulators and SopB-dependent host phosphorylation events. *Science Signaling* **4,** rs9 (2011).
49. Verreck, F. A. W., de Boer, T., Langenberg, D. M. L., van der Zanden, L. & Ottenhoff, T. H. M. Phenotypic and functional profiling of human proinflammatory type-1 and anti-inflammatory type-2 macrophages in response to microbial antigens and IFN-gamma- and CD40L-mediated costimulation. *Journal of Leukocyte Biology* **79,** 285–293 (2006).
50. Jett, B. D., Hatter, K. L., Huycke, M. M. & Gilmore, M. S. Simplified agar plate method for quantifying viable bacteria. *BioTechniques* **23,** 648–650 (1997).

5 | The DNA Damage-Regulated Autophagy Modulator DRAM1 Links Mycobacterial Recognition via TLR-MYD88 to Autophagic Defense

Michiel van der Vaart, Cornelis J. Korbee, Gerda E.M. Lamers, Anouk C. Tengeler, Rohola Hosseini, Mariëlle C. Haks, Tom H.M. Ottenhoff, Herman P. Spaink and Annemarie H. Meijer

Autophagy is an important defense mechanism against mycobacteria, the causative agents of tuberculosis. The molecular mechanisms that link mycobacterial recognition to autophagy remain unclear. Our analysis in zebrafish and human macrophage models of mycobacterial infection reveals that the DNA damage-regulated autophagy modulator DRAM1 functions downstream of pathogen recognition by the Toll-like receptor (TLR)/interleukin-1 receptor (IL1R)-MYD88-NF-κB innate immune sensing pathway to activate selective autophagy. Mycobacterial infection of human macrophages and zebrafish embryos induced *DRAM1* expression in a MYD88 and NF-κB-dependent manner. DRAM1 knockdown increased mycobacterial infection, whereas overexpression lowered infection by hyperactivating autophagy. DRAM1-mediated selective autophagic defenses require the cytosolic DNA sensor STING and the selective autophagy receptor p62/SQSTM1. Contrary to its known role in autophagy-mediated cell death and cancer, this DRAM1 function is p53 independent. We propose that DRAM1 mediates autophagic defense against a broader range of intracellular pathogens, since *DRAM1* expression was also induced by the common bacterial endotoxin lipopolysaccharide.

Published in:
Van der Vaart, M., **Korbee, C.J.**, Lamers, G.E.M., Tengeler, A.C., Hosseini, R., Haks, M.C., Ottenhoff, T.H.M., Spaink, H.P., Meijer, A.H., 2014. **The DNA damage-regulated autophagy modulator DRAM1 links mycobacterial recognition via TLR-MYD88 to authophagic defense.** *Cell Host and Microbe* **15**, 753–767. doi:10.1016/j.chom.2014.05.005.

Introduction

A growing body of evidence firmly establishes autophagy as a defense mechanism against intracellular pathogens[1]. Autophagy is an evolutionarily conserved process in eukaryotes essential for cellular homeostasis in response to environmental and cellular stressors. During autophagy (or macroautophagy), cytoplasmic components are enveloped in double-membraned autophagosomes that fuse with lysosomes for degradation of their content in a process known as autophagic flux. Selective autophagy specifically degrades unwanted protein aggregates or cellular contents via ubiquitin-mediated targeting, using receptors such as p62/SQSTM1 and NDP52 to link ubiquitinated cargo to the microtubule-associated protein 1 light chain 3 (LC3) [1]. Subsequently, components of the general autophagy machinery, including the ATG12-ATG5-ATG16L1 complex, are required for autophagosome maturation[2]. Autophagy has diverse roles in defense by contributing to cytokine secretion, targeting microbes for lysosomal degradation, and as regulator of innate and adaptive immune responses[1,2].

Studies on *Mycobacterium tuberculosis* (*Mtb*), the causative agent of pulmonary tuberculosis (TB), have been a leading example of how autophagy can counteract the ability of intracellular pathogens to avoid host defenses[1,3-5]. Mycobacteria evade leukocyte bacterial-killing mechanisms by preventing phagosome-lysosome fusion, creating a niche that allows them to survive and proliferate[6]. Infected macrophages (Mϕs) then recruit other immune cells to form highly organized structures known as granulomas[7].

We used the zebrafish model to study the role of autophagy during early stages of mycobacterial infection. *Mycobacterium marinum* (*Mm*) is a natural fish pathogen and a close relative of *Mtb*. It causes a phenotype in zebrafish that highly resembles human TB disease, including the formation of caseating granulomas[8]. *Mm* infection of zebrafish embryos has been successfully used to understand host cell signaling and mycobacterial virulence determinants during TB disease[9]. The zebrafish model allows visualization of host-pathogen interactions during early stages of mycobacterial pathogenesis in the absence of an adaptive immune contribution[10] and has recently been used as an *in vivo* model to study bacterial autophagy[11].

The molecular signaling pathway responsible for autophagic control of mycobacterial disease remains unclear, although there are strong links between pathogen recognition by Toll-like receptors (TLRs) and autophagy induction[12-15]. We employed our myeloid differentiation primary response 88 (*myd88*) mutant zebrafish line to study regulation of autophagy downstream of this central Toll-like receptor (TLR)/interleukin-1 receptor (IL1R)-signaling adaptor[16]. We found that DNA damage-regulated autophagy modulator 1 (*dram1*) expression during mycobacterial infection requires MyD88. *DRAM1* is a known target gene of the tumor suppressor p53 and is required for p53-dependent cell death by inducing autophagy[17]. There is considerable interest in DRAM1 due to its relation with tumor development and cancer therapy[18,19].

Here, we show that *DRAM1*/*dram1* expression during mycobacterial infection in primary human Mϕs and zebrafish embryos depends on the TLR/IL1R-

MYD88-NF-κB signaling pathway central to innate immunity and does not require p53. DRAM1 colocalizes with intracellular mycobacteria, and knockdown results in higher bacterial burdens. Confocal imaging, supported by electron microscopy (EM), showed that Dram1 is needed for the formation of autophagosomes and promotes lysosome formation and autophagic flux. Furthermore, we show that the function of *dram1* requires the selective autophagy receptor p62 and the STING DNA-sensing pathway and that activation of this selective autophagy pathway by overexpressing *dram1* in zebrafish embryos is protective against TB disease.

Results

Activating general autophagy is not beneficial for *in vivo* defense against mycobacteria

To investigate autophagic defense in zebrafish, we first tested widely used autophagy modulators in GFP-Lc3 transgenic embryos[20]. This confirmed that 3-methyladenine (3-MA) inhibits autophagosome formation, while chloroquine (Cq) and Ar-12 increased the number of Lc3 fluorescent punctae (**Figures 1A** and **1B**). The effect of Cq treatment is consistent with its prohibitive action on autophagic flux by preventing autophagosome-lysosome fusion, resulting in accumulation of Lc3-labeled autophagosomes. Ar-12 inhibits PDK1/AKT signaling, causing accumulation of reactive oxygen species (ROS) and triggering a stress-induced autophagic response[21]. We then infected GFP-Lc3 embryos with *Mm* and treated them with 3-MA, Cq, or Ar-12 for the first 24 hr postinfection (hpi). Colocalization with GFP-Lc3 was observed for ±30% of the bacteria in control embryos, consistent with results in cultured MΦs[22]. 3-MA decreased autophagy induction in infected cells (**Figure 1C**). Blocking autophagic flux with Cq led to an accumulation of autophagosomes colocalized with *Mm* (**Figure 1C**). In this example, Cq treatment prevented the maturation of bacterial compartments that were entirely decorated with Lc3. Ar-12-treated embryos showed many small Lc3 punctae throughout infected cells, mostly not associated with bacteria (**Figure 1C**). Next, we quantified the effect of these drugs on the bacterial burden at 3

➡ **Figure 1**. **Stress-induced autophagy is not beneficial for defense of zebrafish embryos against mycobacterial infection.**
A. Schematic representation of the effects of 3-MA, Cq, and Ar-12 on autophagosome formation and autophagic flux. **B.** GFP-Lc3 embryos 2 dpf were treated for 24 hr with DMSO (control), 3-MA, Cq, or Ar-12. Representative confocal micrographs of endothelial cells at 3 dpf are shown. **C.** GFP-Lc3 embryos treated as described for **A** injected with *Mm*. Representative confocal micrographs of infected cells at 3 dpf are shown. Boxed areas are detailed below; arrowheads indicate overlap between *Mm* and Lc3. **D.** AB/Tupfel long fin (AB/TL) embryos treated as described for **A** infected with *Mm*. Bacterial pixel counts were determined at 3 dpi. Data (mean ± SEM) is pooled from at least two individual experiments (n ≥ 50 embryos per group). See also **Figure S1.**

days postinfection (3 dpi) and observed increased infection after treatment with all compounds (**Figure 1D**). The effects of inhibitors, 3-MA and Cq, are consistent with results in mammalian cell cultures infected with mycobacteria[4] and support

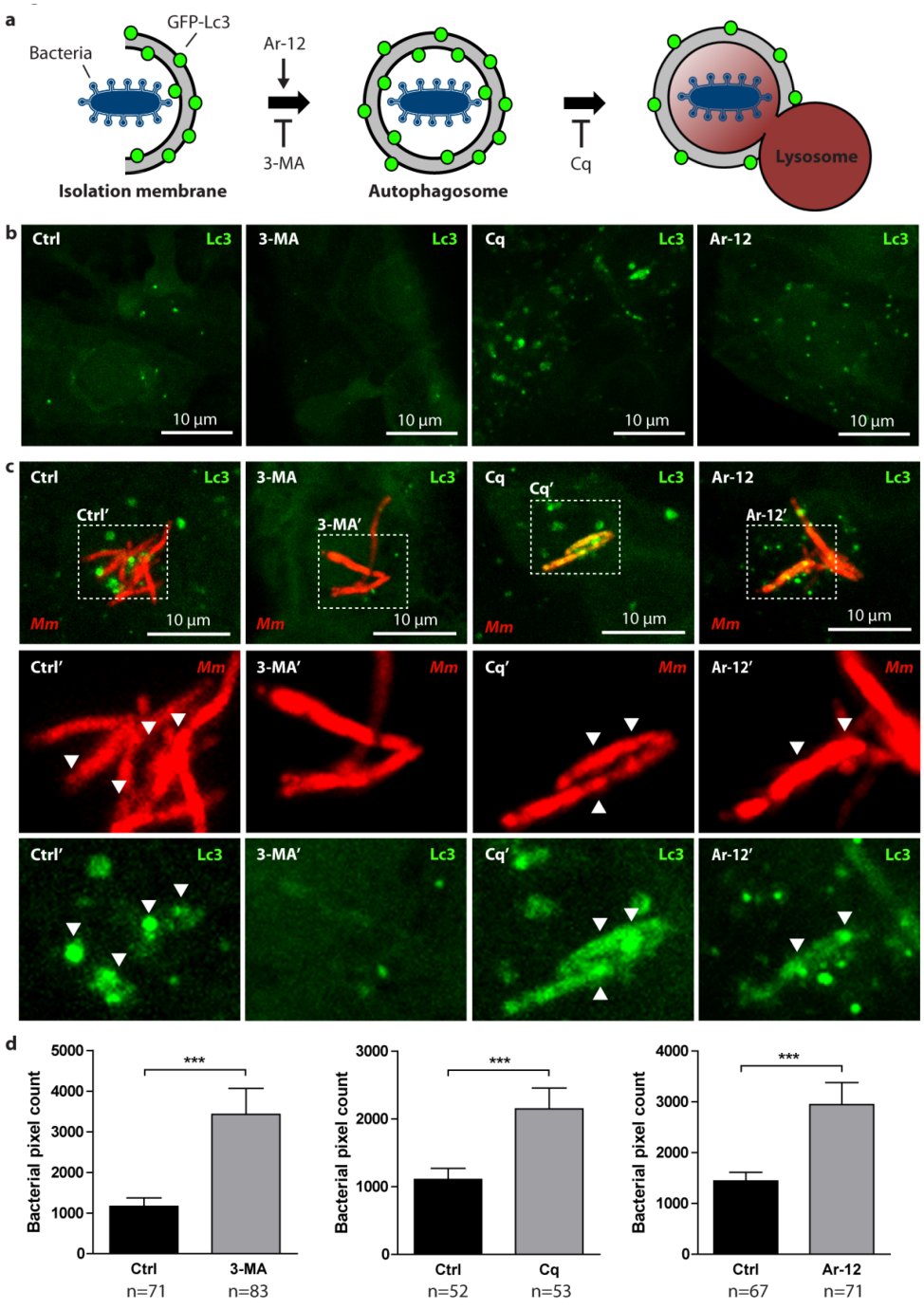

autophagy to function in defense against mycobacteria in zebrafish. However, stimulating ROS-inducible non-targeted autophagy by Ar-12 or the starvation-induced mammalian target of rapamycin (mTOR) pathway using rapamycin (**Figure S1**) was also detrimental to defense against mycobacteria in our zebrafish model.

Induction of autophagy modulator *dram1* by mycobacterial infection is MyD88 dependent in zebrafish

It remains largely unknown how TLR pathogen recognition and autophagy are connected. We have previously demonstrated that *myd88* mutant (*myd88*$^{-/-}$) zebrafish embryos, lacking a signaling adaptor vital to TLR signaling, show impaired induction of genes central to innate immunity and are more susceptible to infection by *Mm*[16]. Microarray profiling of *myd88*$^{+/+}$ and *myd88*$^{-/-}$ embryos infected with *Mm* confirmed the significantly lower expression of proinflammatory genes, such as *il1b*, *tnfa*, and *mmp9*, in the absence of MyD88 signaling (**Figure 2A**). In our search for regulators linking pathogen recognition to autophagy, we found that expression of *dram1* was significantly reduced during *Mm* infection in the absence of functional MyD88 (**Figure 2A**). This gene encodes a transmembrane protein that is highly conserved among vertebrates in terms of protein homology and gene synteny[17] (**Figures S2A–2C**). Over a time course of *Mm* infection, dram1 expression progressively increased in infected *myd88*$^{+/+}$, but not in *myd88*$^{-/-}$ (**Figure 2B**). The MyD88 dependency of *dram1* during *Mm* infection was confirmed by RNA sequencing and quantitative PCR (qPCR) in independent experiments (**Figures 2A** and **2C**). Increased expression of the genes encoding p53, Atg5, Lc3, or p62 was not detected on the whole-embryo level.

In silico analysis of the promoter regions of human and zebrafish *DRAM1*/*dram1* revealed conserved binding sites for the hematopoietic transcription factor Pu.1 (**Figure S2D**). Expression of *dram1* in leukocytes was confirmed by qPCR on

➡ Figure 2. dram1 is induced by mycobacterial infection in a Myd88-dependent fashion

A. *myd88*$^{+/+}$ and *myd88*$^{-/-}$ embryos infected with *Mm* were snap frozen individually at 4 dpi, and triplicate samples were compared with PBS-injected controls using a common reference microarray design. Observed differences were confirmed by RNA sequencing of pools (n=20 embryos) of uninfected and *Mm*-infected *myd88*$^{+/+}$ and *myd88*$^{-/-}$ embryos. **B**. Expression of *dram1* at multiple time points after infection was analyzed by qPCR on pools of *Mm*-infected *myd88*$^{+/+}$ and *myd88*$^{-/-}$ embryos, relative to PBS-injected controls (mean ± SEM of n = 2 biological replicates with 20 embryos per pool). **C**. Expression levels of *dram1* at 4 dpi in individual *myd88*$^{+/+}$ and *myd88*$^{-/-}$ embryos with or without infection were determined by qPCR (mean ± SEM of n=3 biological replicates with 10 embryos per pool). **D**. Macrophages, neutrophils, and leukocytes from 5–6 dpf larvae were isolated by FACS. Expression of *dram1* in the positive fractions (e.g., Mpeg1^{+}) relative to the negative fractions (-VE) was determined by qPCR (mean ± SEM of n=4 biological replicates). See also **Figure S2**.

fluorescence-activated cell sorted (FACS) immune cell populations, showing its enrichment in the Mpeg1+ [23], Mpx+ [24], and Lck+ [25] fractions of dissociated transgenic embryos specific for Mϕs, neutrophils, and lymphocytes, respectively (**Figure 2D**). We conclude that zebrafish *dram1* is expressed in myeloid and lymphoid immune cell lineages and induced in a MyD88-dependent fashion following infection by mycobacteria.

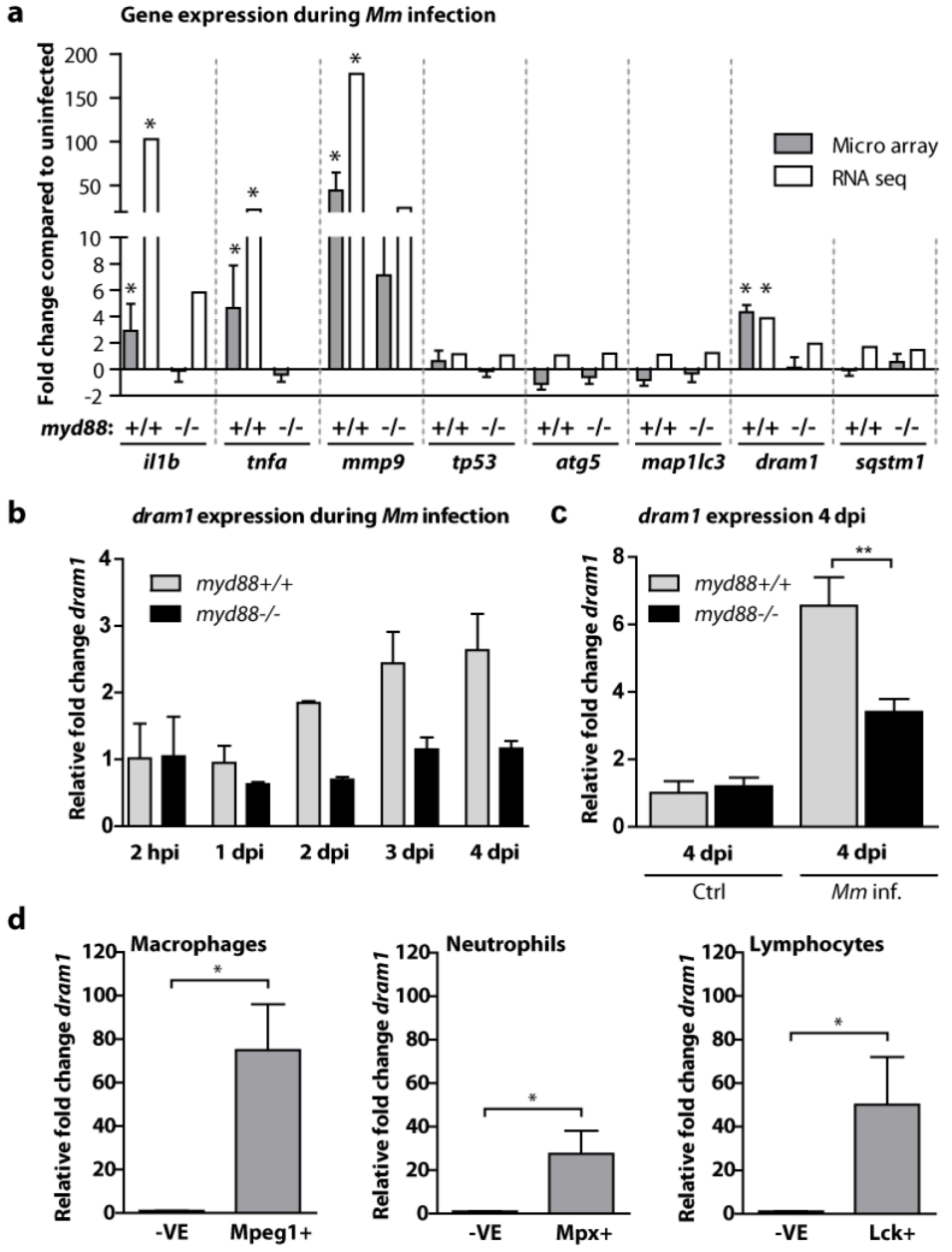

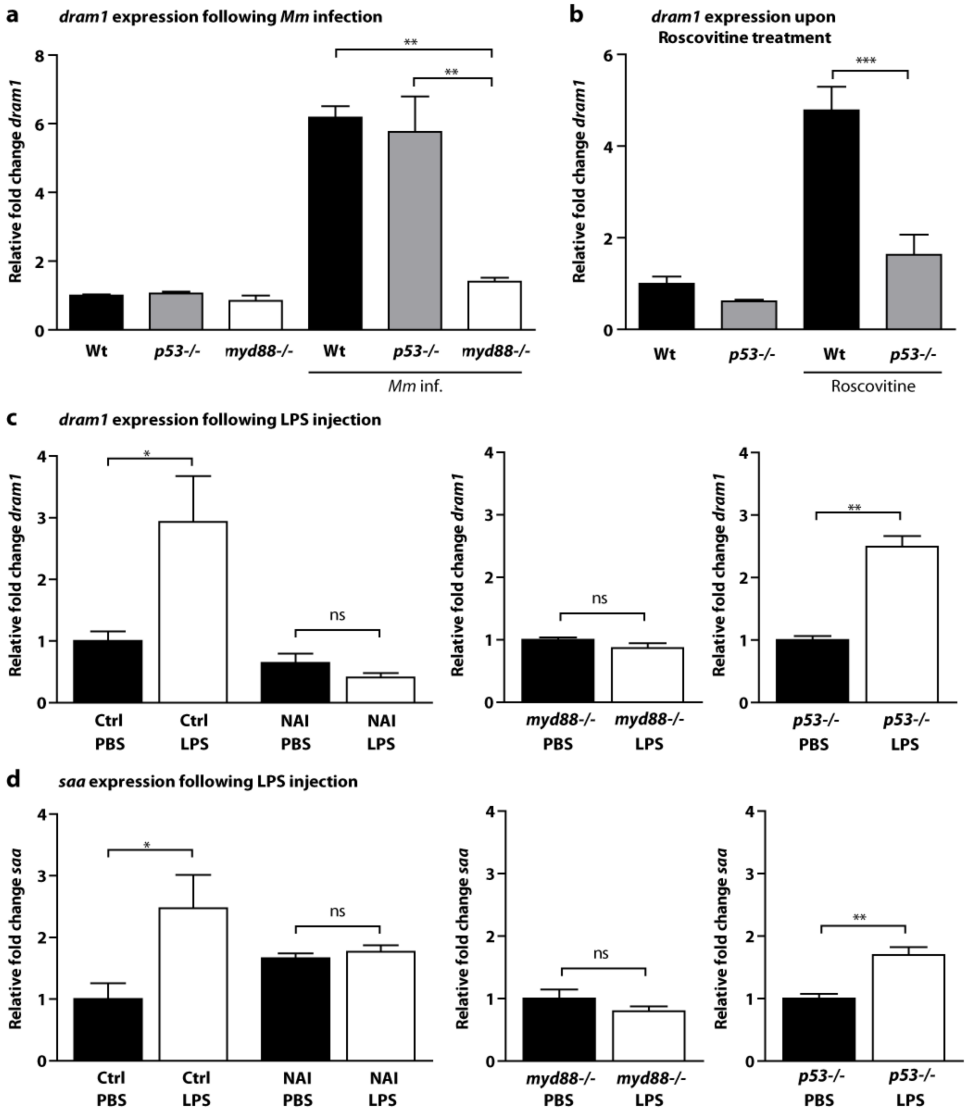

Bacterial-induced expression of *dram1* is independent of p53 but dependent on NF-κB

Since the known functions of DRAM1 are dependent on p53 signaling, we analyzed expression of *dram1* in embryos with a mutation in the DNA-binding domain of p53 (*p53*$^{-/-}$)[26]. *Mm*-infected *p53*$^{-/-}$ mutants showed upregulation of *dram1* to wild-type levels, indicating that infection-induced *dram1* expression is p53 independent (**Figure 3A**). As a control, we treated embryos with the p53-stabilizing agent roscovitin[26]. Unlike wild-type, *p53*$^{-/-}$ embryos were insensitive to roscovitin-induced malformations and did not express *dram1* upon treatment (**Figures S3**, **3B**). These results show that the canonical p53-dependent route to

← Figure 3. *dram1* Expression during Mycobacterial Infection Is Independent of p53 but Dependent on NF-κB

A–C. Expression levels of *dram1* were determined by qPCR for **A:** wild-type, *p53*$^{-/-}$, and *myd88*$^{-/-}$ embryos 4 days after infection with *Mm*, relative to mock-injected controls; **B:** wild-type and *p53*$^{-/-}$ embryos at 5 dpf after 24 hr of treatment with roscovitine, relative to untreated controls (see also **Figure S3**); and **C:** 1 dpf embryos at 2 hpi with LPS, relative to their respective PBS-injected controls (left panel: wild-type embryos with or without NAI treatment [4 hr total, including 2 hr pretreatment]; middle panel: *myd88*$^{-/-}$ embryos; right panel: *p53*$^{-/-}$ embryos). **D.** Expression levels of *saa* were determined by qPCR under the same conditions as those described for **C**.

All graphs show data (mean ± SEM) from three biological replicates with n = 20 embryos pooled per replicate. See also **Figures S2** and **S3**.

dram1 induction is functional in zebrafish but not employed during *Mm* infection. Autophagy can be regulated by NF-κB activation[27], and the promoter regions of human and zebrafish *dram1* contain predicted NF-κB consensus binding sites (**Figure S2D**). We hypothesized that NF-κB is the essential transcription factor downstream of MyD88 regulating *dram1* expression during mycobacterial infection. Since the application of a previously described NF-κB activation inhibitor (NAI) for the duration of early *Mm* pathogenesis (2–4 dpi) was harmful to embryonic development[28], we developed an alternative assay to test for the involvement of NF-κB activity based on two previous findings: (1) zebrafish *dram1* expression is induced by *Salmonella enterica* serovar Typhimurium (*Stm*) infection[29] and (2) TLR recognition of *Stm*-derived lipopolysaccharide (LPS) in zebrafish depends on MyD88[16]. Since LPS-induced gene expression occurs rapidly after exposure, this allowed us to avoid harmful effects of NAI treatment by blocking NF-κB activity for only 4 hr. We found that LPS exposure significantly increased *dram1* expression in control-treated embryos, which was completely abrogated by NAI (**Figure 3C**). Furthermore, *myd88*$^{-/-}$ embryos did not increase *dram1* expression in response to LPS, while *p53*$^{-/-}$ embryos behaved identical to wild-type controls (**Figure 3C**). Expression levels of the known NF-κB target gene serum amyloid A (*saa*) displayed a similar pattern following LPS exposure (**Figure 3D**). Together, these data demonstrate that bacterial induced expression of *dram1* is dependent on MyD88-NF-κB, but not on p53.

DRAM1 is under control of NF-κB and colocalizes with *Mtb* in human Mϕs

In view of the strong evolutionary conservation of DRAM1, we hypothesized that the signaling pathway controlling *dram1* during mycobacterial infection is conserved between human and zebrafish. We obtained human primary Mϕs type 1 (Mϕ1) and type 2 (Mϕ2) from peripheral blood mononuclear cells and infected them with *Mtb*. At 4 hpi we detected elevated expression levels of *DRAM1* in infected Mϕ1 and Mϕ2 (**Figure 4A**). In addition, *SQSTM1* (p62) was significantly induced in *Mtb*-infected Mϕ1s and Mϕ2s (**Figure 4B**), suggesting a collaboration

➡ Figure 4. DRAM1 Colocalizes with *Mtb* and Is Regulated by MYD88-NF-κB Signaling in Human Primary Macrophages
A–C. The effect of NAI treatment on expression of **A:** *DRAM1*, **B:** *SQSTM1*, and **C:** *IL1B* in Mϕ1 and Mϕ2 in the presence or absence of *Mtb* was determined by qPCR, relative to uninfected controls. All graphs show data (mean ± SEM) from three biological replicates. **D.** Expression of *DRAM1* in Mϕ1 and Mϕ2 transfected with siCTRL or siMYD88 with and without *Mtb* infection. All graphs show data (mean ± SEM) from three biological replicates. **E and F.** Immunohistochemistry for **E:** DRAM1 (green) or **F:** LC3 (green) performed on Mϕ1 and Mϕ2 at 72 hpi with *Mtb* (red); Hoechst staining (blue) was used to outline the nuclei and cell boundaries. See also **Figure S4**.

between the autophagy-related proteins DRAM1 and p62 during mycobacterial infection. IL1β expression was also induced in these Mϕs, confirming the inflammatory response to infection (**Figure 4C**). Treatment with NAI prevented the expression of *DRAM1* in infected Mϕ1 and Mϕ2 (**Figure 4A**), while SQSTM1 and IL1β were partially dependent on NF-κB activity in Mϕ1 and independent of NF-κB in Mϕ2s (**Figures 4B** and **4C**). Using siRNA depletion of MYD88, we could confirm the conservation of the MYD88-NF-κB-DRAM1 signaling route during *Mtb* infection of human Mϕ2, but not Mϕ1 (**Figure 4D**), indicating further complexity in DRAM1 regulation in differentiated human Mϕs. In both Mϕ1s and Mϕ2s we observed clear colocalization of DRAM1 and LC3 with *Mtb* at 72 hpi (**Figures 4E** and **4F**). siRNA against *DRAM1*, while effectively reducing *DRAM1* mRNA levels, unexpectedly did not lead to reduced protein expression (**Figure S4**). As the stability of DRAM1 protein therefore precludes the use of genetic knockdown as an experimental approach to study the impact of DRAM1 on mycobacterial infection in human cells, we performed further functional studies in the zebrafish *in vivo* model.

Dram1 is required to contain mycobacterial growth inside Mϕs

To investigate the hypothesis that Dram1 functions in autophagic defense against mycobacterial infection, we used an antisense morpholino oligonucleotide approach in zebrafish to block intron-exon splicing (**Figure S5**), thus preventing the production of functional Dram1 protein. Dram1 deficiency caused by two unique morpholino sequences significantly increased *Mm* bacterial burdens (**Figure 5A**). It was previously shown in glioblastoma stem cells that DRAM1 is required for localization of p62 to autophagosomes, suggesting a role for DRAM1 in p62-dependent selective autophagy[18]. *Mtb* can permeabilize the phagosomal membrane using virulence factors encoded by the bacterial region of difference 1 (RD1), allowing cytosolic components of the selective autophagy pathway access to bacteria inside these vacuoles[30]. Recognition of extracellular bacterial DNA by the STING DNA-sensing pathway leads to degradation of ubiquitinated *Mtb* in mature autophagolysosomes via p62[30]. We therefore depleted the zebrafish homologs of p62 and STING using morpholinos and found that this significantly increased mycobacterial burdens (**Figures 5A** and **S5**).

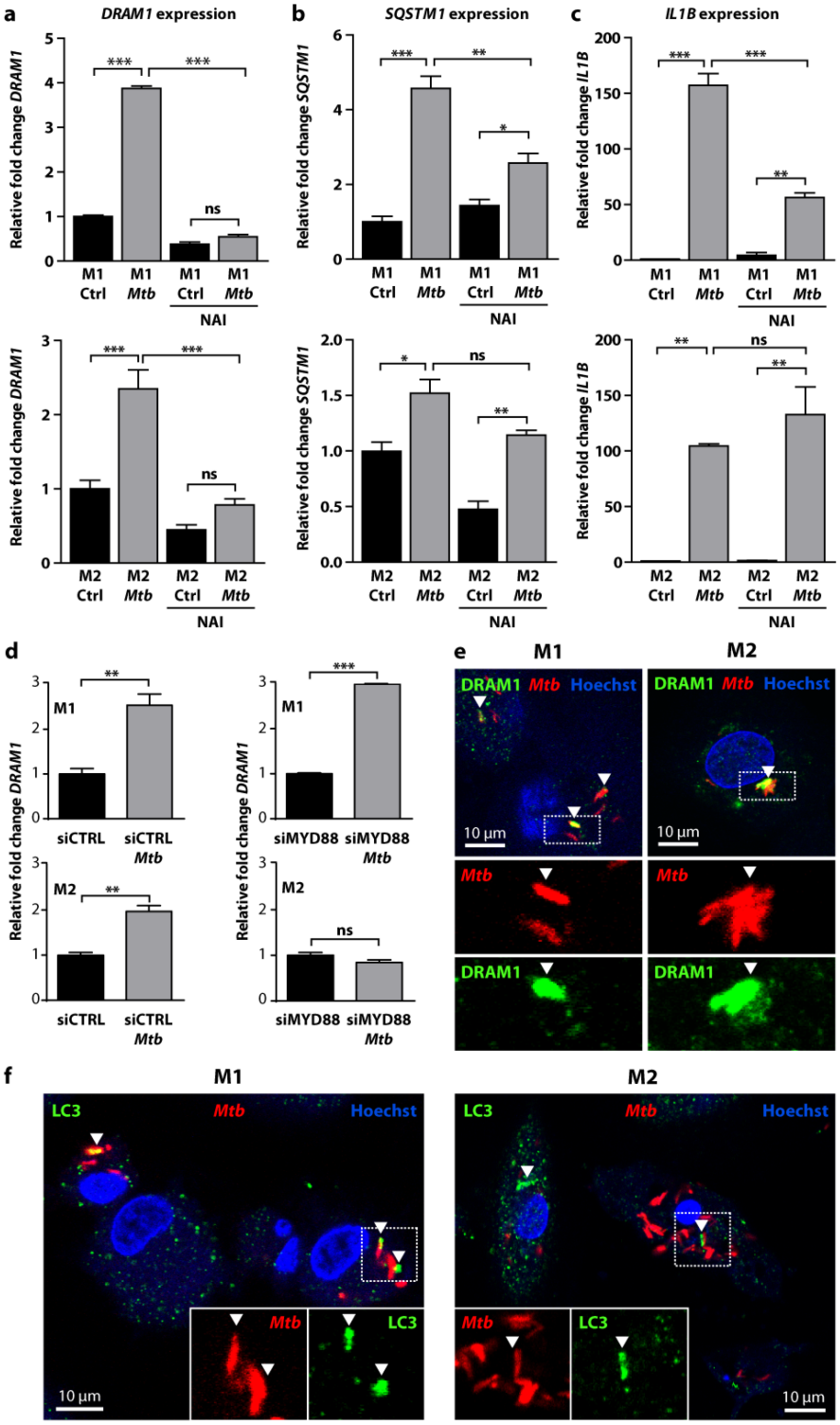
a
DRAM1 expression
Relative fold change DRAM1
M1 Ctrl
M1 Mtb
M1 Ctrl
M1 Mtb
NAI
M2 Ctrl
M2 Mtb
M2 Ctrl
M2 Mtb
b
SQSTM1 expression
Relative fold change SQSTM1
c
IL1B expression
Relative fold change IL1B
ns
d
siCTRL
siCTRL Mtb
siMYD88
siMYD88 Mtb
e
M1
M2
DRAM1 Mtb Hoechst
10 µm
Mtb
DRAM1
f
LC3 Mtb Hoechst
LC3

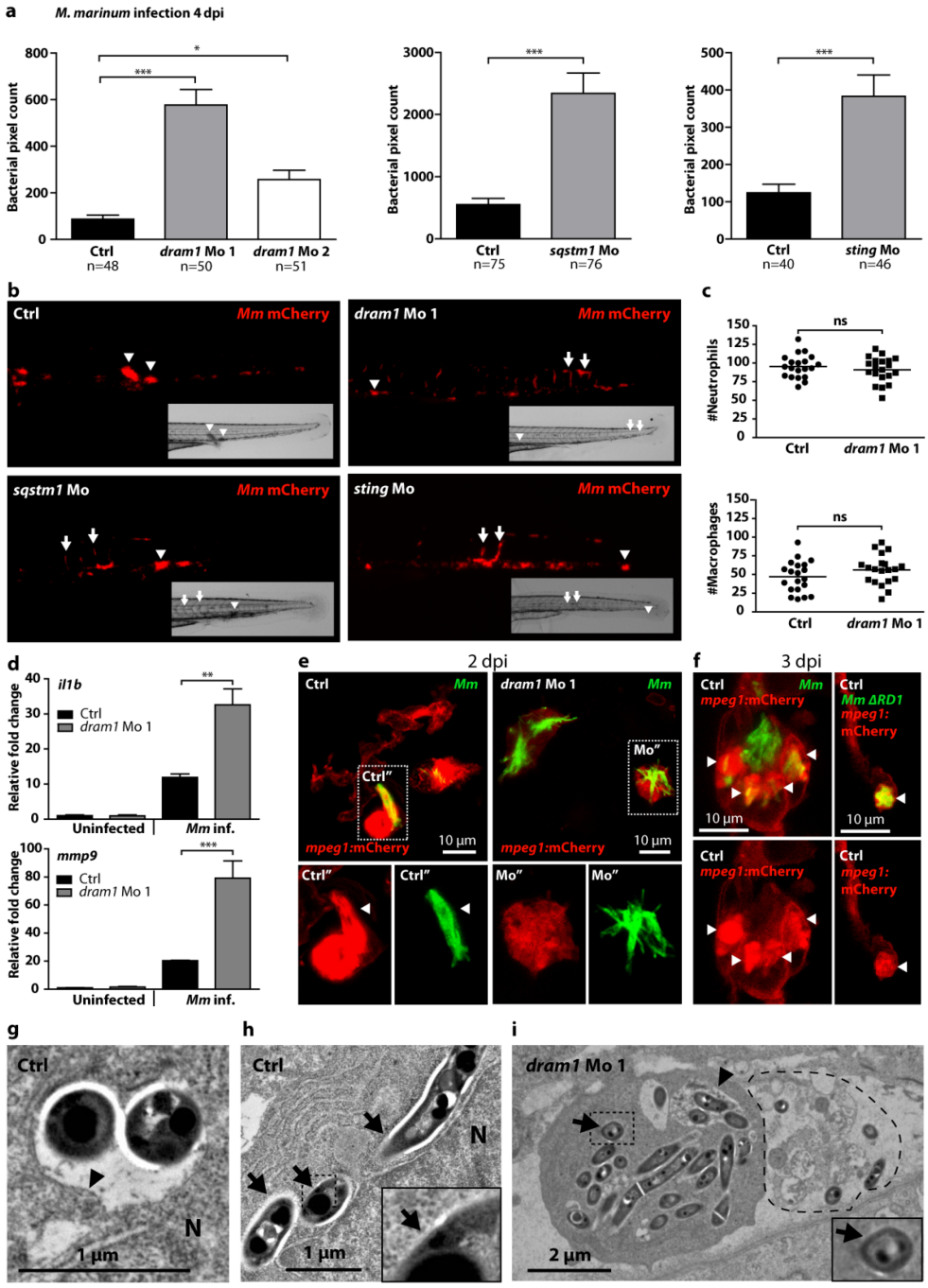
a
M. marinum infection 4 dpi
Bacterial pixel count
Ctrl n=48
dram1 Mo 1 n=50
dram1 Mo 2 n=51
Ctrl n=75
sqstm1 Mo n=76
Ctrl n=40
sting Mo n=46
b
Ctrl
Mm mCherry
dram1 Mo 1
sqstm1 Mo
sting Mo
c
#Neutrophils
#Macrophages
ns
d
il1b
mmp9
Relative fold change
Uninfected
Mm inf.
e
2 dpi
Mm
mpeg1:mCherry
10 µm
f
3 dpi
Mm ΔRD1
g
h
i
1 µm
2 µm
N

⬅ Figure 5. Dram1 Is Required to Contain *Mm* Growth inside Macrophages

A. Zebrafish embryos injected with standard control morpholino, morpholino against *dram1* (*dram1* Mo 1 and Mo 2), *sqstm1* (*sqstm1* Mo), or *sting* (*sting* Mo) were injected with mCherry-labeled *Mm* (see also **Figure S5**). Bacterial pixel counts were determined at 4 dpi. Data (mean ± SEM) is pooled from at least two individual experiments (n = 48–76 embryos per group). **B.** Stereo micrographs of the tail region of highly infected standard control, *dram1* Mo 1-, *sqstm1* Mo-, or *sting* Mo-injected embryos. Arrowheads indicate granuloma formation, and arrows indicate accumulation of bacteria in intersegmental veins. **C.** Total numbers of neutrophils and macrophages in 2 dpf control- or *dram1* Mo 1-injected embryos were quantified using a fluorescence stereo microscope (n = 20 per condition, blinded). Total numbers of macrophages were determined by performing whole-mount L-plastin immunohistochemistry and deducting the number of cells positive for neutrophil-specific myeloperoxidase activity from the number of L-plastin-positive total leukocytes per embryo. Each data point represents an individual embryo, and lines indicate the mean. **D.** Expression levels of *il1b* and *mmp9* at 4 dpi in control morpholino-injected and *dram1* Mo 1-injected embryos with or without *Mm* infection (200 colony-forming units [cfu] for control and 50 cfu for *dram1* Mo 1 to obtain equal bacterial burdens) were determined by qPCR (mean ± SEM from n = 3 biological replicates with 20 embryos per pool). **E and F.** Representative confocal micrographs of *mpeg1*:mCherry transgenic embryos injected with control or *dram1* morpholino 1 and infected with GFP-labeled *Mm* or DRD1 *Mm* **E:** 2 dpi or **F:** 3 dpi. Boxed areas are detailed below, with the green and red channels shown separately. Arrowheads indicate bacteria enclosed by membranes. **G–I.** Transmission electron micrograph of control morpholino-injected embryos with bacteria inside a phagosome (**G**) or bacteria in the cytoplasm (**H**) or *dram1* morpholino-injected embryos with bacteria present both in phagosomes and in the cytoplasm (**I**). Arrows indicate cytoplasmic bacteria, while arrowheads indicate phagosomal membranes. Boxed areas are enlarged in the insets, and the dashed line in **I** indicates the remnants of a dead infected cell. See also **Figure S5**.

Interestingly, highly infected embryos with abrogated *dram1*, *sqstm1*, or *sting* expression displayed a similar phenotype with accumulation of bacteria inside intersegmental blood vessels, indicative of extracellular growth of bacteria (**Figure 5B**). In contrast, highly infected control embryos only displayed large granuloma-like aggregates of *Mm*-infected cells. The phenotype of *dram1* knockdown embryos was not caused by a reduced number of neutrophils or Mϕs (**Figure 5C**). Neither did *dram1* knockdown lead to decreased expression of the proinflammatory genes *il1b* and *mmp9*, ruling out the possibility that Dram1 is required for the initiation of inflammation. In contrast, Dram1-depleted embryos displayed significantly higher expression levels of *il1b* compared to control embryos with equal bacterial burdens at the time point of RNA isolation (**Figures 5D** and **S5F**).

Upon infection of zebrafish embryos, mycobacteria are rapidly phagocytosed by Mϕs[10]. We used a Mϕ-specific reporter line with mCherry localized to all cellular membranes[31] to study the intracellular localization of *Mm* upon knockdown of *dram1*. In both the control and *dram1* knockdown group, virtually all *Mm* were phagocytosed at 1 dpi, and bacteria inside Mϕs were enclosed by membranes (**Figure S5G**). At 2 dpi, bacteria remained intracellular and enclosed by membranes in control-infected embryos (**Figure 5E**). In contrast, we frequently found overgrown Mϕs unable to contain *Mm* inside vesicles in the *dram1* knockdown group (**Figure 5E**), which coincided with the appearance of extracellular bacteria (**Figure S5H**). At 3 dpi, *Mm* in control-infected embryos were residing either in intracellular enclosures or freely in the cytoplasm, indicating that phagosomal escape eventually also occurred in wild-type embryos. However, this only occurred for *Mm* with a functional RD1 locus (**Figure 5F**), similar to the RD1-dependent phagosomal escape of *Mtb* in human cells[32]. Using EM, we could confirm that most bacteria were contained inside phagosomes for control-infected embryos at 2 dpi (**Figure 5G**), with a small proportion of bacteria residing freely in the cytoplasm (**Figure 5H**). At the same time point, infected cells of Dram1-depleted embryos were overgrown by *Mm* and the vast majority of bacteria was cytoplasmic (**Figure 5I**). The inability of Dram1 morphants to control intracellular growth of mycobacteria frequently resulted in rupture of infected cells and the presence of extracellular bacteria inside blood vessels (**Figures 5I** and **S5I**).

➡ Figure 6. Dram1 Modulates an Autophagic Defense Mechanism that Requires Bacterial RD1 Virulence, Host p62/Sqstm1, and Sting

A. GFP-Lc3 embryos were injected with 100 pg *dram1* RNA. Representative confocal micrographs of epithelial cells at 3 dpf are shown. **B.** The number of GFP-Lc3 punctae was determined for n = 50 cells per group and quantified based on confocal micrographs of control- and *dram1* RNA-injected embryos (n ≥ 5, blinded). **C.** Bacterial pixel counts were determined at 3 dpi for infected control- or *dram1* RNA-injected embryos. Data (mean ± SEM) is pooled from two individual experiments (n ≥ 94 embryos per group). **D.** Representative stereo micrographs of the tail of infected control- or *dram1* RNA-injected embryos at 3 dpi. **E.** Representative confocal micrographs of GFP-Lc3 embryos infected with *Mm M* ΔRD1 (400 cfu) and wild-type *Mm M* bacteria (200 cfu). **F.** Bacterial pixel counts following these infections were determined with or without *dram1* knockdown. Data (mean ± SEM) are pooled from two individual experiments (n > 62 embryos per group). **G.** Representative confocal micrographs of GFP-Lc3 embryos injected with control morpholino, *myd88* morpholino, *dram1* morpholino 1, *dram1* RNA (100 pg; inset in the image is a micrograph from a different RNA-injected embryo), *sqstm1* morpholino, *dram1* RNA + *sqstm1* morpholino, *sting* morpholino, and *dram1* RNA + *sting* morpholino. All groups were injected with *Mm*. **H–J.** Confocal micrographs were used to quantify GFP-Lc3 punctae per infected cell (n ≥ 5 embryos per group, blinded) to evaluate the effect of *dram1* RNA (**H**), *dram1* RNA combined with *sqstm1* Mo (**I**), or *dram1* RNA combined with *sting* Mo (**J**). See also **Figure S6**.

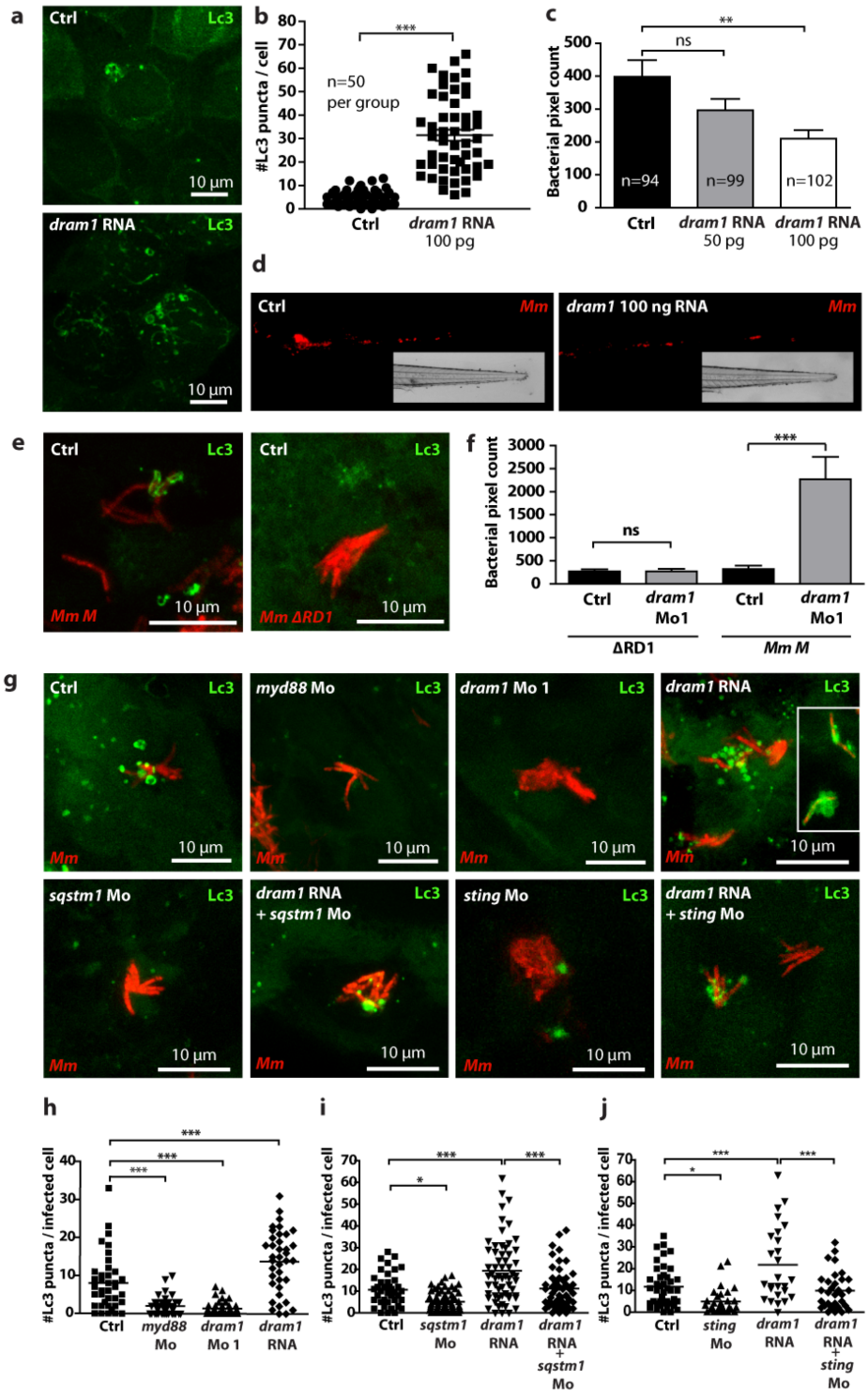
a
Ctrl
Lc3
10 µm
dram1 RNA
Lc3
10 µm
b
#Lc3 puncta / cell
***
n=50
per group
Ctrl
dram1 RNA
100 pg
c
Bacterial pixel count
**
ns
n=94
n=99
n=102
Ctrl
dram1 RNA
50 pg
dram1 RNA
100 pg
d
Ctrl
Mm
dram1 100 ng RNA
Mm
e
Ctrl
Lc3
Mm M
10 µm
Ctrl
Lc3
Mm ΔRD1
10 µm
f
Bacterial pixel count
***
ns
Ctrl
dram1 Mo1
Ctrl
dram1 Mo1
ΔRD1
Mm M
g
Ctrl
Lc3
Mm
10 µm
myd88 Mo
Lc3
Mm
10 µm
dram1 Mo 1
Lc3
Mm
10 µm
dram1 RNA
Lc3
Mm
10 µm
sqstm1 Mo
Lc3
Mm
10 µm
dram1 RNA
+ sqstm1 Mo
Lc3
Mm
10 µm
sting Mo
Lc3
Mm
10 µm
dram1 RNA
+ sting Mo
Lc3
Mm
10 µm
h
#Lc3 puncta / infected cell
***
***
***
Ctrl
myd88 Mo
dram1 Mo 1
dram1 RNA
i
#Lc3 puncta / infected cell
***
***
*
Ctrl
sqstm1 Mo
dram1 RNA
dram1 RNA + sqstm1 Mo
j
#Lc3 puncta / infected cell
***
***
*
Ctrl
sting Mo
dram1 RNA
dram1 RNA + sting Mo

Selective autophagy induced by *dram1* overexpression restricts mycobacterial infection

To further test the hypothesis that Dram1 is involved in autophagic defense against mycobacterial infection, we cloned zebrafish *dram1* and injected mRNA into GFP-Lc3 transgenic embryos at the one-cell stage, leading to ubiquitous overexpression of *dram1* in the developing embryo. Embryos overexpressing *dram1* developed normally and showed no apparent phenotypes (data not shown). At 3 days postfertilization (dpf), *dram1* overexpression resulted in significantly increased numbers of GFP-Lc3 vesicles compared to controls (**Figures 6A** and **6B**), indicating that the function of DRAM1 as an inducer of autophagy is conserved between human and zebrafish[17,33]. Dram1 initiates GFP-Lc3 accumulation via a mechanism that is distinct from the autophagy response to Ar-12 or rapamycin treatment, since Dram1-depleted embryos still displayed a marked increase in GFP-Lc3 vesicles upon exposure to these drugs (**Figures S6A** and **S6B**). We then examined the effect of *dram1* overexpression during mycobacterial infection and observed that it reduced bacterial burden in a dose-dependent manner (**Figures 6C** and **6D**). Mycobacterial clusters decreased in number and size in embryos injected with the highest dose of *dram1* RNA (**Figures S6C** and **S6D**), showing that Dram1 is part of a defense mechanism against mycobacterial infection. Both the induction of autophagy in *Mm*-infected cells and the increase in bacterial burden upon *dram1* knockdown required the mycobacterial RD1 virulence locus (**Figures 6E** and **6F**). To further demonstrate the importance of Dram1 in defense against pathogenic mycobacteria, we knocked down the expression of *myd88* and *dram1* in GFP-Lc3 embryos and infected them with *Mm*. Morpholino knockdown of either *myd88* or *dram1* significantly reduced the number of GFP-Lc3 punctae per cell (**Figures 6G** and **6H**). Strikingly, overexpression of *dram1* RNA increased the autophagy response in infected cells, showing a clear colocalization between Lc3 and bacteria, which occasionally completely encapsulated bacteria (**Figures 6G** and **6H**). Morpholino knockdown of *p62/sqstm1* significantly lowered the number of GFP-Lc3 punctae

➡ Figure 7. Dram1 Mediates Autophagic Flux and Lysosomal Maturation via Multiple Vesicle Fusion Events

A and B. Embryos were infected with crimson-labeled *Mm* and stained with LysoTracker Red (arrowheads indicate colocalization). **A.** Wild-type embryos injected with standard control, *dram1* morpholino, or *dram1* RNA (100 pg). **B.** *dram1* RNA- or control-injected GFP-Lc3 embryos. **C–F.** Embryos transiently expressing mCherry-Dram1, colocalized with **C:** LysoTracker Green, **D:** GFP-Lc3, **E:** crimson-labeled *Mm*, or **F:** crimson-labeled *Mm*, and immunohistochemistry detection of p62 (arrowheads indicate colocalization). **G.** Transmission electron micrograph of *dram1* RNA-injected embryos infected with *Mm* (arrowheads). Arrows indicate (remnants of) vesicle fusion, and « indicates the double membrane of an autophagosome. **H.** Schematic representation of the findings presented in this manuscript, as explained in the **Discussion**. See also **Figure S7**.

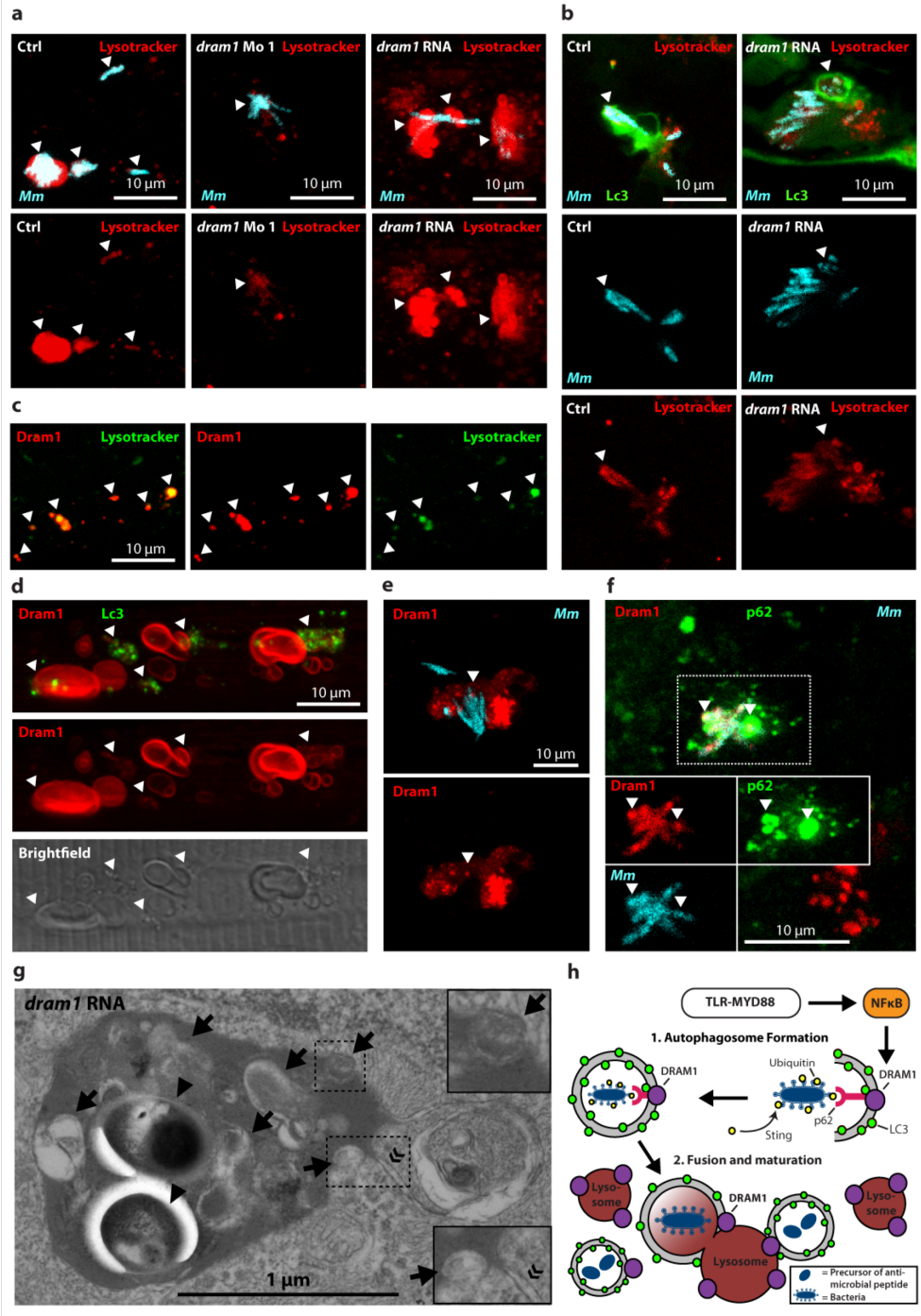
a
Ctrl
Lysotracker
dram1 Mo 1
dram1 RNA
Mm
10 µm
b
Lc3
c
Dram1
d
Brightfield
e
f
p62
g
dram1 RNA
1 µm
h
TLR-MYD88
NFκB
1. Autophagosome Formation
DRAM1
Ubiquitin
Sting
LC3
2. Fusion and maturation
Lyso-some
Lysosome
= Precursor of anti-microbial peptide
= Bacteria

per infected cell in zebrafish embryos (**Figures 6G** and **6I**), consistent with previous observations in human cell cultures[13,30]. If autophagic defense initiated by Dram1 requires p62, Dram1-dependent autophagy should be blocked by depletion of p62. Indeed, coinjection of *sqstm1* morpholino with *dram1* RNA counteracted the increased formation of *Mm*-associated autophagosomes caused by *dram1* overexpression (**Figures 6G** and **6I**). As was observed for p62, knockdown of *sting* also significantly lowered the number of GFP-Lc3 punctae per infected cell and could counteract the effect of *dram1* overexpression (**Figures 6G** and **6J**). Together, these data demonstrate that Dram1 stimulates the targeting of autophagosomes to bacteria or bacteria-containing compartments, requiring Sting and the selective autophagy receptor p62. We conclude that this Dram1-mediated mechanism downstream of MyD88 has a protective function during mycobacterial infection *in vivo*.

Dram1 mediates autophagic flux and lysosomal maturation via multiple vesicle fusion events

Autophagosomes require fusion with lysosomes to obtain mycobactericidal characteristics[2]. It was previously reported that DRAM1 regulates autophagic flux through lysosomes following mitochondrial dysfunctioning[34]. We therefore used LysoTracker to examine the role of Dram1 in lysosomal acidification during *Mm* infection. Dram1 depletion abrogated colocalization of acidified lysosomes with *Mm*-containing vesicles, while Dram1 overexpression dramatically increased lysosomal acidification surrounding *Mm* (**Figure 7A**). Next, we demonstrated that autophagic flux contributes to this process by visualizing *Mm*-containing vesicles that are positive for LysoTracker as well as GFP-Lc3 (**Figure 7B**).

Human DRAM1 was described as a lysosomal protein with six predicted transmembrane domains and has also been localized to autophagosomes[17,33]. In agreement, zebrafish mCherry-Dram1 predominantly localized to LysoTracker-positive vesicles (**Figure 7C**). To express mCherry-Dram1, we injected a DNA construct with beta-actin promoter, resulting in transient mosaic expression and frequently showing high expression in muscle cells. Cells with high levels of mCherry-Dram1 contained large Dram1-positive vacuoles, while neighboring muscle cells retained their characteristic striated pattern (**Figure 7D**). The mCherry-Dram1 pattern confirms the predicted membrane localization of Dram1, and Dram1-positive vacuoles were frequently highly decorated by GFP-Lc3 (**Figures 7D** and **S7A**). As observed for human Mϕs infected with *Mtb* (**Figure 4E**), zebrafish mCherry-Dram1 colocalizes with and accumulates around *Mm* (**Figure 7E**). Furthermore, mCherry-Dram1 colocalized with p62 antibody staining during the autophagic response to mycobacterial infection (**Figure 7F**).

With EM, we determined the ultrastructural composition of *Mm*-containing compartments and regularly observed *Mm* inside autophagolysosomes, as characterized by the presence of cytoplasmic material inside the single-membraned vesicles (**Figure S7B**). Importantly, we also captured the exact moment at which a double-membraned autophagosome fuses with an *Mm*-containing, electron-dense compartment with the characteristics of a lysosome (**Figure 7G**). Notably, this event was imaged in a Dram1-overexpressing embryo,

and we frequently observed large *Mm*-containing compartments in this treatment group (**Figures S7C** and **S7D**). Vesicle fusion would facilitate the delivery of neo-antimicrobial peptides to the bacteria-containing compartment, in line with findings by[13]. The remnants of many membranes inside these compartments demonstrate that these vacuoles have grown to their unusual large size by multiple fusion events.

Discussion

Besides the fundamental cellular homeostatic function of autophagy, selective autophagy has emerged as an important effector mechanism of immune defense[1]. Until now, the autophagy modulator DRAM1 was exclusively known as a p53-target gene that induces autophagy and cell death in response to cellular stresses related to cancer[17] and HIV infection of $CD4^+$ T cells[35]. Here, we show how this important modulator of autophagy also functions downstream of the TLR/IL1R-MYD88-NF-κB pathway in controlling infection with intracellular mycobacteria independently of p53.

We show that zebrafish Dram1 is capable of modulating autophagy, like its human ortholog[17,33], and that *DRAM1* expression is increased in response to infection with mycobacterial pathogens in human Mϕs as well as zebrafish embryos. DRAM1/Dram1 colocalizes with mycobacteria and is important for defense against mycobacterial infection. To further support a function of DRAM1 in TB disease progression, we examined published microarray datasets of human patient material for *DRAM1* expression levels and found that *DRAM1* was upregulated in the whole-blood transcript signature of active TB patients[36] and in Mϕs obtained from *Mtb*-infected patients[37].

Mϕs in *dram1*-deficient zebrafish embryos had difficulty maintaining mycobacteria inside vesicles and were frequently overgrown by bacteria, resulting in large accumulations of extracellular bacteria at later stages of infection. Dram1 and p62 were required for the formation of autophagosomes associated with mycobacterial infection foci. Based on our results, we believe that Dram1 controls intracellular mycobacterial growth in two ways (**Figure 7H**). First, Dram1 mediates p62-dependent selective autophagy that can engulf entire mycobacteria. Second, Dram1 aids in the maturation of mycobacteria-containing compartments by facilitating multiple fusion events with lysosomes and autophagosomes. It has been shown previously that ribosomal and cytoplasmic peptides taken up via p62-dependent autophagy are proteolytically converted into products capable of killing *Mtb* inside lysosomes[13]. The stimulation of autophagosomal and lysosomal vesicle fusion by Dram1 can enhance the delivery of such neo-antimicrobial peptides. In the absence of *dram1*, GFP-Lc3 accumulation could still be induced by Ar-12 or rapamycin, indicating that these drugs stimulate non-selective autophagy pathways independent of Dram1. Ar-12 and rapamycin enhance bacterial killing in several model systems[38-40]. However, contrary to the protective effect of *dram1* overexpression, Ar-12 or rapamycin treatments were detrimental to defense in the

zebrafish model, most likely due to susceptibility of zebrafish embryos to broad side effects of these drugs.

The targeting of autophagosomes to mycobacteria by Dram1 required the DNA-sensing Sting pathway. In human Mϕs, the STING pathway was shown to ubiquitinate and target *Mtb* for autophagic destruction after bacteria had permeabilized the phagosomal membrane using a RD1 locus encoded virulence mechanism[30]. In contrast, RD1 virulence was linked with inhibition of autophagy in *Mtb*-infected dendritic cells[40]. While autophagy-evading strategies are likely to have evolved in mycobacteria, our results in the zebrafish model corroborate the essential requirement of RD1 and Sting for selective autophagic defense against mycobacteria[22,30].

TLR/IL1R signaling via the MYD88-dependent and -independent pathways can activate tumor necrosis factor receptor-associated factor (TRAF)-associated NF-κB activator (TANK)-binding kinase-1 (TBK1) [41], which coordinates assembly and function of the autophagic machinery, including phosphorylation of p62 and maturation of autophagosomes[42]. The IKK family member TBK1 can activate NF-κB[43], making it a potential regulator of *DRAM1* and infection-induced autophagy. However, TBK1 can also inhibit the canonical IKK complex[41], known to be involved in initiation of autophagy[27]. It is becoming clear that autophagy is regulated by both the canonical and noncanonical NF-κB activation pathways, as well as the stress-induced p53 pathway[27]. Besides NF-κB-binding motifs, we identified consensus binding sites for AP-1 and STAT in the promoter region of DRAM1, indicating that other immune signaling pathways may also activate DRAM1. Further dissection of DRAM1 regulation will help clarify the complex signaling networks controlling autophagy initiation and flux in response to different stimuli.

The diverse roles of autophagy as both effector and regulator of immune processes are receiving much attention[1]. Here, we showed that the TLR/IL1R-MYD88-NF-κB-dependent expression of *dram1* is required to mobilize autophagic defense to mycobacteria. Zebrafish *dram1* expression is also upregulated by *Salmonella* infection[29], and in the current study we showed it to be responsive to the common bacterial endotoxin LPS. Furthermore, autophagic defense against intestinal bacteria was recently shown to depend on MYD88, but how MYD88 is linked with autophagosome induction remained unknown[44]. In light of these observations, we expect this TLR-MYD88-DRAM1 defense pathway to protect against a range of intracellular pathogens broader than that of mycobacterial species alone. The role of DRAM1 in immunity might even be broader than that. First, autophagy functions as a regulator of inflammation by targeting inflammasomes for degradation, limiting the processing and secretion of IL-1β[45]. Knockdown of zebrafish *dram1* increased *il1b* expression levels following mycobacterial infection, linking DRAM1 to the regulatory immune function of autophagy. Second, particles that stimulate TLRs during phagocytosis trigger the rapid recruitment of LC3 to the phagosome in a process termed LC3-associated phagocytosis (LAP) [14]. With the currently available techniques, we could not ascertain if Dram1 is involved in LAP; however, *dram1* depletion led to a notable absence of autophagolysosomes, consistent with the proposed role in autophagosome maturation (**Figure 7H**).

The increasing occurrence of *Mtb* strains with resistance to multiple drug treatments makes TB a key priority for infectious disease research. Understanding the host-pathogen interactions during *Mtb* pathogenesis is necessary to develop host-directed therapeutic strategies that may complement antibiotic interventions[46,47]. The role of DRAM1 as an inducer of antimycobacterial autophagy makes this pathway a highly interesting therapeutic target, since we have shown in vivo that hyperactivation of the DRAM1-dependent autophagy pathway significantly lowered mycobacterial burden.

Experimental procedures

Zebrafish Culture and Lines

Zebrafish lines (**Table S1**) were handled in compliance with local animal welfare regulations as overseen by the Leiden University animal ethics committee. Embryos were grown at 28.5°C and kept under anesthesia with egg water containing 0.02% buffered 3-aminobenzoic acid ethyl ester (Tricaine) during bacterial injections or imaging.

Injection Conditions

Mycobacteria or LPS was injected into zebrafish embryos as described in the **Supplemental Experimental Procedures**. Splice morpholinos (**Table S2**) and RNA were injected into the yolk, and mCherry-Dram1 was injected into the cell, at the one-cell stage (details in **Supplemental Experimental Procedures**). Morpholino knockdown of mRNA was tested using the SuperScript One-Step RT-PCR System (Invitrogen, #10928-034).

Gene Expression Analysis

RNA was isolated using TRI Reagent (Life Technologies) and purified with RNeasy MinElute Cleanup kit (QIAGEN). cDNA synthesis and qPCR (**Table S3** for primer sequences) were performed as described previously[16], and gene expression was normalized against housekeeping genes. Microarray and RNA sequencing analysis was performed as described in the **Supplemental Experimental Procedures**. Mϕs, neutrophils, and lymphocytes were isolated by FACS from 5–6 dpf zebrafish larvae.

Drug Treatments

The following drugs were used: 3-methyladenine (3-MA; 10 mM; Sigma, #M9281), chloroquine (100 μM; Sigma, #C6628), Ar-12 (1 μM; Selleck Chemicals, #S1106), Rapamycin (1 μM; Sigma, #44532-U), NF-κB activation inhibitor (50 nM in embryos, 30 nM in Mϕs; Calbiochem, #481406), and Roscovitin (50 μM; Sigma, #R7772). Drugs were administered via the water or culture medium for zebrafish embryos and human Mϕs, respectively.

Microscopy and Fluorescent Pixel Quantification

Embryos were imaged using a Leica MZ16FA stereo fluorescence microscope with DFC420C camera or a Leica TCS SPE confocal microscope. Maximal intensity projections of confocal micrograph z stacks are shown. Total fluorescent pixels per infected fish were determined on whole-embryo stereo fluorescent micrographs using dedicated software[48]. Electron microscopy images were obtained with a JEOL JEM-1010 transmission electron microscope equipped with an Olympus MegaView camera (see **Supplemental Experimental Procedures** for sample preparation).

Immunohistochemistry

Identification of neutrophils and Mϕs was done by immunolabeling with a leukocyte-specific L-plastin antibody and Alexa 568 conjugated secondary antibody combined with neutrophil-specific staining for myeloperoxidase activity[48]. p62 was detected by a sheep polyclonal antibody (ab31545, Abcam); human DRAM1 (AP21751PU-N, Acris Antibodies) and LC3 (PA1-46286, Thermo Scientific) were detected by rabbit polyclonal antibodies combined with donkey-anti-sheep/goat-anti-rabbit Alexa488 conjugated secondary antibody (Invitrogen).

LysoTracker Staining

Embryos were incubated for 1 hr in egg water with 10 μM LysoTracker Green or Red (Invitrogen) and rinsed several times before imaging.

Infection of Human Mϕs

Type 1 and 2 human Mϕs were generated from buffy coats of anonymous blood bank donors with approval of the medical ethical committee of the Leiden University Medical Center, and they were maintained and transfected with siRNA as described in detail in the **Supplemental Experimental Procedures**. *Mtb* was cultured in Difco Middlebrook 7H9 broth (Becton Dickinson) supplemented with 10% albumin dextrose catalase (ADC) (Becton Dickinson) and 0.5% Tween-80 (Sigma). Primary human Mϕs were infected at a multiplicity of infection (MOI) of 10. Wells containing the cell cultures were inoculated with 100 μl of *Mtb* suspension, centrifuged for 3 min at 800 rpm, and incubated at 37°C/5% CO_2 for 60 min. Plates were then washed with medium containing 30 mg/ml gentamicin sulfate (Lonza BioWhittaker) and incubated at 37°C/5% CO_2 in medium containing 5 mg/ml gentamicin and inhibitors, if appropriate.

Statistical Analysis

All data (mean ± SEM) were analyzed using unpaired, two-tailed t tests for comparisons between two groups and one-way ANOVA with Tukey's multiple comparison method as a post-hoc test for other data. (ns, no significant difference; *$p < 0.05$; **$p < 0.01$; ***$p < 0.001$). For microarray, significant differences were calculated using Rosetta Resolver re-ratio analysis (* = fold change > 2, $p < 10^{-5}$). For RNA deep sequencing, significant differences were calculated by DESeq analysis of transcript count data (* = fold change > 2, $p < 0.05$).

Accession Numbers

Microarray and RNA sequencing data were deposited in the Gene Expression Omnibus (GEO) database under accession number GSE49188.

References

1. Deretic, V., Saitoh, T. & Akira, S. Autophagy in infection, inflammation and immunity. *Nat Rev Drug Discov* **13,** 722–737 (2013).
2. Levine, B., Mizushima, N. & Virgin, H. W. Autophagy in immunity and inflammation. **469,** 323–335 (2011).
3. Alonso, S., Pethe, K., Russell, D. G. & Purdy, G. E. Lysosomal killing of Mycobacterium mediated by ubiquitin-derived peptides is enhanced by autophagy. *Proc. Natl. Acad. Sci. U.S.A.* **104,** 6031–6036 (2007).
4. Gutierrez, M. G. *et al.* Autophagy is a defense mechanism inhibiting BCG and Mycobacterium tuberculosis survival in infected macrophages. *Cell* **119,** 753–766 (2004).
5. Singh, S. B., Davis, A. S., Taylor, G. A. & Deretic, V. Human IRGM induces autophagy to eliminate intracellular mycobacteria. *Science* **313,** 1438–1441 (2006).
6. Vergne, I., Chua, J., Singh, S. B. & Deretic, V. Cell biology of mycobacterium tuberculosis phagosome. *Annu. Rev. Cell Dev. Biol.* **20,** 367–394 (2004).
7. Ramakrishnan, L. Revisiting the role of the granuloma in tuberculosis. *Nat Rev Drug Discov* **12,** 352–366 (2012).
8. Swaim, L. E. *et al.* Mycobacterium marinum infection of adult zebrafish causes caseating granulomatous tuberculosis and is moderated by adaptive immunity. *Infection and Immunity* **74,** 6108–6117 (2006).
9. Berg, R. D. & Ramakrishnan, L. Insights into tuberculosis from the zebrafish model. *Trends Mol Med* **18,** 689–690 (2012).
10. Clay, H. *et al.* Dichotomous role of the macrophage in early Mycobacterium marinum infection of the zebrafish. *Cell Host and Microbe* **2,** 29–39 (2007).
11. Mostowy, S. *et al.* The zebrafish as a new model for the in vivo study of Shigella flexneri interaction with phagocytes and bacterial autophagy. *PLoS Pathog* **9,** e1003588 (2013).
12. Delgado, M. A., Elmaoued, R. A., Davis, A. S., Kyei, G. & Deretic, V. Toll-like receptors control autophagy. *The EMBO Journal* **27,** 1110–1121 (2008).
13. Ponpuak, M. *et al.* Delivery of cytosolic components by autophagic adaptor protein p62 endows autophagosomes with unique antimicrobial properties. *Immunity* **32,** 329–341 (2010).
14. Sanjuan, M. A. *et al.* Toll-like receptor signalling in macrophages links the autophagy pathway to phagocytosis. **450,** 1253–1257 (2007).
15. Shi, C.-S. & Kehrl, J. H. MyD88 and Trif target Beclin 1 to trigger autophagy in macrophages. *J. Biol. Chem.* **283,** 33175–33182 (2008).

16. van der Vaart, M., van Soest, J. J., Spaink, H. P. & Meijer, A. H. Functional analysis of a zebrafish myd88 mutant identifies key transcriptional components of the innate immune system. *Dis Model Mech* **6,** 841–854 (2013).
17. Crighton, D. *et al.* DRAM, a p53-induced modulator of autophagy, is critical for apoptosis. *Cell* **126,** 121–134 (2006).
18. Galavotti, S. *et al.* The autophagy-associated factors DRAM1 and p62 regulate cell migration and invasion in glioblastoma stem cells. *Oncogene* **32,** 699–712 (2013).
19. Ryan, K. M. p53 and autophagy in cancer: guardian of the genome meets guardian of the proteome. *Eur. J. Cancer* **47,** 44–50 (2011).
20. He, C., Bartholomew, C. R., Zhou, W. & Klionsky, D. J. Assaying autophagic activity in transgenic GFP-Lc3 and GFP-Gabarap zebrafish embryos. *Autophagy* **5,** 520–526 (2009).
21. Gao, M. *et al.* OSU-03012, a novel celecoxib derivative, induces reactive oxygen species-related autophagy in hepatocellular carcinoma. *Cancer Res.* **68,** 9348–9357 (2008).
22. Lerena, M. C. & Colombo, M. I. Mycobacterium marinum induces a marked LC3 recruitment to its containing phagosome that depends on a functional ESX-1 secretion system. *Cellular Microbiology* **13,** 814–835 (2011).
23. Ellett, F., Pase, L., Hayman, J. W., Andrianopoulos, A. & Lieschke, G. J. mpeg1 promoter transgenes direct macrophage-lineage expression in zebrafish. *Blood* **117,** e49–56 (2011).
24. Renshaw, S. A. *et al.* A transgenic zebrafish model of neutrophilic inflammation. *Blood* **108,** 3976–3978 (2006).
25. Langenau, D. M. *et al.* In vivo tracking of T cell development, ablation, and engraftment in transgenic zebrafish. *Proc. Natl. Acad. Sci. U.S.A.* **101,** 7369–7374 (2004).
26. Guo, L. *et al.* Ionizing radiation induces a dramatic persistence of p53 protein accumulation and DNA damage signaling in mutant p53 zebrafish. *Oncogene* **32,** 4009–4016 (2013).
27. Criollo, A. *et al.* IKK connects autophagy to major stress pathways. *Autophagy* **6,** 189–191 (2010).
28. Kanther, M. *et al.* Microbial colonization induces dynamic temporal and spatial patterns of NF-κB activation in the zebrafish digestive tract. *Gastroenterology* **141,** 197–207 (2011).
29. Stockhammer, O. W. *et al.* Transcriptome analysis of Traf6 function in the innate immune response of zebrafish embryos. *Molecular Immunology* **48,** 179–190 (2010).
30. Watson, R. O., Manzanillo, P. S. & Cox, J. S. Extracellular M. tuberculosis DNA targets bacteria for autophagy by activating the host DNA-sensing pathway. *Cell* **150,** 803–815 (2012).
31. Bernut, A. *et al.* Mycobacterium abscessus cording prevents phagocytosis and promotes abscess formation. *Proc Natl Acad Sci USA* **111,** E943–52 (2014).
32. van der Wel, N. *et al.* M. tuberculosis and M. leprae translocate from the phagolysosome to the cytosol in myeloid cells. *Cell* **129,** 1287–1298 (2007).

33. Mah, L. Y., O'Prey, J., Baudot, A. D., Hoekstra, A. & Ryan, K. M. DRAM-1 encodes multiple isoforms that regulate autophagy. *Autophagy* **8,** 18–28 (2012).
34. Zhang, X.-D., Qi, L., Wu, J.-C. & Qin, Z.-H. DRAM1 regulates autophagy flux through lysosomes. *PLoS ONE* **8,** e63245 (2013).
35. Laforge, M. *et al.* DRAM triggers lysosomal membrane permeabilization and cell death in CD4(+) T cells infected with HIV. *PLoS Pathog* **9,** e1003328 (2013).
36. Berry, M. P. R. *et al.* An interferon-inducible neutrophil-driven blood transcriptional signature in human tuberculosis. **466,** 973–977 (2010).
37. Thuong, N. T. T. *et al.* Identification of tuberculosis susceptibility genes with human macrophage gene expression profiles. *PLoS Pathog* **4,** e1000229 (2008).
38. Chiu, H.-C. *et al.* Eradication of intracellular Francisella tularensis in THP-1 human macrophages with a novel autophagy inducing agent. *J Biomed Sci* **16,** 110 (2009).
39. Chiu, H.-C. *et al.* Eradication of intracellular Salmonella enterica serovar Typhimurium with a small-molecule, host cell-directed agent. *Antimicrobial Agents and Chemotherapy* **53,** 5236–5244 (2009).
40. Romagnoli, A. *et al.* ESX-1 dependent impairment of autophagic flux by Mycobacterium tuberculosis in human dendritic cells. *Autophagy* **8,** 1357–1370 (2012).
41. Clark, K. *et al.* Novel cross-talk within the IKK family controls innate immunity. *Biochem. J.* **434,** 93–104 (2011).
42. Pilli, M. *et al.* TBK-1 promotes autophagy-mediated antimicrobial defense by controlling autophagosome maturation. *Immunity* **37,** 223–234 (2012).
43. Pomerantz, J. L. & Baltimore, D. NF-kappaB activation by a signaling complex containing TRAF2, TANK and TBK1, a novel IKK-related kinase. *The EMBO Journal* **18,** 6694–6704 (1999).
44. Benjamin, J. L., Sumpter, R., Levine, B. & Hooper, L. V. Intestinal epithelial autophagy is essential for host defense against invasive bacteria. *Cell Host and Microbe* **13,** 723–734 (2013).
45. Shi, C.-S. *et al.* Activation of autophagy by inflammatory signals limits IL-1β production by targeting ubiquitinated inflammasomes for destruction. *Nat Immunol* **13,** 255–263 (2012).
46. Koul, A., Arnoult, E., Lounis, N., Guillemont, J. & Andries, K. The challenge of new drug discovery for tuberculosis. **469,** 483–490 (2011).
47. Kuijl, C. *et al.* Intracellular bacterial growth is controlled by a kinase network around PKB/AKT1. **450,** 725–730 (2007).
48. Cui, C. *et al.* Infectious disease modeling and innate immune function in zebrafish embryos. *Methods Cell Biol.* **105,** 273–308 (2011).

Supplemental Information

Supplementary figure 1

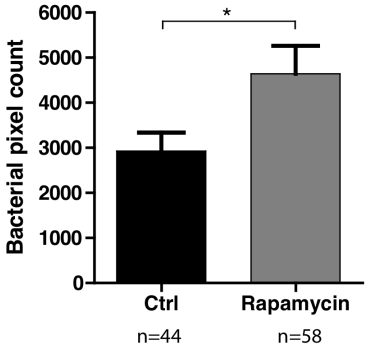

Supplementary figure 1. Effect of Rapamycin treatment on mycobacterial infection in zebrafish embryos. Zebrafish embryos were infected with 200 CFU of *Mycobacterium marinum* at 1 dpf. At 2 dpf, embryos were treated with DMSO (Ctrl) or Rapamycin (1 µM) for 24 hours, after which bacterial fluorescent pixels were quantified based on micrographs. Data (mean ± SEM) represents two individual experiments (*: p≤0,05, as determined by T-test).

Supplementary figure 2

a Gene synteny

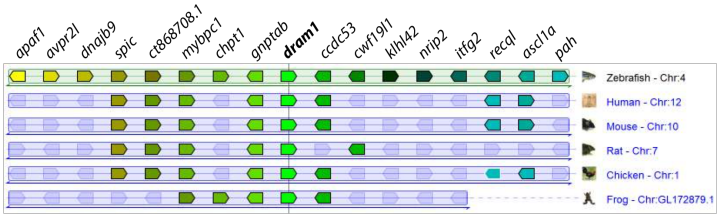

b Protein homology

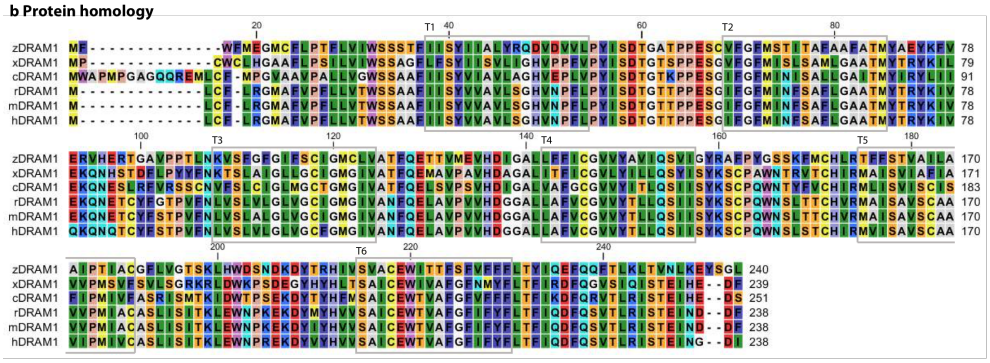

c Alignment tree

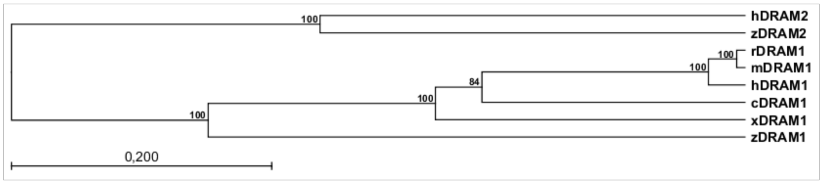

Supplementary figure 2. Conservation of vertebrate DRAM1.
Genomic structure and sequence analysis of the zebrafish *dram1* gene. (A) Physical synteny of the region containing the *dram1* gene in zebrafish chromosome 4 (Chr:4) with human chromosome 12 (Chr:12), mouse chromosome 10 (Chr:10), rat chromosome 7 (Chr:7), chicken chromosome 1 (Chr:1) and frog scaffold GL172879.1. Surrounding *dram1* the genes SPIC, CT8868708.1, MYBPC1, GNPTAB, CCDC53, RECQL, ASCL1A are arranged in the same order on zebrafish Chr:4 as on human Chr:12, and appeared in the same position in the majority of the vertebrate species analyzed. Coding direction of the genes is indicated by the pointed end. Empty pale blue symbols indicate non-syntenic genes. (B) Multiple alignment of the vertebrate DRAM1 proteins. Identical residues identified are indicated with the same color. Grey boxes the transmembrane domains based on human DRAM1 (Crighton et al., 2006). (C) Unrooted phylogenetic tree of DRAM1 amino acid sequences. The tree was created by UPGMA method using ClustalW multiple alignment and bootstrapped 5000 times. The scale for the given branch length indicates 0.200 amino acid substitutions per site. Sequences were retrieved from the following accession numbers in public databases: zebrafish (zDRAM1): ENSDARG00000045561; xenopus (xDRAM1): ENSXETG00000027990; chicken (cDRAM1): ENSGALG00000012761; rat (rDRAM1): ENSRNOG00000038916; mouse (mDRAM1): ENSMUSG00000020057; human (hDRAM1): ENSG00000136048.

Supplementary figure 3

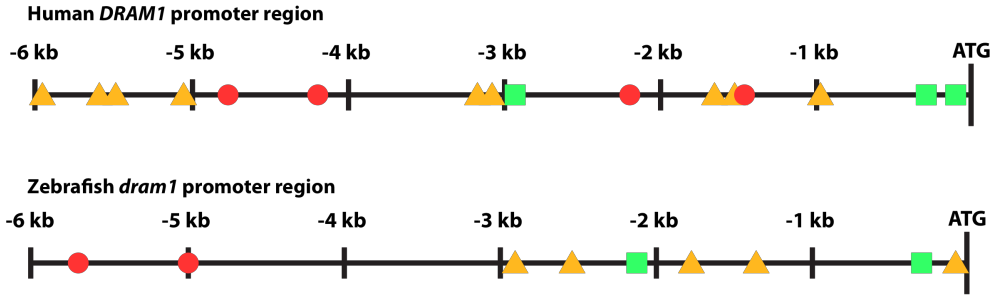

Supplementary figure 3. Transcription factor binding sites in the promoter region of *DRAM1*.
We used Patch 1.0 (http://www.gene-regulation.com/cgi-bin/pub/programs/patch/bin/patch.cgi) to predict the presence of p53, NFκB, and Pu.1 transcription factor binding sites in a 6 kb region upstream of the transcription start site of human and zebrafish DRAM1. Patch is a pattern-based program for predicting transcription factor binding sites in DNA sequences. It uses the set of binding sites from TRANSFAC® Public 6.0. Since the consensus binding sites for zebrafish transcription factors are unknown, we depict predicted vertebrate binding sites.

Supplementary figure 4

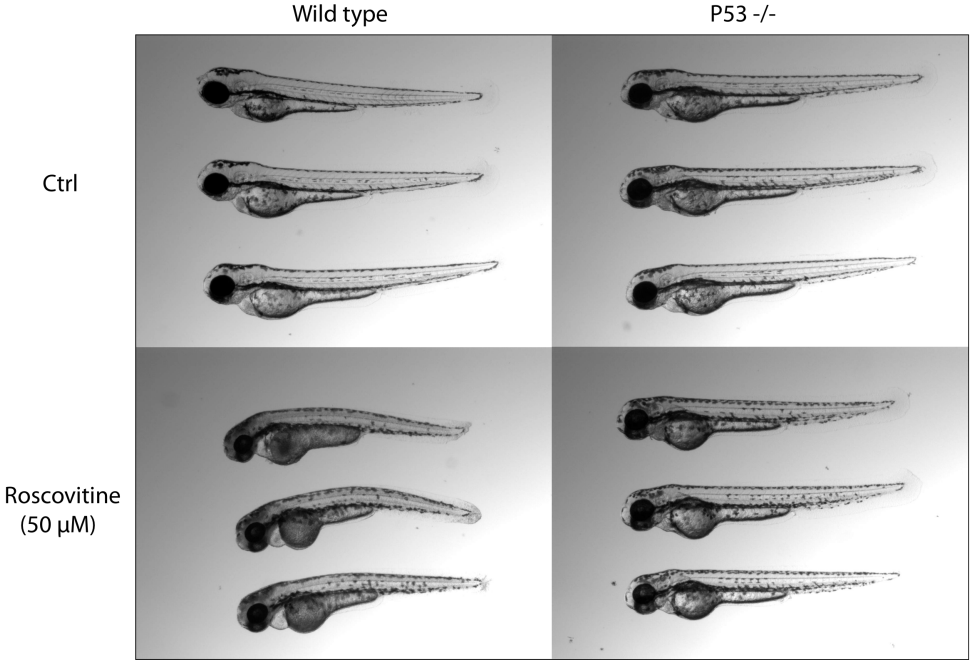

Supplementary figure 4. *p53*$^{-/-}$ embryos are resistant to roscovitin-induced malformations.
Representative images are shown for AB/TL (wild type) and *p53*$^{-/-}$ embryos at 5 days post fertilization after 24 hours of treatment with 50 µM roscovitine.

Supplementary figure 5

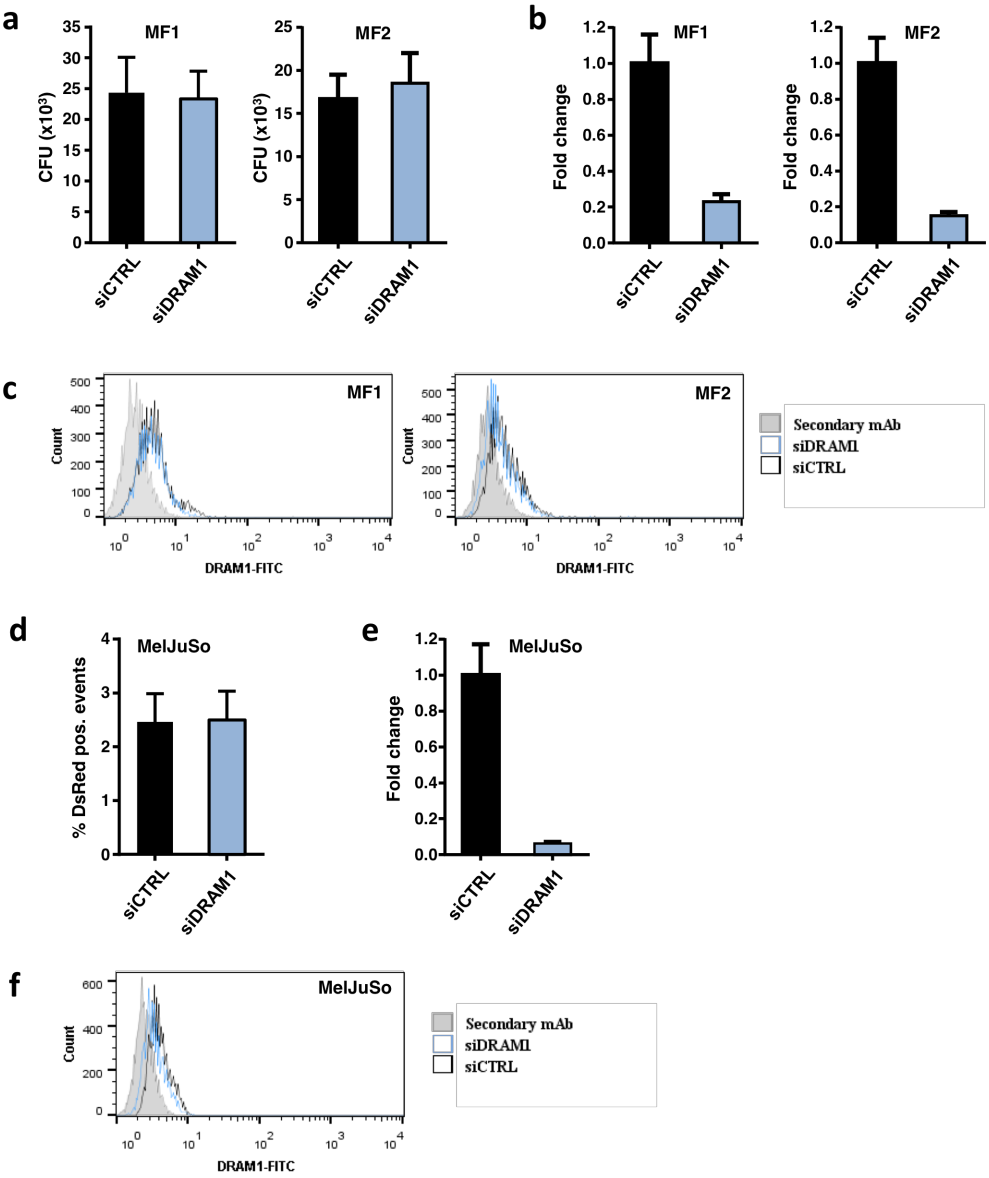

Supplementary figure 5. DRAM1 protein stability precludes the use of genetic knockdown to study DRAM1 function in human primary macrophages and MelJuSo cells. We used an ON-TARGETplus siRNA pool (siDRAM1) to knockdown human *DRAM1* in type 1 (M1) and type 2 (M2) primary human macrophages and MelJuSo cells. (A) siDRAM1 did not affect bacterial burdens in M1 or M2, as determined by an colony forming unit (CFU) assay. (B) Although siDRAM1 effectively reduced *DRAM1* mRNA levels in M1 and M2, (C) DRAM1 protein levels were unaffected. This precludes the use of genetic knockdown by siRNA to study DRAM1 function in M1 and M2. We then tested the effect of siDRAM1 on MelJuSo cells to verify these results. (D) siDRAM did not affect the percentage of MelJuSo cells infected by *Mtb* as determined by FACS analysis. Again, (E) siDRAM1 effectively reduced *DRAM1* mRNA levels, (F) while having no effect on DRAM1 protein levels.

Supplementary figure 6

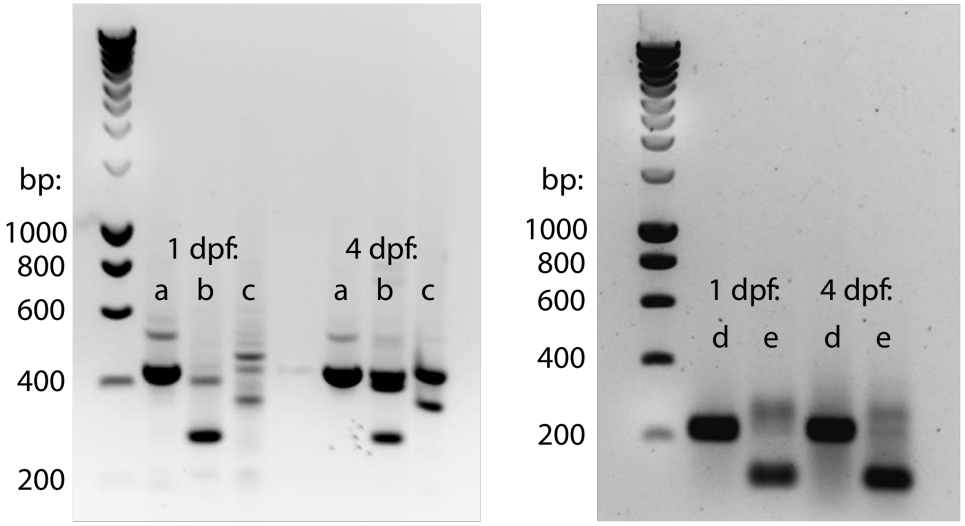

a: SC Mo 0,1 mM
b: *dram1* Mo i2e3 0,1 mM
c: *dram1* Mo i3e4 0,225mM

d: SC Mo 0,1 mM
e: *sqstm1* i1e2 Mo 0,5 mM

Supplementary figure 6. RT-PCR confirmation of splice-blocking morpholinos.
Reverse transcription polymerase chain reaction (RT-PCR) was used to confirm antisense morpholino blocking of intron-exon splicing events in zebrafish *dram1* or *sqstm1* at 1 and 4 days post fertilization. (A) and (D) 0,1 mM Standard control (SC) morpholino; (B) 0,1 mM *dram1* Mo 1 (i2e3, targeting the splicing event between the second intron and the third exon); (C) 0,225 mM *dram1* Mo 2 (i3e4, targeting the splicing event between the third intron and the fourth exon); (E) 0,5 mM *sqstm1* Mo (i1e2, targeting the splicing event between the second intron and the third exon). For both *dram1* and *sqstm1*, the RT-PCR product (approximately 400 and 200 bp in size, respectively) is disrupted upon morpholino injection. Morpholino sequences and primers used for the RT-PCR are listed in supplementary tables 1 and 2.

Supplementary figure 7

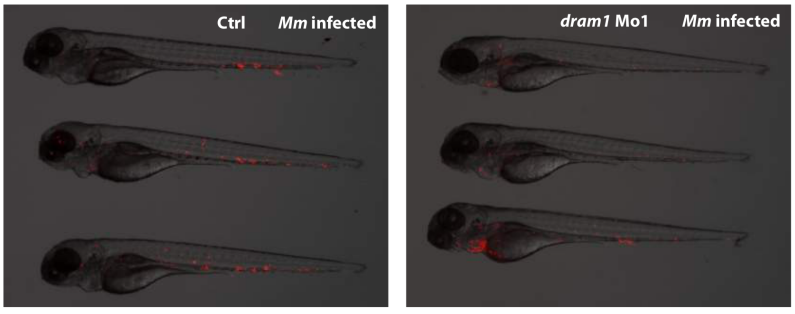

Supplementary figure 7. Equal bacterial burdens in control and *dram1* morpholino injected embryos
Representative stereo micrographs of standard control or *dram1* morpholino injected embryos. Control injected embryos were infected with 200 CFU *Mm* versus 50 CFU for *dram1* morphants to obtain equal bacterial burdens at the time point of RNA isolation.

Supplementary figure 8

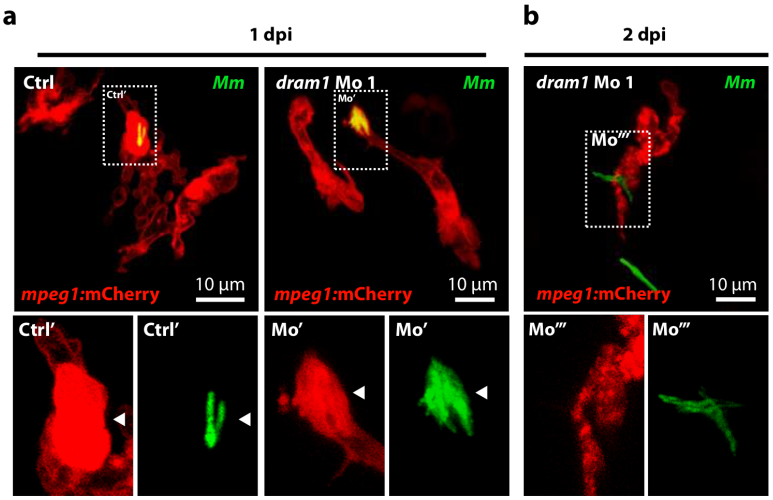

Supplementary figure 8. Localization of *Mm* in- or outside of macrophages
(A-B) Representative confocal micrographs of *mpeg1*:mCherry transgenic embryos injected with standard control or *dram1* morpholino 1 and infected with GFP-labeled *Mm* (A: 1 dpi; B: 2 dpi). Boxed areas are detailed below with the green and red channel shown separately. Arrowheads indicate bacteria enclosed by membranes.

Supplementary figure 9

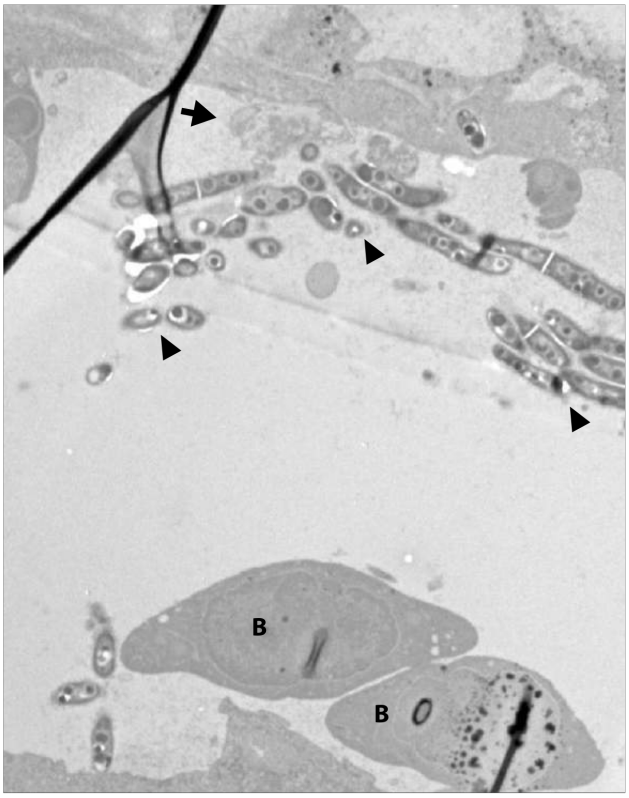

Supplementary figure 9. TEM of extracellular *Mm* in a blood vessel of a *dram1* morphant
Transmission electron microscopy micrograph of a *dram1* morpholino injected embryo infected with *Mm*. Clusters of extracellular bacteria (arrowheads) are residing inside a blood vessel, as illustrated by the presence of red blood cells (B). The remnants of a ruptured cell are indicated by an arrow.

Supplementary figure 10

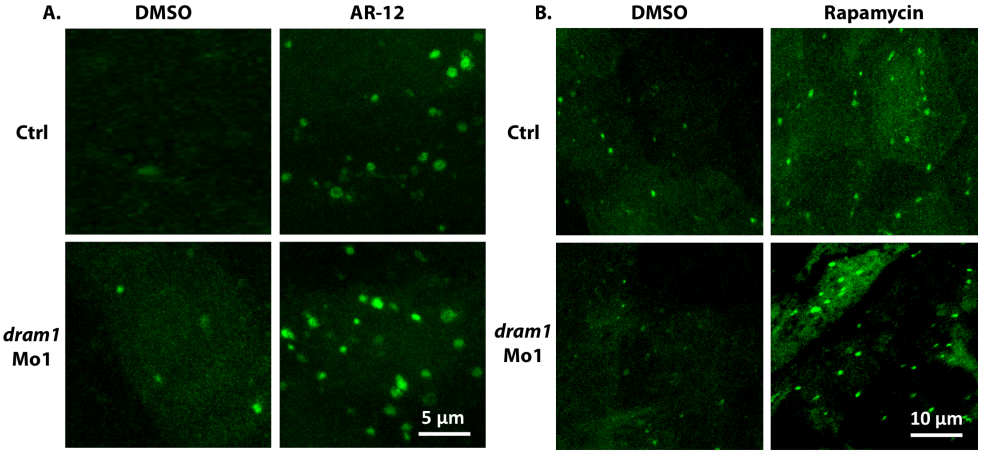

Supplementary figure10. The effect of Ar-12 or rapamycin treatment on *dram1* morphants
Representative confocal micrograph of standard control or *dram1* morpholino injected embryos treated with Ar-12 (A), rapamycin (B), or DMSO as control. Embryos were treated at 2 dpf for 24h.

Supplementary figure 11

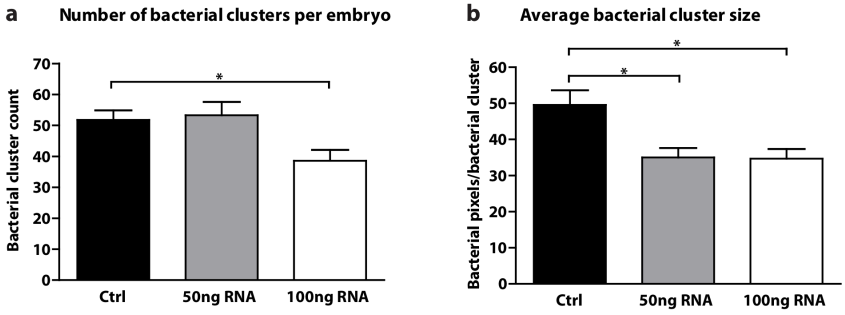

Supplementary figure 11. *dram1* overexpression effect on the formation of granuloma-like aggregates. Wild type embryos were mock-injected or injected with 50 or 100 pg *dram1* RNA immediately after fertilization. Embryos were infected with 200 CFU *Mm* at 1 dpf. Whole embryo stereo fluorescent micrographs were taken at 3 dpi and (A) the total number of bacterial clusters and (B) the average bacterial cluster size were determined using dedicated software (Stoop et al., 2010). Data (mean ± SEM) is pooled from two individual experiments (n>94 embryos per group). Significant differences were calculated by one-way ANOVA with Tukey's Multiple Comparison method as a post-hoc test (*= $p<0.05$). Significant reduction of both the total number of clusters and cluster size by *dram1* overexpression is in agreement with the reduction of total bacterial pixel counts shown in figure 6C.

Supplementary figure 12

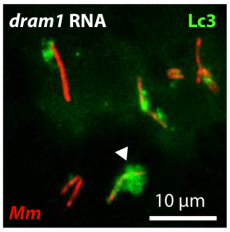

Supplementary figure 12. *Mm* entirely encapsulated by GFP-Lc3 in *dram1* overexpressing embryo
Representative confocal micrograph of a *dram1* RNA injected embryo infected with *Mm*. The bacteria indicated by an arrowhead are entirely engulfed by a GFP-Lc3 positive vesicle, most likely an autophagosome.

Supplementary figure 13

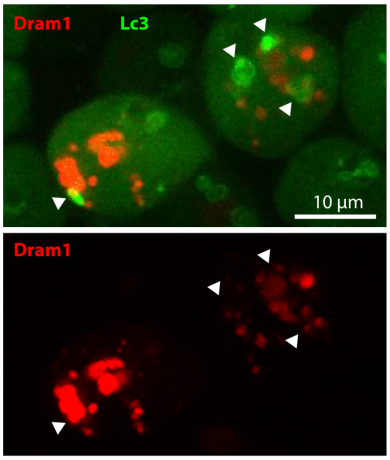

Supplementary figure 13. mCherry-Dram1 co-localizes with GFP-Lc3 postive vesicles
Representative confocal micrograph of GFP-Lc3 embryos transiently expressing mCherry-Dram1. Co-localization is indicated with arrowheads

Supplementary figure 14

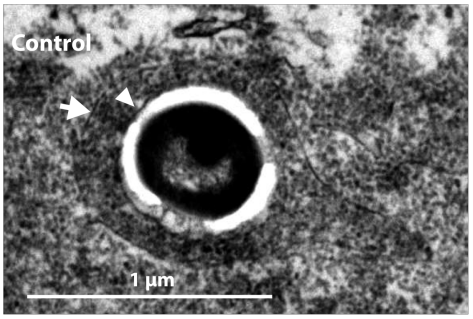

Supplementary figure 14. TEM of control or dram1 overexpressing embryos infected with Mm
Transmission electron micrograph of control or dram1 RNA injected embryos infected with Mm. (A) Bacteria (indicated by an arrowhead) inside an autophagolysome, as characterized by the presence of cytoplasmic material inside a single-membraned vesicle (indicated by an arrow). (B-C) Two examples of large bacteria-containing vesicles, as frequently observed in dram1 overexpressed embryos infected with Mm. V= remnants of vesicular fusion; N = nucleus; « = double-membrane.

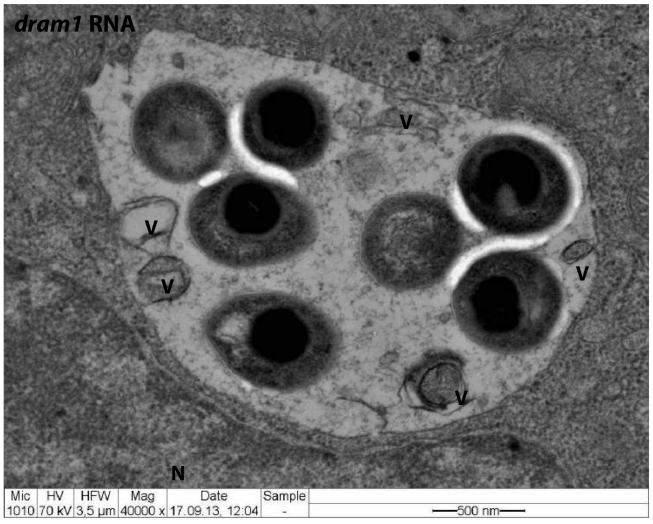

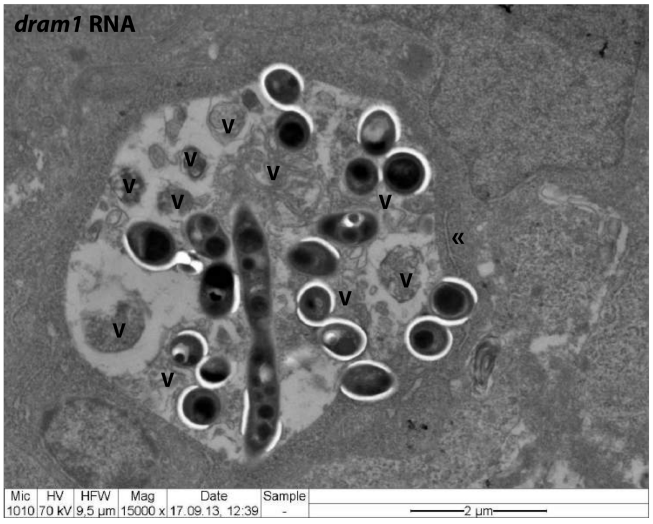

Supplementary table 1: Zebrafish lines

Name	Description	Reference
AB/TL	wild type strain	-
myd88^{hu3568}	Mutant line with truncated MyD88	van der Vaart et al., 2013
tp53^{m214k}	p53 with mutated DNA-binding domain	Guo et al., 2012
Tg(CMV:GFP-Lc3)	GFP-tagged zebrafish Lc3	He et al., 2009
Tg(mpx::egfp)^{i114}	Neutrophil marker	Renshaw et al., 2006
Tg(mpeg1:Gal4-VP16)^{gl24}; *Tg(UAS-E1b:Kaede)*^{s1999t}	Macrophage marker	Ellett et al., 2011
Tg(lck::egfp)^{cz2}	Leukocyte marker	Langenau et al., 2004
Tg(mpeg1::mCherry-F)^{UMSF001}		Georges Lutfalla, kind gift

Supplementary table 2: Morpholino sequences

Gene	Name	Location	Sequence
dram1	Dram1 Mo1	Intron 2 > exon 3	AAGGCTGGAAAACAAACGTACAGTA
dram1	Dram1 Mo2	Intron 3 >exon 4	GTCGTCTCCTGTAACAAAACATGCA
sqstm1	Sqstm1 Mo	Intron 1 > exon 2	CTTCATCTAGAGACAAAGTTCAGGA
sting	Sting Mo	Intron 1 > exon 2	GCCATGATACCTGGAAAACACCAAA
myd88	MyD88 Mo	Exon 2 > intron 2	GTTAAACACTGACCCTGTGGATCAT

Supplementary table 3: Primer sequences

Gene	Type	Species	Accession #	Forward qPCR primer	Reverse qPCR primer
dram1	qPCR	ZF	NM_001006049.1	ATGGTGATGAGCCGATTAGC	TGCTCGATGACCAGATAACC
ppial	qPCR	ZF	AY391451	ACACTGAAACACGGAGGCAAAG	CATCCACAACCTTCCCGAACAC
il1b	qPCR	ZF	NM_212844	GAACAGAATGAAGCACATCAAACC	ACGGCACTGAATCCACCAC
mmp9	qPCR	ZF	NM_213123	CATTAAAGATGCCCTGATGTATCCC	AGTGGTGGTCCGTGGTTGAG
saa	qPCR	ZF	NM_001005599.1	CGCAGAGGCAATTCAGAT	CAGGCCTTTAAGTCTGTATTTGTTG
dram1	RT	ZF	NM_001006049.1	GGATTCATGTCGACAATTACGGC	CCGACAAGAAACCCACATGC
sqstm1	RT	ZF	NM_213173.1	ATTTGCAGCGAAAAGTGCTC	AGTGAACGGAAACCCAGGAA
dram1	Cloning	ZF	NM_001006049.1	TCCGCCAGTCTCTTCACTTT	AACTGCACCAAAAACAGTGG
DRAM1	qPCR	Human	NM_018370.2	TGTCTGTGCTTCACTAATTTCCA	TCACAGATCGCACTCACTACG
SQSTM1	qPCR	Human	NM_003900.4	TCCCGCCGGCACTCTTTTTT	TCCAGTGACGAGGAATTGACAATGG
IL1B	qPCR	Human	M15840.1	CCACGGCCACATTTGGTT	AGGGAAGCGGTTGCTCATC
GAPDH	qPCR	Human	NM_002046.4	AATCCCATCACCATCTTCCA	TGGACTCCACGACGTACTCA

Supplemental experimental procedures

Injection conditions for bacteria and LPS

Mycobacterium marinum Mma20, Mma M, or Mma M ΔRD1 labeled with mCherry, GFP, or Crimson (Swaim et al., 2006) were prepared for the infection of zebrafish embryos by growing them overnight in Difco Middlebrook 7H9 agar (BD and company) supplemented with 10% oleic acid-albumin-dextrose-catalase (OADC, BD and company), 0.5% glycerol, and with appropriate antibiotics to select for fluorescence expression vectors (Benard et al., 2012). Embryos were manually dechorionated at 24 hpf and 200 colony forming units (CFUs) were injected into the caudal vein after the onset of blood flow (28 hpf), or PBS was injected as a control. The same conditions were used for injection of 1 nl of LPS from S. enterica serovar typhimurium dissolved in PBS (10 µg/ml, Sigma, #L6511).

Microarray analysis

Per sample, 500 ng total RNA was combined with Spike A and amplified according to the Agilent Two-Color Microarray-Based Gene Expression Analysis guide version 5.5 (G4140-90050, Agilent technologies). For the common reference an equimolar pool of all test samples was made and 500 ng samples were amplified similarly as the test samples with the exception that Spike B was used. Amino-allyl modified nucleotides were incorporated during the aRNA synthesis (2.5 mM rGAC (GE Healthcare), 0.75 mM rUTP (GE Healthcare), 0.75 mM AA-rUTP (TriLink Biotechnologies). Synthesized aRNA was purified with the E.Z.N.A. MicroElute RNA Clean Up Kit (Omega Bio-Tek). The quality was inspected on the BioAnalyzer (Agilent Technologies) with the Agilent RNA 6000 kit (5067–1511, Agilent Technologies). Test samples were labelled with Cy3 and the Reference sample was labelled with Cy5. For Mycobacterium infected embryos a dye swap technical duplicate was performed in which the control was either labelled with Cy3 or Cy5. The overlap of the technical duplicates was used for the output files. Five µg of aRNA was dried down and dissolved in 50 mM carbonate buffer pH 8.5. Individual vials of Cy3/Cy5 from the mono-reactive dye packs (GE Healthcare) were dissolved in 200 µl DMSO. To each sample, 10 µl of the appropriate CyDye dissolved in DMSO was added and the mixture was incubated for 1 h. Reactions were quenched with the addition of 5 µl 4 M hydroxylamine (Sigma-Aldrich). The labelled aRNA was purified with the E.Z.N.A. MicroElute RNA Clean Up Kit. Yields of aRNA and CyDye incorporation were measured on the NanoDrop ND-1000. Each hybridization mixture was made up from 825 ng Test (Cy3) and 825 ng Reference (Cy5) material. Hybridization mixtures were made as described in the Agilent Two-Color Microarray-Based Gene Expression Analysis guide version 5.5 (G4140-90050, Agilent technologies). The samples were loaded onto 4x180k D. rerio micro-arrays (Design ID:028233, Agilent Technologies) and hybridized for 17 hours at 65°C. Afterwards the slides were washed and scanned (20 bit, 3 µm resolution) in an ozone-free room with the Agilent G2505C scanner as described in the Agilent Two-Color Microarray-Based Gene Expression Analysis guide version 5.5 (G4140-90050, Agilent technologies). Data was extracted with Feature Extraction (v10.7.3.1, Agilent Technologies) with the GE2_107_Sep09 protocol for two-color Agilent micro-arrays. Micro-array data was processed using Rosetta Resolver 7.2 (Rosetta Biosoftware). To compare wild-type control, mutant control, infected wild-type and infected mutant samples, a re-ratio experiment was performed using the Rosetta built-in re-ratio with common reference application. Data were analyzed at the level of probes with significant cut-offs for the ratios set at twofold change at P<10^−5.

RNA deep-sequencing

A total of 3 µg of RNA was used to make RNA-Seq libraries using the Illumina TruSeq RNA Sample Preparation Kit v2 (Illumina Inc., San Diego, USA). In the manufacturer's instructions two modifications were made. In the adapter ligation step 1 µl instead of 2.5 µl adaptor was used. In the library size selection step the library fragments were isolated with a double Ampure XP purification with a 0.7x beads to library ration. The resulting mRNA-Seq library was sequenced using an Illumina HiSeq2000 instrument according to the manufacturer's description with a read length of 2 × 50 nucleotides. Image analysis and base calling was done by the Illumina HCS version 1.15.1. Sequence reads were quality trimmed using the quality_trim module in the CLCbio Assembly Cell v4.0.6. Filtered reads were mapped to ENSEMBL transcripts (Zv9_63) using the ref_assemle_short module in the CLCbio Assembly Cell v4.0.6. Accumulation of transcripts to ENSEMBL genes was done by first converting the mapping files to a table with the assembly_table module in the CLCbio Assembly Cell v4.0.6. Secondly, a custom script was used that sums all reads belonging to the same gene. Non-uniquely mapped reads were divided between genes according to their ratio of uniquely mapped reads. Finally, read counts of transcripts belonging to the same gene were summed to obtain count data at ENSEMBL gene level. Fold-change and differential expression significance values were calculated from gene level read counts using the DESeq package (version 1.8.3) available in Bioconductor (version 2.10).

Dram1 RNA preparation and injection
RNA was isolated from wild type zebrafish embryos using TRI reagent (Life Technologies Europe BV, Bleijswijk, the Netherlands) and purified using the RNeasy MinElute Cleanup kit (QIAGEN Benelux B.V., Venlo, Netherlands). cDNA synthesis was performed using the iScript cDNA synthesis kit (Bio-Rad Laboratories BV, Veenendaal, Netherlands). Full-length Dram1 cDNA was obtained by PCR (primers in Supplementary table 2), using a proof-reading polymerase enzyme (Phusion High-Fidelity DNA Polymerase, New England Biolabs), which was ligated into a ZERO BLUNT TOPO vector (Invitrogen) and subsequently transferred into a pCS2+ expression vector (Invitrogen). Dram1 RNA was generated using the SP6 mMessage mMachine kit (Life Technologies), purified using the RNeasy MinElute Cleanup kit (QIAGEN Benelux B.V., Venlo, Netherlands) and injected into the yolk sac at the one cell stage of zebrafish development.

mCherry-Dram1 preparation and injection
Using the pCS2+ expression vector containing Dram1 cDNA as a template, we added attB sites to the sequence by PCR and used this fragment to create a 3' Gateway entry vector (Invitrogen). This 3' Gateway entry vector was combined with a 5' Gateway entry vector containing the beta actin promoter and a Gateway middle entry vector containing mCherry with the stopcodon removed into a Tol2 containing destination vector, generating the following DNA construct: bactin:mCherry-Dram1. 1 nl of this DNA construct was injected at 50 ng/µl into the cell of a developing zebrafish embryo at the one cell stage, together with Tol2 transposase mRNA for more efficient integration into the genome.

Isolation of zebrafish immune cells by FACS
Dissociation of Tg(mpeg1:Gal4-VP16)gl24;Tg(UAS-E1b:Kaede)s1999t (Ellett et al., 2011), Tg(mpx::egfp)i114 (Renshaw et al., 2006), and Tg(lck::egfp)cz2 (Langenau et al., 2004) zebrafish larvae was performed according to Covassin et al. (2006). In short, embryos were dechorionated using pronase treatment, rinsed in calcium-free Ringer solution, followed by digestion with 0.25% trypsin. The obtained cell suspension was centrifuged, rinsed with PBS and resuspended in Leibovitz medium L15 without phenol red, 1% fetal calf serum, 0.8mM CaCl2, penicillin 50 U/ml and streptomycin 0.05 mg/ml. The single cell suspension was subject to FACS at room temperature using a FACSAria (Becton Dickinson) with the BD FACSDiva software version 5.0.3 and a Coherent Sapphire solid state laser 488 nm with 13 mW power. The GFP+ and GFP- cell fractions were collected as above but with 10% fetal calf serum.

Generation of M1 and M2 macrophages
Type 1 and type 2 macrophagess were generated from buffy coats of healthy donors by FICOLL gradient separation and CD14 MACS sorting (Miltenyi Biotec, Teterow, Germany) followed by stimulation for 6 days with 5 ng/ml recombinant granulocyte macrophage-colony stimulating factor (GM-CSF, BioSource Life Technologies-Invitrogen) or 50 ng/ml recombinant macrophage-colony stimulating factor (M-CSF, R&D Systems, Abingdon, United Kingdom) respectively, as previously reported (Verreck et al., 2006). Macrophages were maintained in Gibco Roswell Park Memorial Institute (RPMI) 1640 medium (Life Technologies-Invitrogen, Bleiswijk, The Netherlands) supplemented with 10% FBS and 2 mM L-Alanyl-L-Glutamine (PAA, Linz, Austria). *Mycobacterium tuberculosis* was cultured in Difco Middlebrook 7H9 broth (Becton Dickinson) supplemented with 10% ADC (Becton Dickinson, Breda, The Netherlands), 0.5% Tween-80 (Sigma-Aldrich).

siRNA transfections
24 hours prior to infection experiments 3,000 cells were transfected with ON-TARGETplus siRNA pools (Thermo Fisher Dharmacon, Waltham Massachusetts, USA) at a 50 nM concentration using 0.2 µl Dharmafect1 (Thermo Fisher Dharmacon) per well in a flat-bottom 96-well plate. Knockdown efficiency was verified by immunoblotting.

Transmission electron microscopy sample preperation
Zebrafish embryos were fixed in 2% glutaraldehyde (GA) and 2% PFA in sodium cacodylate buffer pH 7.2 for 3 hours at room temperature followed by fixation for 16 hours at 4°C. Post fixation was performed in 1% osmium tetroxide in sodium cacodylate buffer for 1 hour at room temperature. After dehydration through a graded series of ethanol all specimens were kept in epoxy resin (Agar scientific) for 16 hours before embedding. Ultrathin sections were collected on Formvar coated 200 mesh or one hole copper grids stained with 2% uranyl acetate in 50% ethanol and lead citrate for 10 minutes each.

Flowcytometric analysis of DRAM1 protein levels
MelJuSo cells, MF1 and MF2 macrophages were stained intracellularly for human DRAM1 following fixation and permeabilization according to the manufacturers protocol (ADG, ITK Diagnostics, Uithoorn, The Netherlands). Protein levels were then determined by subjecting the cells to FACS at room temperature using a FACSAria (Becton Dickinson) with the BD FACSDiva software version 5.0.3.

Flowcytometric analysis of infection and colony forming unit (CFU) assay
The *M. tuberculosis* infection status of MelJuSo cells was deterimend by subjecting the cells to FACS at room temperature using a FACSAria (Becton Dickinson) with the BD FACSDiva software version 5.0.3. The percentage of cells positive for red fluorscently labeled *Mtb* per condition was used as a read out for the bacterial burden. CFU assays were performed using the track dilution method described previously (Jett et al., 1997).

References for supplementary information

Benard EL, van der Sar AM, Ellett F, Lieschke GJ, Spaink HP, Meijer AH. Infection of zebrafish embryos with intracellular bacterial pathogens. J Vis Exp. 2012 Mar 15;(61). pii: 3781.

Covassin L, Amigo JD, Suzuki K, Teplyuk V, Straubhaar J, Lawson ND. Global analysis of hematopoietic and vascular endothelial gene expression by tissue specific microarray profiling in zebrafish. Dev Biol. 2006;(299):551-562.

Verreck, F.A., de Boer, T., Langenberg, D.M., van der Zanden, L., and Ottenhoff, T.H. (2006). Phenotypic and functional profiling of human proinflammatory type-1 and anti-inflammatory type-2 macrophages in response to microbial antigens and IFN-gamma- and CD40L-mediated costimulation. Journal of leukocyte biology 79, 285-293.

Jett, B. D., Hatter, K. L., Huycke, M. M. & Gilmore, M. S. Simplified agar plate method for quantifying viable bacteria. BioTechniques. 23, 648–650 (1997).

6 | Summary and Discussion

As outlined in **Chapter 1**, there are many challenges that accompany the relatively new field of research on host-directed therapies (HDT) in infectious diseases, including technical limitations and obstacles. This particularly holds true for the study of virulent pathogens such as *Mycobacterium tuberculosis* (*Mtb)*, and requires the development of novel technologies and approaches. Against this background we set out to develop novel models and tools visualize and quantify bacterial infection in human cellular models, as described in detail in **Chapters 2** and **3**.

Development of a novel flow cytometry-based screening assay for intracellular bacterial infections in human cells

There is a clear need for high-throughput analyses of interactions at the host-pathogen interface as well as the rapid identification of new candidate molecules, including drugs that target the host molecules regulating these interactions. To address these issues, several reports describing high-throughput screens for HDT discovery have been published in recent years. These studies employed a range of different assays, including traditional colony forming unit (CFU) assays[1,2], bioluminescent assays[3,4] and automated microscopy[5,6] to enumerate bacterial loads. CFU assays have been the golden standard in TB research for over a century, but these are not ideal for high-throughput screening as *Mtb* proliferates very slowly, resulting in a 2-3 week minimum waiting period between bacterial plating and colony count readout, which can extend even to 4-6 weeks. Moreover, performing the assay is very laborious, limiting the throughput. Furthermore, on a more technical note *Mtb* colonies have irregular morphologies and sizes, making it hard to distinguish and quantify them accurately. Employing bioluminescence has been proposed as an alternative[3,4], but even though bioluminescent assays are well quantifiable, reliable and rapid, these assays offer only a single-parameter readout and cannot provide information about exact bacterial loads per cell or the fraction of infected cells. Bridging this gap, several studies have used phenotypic screens employing automated microscopy[5,6]. Using these assays, many different parameters can be derived from images, resulting in large quantities of data. This is both an advantage and a drawback of this methodology, as costly storage facilities, computational infrastructure and computational time needed for analysing such large quantities of data in a high-throughput setting are limited in most laboratories. Moreover this technique is often dependent on automated microscopy platforms and proprietary image analysis software that is not widely available. Therefore, we set out to develop a novel flow cytometry-based screening assay that allows quantification of bacterial loads, infected cell populations and host cell viability, employing novel fluorescent reporter strains of *Mtb* and *Salmonella enterica* serovar Typhimurium (*Stm*). The development of this assay is discussed in **Chapter 2**, in which we report the successful application of the assay in chemical compound screens, using up to 1,200 compounds, and in

siRNA screens testing up to 1,000 siRNA pools (used in **Chapters 3** and **4**). Besides the visualization of infected cells, the quantification of bacterial loads per cell and the exclusion of dead cells, another important advantage of this assay is the strongly decreased time between initiation of the experiment and the readout, which is 24-72 hours instead of 2-4 weeks for classical *Mtb* CFU assays.

The first step towards developing this fluorescence-based assay was engineering novel *Mtb* fluorescent reporter strains expressing stable and destabilized DsRed fluorophore variants, respectively. As *Mtb* is a slowly proliferating bacterium, high stability of fluorescent reporters could potentially cause problems, as accumulation of fluorescent proteins can yield a false positive signal from dead bacteria. Although the stability of the fluorophore did not seem to affect the results obtained in our chemical compound treatment experiments in *Mtb*-infected cells, a more sensitive system was required when performing siRNA experiments, as siRNA-mediated genetic silencing typically resulted in more subtle phenotypes than following chemical compound treatment. To this end we developed a destabilized DsRed reporter construct, which decreases the half-life of DsRed from 4.6 days to several hours[7,8], for expression in *Mtb* and showed that this enabled siRNA screening with an excellent signal-to-noise window.

Since they are the natural target cells for *Mtb* infection, human primary macrophages (Mϕs) represent the ideal model system for in *vitro* TB studies. However, in high-throughput settings the use of these cells suffers from several major drawbacks, a major one of which is that isolating sufficient quantities of human primary Mϕs from single donors is not possible and donor-dependent variation cannot easily be controlled for. An alternative often used by researchers is the human monocytic cell line THP-1. However, differentiation and maturation of this cell line towards a Mϕ-like phenotype requires phorbol 12-myristate 13-acetate (PMA) stimulation, which induces significant Protein Kinase C (PKC) activation[9,10]. This altered signaling background is not desirable for HDT studies, as many host-pathogen interactions take place at the cell signaling level. Therefore we sought a suitable human cell line that is able to phagocytose *Mtb* without the need for chemically induced differentiation and which could be validated in our experimental setting (that is: in which HDT results from literature could be faithfully replicated). As we have previously shown that melanocytes possess phagocytic capability[11], we used and validated the human melanoma cell line MelJuSo as a novel *Mtb* infection model in **Chapter 2**. This model has several important advantages compared to the Mϕ and THP-1 models described above. Firstly, MelJuSo is an established cell line, and is more homogeneous than primary cells from different donors. This enabled both upscaling and greater reproducibility. Secondly, in contrast to the THP-1 model, MelJuSo cells do not require additional stimulation to induce a phagocytic phenotype, thereby providing a 'clean' signaling background for chemical and siRNA screens. Thirdly, as we have shown in **Chapter 2**, MelJuSo cells are efficiently transfectable and near-complete knockdown of specific target gene expression can be achieved using siRNA, while siRNA transfection of THP-1 cells was heterogeneous and resulted in incomplete gene knockdown in our experiments. The high transfectability of MelJuSo cells also offers opportunities for studying *Mtb* infection in cells overexpressing genes or expressing (fluorescently) tagged proteins. More

importantly, we show in **Chapter 2** that results obtained using HDT compounds reported in literature can be faithfully reproduced in MelJuSo cells. Of further importance with regard to validating the MelJuSo model, we demonstrated in **Chapters 3** and **4** that our chemical compound screening results obtained in the MelJuSo-*Mtb* model could be validated in a primary Mϕ *Mtb* infection model. Taken together, these findings firmly establish MelJuSo as a suitable and highly versatile novel *Mtb* infection model for chemical genetics studies, including TB HDT studies.

Beyond wet-lab screens: employing *in silico* prediction tools to accelerate HDT drug discovery for TB

In **Chapter 3** we introduce an *in silico* prediction model as a novel approach to accelerate drug discovery, allowing us to identify novel candidate HDT compounds from a virtually unlimited library of compounds (the PubChem repository) by inferring compound target profiles from compound library screening data. As chemical compounds rarely have a single target and their efficacy in a HDT setting may depend on simultaneously targeting multiple host molecules, our prediction tool was geared towards the ranking of target profiles rather than single target species and on subsequently identifying those compounds in the PubChem repository that have similar target profiles to compounds that were efficacious in our compound library screen. This allowed identification of novel active compounds not just by structural similarity, but rather by confirmed target profiles, allowing a search for compounds that have the desired target profile with reduced toxicity. Moreover, by further focusing our search on active target profiles, the prediction model allowed us to identify host molecules and combinations of these molecules that are essential for bacterial survival. Importantly, we identified novel candidate drugs for HDT against *Mtb* (Dovitinib, AT9283 and ENMD-2076) as well as *Stm* (Nafoxidine and Opipramol), which were shown to be efficacious in our (drug-sensitive (DS) as well as MDR-)*Mtb* and *Stm* infection models, including in human primary Mϕs (discussed below). Moreover, as the prediction model was agnostic to our manual hit compound selection, it allowed fully unbiased validation and follow up of the primary compound screen.

As the prediction model used simple numerical values (in our case z-scores) as input, it can in theory be easily adapted to any screen of chemical compounds (provided that the compounds are submitted to the PubChem repository) and may therefore be of interest for research on other druggable diseases, in particular for drug repurposing studies.

Novel targets and drug candidates for HDT

Applying the novel tools we developed above as well as using a zebrafish TB infection model in several individual studies, we identified multiple novel targets for HDT. These include receptor tyrosine kinases (RTKs), PCTAIRE kinases and the DNA-damage regulated autophagy modulator (DRAM1) as new molecular targets for HDT, as well as chemical inhibitors for several of these molecules as starting points for novel anti-infective therapies. These findings will be discussed below, contextualized by other results and published literature.

Role of receptor tyrosine kinases and their chemical inhibitors in mycobacterial infection

In our screen of a Library Of Pharmacologically Active Compounds (LOPAC) in the MelJuSo-*Mtb* model (discussed in **Chapter 3**), 4 out of 5 validated best hit compounds (which inhibited intracellular *Mtb*) were molecules affecting kinases that participate in RTK signaling pathways. These compounds included: Tyrphostin AG 494 (an EGFR inhibitor), SU 6656 (a SRC Family Kinase (SFK) inhibitor), SB 216763 (a GSK-3 inhibitor) and GW5074 (a RAF1 inhibitor) [12-16]. As an independent validation of these findings, our *in silico* predictive model identified additional RTK inhibitors AT9283, ENMD-2076 and Dovitinib as candidate hits, and their activity was subsequently confirmed in our MelJuSo and human primary MΦ (DS and MDR) *Mtb* infection models. Importantly, an unbiased siRNA screen of the human kinome in the MelJuSo-*Mtb* model again independently identified RTK signaling as a host regulatory pathway of *Mtb* infection, and BLK, ABL1 and NTRK1 were identified as candidate targets for HDT. As RTK inhibitors are already an active topic of studies in cancer research[17] and compounds like AT9283, ENMD-2076 and Dovitinib have already entered clinical trials up to phase III[18-23] (http://www.clinicaltrials.gov), RTK inhibitors are promising candidates for drug repurposing and rapid development into HDT drugs for intracellular bacterial infections.

The relevance of (growth factor) RTK signaling pathways for mycobacterial infection is supported by multiple independent studies. Firstly, the growth factor VEGF was shown to be responsible for enhanced angiogenesis in TB granulomas and thereby to support mycobacterial survival in zebrafish *Mycobacterium marinum* (*Mm*) [24] and rabbit *Mtb*[25] infection models. In the study by Oehlers *et al*., Pazopanib (one of the compounds identified by our predictive model) was used to inhibit the VEGF receptor (VEGFR), and this limited granuloma vascularization while decreasing the bacterial burden in their zebrafish *Mm* infection model. Our study showed that VEGFR inhibition may also result in (yet unidentified) intracellular events leading to inhibition of mycobacterial growth, as angiogenesis could not be a contributing factor in our cellular infection model. Secondly, in a chemical screen Stanley *et al*. identified Gefitinib as a compound that inhibits *Mtb* growth by targeting epidermal growth factor receptor (EGFR) signaling. Inhibitors of both these pathways were also identified as host-directed inhibitors of *Mtb*, first in our LOPAC screen (the EGFR inhibitor Tyrphostin AG 494) and subsequently *in silico* in our predictive model (the VEGFR inhibitors Dovitinib and Pazopanib).

Chemical optimization of the H-89 inhibitor scaffold identifies 97i as a novel HDT drug candidate and reveals a role for PCTAIRE kinases in regulation of intracellular bacterial infection

The study by Kuijl *et al*. laid the groundwork for the research reported in this thesis and introduced AKT1 as a promising target for HDT for intracellular bacterial infections[26]. Currently, the role of AKT1 in *Stm* infection remains undisputed. However, the work reported in this thesis sheds new light on its role in regulating *Mtb* infection. Our results reported in **Chapters 3** and **4** confirmed the involvement of AKT1 in *Mtb* infection but also indicated that other host molecules (as discussed above) may be highly significant additional determinants of *Mtb* infection outcome. In contrast to AKT1 as a strong host regulator of *Stm* infection, a single host 'master regulator' of *Mtb* might not exist or has not yet been identified. Our results in **Chapter 4** indicated that indeed a combination of host molecules must be perturbed in order to successfully control intracellular *Mtb*. Our experiments with *Stm* suggested that supplementation of H-89 treatment with silencing of CDK18 could further enhance control of *Stm* bacteria, but this remains currently unproven for *Mtb*. A possible explanation for the requirement for targeting multiple host molecules might be functional redundancy of these targets. However, another possibility might be that *Mtb* employs multiple (simultaneous or consecutive) strategies for evading host control, which should be targeted simultaneously (or consecutively) by novel therapeutics. Further research should therefore focus on identifying the minimal core host molecules that control *Mtb* infection and identifying or developing specific compounds targeting these.

Directly building upon the study by Kuijl et al. [26], we used the kinase inhibitor H-89 as a starting point for further development of host-directed compounds that inhibit intracellular bacterial infections (**Chapter 4**). In **Chapters 3** and **4** we demonstrated that host-mediated bacterial inhibition was significantly stronger in *Stm*-infected cells than in cells infected with *Mtb,* sparking our efforts to enhance the target specificities of the H-89 scaffold in search of the minimal core host molecules that control *Mtb*. This study represents an example of how lead compound optimization can result in significantly enhanced bacterial inhibition by optimizing target specificities. By altering the chemical structure of H-89, we were able to generate host-directed compounds with significantly enhanced activity against intracellular *Mtb*. From this library, compound 97i was identified as the lead molecule with the greatest potential for drug development. Using kinome profiling, we were able to identify the PCTAIRE kinases, a cyclin-dependent kinase (CDK) subfamily consisting of CDK16, CDK17 and CDK18 (PCTAIRE-1, PCTAIRE-2 and PCTAIRE-3, respectively), as host molecules that were targeted by 97i. While H-89 inhibits CDK16 and CDK17, we demonstrated that 97i targets all three PCTAIRE kinases. When CDK18 was genetically silenced in combination with H-89 treatment, inhibition of the outgrowth of intracellular *Stm* was indeed improved, suggesting that all three PCTAIRE kinases must be inhibited for optimal inhibition of bacterial growth, possibly due to functional redundancy of the members of this kinase family. Follow-up studies will need to extend this to *Mtb*.

The PCTAIRE kinases are cytosolic kinases that up until now have been poorly characterized[27]. Their contribution to cell cycle regulation (a hallmark of many CDKs) is disputed and their cellular-molecular functions are largely unknown. However, several recent studies have provided possible avenues for further research to elucidate their role in controlling intracellular bacterial infections. Firstly, different PCTAIRE kinases have previously been linked to intracellular vesicle transport. In a study by Palmer *et al*., direct interactions of the PCTAIRE kinases CDK16 and CDK18 with COPII coatomer proteins, which regulated vesicle transport from the endoplasmic reticulum (ER) were demonstrated and this process could be partially blocked by H-89 treatment[28]. COPII-coated vesicles are involved in anterograde transport of protein products from the ER tot the Golgi apparatus and can therefore directly impact delivery of proteins to the phagosome or other vesicles[29]. The notion that inhibition of PCTAIRE kinases blocks both ER export as well as *Stm* (and possibly *Mtb*) outgrowth suggests that these intracellular bacteria might either require functional protein transport in the host cell for their survival or that the bacteria 'hijack' cellular processes involved in vesicle transport. As we showed in **Chapter 4** that 97i inhibits all three PCTAIRE kinases, the study by Palmer *et al*. might thus provide a basis for elucidating the mechanism responsible for bacterial inhibition by the host. A role for PCTAIRE kinases in vesicle transport is further supported by a study from Matsuda *et al*. [30]. The authors demonstrated that CDK18 regulates the RhoGTPases RAC1 and RHOA through inhibition of the kinase FAK, indicating that CDK18 might be indirectly involved in regulation of cell motility and adhesion, phagocytosis and phagosome maturation through reorganization of the actin cytoskeleton[31,32]. We previously also identified a role for RAC1 and RHOA during *Stm* infection and AKT1 was shown to be a regulator of this process by targeting PAK4 and thereby modulating GEF-H1 activity. The CDK18-FAK axis might present an alternative route to modulate RAC1 and RHOA activity during bacterial infection[26]. Our own preliminary siRNA screening data also support a role for FAK in controlling intracellular bacteria, as silencing of this kinase promoted outgrowth of both *Stm* and *Mtb*. Secondly, PCTAIRE kinases might be involved in immune modulation, which could impact bacterial control. CDK16 knockdown was recently shown to enhance sensitivity of tumor cells to TNF-family cytokines[33], and TNF is a major protection-associated cytokine in TB[34]. Whether inhibition of PCTAIRE kinases (for instance by 97i) might have an additional beneficial effect through sensitization of infected Mϕs to TNF-family cytokines remains to be studied in more complex models than the cell lines and Mϕs that we employed in our studies. So far, our own preliminary data indicated that 97i might shift *Mtb*-infected Mϕs towards a pro-inflammatory Mϕ1-like phenotype, as we observed decreased cell-surface expression of the Mϕ2 marker CD163 and a shift towards pro-inflammatory cytokine secretion upon treatment with 97i. Another possible immunomodulatory role for PCTAIRE kinases, namely at the level of the IL-1β-induced inflammatory response, was reported by Frank *et al*. [35]. In their study, the authors identified CDK18 as one of the proteins required for inhibition of the IL-1β-induced inflammatory response by *Klebsiella pneumoniae* (*K. pneumoniae*). As an important role for IL-1β in skewing the type I interferon response towards a protective phenotype during *Mtb* infection was recently demonstrated[36], this may

suggest another possible mechanism for PCTAIRE kinase-mediated control of intracellular bacteria. Interestingly, inhibition of the IL-1β-induced inflammatory response by *K. pneumoniae* was shown to be EGFR-dependent by Frank *et al.*, providing an interesting link between RTK inhibitors (discussed above and in **Chapter 3**) and PCTAIRE kinase-mediated modulation of IL-1β-induced inflammation.

DRAM1

In another series of studies that focused on the zebrafish-*Mm* infection model and on *Mtb* infection of human Mϕs, we described the identification of DNA Damage-Regulated Autophagy Modulator (DRAM1) as a new molecule in host resistance against mycobacteria, and thus also as a new candidate target for HDT (**Chapter 5**). DRAM1 was previously known as a protein that induces autophagic and cell death responses following cancer-related cellular stress or HIV infection, both in a p53-dependent manner. In the embryonic zebrafish-*Mm* infection model, however, we observed that Dram1 is also regulated by the TLR/IL1R-MYD88-NF-κB axis, in a manner independent from p53. Importantly, we demonstrated that *DRAM1*/*dram1* is upregulated in response to mycobacterial infection in zebrafish (*Mm*) as well as in human primary Mϕs (*Mtb*) and that DRAM1/Dram1 colocalizes with intracellular mycobacteria in both models. As *dram1*-deficient zebrafish embryos were incapable of containing mycobacteria in vesicles, *Mm* infections resulted in excessive bacterial loads in these embryos, indicating a direct involvement of Dram1 in mycobacterial control. We further demonstrated that TLR/IL1R-MYD88-NF-κB-dependent up-regulation of Dram1 was a prerequisite for targeting the autophagic response to mycobacteria and that this response required p62 as well as the DNA-sensing Sting pathway. In human Mϕs the STING pathway was previously shown to induce ubiquitination of *Mtb* in phagosomes that had been damaged by a *Mtb*-RD1 locus encoded virulence factor[37]. Romagnoli *et al*. showed in *Mtb*-infected dendritic cells that RD1-related virulence may be responsible for inhibition of autophagy and promotion of mycobacterial survival, suggesting that this host-pathogen interaction may be exploited to enhance autophagic control of mycobacterial infection[38]. Our results corroborate this notion, as indeed Sting was essential for induction of selective autophagy during mycobacterial infection. Therefore, targeting the TLR-MYD88-NF-κB axis to activate DRAM1 or downstream effectors is a potential strategy for HDT to overcome inhibition of selective autophagy by mycobacteria.

Additional compounds and targets

Our chemical and siRNA screens in **Chapters 3** and **4** identified additional compounds and host molecules that could not actively be pursued further in our studies but that might be of interest for future HDT research.

In our LOPAC screen, also host-directed compounds other than RTK signaling inhibitors were identified that affected intracellular *Mtb* growth. These compounds target a range of different host molecules (**Chapter 3**). One of these compounds was Quinacrine, an antimalarial drug with reported activity in various other diseases through several different targets[39]. Of note, AKT1 (discussed in detail in **Chapter 1** and below), NF-κB (a possible link with DRAM1, which is

described in **Chapter 5** and discussed above) and phospholipase A2 (a key enzyme in the eicosanoid pathway, previously identified as a regulator of the type I interferon response in *Mtb* control[36]) have been reported as targets of Quinacrine[40]. Furthermore, compounds targeting Ca^{2+} transport were identified in our screens in the MelJuSo-*Mtb* model (3',4'-Dichlorobenzamil[41]) and HeLa-*Stm* model (Mibefradil[42]). As Ca^{2+}-mediated activation of calcineurin was previously proposed as a mechanism inhibiting phagosome maturation in *Mtb*-infected cells[43], modulating intracellular Ca^{2+} transport using 3',4'-Dichlorobenzamil or Mibefradil might promote phagosome maturation and control of intracellular bacteria in infected cells.

Additionally, our screens independently confirmed the significant activity of the previously reported candidate HDT compound Haloperidol[5] and the role of the human kinase ABL1[44,45], further supporting the plausibility of our model system as discussed above. Haloperidol, an antipsychotic that targets dopamine receptors[46], was previously shown to inhibit mycobacterial survival by accelerating endolysosomal trafficking in human cells[5]. We confirmed this in our LOPAC screen in the MelJuSo-*Mtb* model (**Chapter 3**) and extended this finding by showing that Haloperidol also inhibited *Stm*, indicating that this compound may offer a wider range of HDT applications. Interestingly, we also identified the Sigma receptor agonist Opipramol as a host-directed inhibitor of *Stm* using the *in silico* predictions based on the LOPAC screening data and subsequently confirmed the host-mediated anti-bacterial activity of this compound *in vitro*. As Haloperidol has been reported as a high affinity Sigma receptor interactor[47], this finding provides further support for Haloperidol as a promising HDT compound and identifies Sigma receptors as potential host targets that may be exploited for HDT. The siRNA screen of the human kinome reported in **Chapter 3** also independently confirmed a role for the non-receptor tyrosine kinase ABL1. ABL1 was previously reported as a host regulator of mycobacterial infection and its inhibitor Imatinib was efficacious in inhibiting *Mtb in vivo*[44,45]. Importantly, we confirmed the activity of Imatinib in our MelJuSo-*Mtb* model in **Chapter 2**, but Imatinib did not surpass the level of *Mtb* inhibition exerted by H-89 in our model. A possible explanation for this might be that Imatinib, in addition to affecting ABL1 signaling, also modulates the myeloid compartment, which may reduce the bacterial burden[48]. As this cannot be measured in a cellular infection model, the effects of Imatinib on *Mtb* infection were likely limited to ABL1-mediated mechanisms in our model, explaining the discrepancy in efficacy with *in vivo* models.

A future perspective on HDT for intracellular bacterial infections

Apart from the novel compounds and host molecules identified for HDT reported above, our studies also provide important insights for additional HDT strategies and the further identification and development of HDT molecules.

In our studies, we used a chemical compound-centric approach followed by target identification, for several reasons. Firstly, as we demonstrated that

perturbation of multiple host molecules may be required for host control of intracellular *Mtb* (discussed in the previous paragraph) and chemical compounds rarely have a single target, efficacious chemical compounds provide an ideal starting point for elucidation of host-pathogen interactions that regulate intracellular bacterial survival. Conversely, in gene silencing approaches individual genes are targeted. In our own experiments, the effect of knockdown of single genes on *Mtb* bacterial loads was limited and relatively few targets were identified that significantly affected *Mtb* survival. However, our siRNA screen of the human kinome confirmed HDT targets reported in literature like ABL1 (discussed above) and provided a significant and valuable complementary approach to chemical compound screening, particularly when studying the dataset using network or pathway analyses rather than by focusing on individual targets, as we demonstrated in **Chapter 3**. Secondly, screening for efficacious compounds instantly provides starting points for drug development, whereas in genetic approaches compounds targeting the identified gene products must first be found before further development into clinically applicable drugs is possible, if at all. Thirdly, performing chemical screens of existing drugs for drug repurposing may further accelerate HDT drug development as generally a wealth of drug safety and pharmacokinetic data is available and the drugs may either be in, or already have passed the stage of clinical trials, thus enhancing the chances of successful clinical application. This is exemplified by our LOPAC screen and the subsequent *in silico* predictions in **Chapter 3**, where we identified multiple compounds as HDT candidates that were already studied in clinical trials.

Even though the focus on chemical compounds described above is the fastest way towards clinically applicable HDT drugs, fundamental research (and systems biology approaches) will remain essential to expand our understanding of the host-pathogen interactions that underlie the successful survival of major pathogens like *Mtb* inside host cell niches. By definition, pathogens are organisms that have acquired some level of resistance against innate host microbicidal mechanisms as this is a prerequisite for successful colonization. Even though HDT approaches are less likely to cause resistance than direct anti-microbials (as discussed in **Chapter 1**), because the former do not act on bacterial targets that can be rapidly mutated, but rather on host targets that cannot, selective multi-pronged host-mediated immune pressure is still exerted on the bacteria. Therefore, at least in theory, it cannot be excluded that chemical perturbation of host mechanisms may lead to the emergence of pathogens that have developed alternative methods for escaping host immune functions. A thorough understanding of the interactions taking place at the host-pathogen interface and downstream pathways and effector mechanisms is therefore essential to prevent development of novel 'HDT-resistant' pathogens.

By performing our studies in both *Stm* and *Mtb* infection models we gained important insights in the applicability of HDT for different pathogens. As a basis for our studies, we showed in **Chapters 2** and **4** that H-89 is not equally effective in *Stm* and *Mtb* infection models. In addition, the chemical compound screens described in **Chapters 3** and **4** showed limited agreement between the *Stm* and *Mtb* models. This indicated that future HDT approaches must take specific perturbations of host immune mechanisms by different pathogens into

account, again underscoring the need for fundamental understanding of host-pathogen interactions. Despite this, we identified several compounds that displayed activity in both the *Stm* and *Mtb* infection models. Most notably, H-89-derived kinase inhibitor 97i (**Chapter 4**) was highly potent in inhibiting both *Stm* as well as *Mtb* in our experiments and we showed in **Chapter 3** that Haloperidol (which was previously shown to inhibit mycobacterial infection) also inhibits intracellular *Stm*, providing important proof-of-principle for wide-spectrum HDT. Therefore, identifying the strategies for bacterial survival that are employed by multiple pathogens may identify critical host molecules or pathways that can be exploited for wide-spectrum HDT.

In conclusion, HDT presents a promising novel strategy in the fight against global antibiotic resistance. In this newly emerging field, significant efforts will be required to develop clinically applicable HDT drugs. Detailed knowledge of the interactions taking place at the host-pathogen interface should be expanded to identify the most promising avenues for HDT against rampant anti-microbial resistant infections such as MDR, XDR and TDR TB and typhoid disease. The work described in this thesis contributes to this through the identification of multiple new targets and chemical compounds that can help accelerate development of novel HDT drugs, either directly by providing repurposable drugs with established clinical applicability, as well as by identifying novel host molecules and pathways contributing to the fundamental understanding of host-pathogen interactions in TB and typhoid disease.

References

1. Kumar, D. *et al.* Genome-wide analysis of the host intracellular network that regulates survival of Mycobacterium tuberculosis. *Cell* **140,** 731–743 (2010).
2. Jayaswal, S. *et al.* Identification of host-dependent survival factors for intracellular Mycobacterium tuberculosis through an siRNA screen. *PLoS Pathog* **6,** e1000839 (2010).
3. Andreu, N. *et al.* Optimisation of bioluminescent reporters for use with mycobacteria. *PLoS ONE* **5,** e10777 (2010).
4. Eklund, D. *et al.* Validation of a medium-throughput method for evaluation of intracellular growth of Mycobacterium tuberculosis. *Clin. Vaccine Immunol.* **17,** 513–517 (2010).
5. Sundaramurthy, V. *et al.* Integration of chemical and RNAi multiparametric profiles identifies triggers of intracellular mycobacterial killing. *Cell Host and Microbe* **13,** 129–142 (2013).
6. Brodin, P. *et al.* High content phenotypic cell-based visual screen identifies Mycobacterium tuberculosis acyltrehalose-containing glycolipids involved in phagosome remodeling. *PLoS Pathog* **6,** e1001100 (2010).
7. Verkhusha, V. V. *et al.* High stability of Discosoma DsRed as compared to Aequorea EGFP. *Biochemistry* **42,** 7879–7884 (2003).

8. Li, X. *et al.* Generation of destabilized green fluorescent protein as a transcription reporter. *J. Biol. Chem.* **273,** 34970–34975 (1998).
9. Liu, W. S. & Heckman, C. A. The sevenfold way of PKC regulation. *Cell. Signal.* **10,** 529–542 (1998).
10. Wu-zhang, A. X. & Newton, A. C. Protein kinase C pharmacology: refining the toolbox. *Biochem. J.* **452,** 195–209 (2013).
11. Le Poole, I. C. *et al.* Phagocytosis by normal human melanocytes in vitro. *Exp. Cell Res.* **205,** 388–395 (1993).
12. Lemmon, M. A. & Schlessinger, J. Cell signaling by receptor tyrosine kinases. *Cell* **141,** 1117–1134 (2010).
13. Levitzki, A. & Gazit, A. Tyrosine kinase inhibition: an approach to drug development. *Science* **267,** 1782–1788 (1995).
14. Varga, E. V. *et al.* Involvement of Raf-1 in chronic delta-opioid receptor agonist-mediated adenylyl cyclase superactivation. *Eur. J. Pharmacol.* **451,** 101–102 (2002).
15. Cicha, I., Zitzmann, R. & Goppelt-Struebe, M. Dual inhibition of Src family kinases and Aurora kinases by SU6656 modulates CTGF (connective tissue growth factor) expression in an ERK-dependent manner. *Int. J. Biochem. Cell Biol.* **46,** 39–48 (2014).
16. Coghlan, M. P. *et al.* Selective small molecule inhibitors of glycogen synthase kinase-3 modulate glycogen metabolism and gene transcription. *Chem. Biol.* **7,** 793–803 (2000).
17. Gaumann, A. K. A. *et al.* Receptor tyrosine kinase inhibitors: Are they real tumor killers? *Int. J. Cancer* **138,** 540–554 (2016).
18. Hay, A. E. *et al.* A phase II study of AT9283, an aurora kinase inhibitor, in patients with relapsed or refractory multiple myeloma: NCIC clinical trials group IND.191. *Leuk. Lymphoma* **57,** 1463–1466 (2016).
19. Moreno, L. *et al.* A phase I trial of AT9283 (a selective inhibitor of aurora kinases) in children and adolescents with solid tumors: a Cancer Research UK study. *Clinical Cancer Research* **21,** 267–273 (2015).
20. Schäfer, N. *et al.* Phase I trial of dovitinib (TKI258) in recurrent glioblastoma. *J. Cancer Res. Clin. Oncol.* **142,** 1581–1589 (2016).
21. Cheng, A.-L. *et al.* Randomized, Open-Label Phase 2 Study Comparing Frontline Dovitinib vs Sorafenib in Patients With Advanced Hepatocellular Carcinoma. *Hepatology* (2016). doi:10.1002/hep.28600
22. Lim, S. H. *et al.* Efficacy and safety of dovitinib in pretreated patients with advanced squamous non-small cell lung cancer with FGFR1 amplification: A single-arm, phase 2 study. *Cancer* (2016). doi:10.1002/cncr.30135
23. Yee, K. W. L. *et al.* A phase I trial of the aurora kinase inhibitor, ENMD-2076, in patients with relapsed or refractory acute myeloid leukemia or chronic myelomonocytic leukemia. *Invest New Drugs* (2016). doi: 10.1007/s10637-016-0375-2
24. Oehlers, S. H. *et al.* Interception of host angiogenic signalling limits mycobacterial growth. **517,** 612–615 (2015).
25. Datta, M. *et al.* Anti-vascular endothelial growth factor treatment normalizes tuberculosis granuloma vasculature and improves small molecule delivery. *Proc Natl Acad Sci USA* **112,** 1827–1832 (2015).

26. Kuijl, C. *et al.* Intracellular bacterial growth is controlled by a kinase network around PKB/AKT1. **450,** 725–730 (2007).
27. Mikolcevic, P., Rainer, J. & Geley, S. Orphan kinases turn eccentric: a new class of cyclin Y-activated, membrane-targeted CDKs. *Cell Cycle* **11,** 3758–3768 (2012).
28. Palmer, K. J., Konkel, J. E. & Stephens, D. J. PCTAIRE protein kinases interact directly with the COPII complex and modulate secretory cargo transport. *Journal of Cell Science* **118,** 3839–3847 (2005).
29. Hughes, H. & Stephens, D. J. Assembly, organization, and function of the COPII coat. *Histochem. Cell Biol.* **129,** 129–151 (2008).
30. Matsuda, S., Kawamoto, K., Miyamoto, K., Tsuji, A. & Yuasa, K. PCTK3/CDK18 regulates cell migration and adhesion by negatively modulating FAK activity. *Sci Rep* **7,** 45545 (2017).
31. Groves, E., Dart, A. E., Covarelli, V. & Caron, E. Molecular mechanisms of phagocytic uptake in mammalian cells. *Cell. Mol. Life Sci.* **65,** 1957–1976 (2008).
32. Kinchen, J. M. & Ravichandran, K. S. Phagosome maturation: going through the acid test. *Nat Rev Mol Cell Biol* **9,** 781–795 (2008).
33. Yanagi, T., Shi, R., Aza-Blanc, P., Reed, J. C. & Matsuzawa, S.-I. PCTAIRE1-knockdown sensitizes cancer cells to TNF family cytokines. *PLoS ONE* **10,** e0119404 (2015).
34. Ottenhoff, T. H. M. New pathways of protective and pathological host defense to mycobacteria. *Trends Microbiol.* **20,** 419–428 (2012).
35. Frank, C. G. *et al.* Klebsiella pneumoniae targets an EGF receptor-dependent pathway to subvert inflammation. *Cellular Microbiology* **15,** 1212–1233 (2013).
36. Mayer-Barber, K. D. *et al.* Host-directed therapy of tuberculosis based on interleukin-1 and type I interferon crosstalk. **511,** 99–103 (2014).
37. Watson, R. O., Manzanillo, P. S. & Cox, J. S. Extracellular M. tuberculosis DNA targets bacteria for autophagy by activating the host DNA-sensing pathway. *Cell* **150,** 803–815 (2012).
38. Romagnoli, A. *et al.* ESX-1 dependent impairment of autophagic flux by Mycobacterium tuberculosis in human dendritic cells. *Autophagy* **8,** 1357–1370 (2012).
39. Al-Bari, M. A. A. Chloroquine analogues in drug discovery: new directions of uses, mechanisms of actions and toxic manifestations from malaria to multifarious diseases. *J. Antimicrob. Chemother.* **70,** 1608–1621 (2015).
40. Ehsanian, R., Van Waes, C. & Feller, S. M. Beyond DNA binding - a review of the potential mechanisms mediating quinacrine's therapeutic activities in parasitic infections, inflammation, and cancers. *Cell Commun. Signal* **9,** 13 (2011).
41. Blaustein, M. P. & Lederer, W. J. Sodium/calcium exchange: its physiological implications. *Physiol. Rev.* **79,** 763–854 (1999).
42. Osterrieder, W. & Holck, M. In vitro pharmacologic profile of Ro 40-5967, a novel Ca2+ channel blocker with potent vasodilator but weak inotropic action. *J. Cardiovasc. Pharmacol.* **13,** 754–759 (1989).

43. Jayachandran, R. *et al.* Survival of mycobacteria in macrophages is mediated by coronin 1-dependent activation of calcineurin. *Cell* **130,** 37–50 (2007).
44. Napier, R. J. *et al.* Imatinib-sensitive tyrosine kinases regulate mycobacterial pathogenesis and represent therapeutic targets against tuberculosis. *Cell Host and Microbe* **10,** 475–485 (2011).
45. Hawn, T. R., Shah, J. A. & Kalman, D. New tricks for old dogs: countering antibiotic resistance in tuberculosis with host-directed therapeutics. *Immunol. Rev.* **264,** 344–362 (2015).
46. Lako, I. M., van den Heuvel, E. R., Knegtering, H., Bruggeman, R. & Taxis, K. Estimating dopamine D_2 receptor occupancy for doses of 8 antipsychotics: a meta-analysis. *J Clin Psychopharmacol* **33,** 675–681 (2013).
47. Maurice, T. & Su, T.-P. The pharmacology of sigma-1 receptors. *Pharmacol. Ther.* **124,** 195–206 (2009).
48. Napier, R. J. *et al.* Low doses of imatinib induce myelopoiesis and enhance host anti-microbial immunity. *PLoS Pathog* **11,** e1004770 (2015).

Nederlandse Samenvatting (Summary in Dutch)

Antibioticumresistentie is een snel toenemend en ernstig wereldwijd probleem in de strijd tegen (bacteriële) infectieziekten. Door de opkomst van meervoudig en zelfs volledig antibioticumresistente *Mycobacterium tuberculosis* (*Mtb*) stammen dreigt de ernstige infectieziekte tuberculose (TB) onbehandelbaar te worden. Pogingen om nieuwe antibiotica te identificeren of ontwikkelen zijn weinig succesvol gebleken en dus vraagt het antibioticumresistentieprobleem om nieuwe strategieën om infecties aan te pakken. De kennis dat intracellulaire bacteriën zoals *Mtb* en *Salmonella* kunnen overleven door signaleringsroutes van de gastheercel te manipuleren biedt mogelijkheden voor zogenaamde gastheergerichte therapieën. Hierbij worden door middel van chemische stoffen of genetische technieken de signaleringsroutes van de gastheercel dusdanig gestuurd dat de manipulaties door de bacterie ongedaan gemaakt worden. Dit heeft als gevolg dat de bacterie door het immuunsysteem gedood wordt. Op dit moment is het onderzoeksveld echter nog niet zo ver dat gastheergerichte therapie klinisch toegepast kan worden en veel van de interacties die plaatsvinden tussen de bacteriën en de gastheercel zijn tot dusver niet bekend. Om de ontwikkeling van gastheergerichte therapieën tegen TB (en *Salmonella* infecties) te versnellen hebben we een aantal verschillende strategieën gevolgd, welke hieronder worden uiteengezet.

Allereerst hebben we geïnvesteerd in de ontwikkeling van nieuwe technieken waarmee we versneld 1) de menselijke genen en eiwitten kunnen identificeren die een belangrijke rol spelen bij de overleving van *Mtb* en *Salmonella* in de gastheercel en 2) chemische stoffen kunnen identificeren die kunnen worden gebruikt om deze eiwitten of de signaleringsroutes waarin de eiwitten een rol spelen dusdanig te sturen dat intracellulaire bacteriën niet langer kunnen overleven (**Hoofdstuk 2**). Dit heeft geleid tot de ontwikkeling van een nieuwe screeningsmethode, gebaseerd op geautomatiseerde flow cytometrie, waarmee we snel grote chemische en genetische bibliotheken kunnen screenen, gebruikmakend van nieuwe infectiemodellen op basis van menselijke cellen en fluorescente *Mtb* en *Salmonella* stammen. De screeningsmethode bleek in onze uitgebreide validatie-experimenten snel en zeer reproduceerbaar, en resultaten behaald door middel van traditionele testen voor bacteriële groei en *Mtb* infecties in humane primaire macrofagen konden goed gereproduceerd worden in dit systeem. In **Hoofstukken 3** en **4** hebben we de nieuwe methode vervolgens toegepast voor het screenen van grote bibliotheken van chemische stoffen en siRNA's om chemische stoffen en mensenlijke genen te identificeren die kunnen worden gebruikt voor gastheergerichte therapieën.

Allereerst hebben we in **Hoofdstuk 3** een screening uitgevoerd van de Library Of Pharmacologically Active Compounds (LOPAC), waarbij we meerdere chemische stoffen (die reeds worden toegepast voor andere aandoeningen)

hebben gevonden die Receptor Tyrosine Kinases (RTKs) als doelwit hebben en die de groei van intracellulaire bacteriën sterker remmen dan reeds bekende stoffen. Vervolgens hebben we een computermodel gebouwd dat, op basis van de screeningsdata en de menselijke eiwitten die de chemische stoffen in de LOPAC bibliotheek als doelwit hebben, nieuwe chemische stoffen kan voorspellen die ook activiteit zouden moeten vertonen in onze infectiemodellen. De stoffen die door dit model voorspeld werden bleken in onze experimenten inderdaad de groei van *Mtb* en *Salmonella* te remmen. Bovendien hadden de stoffen die (antibioticumresistente en -gevoelige) *Mtb* remden wederom RTK's als doelwit. Door vervolgens onze screeningsmethode in te zetten voor een siRNA screen van het volledige humane kinoom bevestigden we wederom dat RTK's een rol spelen bij de overleving van *Mtb* in de humane cel. Bij elkaar leveren deze resultaten dus zowel een nieuwe signaleringsroute op die als doelwit gebruikt kan worden voor gastheergerichte therapieën én werden er chemische stoffen geïdentificeerd die als basis kunnen dienen voor de ontwikkeling van nieuwe gastheergerichte therapeutica.

Resultaten van een tweede screening van chemische stoffen worden beschreven in **Hoofdstuk 4**. Hierbij hebben we ons gericht op een nieuw ontwikkelde bibliotheek van stoffen die afgeleid zijn van de kinase-remmer H-89, welke we in een eerdere studie hebben geïdentificeerd als een gastheergerichte remmer van *Salmonella* en *Mtb*. Uit deze screen kwam de kinase-remmer 97i als meest veelbelovend naar voren, aangezien deze intracellulaire groei van (antibioticumresistente en -gevoelige) *Mtb* en *Salmonella* aanzienlijk sterker remde dan H-89, zowel in menselijke cellijnen als in primaire macrofagen. Bovendien toonden we hier aan dat 97i de zogenaamde PCTAIRE-familie van kinases als doelwit heeft en lieten we zien dat het uitschakelen van het gen coderend voor de PCTAIRE kinase CDK18 bovenop H-89 behandeling een sterkere remming van *Salmonella* gaf. Om deze reden zijn de PCTAIRE kinases interessante doelwitten voor verder onderzoek naar gastheergerichte therapieën en is 97i een sterke basis voor de ontwikkeling van gastheergerichte therapeutica.

Door gebruik te maken van een model voor TB in zebravisembryo's beschrijven we in **Hoofdstuk 5** een andere invalshoek voor de identificatie van doelwitten voor gastheergerichte therapie. Hierbij richtten we ons op autofagie, een belangrijk afweermechanisme tegen mycobacteriën zoals *Mtb*. Tot dusver was het onduidelijk hoe de herkenning van van mycobacteriën door het aangeboren immuunsysteem verband houdt met autofagie. Door het bestuderen van zebravis en humane macrofaag infecties met mycobacteriën lieten we zien dat DNA damage-regulated autophagy modulator (DRAM1) wordt aangestuurd door de Toll-like receptor (TLR)/interleukine-1 receptor (IL1R)-MYD88-NF-κB signaleringsroute. Dit leidt vervolgens tot activatie van selectieve autofagie. Het uitschakelen van het gen dat codeert voor DRAM1 leidde in onze infectiemodellen tot verhoogde mycobacteriële groei, terwijl overexpressie van DRAM1 de infectie remde door hyperactivatie van autofagie. Inductie van autofagie door DRAM1 was tevens afhankelijk van de cytosolische DNA sensor STING en het selectieve autofagie herkenningsmolecuul p62/SQSTM1. Voorheen was DRAM1 enkel bekend in de context van celdood geïnduceerd door autofagie en in kanker, waarbij DRAM1 afhankelijk was van p53. Hier lieten we zien dat er alternatieve

routes zijn om DRAM1 te activeren en dat deze route kan leiden tot selectieve autofagie van mycobacteriën en waarschijnlijk ook andere intracellulaire pathogenen.

Het werk beschreven in dit proefschrift draagt bij aan het versnellen van de ontwikkeling van gastheergerichte therapieën voor intracellulaire bacteriële infecties allereerst door de identificatie van nieuwe moleculaire aangrijpingspunten en chemische stoffen die als basis kunnen dienen voor de ontwikkeling van gastheergerichte therapeutica, alsmede door het uitbreiden van onze fundamentele kennis van de interacties die plaatsvinden tussen de humane cel en klinisch relevante bacteriële pathogenen zoals *Mtb* en *Salmonella*.

Curriculum Vitae

Born in Leiden on November 29th, 1982, Cornelis Jacob (Kees) Korbee grew up in Noordwijk aan Zee. There, his interest for medical biology was sparked during his VWO education while attending a practical course in biology class, dissecting heart tissue. However, this did not directly lead him to higher education in biology. After a brief departure to study multimedia design in Rotterdam in 2001, he saw the light and was drawn back to his city of birth in 2002 to study Biomedical Sciences. Upon graduation in 2008, he started his research to attain his Ph.D. at the Department of Infectious Diseases of the Leiden University Medical Center, resulting in this thesis.

His frequent work with (genetically modified) human pathogens at a high containment level, combined with his more than frequent student supervision activities in the laboratory, subsequently led him to a career in biological safety. Kees placed his first steps in this field as a Biological Safety Officer at Erasmus MC in 2017, where he learned the trade for half a year. The lessons learned during his Ph.D. regarding genetic modification, infectious diseases and safely working in a BSL-3 facility will be more than valuable in his current occupation as Biological Safety Officer at the Netherlands Cancer Institute - Antoni van Leeuwenhoek in Amsterdam.

List of Publications

1. **Novel Host-Directed Chemical Compounds Inhibit Intracellular Bacteria by Targeting PCTAIRE Kinases.**
   Korbee, C.J.*, Heemskerk, M.T.*, Walburg, K.V., Van den Nieuwendijk, R., Van Strijen, E., Kuijl, C., Schreuders, C., Eken, J., Savage, N.D.L., Neefjes, J.J., Overkleeft, H.S., Ottenhoff, T.H.M.**, Haks, M.C.**.
   Manuscript in preparation.

2. **Combined chemical genetics and data-driven bioinformatics approach identifies receptor tyrosine kinase inhibitors as host-directed antimicrobials.**
   Korbee, C.J.*, Heemskerk, M.T.*, Kocev, D., Van Strijen, E., Rabiee, O., Franken, K.L.M.C., Wilson, L., Savage, N.D.L., Džeroski, S., Haks, M.C.**, Ottenhoff, T.H.M.**.
   Nature Communnications **9**, 358. doi:10.1038/s41467-017-02777-6 (2018)**.**

3. **The DNA damage-regulated autophagy modulator DRAM1 links mycobacterial recognition via TLR-MYD88 to authophagic defense.**
   Van der Vaart, M., **Korbee, C.J.**, Lamers, G.E.M., Tengeler, A.C., Hosseini, R., Haks, M.C., Ottenhoff, T.H.M., Spaink, H.P., Meijer, A.H..
   Cell Host and Microbe **15**, 753–767. doi:10.1016/j.chom.2014.05.005 (2014).

4. **Systems Microbiology: Current Topics and Applications; Chapter 5 - Manipulating the Fight Between Human Host Cells and Intracellular Pathogens.**
   Barsacchi, R.*, Sundaramurthy, C.*, **Korbee, C.J.**, Neefjes, J.J., Ottenhoff, T.H.M., Scanu, T., Zerial, M..
   Caister Academic Press. ISBN: 978-1-908230-02-7 (2012).

5. **Mycobacterial secretion systems ESX-1 and ESX-5 play distinct roles in host cell death and inflammasome activation.**
   Abdallah, A.M.*, Bestebroer, J.*, Savage, N.D.L., De Punder, K., Van Zon, M., Wilson, L., **Korbee, C.J.**, Van der Sar, A.M., Ottenhoff, T.H.M., Van der Wel, N.N., Bitter, W., Peters, P.J..
   The Journal of Immunology **187**, 4744–4753. doi:10.4049/jimmunol.1101457 (2011).

6. **Nuclear Localization of CXCR4 Determines Prognosis for Colorectal Cancer Patients.**
   Speetjens, F.M., Liefers, G.J., **Korbee, C.J.**, Mesker, W.E., Van de Velde, C.J.H., Van Vlierberghe, R.L., Morreau, H., Tollenaar, R.A., Kuppen, P.J.K..
   Cancer Microenvironment **2**, 1-7. doi:10.1007/s12307-008-0016-1 (2009).

* Contributed equally
** Contributed equally

Portfolio

Courses	Year
Basiscursus Regelgeving en Organisatie voor Klinisch Onderzoekers (BROK)	2016
PhD Introductory Meeting	2016
Basic Methods and Reasoning in Biostatistics	2015
LIFI Course in Immunology	2011
Conferences	**Year**
Antibiotics Alternatives for the New Millennium (London). *Invited speaker.*	2014
Keystone Symposium - (Keystone, CO, USA). *Presented work;* *2 Posters at poster session.*	2014
CiPKeBIP Annual Conference on: Immune response and host microbiota in disease development (Ljubljana, Slovenia). *Presented work (invited speaker).*	2012
NVVI Conference (Noordwijkerhout, The Netherlands). *Presented work.*	2011
Keystone Keystone Symposium - Tuberculosis: Immunology, Cell Biology and Novel Vaccination Strategies (Vancouver, BC, Canada). *Attended conference.*	2011
NVVI Conference (Noordwijkerhout, The Netherlands). *Attended conference.*	2010
Teaching	**Period**
Supervision of student internships. *8 Students in total (BSc., MSc., HLO).*	2010-2015
Biomedical Sciences Bachelor's Course Pathogen-Host Interactions. *Gave lectures;* *Supervised work groups;* *Prepared and evaluated exam questions.*	2011-2014
Biomedical Sciences Master's Course Pathogen-Host Interactions. *Prepared and supervised practical course.*	2011-2014
Supervised research proposal writing *2 Students*	2013-2014

List of Abbreviations

3-MA	3-Methyladenine
ADC	Albumin dextrose catalase
AMPK	Adenosine monophosphate-activated protein kinase
ANOVA	Analysis of variance
AUC	Area under the curve
AVG	Average
CDK	Cyclin-dependent kinase
CFU	Colony forming unit
Cq	Chloroquine
DMSO	Dimethyl sulphoxide
Dpf	Days post-fertilization
Dpi	Days post-infection
DRAM1	DNA-damage regulated autophay modulator
DS	Drug-sensitive
ECL	Enhanced chemiluminescence
EGFR	Epidermal growth factor receptor
EM	Electron microscopy
ER	Endoplasmic reticulum
FACS	Fluorescence-activated cell sorting
FBS	Fetal bovine serum
FDR	False discovery rate
GEO	Gene Expression Omnibus
GFP	Green fluorescent protein
GM-CSF	Granulocyte macrophage-colony stimulating factor

GO	Gene ontology
HDT	Host-directed therapy
Hpi	Hours post-infection
HTS	High-throughput sampler
IFNγ	Interferon gamma
IFNγR	Interferon gamma receptor
IL1R	Interleukin-1 receptor
IMDM	Iscove's Modified Dulbecco's Medium
K. pneumoniae	*Klebsiella pneumoniae*
K_i	Dissociation constant
LAM	Lipoarabinomannan
LAP	LC3-associated phagocytosis
LB	Luria-Bertani
LC3	Microtubule-associated protein 1 light chain 3
LOPAC	Library of pharmacologically active compounds
LPS	Lipopolysaccharide
M-CSF	Macrophage-colony stimulating factor
MDR	Multi-drug resistant
Mm	*Mycobacterium marinum*
MODC	Mouse ornithine decarboxylase
MOI	Multiplicity of infection
Mϕ	Macrophage
Mϕ1	Type 1 macrophage
Mϕ2	Type 2 macrophage
Mtb	*Mycobacterium tuberculosis*
mTOR	Mammalian target of rapamycin
Myd88	Myeloid differentiation primary response 88

NAI	NF-κB activation inhibitor
ns	Not significant
NTRK1	Neurotrophic receptor tyrosine kinase 1
OD	Optical density
OD_{600}	Optical density at 600 nm
PCT	Predictive clustering tree
Pfal	*Plasmodium falciparum*
PFDHOD	*Plasmodium falciparum* dihydro orotate dehydrogenase
PI(3)P	Phosphatidylinositol 3-phosphate
PKC	Protein kinase C
PknG	Protein kinase G
PMA	Phorbol 12-mystirate 13-acetate
qPCR	Quantitative polymerase chain reaction
RD1	Region of difference 1
RNA	Ribonucleic acid
RNAi	RNA interference
ROS	Reactive oxygen species
RPMI	Roswell Park Memorial Institute
RTK	Receptor tyrosine kinase
***S.* Paratyphi**	*Salmonella enterica* serovar Paratyphi
***S.* Typhi**	*Salmonella enterica* serovar Typhi
Saa	Serum amyloid A
SCV	*Salmonella*-containing vesicle
SDF	Structure-data format
SEM	Standard error of the mean
SFK	SRC family kinase
siRNA	Small interfering RNA

SPI1	*Salmonella* pathogenicity island 1
SPI2	*Salmonella* pathogenicity island 2
STDEV	Standard deviation
Stm	*Salmonella enterica* serovar Typhimurium
T3SS	Type III secretion system
TANK	TRAF-associated NF-κB activator
TB	Tuberculosis
TBK1	TANK-binding kinase-1
TDR	Totally drug resistant
TGFßI	Tumor growth factor ß type-1
TGFßII	Tumor growth factor ß type-2
TGFßRI	TGFß type-1 receptor
TGFßRII	TGFß type-2 receptor
TLR	Toll-like receptor
TRAF	Tumor necrosis factor receptor-associated factor
TTSS	Type III secretion system
VEGFR	Vascular endothelial growth factor receptor
XDR	Extensively drug resistant